Final Research Report
Research Project Agreement No. Y8265
Implementation of Infiltration Ponds Research

IMPLEMENTATION OF INFILTRATION PONDS RESEARCH

by

Joel W. Massmann
6520 East Mercer Way
Mercer Island, Washington 98040

Washington State Department of Transportation
Technical Monitor
Tony Allen
State Geotechnical Engineer

Prepared for

Washington State Transportation Commission
Department of Transportation
and in cooperation with
U.S. Department of Transportation
Federal Highway Administration

October 2003

TECHNICAL REPORT STANDARD TITLE PAGE

1. REPORT NO.	2. GOVERNMENT ACCESSION NO.	3. RECIPIENT'S CATALOG NO.
WA-RD 578.1		

4. TITLE AND SUBTITLE	5. REPORT DATE
IMPLEMENTATION OF INFILTRATION PONDS RESEARCH	October 2003
	6. PERFORMING ORGANIZATION CODE
7. AUTHOR(S)	8. PERFORMING ORGANIZATION REPORT NO.
Joel Massmann	
9. PERFORMING ORGANIZATION NAME AND ADDRESS	10. WORK UNIT NO.
Joel Massmann 6520 East Mercer Way Mercer Island, Washington 98040	11. CONTRACT OR GRANT NO. Contract no. Y8265
12. SPONSORING AGENCY NAME AND ADDRESS	13. TYPE OF REPORT AND PERIOD COVERED
Research Office Washington State Department of Transportation Transportation Building, MS 47370 Olympia, Washington 98504-7370 Keith Anderson, Project Manager, 360-709-5405	Final Research Report
	14. SPONSORING AGENCY CODE

15. SUPPLEMENTARY NOTES

This study was conducted in cooperation with the U.S. Department of Transportation, Federal Highway Administration.

16. ABSTRACT

Stormwater infiltration facilities help reduce the hydrologic impacts of residential and commercial development. The design of these facilities is particularly challenging because of large uncertainties associated with predictions of both short-term and long-term infiltration rates.

Full-scale "flood tests" conducted at four infiltration facilities in western Washington suggest that lateral flow along the sides of the ponds may be significant. This is similar to "bank storage" that occurs in stream channels. More efficient designs may require a larger ratio of side area to bottom area and that maintenance activities should be considered for the sides as well as the bottom of the pond.

Saturated hydraulic conductivity values estimated from measuring air conductivity and from regression equations derived from grain size parameters were compared to full-scale infiltration rates for 15 sites in western Washington. The estimated values for saturated hydraulic conductivity were up to two orders-of-magnitude larger than the full-scale infiltration rates for some sites and were two orders-of-magnitude smaller at others. These results show that infiltration rates cannot be reliability estimated on the basis of soil properties alone; information related to the hydraulic gradient is also important.

Computer models were compared to identify the flow systems for which saturated models provide reasonable approximations. The difference between saturated and unsaturated flow models was lowest in highly permeable soils and increased as the hydraulic conductivity of the soil decreased. The simulations suggest that steady-state infiltration rates calculated with a saturated model will be 20 to 30 percent smaller than rates calculated with an unsaturated model for the range of hydraulic conductivities typically found beneath Western Washington infiltration ponds. A comparison of steady-state and transient simulations showed that the steady-state assumption may significantly underestimate infiltration rates.

17. KEY WORDS	18. DISTRIBUTION STATEMENT
Stormwater infiltration facilities, infiltration rates, hydraulic conductivity estimates, full-scale infiltration tests, stormwater infiltration design, numerical simulations	No restrictions. This document is available to the public through the National Technical Information Service, Springfield, VA 22616

19. SECURITY CLASSIF. (of this report)	20. SECURITY CLASSIF. (of this page)	21. NO. OF PAGES	22. PRICE
None	None		

DISCLAIMER

The contents of this report reflect the views of the author, who is responsible for the facts and the accuracy of the data presented herein. The contents do not necessarily reflect the official views or policies of the Washington State Transportation Commission, Department of Transportation, or the Federal Highway Administration. This report does not constitute a standard, specification, or regulation.

TABLE OF CONTENTS

TABLES

FIGURES

APPENDICES

EXECUTIVE SUMMARY

E.1 INTRODUCTION

Storm water infiltration facilities are used to reduce the hydrologic impacts of residential and commercial development. These infiltration facilities - which may include ponds, dry wells, infiltration galleries, and swales – are designed to capture and retain runoff and allow it to infiltrate rather than to discharge directly to surface water. The design of infiltration facilities is particularly challenging because of the large uncertainties associated with predictions of both short-term and long-term infiltration rates. These uncertainties in infiltration rates translate into uncertainties in the area and volume that are required for infiltration ponds. The overall objective of the studies described in this report was to provide recommendations for improving approaches used to design infiltration facilities, with particular emphasis on infiltration ponds. These studies involved two main components: a data-collection component and a numerical-modeling component.

E.1.1 Data-collection component

The primary objective of the data-collection component was to investigate the relationship between field-measured infiltration rates and estimates of saturated hydraulic conductivity. The data-collection component involved compiling existing data on field-scale infiltration rates from previous studies. Field-scale infiltration rates were also measured at selected ponds in western Washington. These field-measured infiltration rates were then compared to estimates of hydraulic conductivity obtained from soil samples collected in the field. The hydraulic conductivity estimates were based on soil gradation analyses and air conductivity tests. The goal was to evaluate how the hydraulic conductivity of near-surface soils compares to field-scale values of infiltration rates. The description of the data collection component is derived from Butchart (2001) and is included in sections 2, 3, and 4.

E.1.2 Numerical-modeling component

The primary objectives of the numerical-modeling component were to compare different modeling approaches, to quantify the sensitivity in the overall function of infiltration ponds to different input parameters, and to develop recommendations for site characterization and design alternatives for these facilities. Models that simulate both saturated and unsaturated flow were compared with models that consider only saturated flow to identify those flow systems for which saturated models provide reasonable approximations. Both steady-state and transient simulations were developed and compared. The models were used to evaluate the sensitivity of infiltration rates to subsurface stratigraphy, depth to water table, and pond geometry. The models were also used to illustrate the importance of hydraulic gradient in estimating infiltration rates from these facilities. The description of the numerical-modeling component is derived from Stolar (2001) and is included in sections 5 and 6.

E.2 SUMMARY OF CONCLUSIONS AND DESIGN RECOMMENDATIONS

The following conclusions and design recommendations can be developed from the results of the studies described in this report.

E.2.1. Effects of hydraulic gradient

- Short-term infiltration tests will tend to over-estimate long-term infiltration rates. The initial infiltration rate is significantly larger than the saturated hydraulic conductivity because the hydraulic gradient term is larger than one. As more water infiltrates, the gradient approaches a value of one and the infiltration rate approaches the saturated hydraulic conductivity.
- If recharge or infiltration is sufficient to cause the wetting front to reach a regional or perched water table, the hydraulic gradient may drop to a value significantly less than one and the infiltration rate may be much less than the saturated hydraulic conductivity. This is a very important concept and one that is overlooked in design approaches in which infiltration rates are estimated solely on the basis of soil types or saturated hydraulic conductivity estimates.

- The results of computer simulations demonstrate that, in highly permeable soils, assuming a hydraulic gradient of one is not a conservative estimate. Conversely, in low permeable soils, assuming a hydraulic gradient of one may be conservative.

E.2.2 Regressions for saturated hydraulic conductivity

- An equation was developed to give estimates of hydraulic conductivity based on data that are readily available from grain size analyses. For the set of soils used in this study, the equation was shown to result in significantly less error than the typically-used Hazen equation. This equation should be considered an alternative for the Hazen equation.

E.2.3 Full-scale infiltration tests

- Full-scale infiltration tests conducted at four sites in western Washington showed that the infiltration rate increases with time during the filling portion of the test. After the discharge to the pond is stopped, the infiltration rate quickly decreases to a rate that may be several times smaller than the initial rate. The rapid increase in infiltration during the filling portion of the test may be caused in part by lateral flow along the sides of the ponds. This is similar to "bank storage" that occurs in stream channels. As the water level in the pond increases, flow is induced horizontally into the banks of the pond. This infiltration is in addition to the infiltration that occurs along the pond bottom. Once the water level in the pond begins to decrease, the horizontal flow is reversed and water drains into the pond along the sides and out of the pond along the bottom. This inflow, which reduces the net infiltration rate, decreases with time.
- Saturated hydraulic conductivity values estimated from measuring air conductivity and from regression equations derived from grain size parameters were compared to full-scale infiltration rates performed during this study and given in literature. The estimated saturated hydraulic conductivity values were up to two orders-of-magnitude larger that the full-scale infiltration rates for some sites and were two orders-of-magnitude smaller in other cases. This reinforces that grain size texture alone does not include site-specific characteristics that may affect infiltration rate

E.2.4 Comparison of modeling approaches

- Results from a steady-state saturated flow model were compared to results from a transient unsaturated model to evaluate errors that are introduced when the simplified model is used to simulate flow from infiltration ponds. These results show that the steady-state assumption may significantly under-estimate infiltration rates and that the amount of this under-estimation is dependent upon site-specific hydrologic information.
- Computer simulations were used to quantify the difference in estimated infiltration rates that occur when using a saturated flow model versus an unsaturated flow model. The difference between the saturated and unsaturated flow models is lowest in highly permeable soils and increases as the hydraulic conductivity of the soil is reduced. The modeling results suggest that the error in the final steady-state infiltration rate varies from 20 to 40% over a range of hydraulic conductivities typically found beneath infiltration ponds in Western Washington.

E.2.5 Design alternatives from computer simulations

- The results of computer simulations suggest the infiltration rate increases linearly as the pond becomes more elongate. The increase in the infiltration rate can be attributed to the increase in the lateral flow that occurs as the pond perimeter increases.
- If lateral flow is consistently important, more efficient designs may require a larger ratio of side area to bottom area. This design approach would necessitate maintenance for the sides as well as the bottom of the pond. If the soil on the sides and bottom are preserved with respect to vegetation and silt build-up, the horizontal as well as the vertical flow could be an effective means of infiltrating storm-water runoff into the subsurface.

1 INTRODUCTION

Storm water infiltration facilities are used to reduce the hydrologic impacts of residential and commercial development. Increased runoff caused by impervious surfaces may destabilize stream channels and may degrade or destroy fish and wildlife habitat. Impervious surfaces also prevent rain and snowmelt from seeping into the ground and recharging streams, wetlands, and aquifers (Ferguson, 1994). Infiltration facilities, such as ponds, dry wells, infiltration galleries, and swales, are designed to capture and retain runoff and allow it to infiltrate rather than to discharge directly to surface water.

Important benefits of groundwater infiltration facilities include reducing surface-runoff volume, reducing pollutant discharge, reducing thermal impacts on fisheries, increasing groundwater recharge, and augmenting low-flow stream conditions (Duchene et al., 1992).

The design of infiltration facilities is particularly challenging because of the large uncertainties associated with predictions of both short-term and long-term infiltration rates. These uncertainties in infiltration rates translate into uncertainties in the area and volume that are required for infiltration ponds. Under-sized ponds may result in flooding, while over-size ponds may be inefficient in terms of land use and expensive in terms of property acquisition.

The overall objective of the studies described in this report was to provide recommendations for improving approaches used to design infiltration facilities, with particular emphasis on infiltration ponds. These studies involved two main components: a data-collection component and a numerical-modeling component. The primary objective of the data-collection component was to investigate the relationship between field-measured infiltration rates and estimates of saturated hydraulic conductivity. The data-collection component involved compiling existing data on field-scale infiltration

rates from previous studies. Field-scale infiltration rates were also measured at selected ponds in western Washington. These field-measured infiltration rates were then compared to estimates of hydraulic conductivity obtained from soil samples collected in the field. The hydraulic conductivity estimates were based on soil gradation analyses and air conductivity tests. The goal was to evaluate how the hydraulic conductivity of near-surface soils compared to field-scale values of infiltration rates. The data collection component of this report is from Butchart (2001) and is included in sections 2, 3, and 4 of this report.

The primary objectives of the numerical-modeling component were to compare different modeling approaches, to quantify the sensitivity in the overall function of infiltration ponds to different input parameters, and to develop recommendations for site characterization of and design alternatives for these facilities. Models that simulate both saturated and unsaturated flow were compared with models that consider only saturated flow to identify those flow systems for which saturated models provide reasonable approximations. Both steady-state and transient simulations were developed and compared. The models were used to evaluate the sensitivity of infiltration rates to subsurface stratigraphy, depth to water table, and pond geometry. The models were also used to illustrate the importance of hydraulic gradient in estimating infiltration rates from these facilities. The numerical-modeling component of this report is from Stolar (2001) and is included in sections 5 and 6 of this report.

The data-collection and numerical-modeling components of this research considered various issues and aspects related to infiltration facilities. The research relates to the relative importance of soil type in controlling infiltration. It relates to the effects of hydraulic gradients and water table configuration. It considered design methodologies that are currently in practice, and it included an evaluation of the importance of lateral flow from infiltration ponds. An overview of these issues and aspects is presented below.

1.1 Quantitative Descriptions of Infiltration Processes

The design of infiltration facilities requires quantitative estimates of infiltration rates. The size and geometry of the infiltration facilities are selected by comparing infiltration rates with estimates of runoff volumes calculated for specified precipitation events. Two equations that are commonly used to describe infiltration are Darcy's Law and the Green-Ampt equation. These equations are described below as a means to illustrate the processes and parameters that control infiltration and that dictate success or failure at infiltration facilities.

1.1.1 Darcy's Law

Darcy's Law can be written in terms of infiltration rate in the following form:

$$f = \frac{Q}{A} = -K\left(\frac{dh}{dz}\right) = -Ki \tag{1.1}$$

where f is the specific discharge or infiltration rate of water through a unit cross-section of the porous material (L/t), Q is the volumetric flow rate (L^3/t), A is the cross-sectional area perpendicular to flow (L^2), K is the hydraulic conductivity (L/t), dh/dz is the hydraulic gradient (L/L), and i is a "short-hand" notation for the gradient (L/L).

Darcy's law illustrates that the two factors that control infiltration are hydraulic conductivity and hydraulic gradient. The hydraulic conductivity, K, is a particularly challenging parameter to estimate because it varies by orders-of-magnitude, depending on the geologic media or soil type (Freeze and Cherry, 1979). Additional uncertainties are introduced in unsaturated soils, where hydraulic conductivity is a function of the water saturation or moisture content.

The hydraulic head in equation 1.1 is the driving force or energy that causes water to move through the soil. This force, which is due to gravity and pressure, is composed of two components: an elevation head, z , and a pressure head, ψ:

$$h = z + \frac{P}{\rho g} = z + \psi \tag{1.2}$$

where h is the total head, z is the elevation of the point above some datum (L), P is the water pressure (M/L·t^2), ρ is the water density (M/L^3), and ψ is the pressure head. At the water table the water pressure is atmospheric (i.e., set equal to 0.0), and the hydraulic head equals the elevation. Water pressure is less than 0.0 in the unsaturated zone above the water table and is greater than 0.0 in the saturated zone below the water table. The negative water pressures in unsaturated soils are caused by capillary forces or capillary pressures (Freeze and Cherry, 1979). These capillary pressures are a function of pore size—smaller pores have greater capillary pressures (Ward and Elliot, 1995). This negative capillary pressure is also a function of soil moisture content. The capillary pressure becomes less negative as the soil moisture content increases. For unsaturated systems with capillary pressures of less than 0.0, pressure or "suction" head is defined as capillary pressure divided by the unit weight of water (Mays, 1996):

$$\psi = \frac{P_c}{\rho g} \tag{1.3}$$

where P_c is capillary pressure (M/L·t^2) and ψ is the suction head (L). Table 1.1 gives typical values for the suction head at the wetting front for various soil types.

Although Darcy's Law was originally developed to describe saturated flow, it also applies to flow in unsaturated systems (e.g., Freeze and Cherry, 1979). In unsaturated flow, the hydraulic conductivity, K, the fluid pressure, P, and the hydraulic gradient, i, are functions of the moisture content. Darcy's Law for unsaturated flow can be rewritten as:

$$f = -K(\theta) \cdot i(\theta) \tag{1.4}$$

where $K(\theta)$ is the unsaturated hydraulic conductivity [L/T], $i(\theta)$ is the head gradient for unsaturated flow, and θ is the volumetric moisture content.

1.1.2 The Green-Ampt Approximation

Darcy's Law is often used to describe infiltration in unsaturated systems through an approximation that is termed the Green-Ampt equation (e.g., Chin, 2000). The Green-Ampt equation was developed by using Darcy's Law in conjunction with a set of assumptions regarding flow field geometry and material properties. This approach assumes ponded water at the ground surface and a wetting front that extends to a depth, *L*, as shown in Figure 1.1. The wetting front is assumed to move downward as a sharp interface. The soil is assumed to be saturated above the wetting front (the water content is assumed equal to the porosity). The water content below the wetting front is assumed to be equal to some lower initial value. The rate of infiltration is approximated by the following expression:

$$f(t) = K_{sat}\left[\frac{H_o + L + h_{wf}}{L}\right] \tag{1.5}$$

where

f(t) = the infiltration rate at time t (L/t),

K_{sat} = saturated hydraulic conductivity (L/t),

H_o = depth of water in the pond or infiltration facility (L),

L = depth of the wetting front below the bottom of the pond (L), and

h_{wf} = average capillary head at the wetting front (L). Approximately equal to the air entry pressure or bubbling pressure.

Equation (1.5) can be solved to estimate infiltration rate as a function of time (e.g., Salvucci and Entekhabi, 1994). Table 1.2 summarizes the values for input variables that were used to compare infiltration rates for different soil types. These values were chosen on the basis of averages reported by Carsel and Parrish (1988) for these soil types. The depth of water in the infiltration facility, H_o, is assumed to be small in these calculations. The general shape of the infiltration curve that derived from Equation 1.5 is shown in Figure 1.2 for a "loamy sand" soil type. Curves for other soil types will have similar shapes, but with different infiltration rates at steady-state and different time periods required to achieve these steady-state rates. The initial infiltration rates are higher than the saturated hydraulic conductivity because of the relatively high gradients

when the wetting front is shallow (L in equation (1.5) is small). As the depth of the wetting front increases, the gradient decreases and the infiltration rate approaches the saturated hydraulic conductivity, K_{sat}. Table 1.2 summarizes the results for three different soil types that are often associated with infiltration facilities.

The results presented in Figure 1.2 and Table 1.3 have important implications for the design of infiltration facilities. These results show that short-term infiltration tests will tend to over-estimate long-term infiltration rates. These results also illustrate the importance of the hydraulic gradient term in controlling infiltration rates. The initial infiltration rate is significantly larger than the saturated hydraulic conductivity because the gradient term is larger than 1.0. As more water infiltrates, the gradient decreases and approaches a value of 1.0.

1.1.3 Impact of Regional or Perched Water Tables

Note that once the wetting front reaches a regional or perched water table, the Green-Ampt approximation is no longer valid. Under these conditions, the hydraulic gradient may drop to a value significantly less than 1.0, and the infiltration rate may be much less than the saturated hydraulic conductivity. This is a very important concept and one that is overlooked in design approaches in which infiltration rates are estimated solely on the basis of soil types or saturated hydraulic conductivity estimates.

Figure 1.3 illustrates a flow system near an infiltration pond in which the wetting front has reached the water table. The soils beneath and adjacent to the pond are saturated with water, and the water table slopes away from the pond. The infiltration rate under these conditions is still described with Darcy's Law (Equation 1.1), but the gradient term is more difficult to quantify or predict. This gradient, which is related to the slope of the water table near the pond, will depend upon the soil type, the depth to the water table, the geometry of the pond, and the depth of water in the pond. Under most conditions this gradient will be significantly less than 1.0, and the infiltration rate will be smaller than the saturated hydraulic conductivity, as shown in Darcy's Law.

1.1.4 Infiltration in Layered Systems

The previous discussions related to Darcy's Law and the Green Ampt approximation have focused on homogeneous soils. Infiltration into layered systems can also be described with Darcy's law, with hydraulic conductivity and gradients changing from layer to layer. For infiltration at a site with a higher conductivity layer overlaying a layer of lower conductivity, the top layer initially controls the infiltration rate. When the wetting front reaches the less conductive layer, the infiltration rate will drop, and the rate of infiltration will be controlled by the less conductive layer (Chow et al., 1988). After a sufficient time, a positive pressure head in the form of a perched water table (mound) can develop above the lower conductivity soil. Ponding, or mounding, results in a head gradient of less than 1.0, much the same way as when the wetting front reaches the water table. The shape and growth of the mound depends on the infiltration rate, the dimensions of the infiltration area, and the hydraulic characteristics of the soil (Ferguson, 1994).

1.2 Infiltration Rates from Design Manuals for Storm Water Infiltration Facilities

Two widely recognized references are used to design of storm water infiltration facilities in Washington State. One is the Washington Department of Ecology's *Stormwater Management Manual for Western Washington* (WDOE, 2001), and the second is the *King County Surface Water Design Manual* (King County, 1998).

The Department of Ecology manual recommends three methods for estimating long-term infiltration rates. The first method is based on a correlation between USDA soil texture and infiltration rates for homogeneous soils. The infiltration rates that the Department of Ecology has recommended, which are reproduced in Table 1.2, are based on a correlation developed by Rawls, et al. (1982) with minor changes based on the Water Environment Federation (1998). The manual indicates that infiltration rates provided through this correlation represent "short-term conservative rates for homogeneous soils." These estimates do not consider the effects of long-term clogging due to siltation and biomass buildup in the infiltration facility. The Department of Ecology recommends that the short-term infiltration rates be reduced by dividing them by

a correction factor of 2 to 4, depending on the soil textural classification. These correction factors, which are included in Table 1.2, can be reduced if approved by the local jurisdiction for sites with little soil variability, sites that will have a high degree of long-term facility maintenance, or sites where pretreatment will be employed to reduce the total suspended solids entering the infiltration facility. The WDOE manual specifies that correction factors must be greater than or equal to 2.0 and that factors higher than those included in Table 1.2 should be considered "for situations where long-term maintenance will be difficult to implement, where little or no pretreatment is anticipated, or where site conditions are highly variable or uncertain."

The second method for estimating infiltration rates included in the Department of Ecology manual is based on soil gradation parameters measured with the ASTM soil gradation procedure. These estimates are based on studies that compare infiltration measurements from full-scale infiltration facilities to soil gradation data developed with the ASTM procedure (ASTM D422). The recommended infiltration rates are included in Table 1.3. These estimates are described as "long-term rates" that represent average conditions regarding site variability, the degree of long-term maintenance, and pretreatment for TSS control. The Ecology manual indicates these long-term infiltration rates may need to be decreased if the site is highly variable, or if maintenance and influent characteristics are not well controlled. The manual also notes that the data that form the basis for the estimates in Table 1.3 were from soils that would be classified as sands or sandy gravels and that no data were available for finer soils. The manual recommends that these vales not be for soils with a d_{10} size (10 percent passing the size listed) of less than 0.05 mm (U.S. Standard Sieve). The estimated infiltration rates included in tables 1.2 and 1.3 apply to homogeneous soils. If more than one soil unit is encountered beneath the facility within a depth of 6 feet (2 meters) or 2.5 times the proposed maximum water design depth, the Ecology manual requires that the lowest infiltration rate determined from each of the soil units be used as the representative site infiltration rate.

The third approach recommended in the Department of Ecology manual is to use large-scale in-situ infiltration measurements by using a procedure termed the Pilot Infiltration Test (PIT). For this test, water is added to a pond or an excavated pit at a rate that will maintain the water level between 3 and 4 feet (1 meter) above the bottom of the pond or pit. The instantaneous flow rate and cumulative volume required to maintain the constant water level are recorded at 15- to 30-minute intervals. Water is added to the pit for a recommended minimum of 17 hours. The infiltration rate is recorded both as the pond is filled and then as it empties. Estimates from these in-situ tests are also considered short-term rates that must be reduced through correction factors to account for site variability and number of tests conducted, degree of long-term maintenance and influent pretreatment/control, and potential for long-term clogging due to siltation and bio-buildup. The typical range of correction factors to account for these issues is summarized in Table 1.4.

The second major reference for storm water management in the state of Washington is the *King County Surface Water Design Manual* (1998). Procedures to estimate the infiltration rate outlined in the King County manual include the EPA falling-head percolation test procedure and the double-ring infiltrometer test. The double-ring infiltrometer test is used more widely than the EPA falling-head procedure. In the double ring infiltrometer test, a cylinder (typically less than 3 feet (1 meter) in diameter) is inserted into the ground. A second, larger-diameter cylinder is then inserted around the first, inner cylinder. Water is poured into the inner cylinder. The water level is held constant by continually adding water from a graduated cylinder. The quantity of water added during a specified time period is recorded, and the infiltration rate versus time can then be calculated. The double-ring system is intended to measure only vertical infiltration by reducing the effects of lateral flow. The outer ring provides a buffer zone, eliminating lateral flow within the inner infiltrometer. The infiltration rate is measured with the inner ring and results in a more accurate vertical rate (Ferguson, 1994).

The King County manual suggests that at least three tests should be performed for each proposed infiltration facility site. Correction factors to be applied to measured

infiltration rates are included in the King County manual. These correction factors account for uncertainties in testing, depth to the water table or impervious strata, infiltration receptor geometry, and long-term reductions in permeability due to bio-buildup and accumulation of fines. Table 1.6 provides the correction factors that are multiplied by the measured infiltration rate to determine a design infiltration rate. The factor $F_{testing}$ refers to uncertainties in small-scale testing; $F_{geometry}$ refers to infiltration receptor geometry; and $F_{plugging}$ refers to biological accumulation on the pond bottom.

1.3 Other Criteria and Considerations for Infiltration Ponds

1.3.1 Siting Criteria and Considerations

Different regulatory organizations have attempted to improve the likelihood of an infiltration pond functioning properly by developing criteria that must be met before a pond location is selected. The common thread in these criteria is that infiltration ponds function best when the soil is highly permeable, the slope of the infiltration surface is low, and the pond is high above the water table. Specifically, the Department of Ecology requires the soil infiltration rate to be at least 0.5 in/hr (1.3 cm/hr), the slope to be no greater than 15 percent, and the bottom of an infiltration facility to be a minimum of 5 feet (1.5 meters) from the seasonal high water mark (WDOE, 2001). The provision for the minimum distance to the water table is in place as an effort to avoid the low hydraulic gradients that develop when the wetting front from the infiltration pond reaches the water table. These types of requirements are similar to those used in other states and jurisdictions. For example, the design guidelines prepared by the State of Maryland (2000) state that the bottom must be 4 feet (1.2 meters) from the water table, the infiltration rate may not be lower than 0.52 in/hr (1.3 cm/hr), and the slope must be less than 20 percent.

The approach used to site infiltration ponds developed by the Swedish Association of Water and Sewage Works is based on a point system (Stahre and Urbonas, 1990). Points are assigned to potential sites according to the ratio between the tributary connected impervious area and the infiltration area, the nature of the surface and underlying soils, the slope of the infiltration surface, the vegetation cover, and the degree

of traffic on the surface. Sites with high scores are considered suitable, whereas sites that score low are not considered.

1.3.2 Clogging

The formation of a clogging layer on the surface of infiltration ponds is a common occurrence along the wetted perimeter. Clogging may be caused by the accumulation of silt, clay, or other fine material that was suspended in the water entering the recharge basin, by algae growth on the bottom or in the water, by precipitation of calcium carbonate in the water due to increases in pH caused by algae activity, and by biological activity on the wetted perimeter (Bouwer and Rice, 1989). Duchene et al. (1992) used a two-dimensional unsaturated flow model to investigate the influence of clogging on the performance of an infiltration trench. They found that placing a 2 inch-thick (5 cm) layer of soil with a low hydraulic conductivity at the bottom of the trench reduced the infiltration rate by 20 percent, 7 percent, and 4 percent for depths of water in the trench of 0.8 ft (0.25 m), 1.6 ft (0.50 m), and 3.3 ft (1.0 m), respectively. Field observations have shown that the formation of a relatively thin clogging layer on the surface of the soils may reduce infiltration rates significantly more than what was shown with the numerical model (Schuh, 1990). These reductions may be due to pore clogging that occurs more deeply than the 2 inches assumed in the numerical model.

1.3.3 Water Table Elevation

Traditional methods of measuring infiltration rates either have no relationship to the water table elevation or do not consider water level fluctuations over time periods longer than several days. Because water table elevations change throughout the year, it is important to understand the effect that these variations have on the infiltration rate. While infiltration ponds are known to function best when they are well above the water table, relatively little quantitative analysis has been conducted to determine how pond performance is affected by fluctuations in the water table.

1.3.4 Lateral Flow

Currently, information in the literature conflicts regarding what area to use as the available infiltration area in the Darcy's law design approach. The design guidelines prepared by the State of Maryland (1984) suggest using only the bottom area of an infiltration pond when calculating the infiltration rate. Conversely, Stahre and Urbanas (1990) suggest using only the sides of the pond, since the bottom will most likely become clogged over time. Duchene et al. (1992) estimated the percentage of infiltration that occurred through the sides of an infiltration trench and concluded that approximately three-quarters of the water flows through the bottom of the trench. The amount of lateral flow depends on site-specific factors such as height-area ratio of the pond and the degree of anisotropy in the soils around the pond.

Table 1.1—Wetting front suction head for different soil textures (after Mays, 1996).

Soil Class	Wetting front soil suction head, ψ, inches (cm)
Sand	2 inches (5 cm)
Loamy sand	2.5 (6.3)
Sandy loam	4 (10)
Loam	3.5 (8.9)
Silt loam	6.5 (16.5m)

Table 1.2—Parameters used to estimate infiltration rates shown in Figure 1.2

	Sand	Loamy Sand	Sandy Loam
Input parameters			
Capillary head at wetting front, inches (cm)	1.6 (4.1)	2.3 (5.8)	4.4 (11.2)
Saturated hydraulic Conductivity, in./min (cm/min)	0.2 (0.49)	0.1 (0.24)	0.03 (0.07)
Output description			
Time at which infiltration rate equals 1.5 times the saturated hydraulic conductivity (hrs)	0.05	0.1	0.9
Time at which infiltration rate equals 1.1 times the saturated hydraulic conductivity (hrs)	0.4	1.1	8.5

Table 1.3—Recommended infiltration rates based on USDA soil textural classification (WDOE, 2001)

	Short-Term Infiltration Rate, in/hr (cm/hr)	Correction Factor	Estimated Long-Term Infiltration (Design) Rate, in/hr (cm/hr)
Clean sandy gravels and gravelly sands (i.e., 90% of the total soil sample is retained in the #10 sieve)	20 (50)	2 (5)	10 (25)
Sand	8 (20)	4 (10)	2 (5)
Loamy Sand	2 (5)	4 (10)	0.5 (1.3)
Sandy Loam	1 (2.5)	4 (10)	0.25 (0.64)
Loam	0.5 (1.3)	4 (10)	0.13 (0.33)

Table 1.4—Recommended infiltration rates based on ASTM gradation testing (WDOE, 2001)

D10 Size from ASTM D422 Soil Gradation Test mm	**Estimated Long-Term (Design) Infiltration Rate, in/hr (cm/hr)**
>0.4	9 (23)
0.3	6.5 (16.5)
0.2	3.5 (8.9)
0.1	2.0 (5)
0.05	0.8 (2)

Table 1.5—Correction factors to be used with in-situ infiltration measurements to estimate long-term design infiltration rates (WDOE, 2001).

Issue	**Partial Correction Factor**
Site variability and number of locations tested	CFv = 1.5 to 6
Degree of long-term maintenance to prevent siltation and bio-buildup	CFm = 2 to 6
Degree of influent control to prevent siltation and bio-buildup	CFi = 2 to 6
Total correction factor	CF = CFv + CFm + CFi

Table 1.6—Correction factors from the *King County Surface Water Design Manual* (King County, 1998).

$\mathbf{F_{testing}}$	$\mathbf{F_{geometry}}$	$\mathbf{F_{plugging}}$
0.30 - 0.50	0.25 - 1.0	0.7 for loams and sandy loams
		0.8 for fine sands and loamy sands
		0.9 for medium sands
		1.0 for coarse sands or cobbles

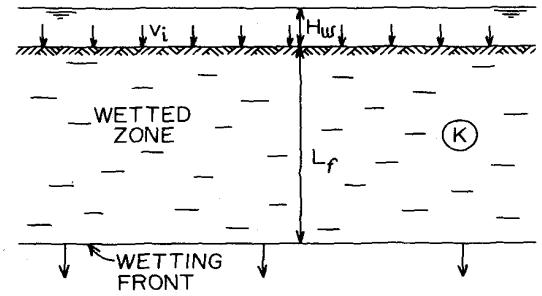

Figure 1.1—Moisture zones during infiltration (Bouwer, 1978).

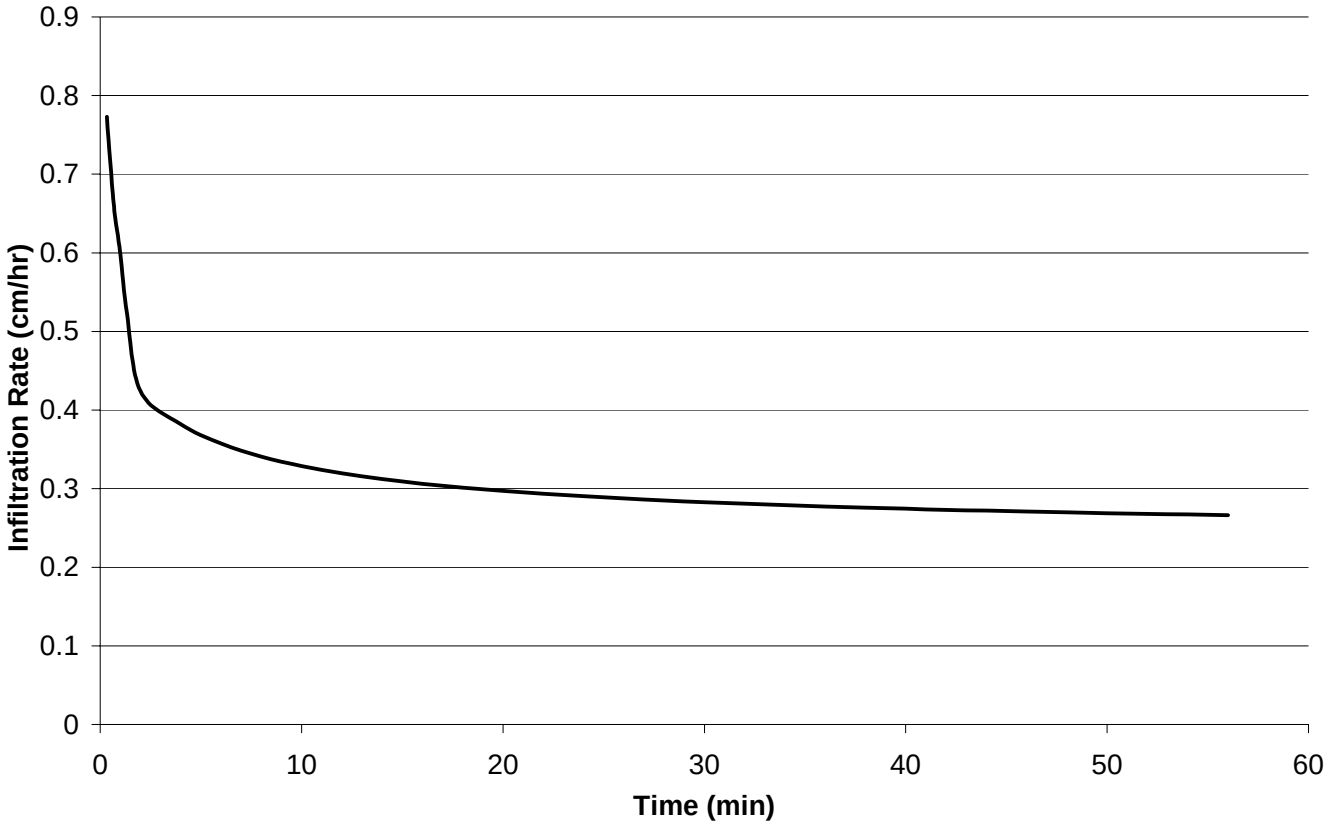

Figure 1.2 —Estimated infiltration rate for loamy sand using the Green and Ampt equation.

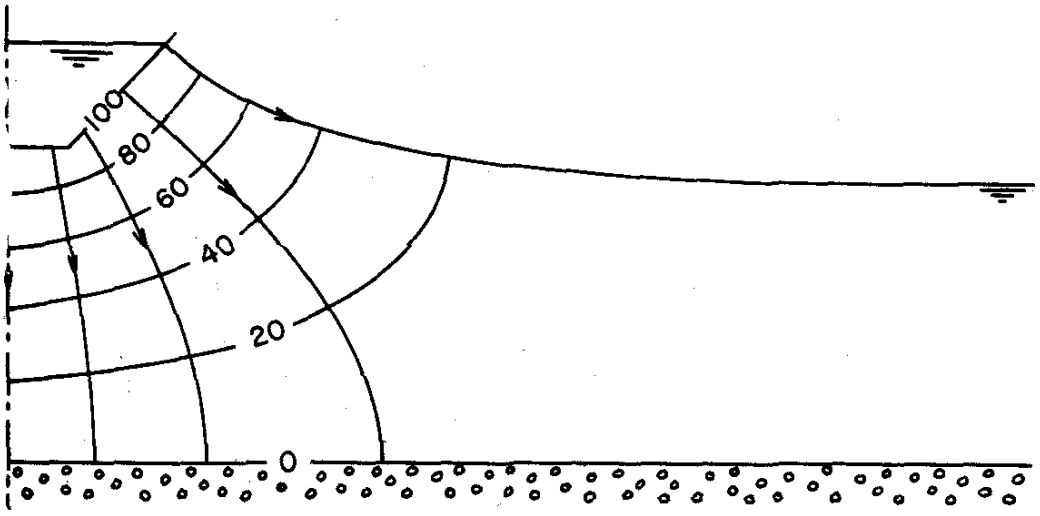

Figure 1.3—Flow system for a wetting front that has reached the water table (Bouwer, 1978).

2 ESTIMATING HYDRAULIC CONDUCTIVITY FROM AIR FLOW EXPERIMENTS

One of the objectives of this study was to develop estimates of the saturated hydraulic conductivity of disturbed soil samples obtained from infiltration ponds. Two approaches were used: one approach was based on measuring air flow in synthetic and natural soil samples, and the second approach was based on soil texture information obtained from grain size curves. Both approaches are relatively simple and do not require sophisticated laboratory techniques or equipment. The intent is to develop an approach for estimating saturated hydraulic conductivity that is more sophisticated and site-specific than the approach based on USDA soil classifications that was described in Chapter 1, but that is also more simple than traditional laboratory methods. The air-flow approach is described in this chapter, and the soil-texture approach is described in Chapter 3.

Finding a relationship between air conductivity and saturated hydraulic conductivity is beneficial because air conductivity can be measured rapidly and with fewer practical problems than saturated hydraulic conductivity (Loll et al., 1999). The approach introduced in this study requires relatively few technical laboratory testing procedures and can be done in minutes for each soil sample.

2.1 Relationship Between Air Conductivity and Hydraulic Conductivity

The approach for estimating saturated hydraulic conductivity using air-flow experiments is based on Darcy's law. Although originally developed for water as the fluid, Darcy's law has been shown to be valid for air flow in most soils (Massmann, 1989). The exceptions are relatively fine-grained soils, such as clays, and systems with very high flow rates. For the pressures and soil types that will be used in this study, the flow of air through soils can be described by the following form of Darcy's law:

$$Q_{air} = -K_{air}\left(\frac{dh_{air}}{dz}\right)A \qquad (2.1)$$

where Q_{air} is the volumetric flow rate for the air (L^3/t), dh_{air}/dz is the head gradient across the permeameter (L/L), and K_{air} is the conductivity of the sample for air (L/t). The subscript *"air"* is used to denote that air is the mobile fluid in this experiment.

The pneumatic head, h_{air}, is a measure of the mechanical energy per unit mass of air. For the relatively low pressures used in the laboratory experiments in this study, the air can be treated as an incompressible fluid (Massmann, 1989), and the fluid head at a point is given by the following expression:

$$h_{air} = z + \frac{P_{air}}{\rho_{air} g} \qquad (2.2)$$

where P_{air} is the air pressure ($M/L \cdot t^2$) and ρ_{air} is the air density (M/L^3).

The air conductivity, K_{air}, is given by the following expression (Massmann, 1989):

$$K_{air} = \frac{k \rho_{air} g}{\mu_{air}} \qquad (2.3)$$

where k is permeability (L^2), ρ_{air} is the air density (M/L^3), and μ_{air} is the dynamic viscosity of the air ($M/L \cdot t$).

The permeability, k, that is measured with air-flow experiments with a dry soil is assumed to be nearly equal to the permeability that is measured with water-flow experiments with saturated soil. Differences in permeability from gas-flow experiments using dry soils and water-flow experiments using the same soils that are saturated with water may arise because of gas slippage along the solid boundaries. For most soils at infiltration sites, the permeability for a dry soil measured with air flow will be slightly larger than the permeability for a saturated soil measured with water flow. This

phenomena is known as the "Klinkenberg effect" (Corey, 1986). The differences in permeability estimates are generally small (less than 10%) for coarse-grained soils such as silts, sands, and gravels (Massmann, 1989). Other factors that may affect the relationship between the permeability that is measured with air-flow experiments and to the permeability that is measured with water-flow experiments are discussed in Section 2.5.

Equation 2.3 can be combined with a similar expression for hydraulic conductivity (e.g., Freeze and Cherry, 1979) to give hydraulic conductivity as a function of air conductivity:

$$K_s = \frac{k\rho_w g}{\mu_w} = \frac{\mu_{air}\rho_w}{\mu_w \rho_{air}} K_{air} = C_f K_{air} \qquad (2.4)$$

The correction factor C_f is dependent upon the viscosity and density of air and water. Each of these variables is in turn dependent upon temperature, as summarized in Table 2.1. If the air conductivity is measured at laboratory temperatures, and if the hydraulic conductivity is also for laboratory temperatures, then the correction factor is equal to 15. This is based on an assumed laboratory temperature of 20° C. If the air conductivity is measured at laboratory temperatures, and if the hydraulic conductivity is for field temperatures, then the correction factor is approximately 11.5. This is based on an assumed field temperature of 10° C.

2.2 Measuring Air Conductivity

The conventional method for measuring the air conductivity of porous media involves continuous-flow permeameters (e.g., Stonestrom and Rubin, 1989; Springer et al., 1998). Air flow is induced through a sample with a mechanical air pump or a source of compressed air. The pressure drop across the sample is measured with pressure transducers or manometers, and the flow rate is measured with rotameters or soap-film flow meters. More recently, air permeameters have also been developed with pistons and

syringes to induce air flow and photosensors to measure flow rates (e.g., Davis et al., 1994).

The stand-alone permeameter that was used in the current study is shown in Figure 2.1. This permeameter, which was developed at the University of Washington (Massmann and Johnson, 2001), is constructed with two sections of clear, rigid plastic tubing connected with a plastic fitting or coupling. The upper section of the tubing holds the soil sample, and the lower section is used as a reservoir for pressurized air. Tubes with an inside diameter of 0.5 to 4 inches (1 to 10 cm) and with upper and lower sections each approximately 12 to 20 inches (30 to 50 cm) long work well for fine to medium sands. Longer sections may be required for more permeable materials. A nylon or steel mesh is glued to the bottom of the upper section to hold the sample.

The air permeability or conductivity is measured by first placing a sample of dry soil in the upper section of the permeameter. The top of the permeameter is sealed, and the lower section is submerged in a container of water. The seal can be made with a cork or rubber stopper or simply with a thumb. Water will enter the bottom section of the permeameter and will pressurize the air. Because the air pressure in the lower section is greater than atmospheric pressure, air will flow through the sand when the top of the permeameter is opened. As the air flows upward through the permeameter, the air pressure in the lower section decreases, and H, the distance from the water level in the lower section of the permeameter to the water level in the water container, becomes smaller. If the diameter of the water reservoir is large relative to the diameter of the permeameter, the rate of flow through the permeameter, Q_{air}, is directly proportional to the rate of change in H.

The air conductivity can be estimated by measuring how quickly the water level in the lower section raises. The following expression gives this relationship (Massmann and Johnson, 2001):

$$K_{air} = \left(\frac{\rho_{air}}{\rho_w} \right) \frac{L}{(t_1 - t_0)} \ln \left(\frac{\frac{\rho_w}{\rho_{air}} H_o + L}{\frac{\rho_w}{\rho_{air}} H_1 + L} \right) \qquad (2.5)$$

where H_o and H_1 are measured at times t_0 and t_1 (Massmann and Johnson, 2001). All values on the right side of the equation (2.5) are either known or can be measured directly with the permeameter. In most cases, the first term on the right side of equation (2.5) will be large relative to L. In these cases, equation (2.5) can be reduced to the following:

$$K_{air} = \left(\frac{\rho_{air}}{\rho_w} \right) \frac{L}{(t_1 - t_0)} \ln \left(\frac{H_o}{H_1} \right) \qquad (2.6)$$

2.3 Sensitivity to Permeameter Scale

Three different sizes of air permeameters were used to evaluate the sensitivity of the results to the scale of the permeameter. The inside diameters of the three permeameters were 0.5 inch, 2.5 inch, and 4.0 inch (1.25 cm, 6.4 cm, and 10.2 cm), and the lengths of the permeameters were 12 inch, 18 inch, and 24 inch ((31 cm, 46 cm, and 61 cm), respectively. The soil samples used in these tests comprised #50 and #125 silica sand. Grain size curves for these soils are included in tables C2 and C3 in Appendix C.

The results for the two larger-diameter permeameters, which are included in Table 2.2, were reasonably consistent, and differences were likely due to differences in sample porosity. However, the smallest permeameter tended to give air conductivity values higher than those obtained with the larger permeameters. This can be seen by comparing the results from the #50 samples in Table 2.2. For #50 samples with similar porosity, the air conductivity estimated with the smallest permeameter was twice as large as the air conductivity estimated using the larger permeameter. Similarly, this can be seen in comparing the first two trials of the #50 samples for the smallest permeameter (the ones with the lowest porosity) with the two trials for the medium and large permeameter. The

lower porosity samples in the small permeameter produced estimates of air conductivity similar to those from the higher porosity samples for the medium and large permeameters. One explanation for the higher values with the smaller permeameter is leakage along the side walls of the permeameter. The side wall area is proportional to the permeameter diameter while the resistance caused by the soil is proportional to the diameter squared. For small diameter samples, the side wall area becomes larger relative to the soil area.

Reproducibility was also investigated for each permeameter. The difference between estimates for samples with approximately the same porosity for the #50 and #125 soils was generally on the order of 30 percent or less. These differences were smaller for the larger permeameters. This magnitude of error may be acceptable for many applications, especially at sites with significant spatial heterogeneity.

The advantages of a larger permeameter include reduced edge effects relative to the soil sample, and the ability for larger soil particles to fit into the column without taking up the whole cross-sectional area of the column. A larger permeameter also allows for larger volumes of soil samples, which achieve more precise results for more permeable and non-uniform soils. The 2.5-inch (6.4-cm) diameter permeameter was chosen for the laboratory tests because it was easier to manage than the 4-inch (10.2-cm) diameter permeameter, and the differences in measured results between the two permeameters were within an acceptable range.

2.4 Measuring Air Conductivity for Synthetic Soils

The objective of measuring air conductivity for synthetic soils was to develop regression equations to estimate saturated hydraulic conductivity, K_s, from grain-size analyses. The measured air conductivity values were converted to saturated water conductivity, and a regression equation was derived to estimate saturated hydraulic conductivity using selected grain-size parameters of the synthetic soil samples. The expectation was to use the regression equation to estimate K_s for field soil samples.

Four different soil textures were selected to encompass a wide range of saturated hydraulic conductivity values. The soil textures included #16 silica sand, #50 silica sand, #125 silica sand, and rock flour (pulverized sand that has the consistency of flour). Mixing different portions of these four soil types created a series of soil textures. The air permeameter was then used to estimate hydraulic conductivity for each different soil sample using a C_f of 15. This is the appropriate correction factor if the air conductivity is measured at laboratory temperatures, and if the hydraulic conductivity is also for laboratory temperatures, with assumed laboratory temperature of 20° C. The mixtures used to develop the different soil samples, the measured K_{air} values, and the estimated saturated hydraulic conductivity are given in Appendix A. These hydraulic conductivity values were used to develop regression equations relating soil texture information and hydraulic conductivity. Limitations and errors associated with this approach are discussed below in Sections 2.5 and 2.6.

Equation 2.6 was used to calculate K_{air}. H_0 was measured from a ruler that was taped to the lower cylinder. When the seal was released from the upper cylinder, a stopwatch was used to record the time for the water to rise inside the lower cylinder. H_1 was measured when the timer was stopped. The length of the soil sample was recorded with a ruler.

The porosity, n, for each sample was estimated by measuring the volumes of solids and the bulk sample. Porosity was then calculated with the following expression:

$$n = \frac{V_{pores}}{V_{sample}} = \frac{V_{sample} - V_{solids}}{V_{sample}} = 1 - \frac{V_{solids}}{V_{sample}} \qquad (2.7)$$

where V_{pores} is the volume of the pore space, V_{sample} is the volume of the soil sample, and V_{solids} is the volume of the solid particles.

The volume of the soil sample, V_{sample}, was determined by multiplying the length of the soil sample by the cross-sectional area of the inside cylinder. The volume of the

solid particles, V_{solids}, was calculated by dividing the weight of the soil sample by 2.65, which is the accepted density for particles (Danielson and Sutherland, 1986).

2.5 Measuring Air Conductivity for Natural Soils

The objective of measuring air conductivity for natural soils was to derive a regression equation relating hydraulic conductivity and soil texture information that could be compared with the regressions derived for the synthetic soils.

A series of air conductivity tests was conducted on samples collected at 15 sites with infiltration ponds. Test holes to collect soil samples were drilled to depths between 10 inches (25 cm) to 70 inches (178 cm). The depths of the test holes depended upon the physical ability to reach lower depths and the soil uniformity. The shallower depths were a result of either soil conditions that prohibited deeper depths, observed uniformity of the soil column throughout and therefore the expectation that deeper depths would not provide new soil textures, or encountering of the water table. Each test hole was visually inspected for a change in soil texture. Soil samples were taken for each soil texture throughout the soil column and identified by the soil layer and depth of the layer. The samples were air dried in the laboratory and tested for air conductivity with the air permeameter. The air conductivity test was repeated for each sample until a minimum of three consistent measurements had been obtained.

Measured air conductivity and the corresponding saturated hydraulic conductivity for each measurement is given in Appendix B.

2.6 Sources of Error in Converting Air Conductivity to Hydraulic Conductivity

Estimates of hydraulic conductivity that are based on air conductivity measurements may differ from true hydraulic conductivities because of two main factors: effects of moisture content and absorption effects. The effects of moisture content may be significant if the air conductivity measurements are made on soils with moisture contents that are large enough so that the soil water blocks pores that would otherwise contribute to air flow. One of the assumptions inherent in estimating hydraulic

conductivity values from air conductivity values is that the pore structure that contributes to air flow is the same as the pore structure that contributes to water flow. For air conductivity tests that are completely dry, this is generally a very good assumption. However, if moisture is present in the samples used to estimate air conductivity, the resulting hydraulic conductivity estimate may be lower than the true hydraulic conductivity because of a reduction in pore space in the air conductivity tests. The samples used in the current study were completely dry and so these moisture effects will not be a factor.

A more important limitation inherent in the current study arises from the effects of water absorption on soil structure. Clay minerals may affect air conductivity in dry soils in ways that are different from their effects on hydraulic conductivity in saturated soils. For example, swelling of montmorillonite clays may result in large reductions in hydraulic conductivity in saturated soils. Even when only non-swelling clays are present, the absorption of water may cause disaggregation and migration of clay particles and subsequent blockage of pores. In either case, the hydraulic conductivity values estimated from air conductivities tests may be significantly larger than the true hydraulic conductivities. Correction factors based on the fraction of clay particles in a soil have been developed to account for these effects (Weeks, 1978). For the soils studied by Weeks, these correction factors, CF, have the following form:

$$K_{corr} = K_{calc}(CF) = K_{calc}\left\{0.3\exp^{-5.7CMC}\right\} \qquad (2.8)$$

where K_{corr} is the corrected hydraulic conductivity, K_{calc} is the hydraulic conductivity calculated from air conductivity measurements on dry soil, and CMC is the quantity of expanding lattice clay minerals of the montmorillonite group, expressed as a decimal fraction of the total mineral content. For the soils used in the current study, the clay fraction was not expanding and CMC was assigned a value of 0.

Several studies have been published that quantify the magnitude of errors in converting air conductivity to hydraulic conductivity (Weeks, 1978; Blackwell et al.,

1990; Loll et al., 1999; Iverson et al., 2001). These studies all involve field and laboratory experiments that compared hydraulic conductivity values estimated from air conductivity tests with values estimated from field-scale recharge experiments or from laboratory-scale hydraulic conductivity tests. In all cases, the soils used in the air conductivity tests were not completely dry and so the effects of errors caused by moisture content are included in the estimates. As previously noted, these moisture effects are not a factor in the current study, in which all soils were completely dry.

Large-scale field tests of both air conductivity and hydraulic conductivity were completed by Weeks (1978). These tests showed that the estimates of hydraulic conducitivty from air conductivity measurements were generally with a factor of 2 or 3 of the value from hydraulic recharge tests. These differences were attributed to structural changes caused by wetting. For shallow layers, the values from air conductivity tests were a few times larger than the values from recharge tests. For deeper layers, where confining pressures tend to limit these structural changes, the values from air conductivity tests were very similar to the values from the recharge tests (Weeks, 1978). Weeks concludes that if the soils are structurally unaffected by wetting, the air conductivity values should give reliable estimates of hydraulic conductivity. It should again be noted that these tests were done in-situ and include effects of moisture on air conductivity values.

The study by Loll et al. (1999) provides one of the more comprehensive datasets comparing hydraulic conductivity estimates from air conductivity with hydraulic conductivity estimates from hydraulic conductivity tests. Results from both hydraulic conductivity and air conductivity tests are report for 1,614 undisturbed, 100 cm^3 core samples. These samples represented soils with hydraulic conductivity values that ranged from 3 $x10^{-6}$ cm/s (0.004 in/hour) to $1x10^{-1}$ cm/s (140 in/hour) with a mean value of $8x10^{-5}$ cm/s (0.1 in/hour). The air conductivity tests were completed on moist soils that were drained with a suction equal to –100 cm of water. For the complete dataset, the general accuracy of the hydraulic conductivity values from air conductivity tests was better than +/- 0.7 orders of magnitude (95% prediction interval). There was more

scatter (larger errors) for soils with hydraulic conductivity values less than 0.0001 cm/s or 0.16 in/hr.

In a follow-up study, Iversen et al. (2001) evaluated air and hydraulic conductivity values in textured soils using two measurement scales. One set of measurements were made on samples with a volume of 100 cm^3 set and a second set was measured on samples with a volume of 6,280 cm^3. In both sets, the samples were described as "undisturbed." Tests were run on a total of 224 samples of "structured loamy soils" and "sandy soils." The samples used for the air conductivity tests were drained using –50 cm of suction and the hydraulic conductivity tests were done on saturated samples. The 95% prediction interval was +/- 1.7 orders of magnitude for the structured loamy samples and was +/- 0.4 orders of magnitude for the sandy soils.

Blackwell et al. (1990) compares hydraulic conductivity estimates from air conductivity and hydraulic conductivity tests for samples of loam, silty loam, and clay loam soils with hydraulic conductivity values ranging from $3x10^{-4}$ to $3x10^{-1}$ cm/s (0.4 to 400 in/hr.) Based on measurements from 60 samples, they report a linear correlation between estimated values with a correlation coefficient (r^2) of 0.955.

These studies suggest that the hydraulic conductivity estimates from air conductivity tests are likely within +/- 0.5 orders of magnitude of values that would have been obtained with hydraulic conductivity tests. For higher permeability sands, the errors may be considerably lower than this while for samples with significant clay fractions, the errors may be considerably larger. An error with an order of magnitude of 0.5 corresponds to a factor of approximately 3. Given the magnitude of errors inherent in sampling errors, laboratory hydraulic conductivity tests, and soil heterogeneity, this factor of 3 may be acceptable.

2.7 Limitations of the Approach

There are limitations in using the air permeameter with coarse-textured soils. When the measured air conductivity is larger than approximately 0.04 inches/second (0.1

cm/s), accurately measuring the time to move air through the soil sample becomes difficult once the upper column seal has been released. This air conductivity value corresponds to a saturated hydraulic conductivity of 0.4 inches/second (1 cm/s), which is typical of coarse gravel.

Non-uniform soil textures within a soil layer resulted in another limitation for the air permeameter. Packing non-uniform soil sometimes resulted in large macropores or continuous air gaps within the soil sample and between the sample and the test cylinder. This can result in preferential flow paths through the column. A large diameter permeameter has the advantage of reducing this effect. The soil can be agitated in the permeameter until the "holes" are filled in with the finer soil.

Table 2.1—Density and viscosity of water and air at different temperatures (from Janna, 1993).

Temperature °C	**ρ_{water}(kg/m^3)**	**μ_{water}(kg/m·s)**	**ρ_{air}(kg/m^3)**	**μ_{air}(kg/m·s)**
10	1000	$1.3(10^{-3})$	1.25	$1.76(10^{-5})$
20	998	$1(10^{-3})$	1.2	$1.8(10^{-5})$
Temperature °F	**ρ_{water}g (lb/ft^3)**	**μ_{water} (lb$_m$/ft·s)**	**ρ_{air}g (lb/ft^3)**	**μ_{air} (lb$_m$/ft·s)**
50	62.4	$1.8(10^{-4})$	0.078	$2.43(10^{-6})$
68	62.3	$1.4(10^{-4})$	0.075	$2.5(10^{-6})$

Table 2.2—Comparison of measured air conductivity values for different size permeameters.

Synthetic Sample	**D = 0.5 inch**		**D = 2.5 inch**		**D = 4 inch**	
	K_{air} (in/s)	***porosity***	**K_{air} (in/s)**	***porosity***	**K_{air} (in/s)**	***porosity***
#16	2.3E-02					`
#50	7.9E-04	0.26	8.3E-04	0.35	7.9E-04	0.34
#50	8.3E-04	0.26	8.7E-04	0.35	9.8E-04	0.35
#50	1.4E-03	0.31				
#50	1.7E-03	0.32				
#50	1.6E-03	0.33				
#125	7.5E-05	0.37	9.8E-05	0.44	9.8E-05	0.43
#125	1.1E-04	0.37	7.1E-05	0.45	1.2E-04	0.46
#125			1.1E-04	0.45		
#125			1.2E-04	0.46		
Synthetic Sample	**D = 1.25 cm**		**D = 6.35 cm**		**D = 10.16 cm**	
	K_{air} (cm/s)	***porosity***	**K_{air} (cm/s)**	***porosity***	**K_{air} (cm/s)**	***porosity***
#16	5.8E-02					
#50	2.00E-03	0.26	2.10E-03	0.35	2.00E-03	0.34
#50	2.10E-03	0.26	2.20E-03	0.35	2.50E-03	0.35
#50	3.60E-03	0.31				
#50	4.30E-03	0.32				
#50	4.10E-03	0.33				
#125	1.90E-04	0.37	2.50E-04	0.44	2.50E-04	0.43
#125	2.70E-04	0.37	1.80E-04	0.45	3.10E-04	0.46
#125			2.80E-04	0.45		
#125			3.00E-04	0.46		

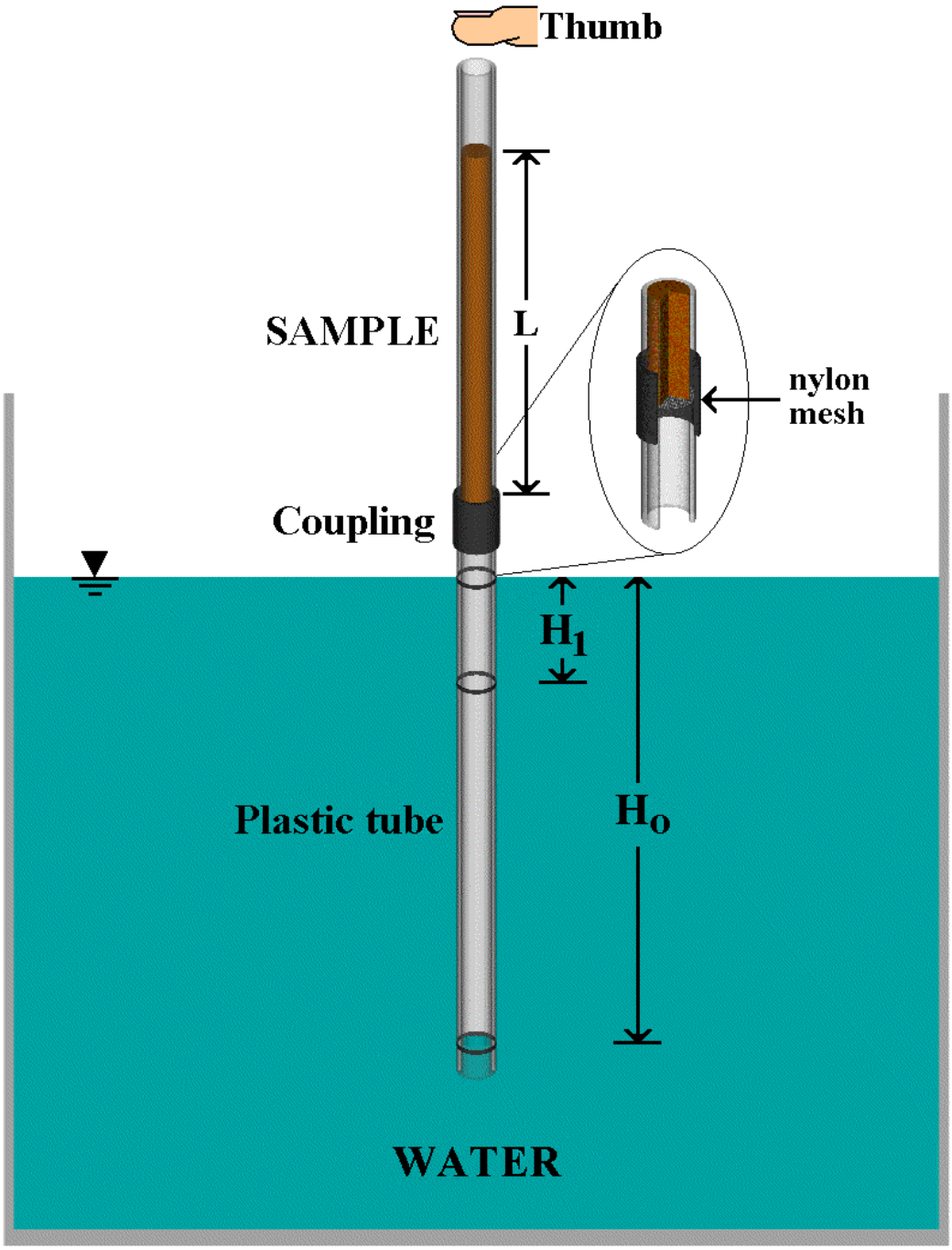

Figure 2.1—Stand-alone air permeameter (from Massmann and Johnson, 2001).

3 ESTIMATING SATURATED HYDRAULIC CONDUCTIVITY FROM GRAIN SIZE CURVES

Regression equations that were derived with grain size parameters from synthetic and field soil samples were used to estimate saturated hydraulic conductivity (K_s). Three different sets of regression equations were developed. The first set of equations was derived from data collected from the synthetic soils described in Chapter 2. The second set of equations was derived from data collected from the field (natural) soils. Data from the synthetic and natural soils were combined to derive the third set.

A relationship between grain size distribution and saturated hydraulic conductivity is of value because grain size information can be obtained more easily than laboratory measurements of hydraulic conductivity. Because grain size analyses are generally simple and inexpensive, estimates from relatively many samples can be obtained rapidly and inexpensively. It may be more effective to obtain rough estimates of saturated hydraulic conductivity from grain size distributions from many samples rather than from a few laboratory measurements that require substantially more effort, especially in soils that exhibit significant spatial heterogeneity. A relationship between grain size and hydraulic conductivity may provide adequate estimates for hydraulic conductivity where more detailed data are not available or justified (Rawls et al., 1982).

3.1 Approaches for Estimating Saturated Hydraulic Conductivity Using Soil Texture Data

Methodologies have been proposed in the literature for estimating hydraulic conductivity and infiltration rates on the basis of soil texture information. These methodologies range from relatively qualitative estimates based on soil type (e.g. Table 2.2, p. 29, Freeze and Cherry, 1979) to relatively quantitative estimates based on data from soil gradation analyses. Estimates of hydraulic conductivity from soil gradation analyses include the Hazen formula, which is based on an effective grain size (Freeze and Cherry, 1979); the Krumbein and Monk equation, which is based on the mean and the standard deviation of the grain size (Davis and DeWeist, 1966); and the Fair-Hatch

equation, which is based on the complete gradation curve (Freeze and Cherry, 1979). These approaches are generally applicable to relatively uniform sands.

One approach that has been proposed for estimating infiltration rates is to use regression equations based on percentage of sand, percentage of clay, and porosity. The general idea is to measure infiltration rates from a large set of samples and to correlate these rates to measurements of the percentage of sand, percentage of clay, and porosity. The resulting regression equations are then assumed to be valid for other similar soils. This approach was used by Rawls and Brakensiek (1985). Regression equations were developed on the basis of measurements taken from more than 5,000 soil horizons from 1,323 soil types in 32 states. The data used to develop these regression equations were collected from soils with clay content ranging from 5 to 60 percent and with a sand content of from 5 to 70 percent. (Clay content was defined as particle sizes smaller than 0.002 mm. Sand was defined as particle sizes between 0.05 and 2 mm.) The data that were used to develop the regressions are described in Rawls et al., 1982.

Although the regresssions developed by Rawls and Brakensiek were developed with soils with clay contents of between 5 to 60 percent and with sand contents of from 5 to 70 percent, they have been used to describe soils with higher sand contents (Carsel and Parrish, 1988; Meyer et al., 1997). The accuracy of these regressions for soils with higher sand content is not known. Soils considered for infiltration facilities generally have a relatively low clay content. This may limit the use of these equations for estimating saturated hydraulic conductivity for soils in western Washington.

Note that for layered systems, the soil texture information should be collected for each individual layer. An effective hydraulic conductivity can be calculated from the values estimated for the individual layers. For example, the effective hydraulic conductivity for flow perpendicular to the layers is given by the harmonic mean (Freeze and Cherry, 1979).

3.2 Regression Equations for Synthetic Soils

A regression equation was derived by using saturated hydraulic conductivity estimates from 71 “synthetic” soil samples comprising different fractions of four different soil textures. The saturated hydraulic conductivity for each soil sample was estimated by using the air permeameter described in Chapter 2.

Measuring saturated hydraulic conductivity of synthetic soils with pre-determined grain size parameters provided a relatively quick method of obtaining a wide distribution of grain size soil samples and simple calculation of the parameters used in the regression equation.

Grain size characteristics were selected to obtain samples over a large range of the gradation curve. Coarse, medium, and fine textures were represented by four homogeneous soil textures: #16, #50, #125, and rock flour. The desired distribution of grain size samples was achieved by using the #16, #50 and #125 soil textures in increments of 20 percent. The rock flour was added to the samples in increments of 5 percent, up to a maximum of 20 percent. The rock flour was used to represent characteristics of clay in a soil. The different synthetic samples used for the regression equation are given in Appendix A.

Five different parameters were initially used in the regression equation: porosity, fraction of fines, and the effective grain diameters d_{10}, d_{60} and d_{90}. The fraction of fines is defined is the fraction of the soil sample that passes the number 200 sieve (mesh size of 0.075 mm). The effective grain diameters d_{10}, d_{60} and d_{90} correspond to an equivalent "percent passing" on the grain size distribution curve (10% of the sample is comprised of soil particles with a grain diameter smaller than d_{10}). Because in-situ porosity cannot be duplicated in the lab, the final evaluation of regression equations did not include porosity.

The grain size parameters for the four soil textures were obtained from grain size curves. The curves were made from sieve analyses for soils #16, #50 and #125. The grain size curve for the rock flour was obtained from a hydrometer test conducted at a

commercial laboratory. The grain size curves for the synthetic soils are given in Appendix C.

Grain size curves for the synthetic samples were calculated based on the grain size curves for the original four soil textures. The percent of the synthetic sample that passes a prescribed mesh diameter is calculated as a summation of the percentage of the original soil texture in the synthetic soil multiplied by the percent of the original soil texture that passes the prescribed mesh diameter. For example, the percentage of a composite or synthetic soil sample comprised of 80 percent #16 soil, 1 percent #50 soil, 5 percent #125 soil, and 5 percent rock flour that would pass the #80 sieve (0.18 mm mesh) would be calculated from the following equation:

$$\%P_{\#80,\ composite} = 0.80(\%P_{\#80,\ 16})+0.01(\%P_{\#80,\ 50})+0.05(\%P_{\#80,\ 125})+0.05(\%P_{\#80,\ flour}) \quad (3.1)$$

where $\%P_{\#80}$ is the percentage of the various soils that pass the number 80 sieve.

Regression equations were derived using different combinations of the four grain size parameters. Each different combination contains one or more of the parameters raised to the power of one or two. The rationale behind the different combinations was taken from the Rawls and Brakensiek (1985) regression equations for saturated hydraulic conductivity. Two general equations were used to predict saturated conductivity:

$$K_{s-predicted} = c_1 + c_2 d_{10}^m + c_3 d_{60}^m + c_4 d_{90}^m + c_5\, fines^m \quad (3.2a)$$

$$\log(K_{s-predicted}) = c_1 + c_2 d_{10}^m + c_3 d_{60}^m + c_4 d_{90}^m + c_5\, fines^m \quad (3.2b)$$

where $K_{s\text{-}predicted}$ is saturated hydraulic conductivity in units of cm/s (L/t); c_1, c_2, c_3, c_4, and c_5 are coefficients; d_{10}, d_{60}, and d_{90} are the grain sizes in mm at which 10, 60, and 90 percent of the material by weight is smaller, fines is the fraction of material passing 0.075 mm (#200) sieve, and the exponent, *m*, is 1 or 2. Equation 3.2a assumes saturated hydraulic conductivity can be described as a polynomial function of the grain size

parameters while equation 3.2b assumes that the logarithm of saturated hydraulic conductivity is a polynomial function of the grain size parameters.

The "Solver" routine in Excel spreadsheets was used to calculate the coefficients for each parameter by minimizing the sum of the square errors, subject to the constraint that the predicted saturated hydraulic conductivity was greater than 0.0. The square error for sample *i* is calculated by

$$\left(K_{measured,i} - K_{predicted,i}\right)^2 \qquad (3.3)$$

where $K_{measured,i}$ is the measured saturated hydraulic conductivity estimated with the air permeameter (L/t), and $K_{predicted,i}$ is the calculated saturated hydraulic conductivity from a regression equation (L/t).

Regression equations were also developed on the basis of the lowest normalized sum of the square error. The normalized square error is calculated by

$$\sqrt{\left(\frac{K_{measured,i} - K_{predicted,i}}{K_{measured,i}}\right)^2} \qquad (3.4)$$

Plots of the regression equations that were derived by minimizing the sum of the square error and the sum of the normalized square error were compared. The comparison revealed that regression equations derived by minimizing the sum of the mean square error resulted in a closer fit between the measured K_s and the predicted K_s. The equations that were tested for minimum sum of the square error are given in Table 3.2.

Two regression equations were selected for a best-fit comparison. These two equations are presented in Table 3.3. Trial 1 was the Hazen equation, which was selected to compare the derived regression with the original Hazen equation. Trial 13 was selected because it gave the best overall fit for the regressions derived from synthetic soil samples, natural soil samples, and natural and synthetic soil samples combined.

The measured K_s values obtained using the air permeameter and the predicted K_s values from regression equations A.1 and A.13 are plotted in figures 3.1 and 3.2. The Hazen equation under-predicted K_s for the majority of the measured samples. Equation A.13 generally over-predicted K_s values for rates of less than 14 in/hr (0.01 cm/s). Predicted K_s values of greater than 14 in/hr (0.01 cm/s) were more evenly spread about the direct correlation line, though predicted values were generally less than measured values.

3.3 Estimating Saturated Hydraulic Conductivity for Natural Soils by Using the Regression Equation from Synthetic Soils

Grain size parameters for "natural" soil samples from 15 sites were used in the regression equations A.1 and A.13 derived from "synthetic" soil samples. Comparisons of predicted versus measured K_s are shown in figures 3.3 and 3.4.

The Hazen equation under- and over-predicted K_s values. Regression equation A.13 over-predicted K_s for the majority of the samples. Regression equation A.6a was non-conservative by up to a factor of 1000 for predicted K_s values measured in this study. This suggests that the coefficients derived for the synthetic soils were too large for estimating K_s for the natural soils.

3.4 Regression Equations from Natural Soil Samples

Regression equations were derived for field soil samples by using the same soil texture parameters as the synthetic-soil regressions. A total of 67 soil samples were taken from 15 sites with infiltration ponds. The K_s values used to derive the regression equations are found in Appendix B. The parameters for the natural soils were obtained from grain size curves generated from sieve analyses. The grain size curves are found in Appendix C.

The results for equations derived by minimizing the sum of the mean square error are given in Table 3.3. Regression equations B.1 and B.13 were developed from the natural soils. Comparisons between the measured and predicted K_s values for the two selected equations are shown in figures 3.5 and 3.6. Similar to the synthetic regression results, the Hazen equation showed a tighter fit for lower K_s rates and was conservative for rates greater than 140 in/hr (0.1 cm/s). Regression equation B.13 does not give as tight as fit as the Hazen for K_s values of less than 140 in/hr (0.1 cm/s) and give less conservative K_s values for rates larger than 140 in/hr (0.1 cm/s).

3.5 Regression Equation from Both Synthetic and Natural Soil Samples

Regression equations were developed by using a combined data set of measured K_s values from both the synthetic and natural soils. The derived regression equations and sum of the mean square errors are included in Table 3.3 as C.1 and C.13. Figures 3.7 and 3.8 compare the measured and predicted K_s values for the two selected equations. For these equations, d_{10}, d_{60}, and d_{90} are the grain sizes in mm at which 10, 60, and 90 percent of the material by weight is smaller, fines is the fraction of material passing 0.075 mm (#200) sieve, and K_s is the saturated hydraulic conductivity and is in units of cm/sec.

The Hazen equation under-predicted the majority of K_s values by up to a factor of 1000. For regression equation C.13, most of the samples were over-predicted for K_s values of lower than 14 in/hr (0.01 cm/s) and under-predicted for K_s values of greater than 140 in/hr (0.1 cm/s).

Figure 3.9 compares the difference between the measured and predicted K_s values for the two equations. The sum of normalized errors shown in Figure 3.9 is given by equation 3.4. This figure confirms that the Hazen equation (C.1) generally provides a better fit for observed values less than 14 in/hr (0.01 cm/s) while the logarithm equation (C.13) provides better fits for observed values greater than 140 in/hr (0.1 cm/s).

Table 3.1—Coefficients for the Hazen Equation, where d_{10} is in mm and K_s is in cm/s (Fetter, 1994).

Very fine sand, poorly sorted	0.40 - 0.80
Fine sand with appreciable fines	0.40 - 0.80
Medium sand, well sorted	0.80 - 1.20
Coarse sand, poorly sorted	0.80 - 1.20
Coarse sand, well sorted, clean	1.20 - 1.50

Table 3.2—Sum of mean square error for synthetic and natural soil samples.

Trial	**Log?**	**d_{10}**	**d_{60}**	**d_{90}**	**d_{10}^2**	**d_{60}^2**	**d_{90}^2**	*Sum of Square Errors*		
								Synthetic	Natural	Combined
1	**No**				**X**			**1.25**	**4.02**	**5.43**
2	No					X		3.83	8.10	11.25
3	No						X	2.18	6.53	10.80
4	No	X	X	X				0.68	2.70	3.50
5	No				X	X	X	0.79	4.28	3.83
6	No	X	X	X	X	X	X	0.53	3.05	3.45
7	No		X	X	X			0.86	3.15	4.28
8	No	X		X		X		0.69	2.74	3.50
9	No	X	X				X	0.65	2.93	3.60
10	No			X	X	X		0.88	3.15	4.28
11	No		X		X		X	0.77	3.38	4.05
12	No	X				X	X	0.65	2.93	3.60
13	**Yes**	**X**	**X**	**X**				**2.08**	**3.36**	**4.72**

Table 3.3—Sum of mean square error of synthetic and natural soils for selected equations.

Trial	**Regression Equation**	**Sum of normalized errors**
A.1	$K_s = 1.07\, d_{10}^2$	49
A.13	$\text{Log}(K_s) = -1.97+1.65\, d_{10} +0.34\, d_{60} +0.21\, d_{90} - 2.48 fines$	140
B.1	$K_{sat} = 0.77\, d_{10}^2$	73
B.13	$\text{Log}(K_s) = -1.62+1.85\, d_{10} +0.013\, d_{60} - 0.012\, d_{90} -0.61 fines$	111
C.1	$K_{sat} = 0.87\, d_{10}^2$	128
C.13	$\text{Log}(K_s) = -1.57+1.90\, d_{10} +0.015\, d_{60} - 0.013\, d_{90} -2.08 fines$	293

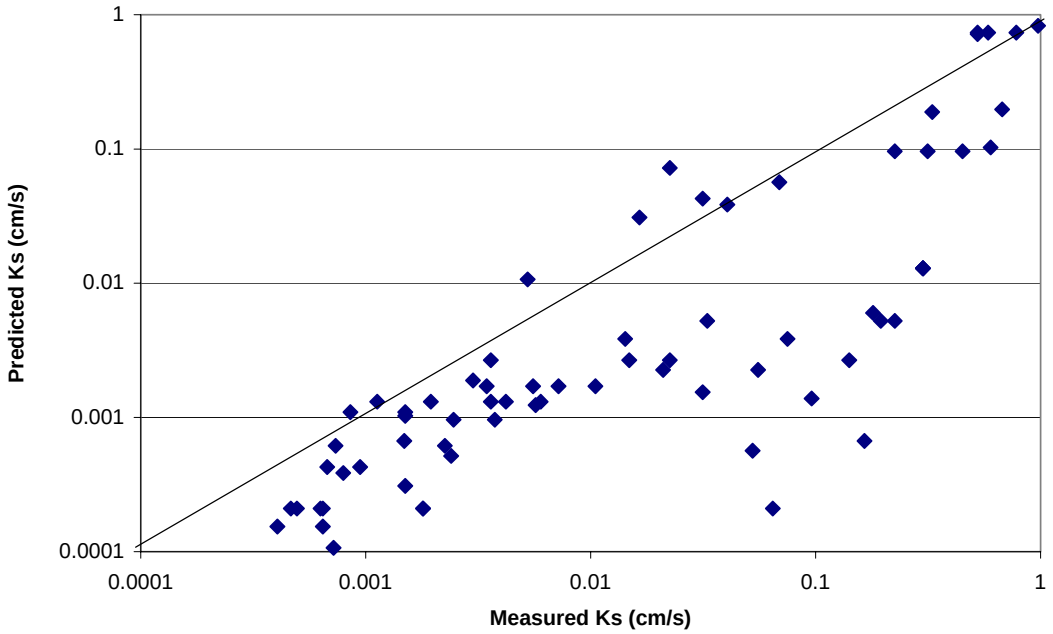

Figure 3.1—A comparison of measured hydraulic conductivity of synthetic soils with predictions made with the Hazen equation (regression equation A.1).

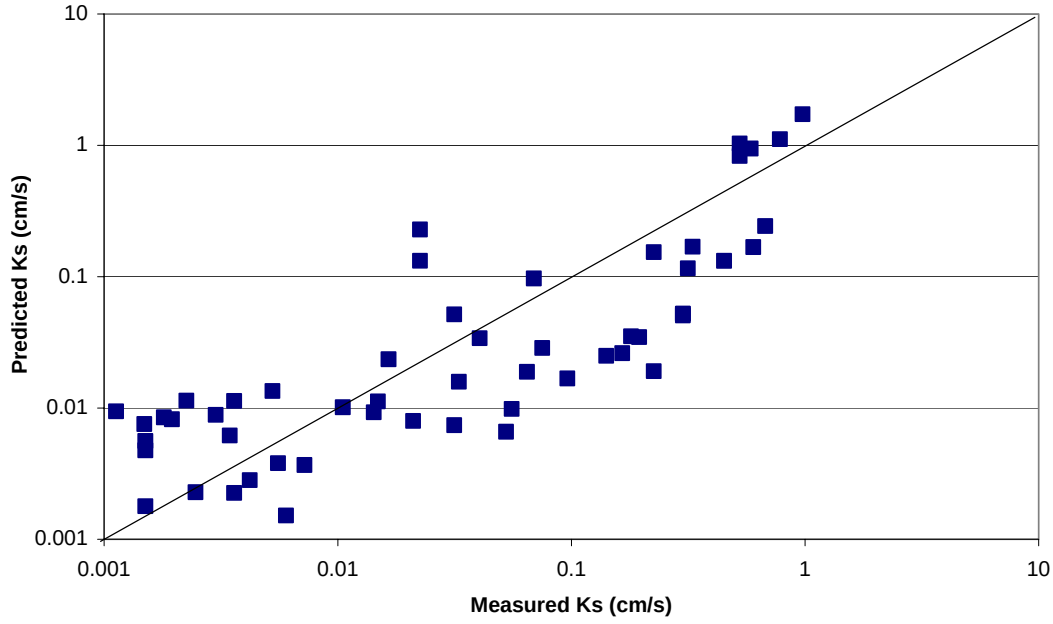

Figure 3.2 - A comparison of measured hydraulic conductivity of synthetic soils with predictions made with regression equation A.13.

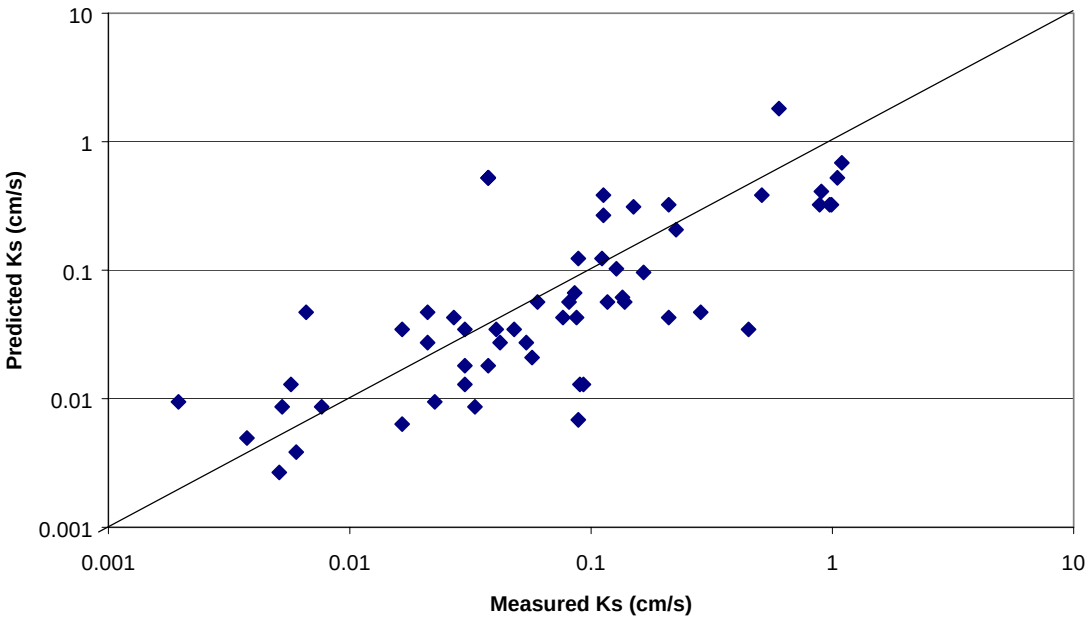

Figure 3.3—Hazen equation A.1 derived from synthetic soil and applied to natural soil parameters.

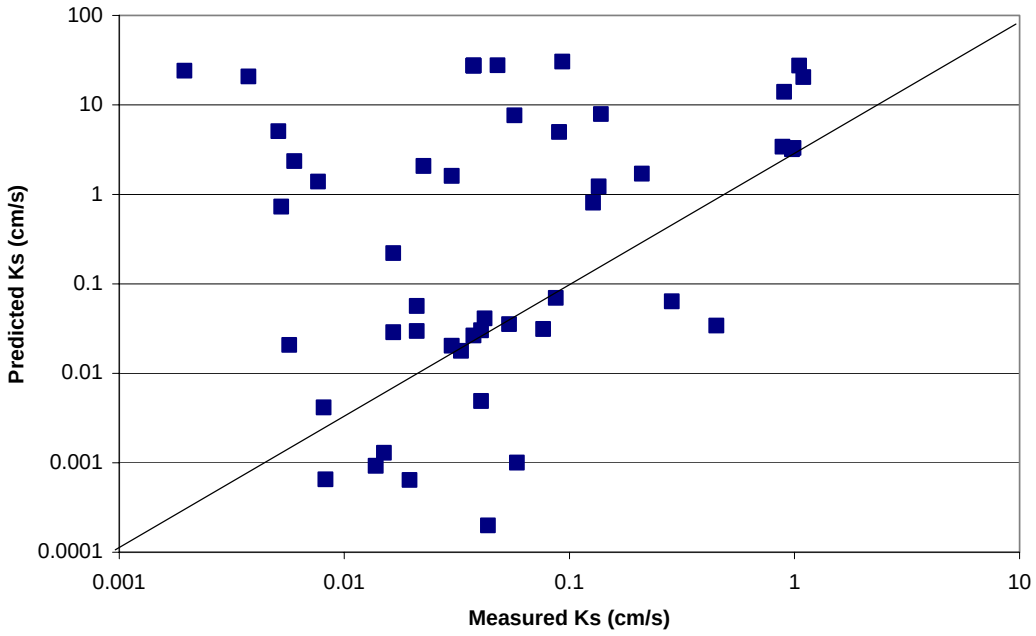

Figure 3.4—Regression equation A.13 derived from synthetic soil and applied to natural soil parameters.

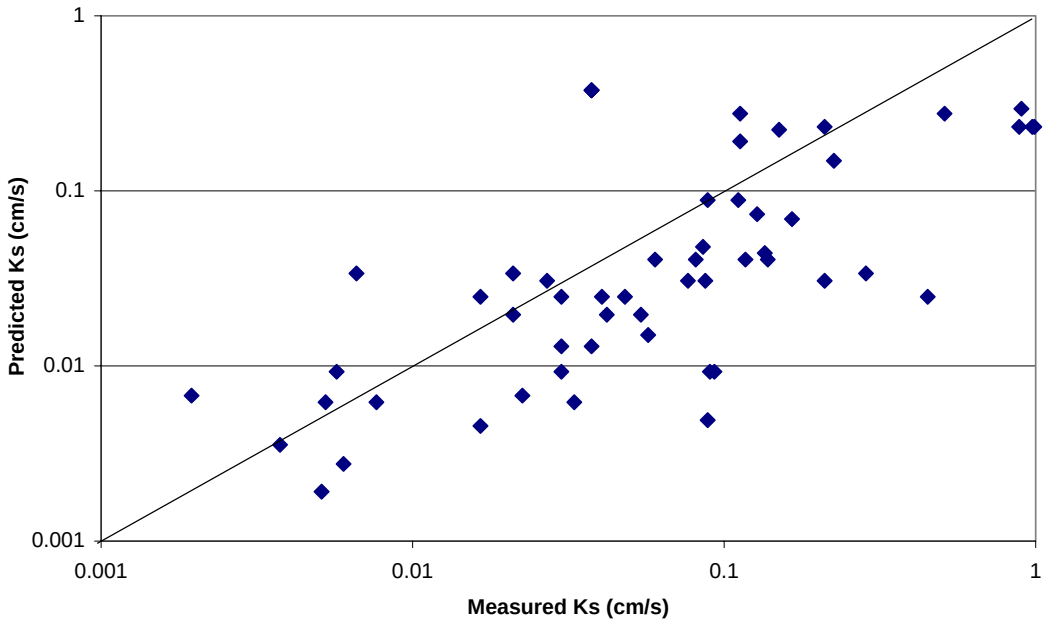

Figure 3.5—A comparison of measured hydraulic conductivity of natural soils with predictions made with the Hazen equation (regression equation B.1).

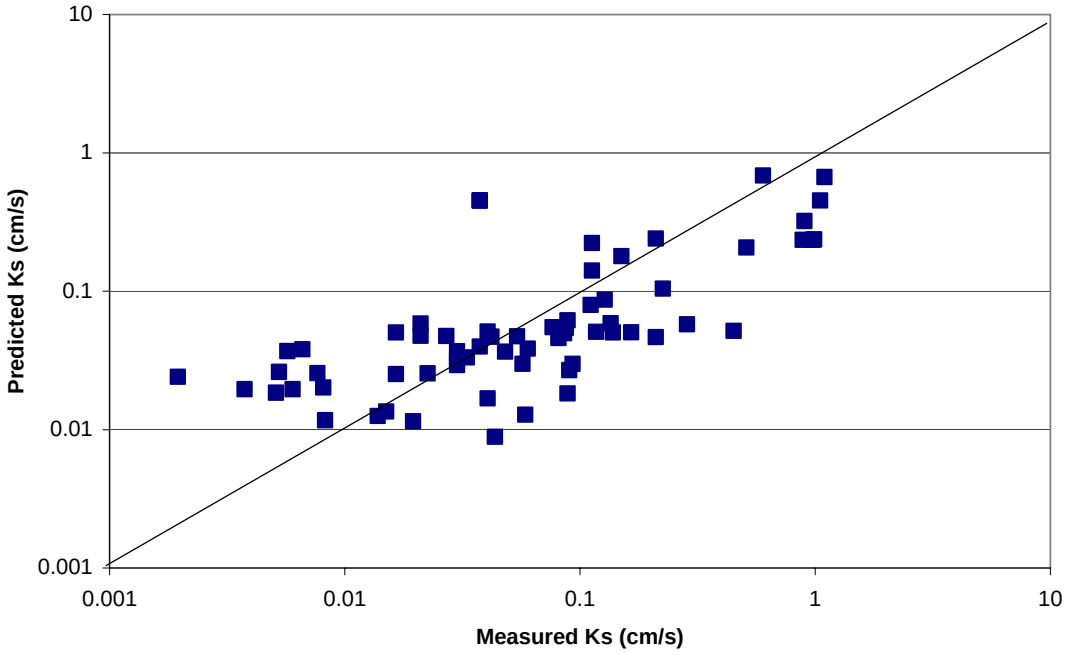

Figure 3.6—A comparison of measured hydraulic conductivity of natural soils with predictions made with regression equation B.13.

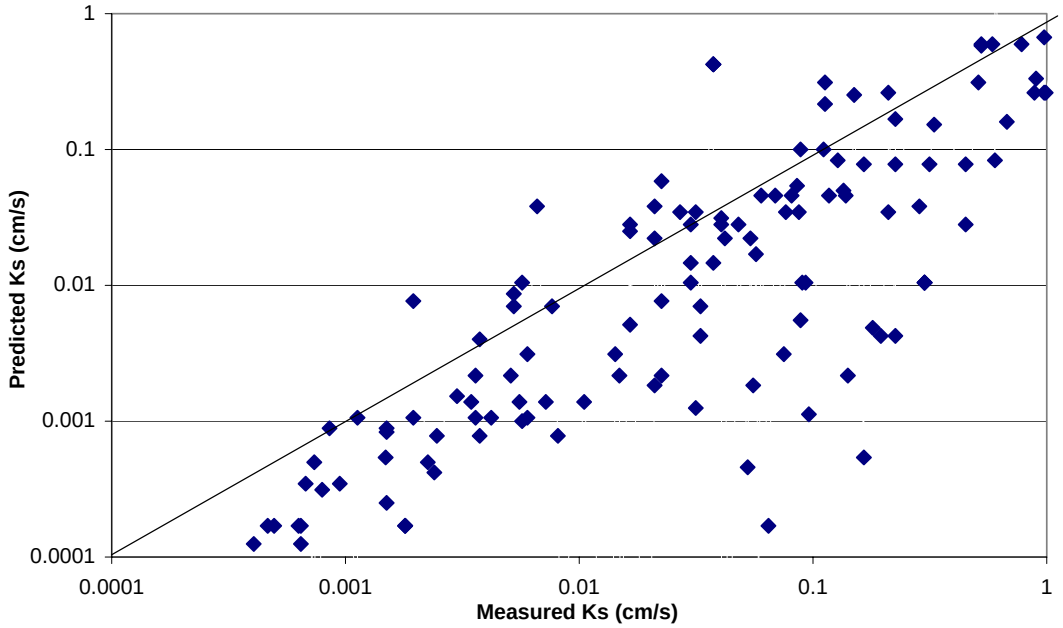

Figure 3.7—A comparison of measured hydraulic conductivity of natural soils and synthetic soils with predictions made with the Hazen equation (regression equation C.1).

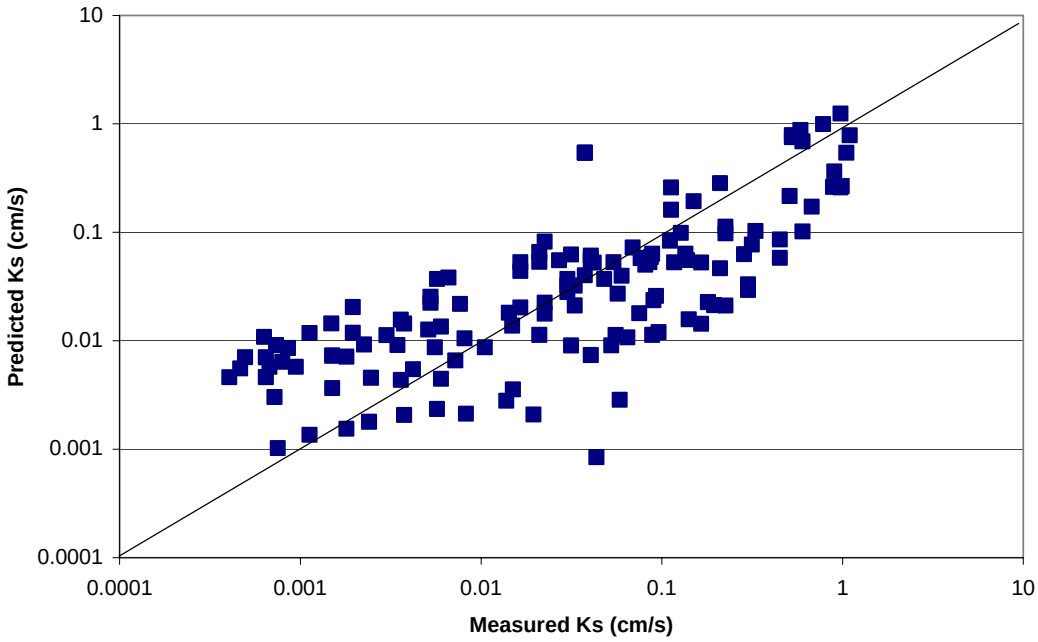

Figure 3.8—A comparison of measured hydraulic conductivity of natural soils and synthetic soils with predictions made with regression equation C.13.

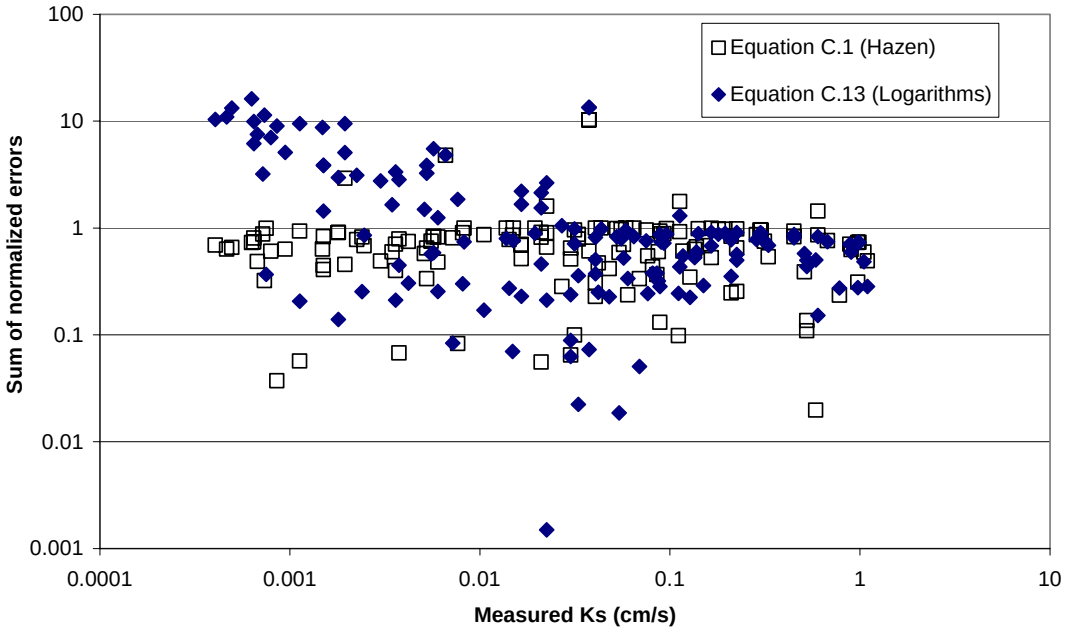

Figure 3.9—Comparison of normalized errors for regressions with natural and synthetic soils.

4 FULL-SCALE INFILTRATION TESTS

This chapter describes the results of full-scale tests that were conducted in this study to estimate infiltration rates for four infiltration facilities in western Washington. The methods used to conduct these tests are described in Section 4.1, and the approach used to analyze the data is described in Section 4.2. The sites that were used for the full-scale test are described in Section 4.3 and the results of the tests are presented in Section 4.4. Some of the implications of the data are discussed in Section 4.5.

In comparison to other field and laboratory methods, full-scale tests provide the most reliable estimates of how infiltration ponds will perform. These tests, which are often termed "flood tests," are conducted by discharging water into a pond and measuring the change in water level in the pond as a function of time. Data are collected both during the filling stage of the test and during the draining stage after the discharge into the pond has been stopped. The primary advantage of these full-scale tests is that the infiltration rate is measured directly. The approach does not require modeling or significant analytical tools to estimate or infer infiltration rate from some other measured parameter. Sampling errors that can be introduced with small-scale measurements in heterogeneous soils are avoided. The primary disadvantage is that these tests require a source of water that can be delivered at a high enough flow rate to cause ponding within the facility.

4.1 Field Methods for the Full-Scale Tests

Figure 4.1 illustrates a typical configuration for the full-scale flood tests that were completed as part of the current study. A pressure transducer was used to measure the water level in the pond as a function of time. During the filling stage of the test, which typically lasted several hours, water was discharged into the pond and the depth of water increased. The draining stage of the test started when the discharge was terminated. The

water level in the pond decreased with time during this draining stage as the water infiltrated through the bottom and sides of the pond. The draining stage lasted from 12 hours to several days, depending upon the rate of infiltration.

The pressure transducer, model 15 PSI PS9800 from Instrumentation Northwest, Inc., has an accuracy of 0.1 percent. For a water level in a pond of 24 inches (61 cm), the degree of accuracy is ± 0.18 inches (0.45 cm). The transducer, supported by a steel post that is driven into the pond bottom, measures the height of water above the bottom of the transducer. The transducer is connected to an automatic data acquisition system that collects measurements at pre-determined time intervals. For this study the time interval was 10 minutes.

The water used to fill the ponds was obtained by connecting a 2.5-inch (6.35-cm) diameter hose to a fire hydrant. The flow rate, which was controlled with a valve at the hydrant, was measured with a water meter provided by the local water utilities. These meters measure to the nearest 10 cubic feet (0.3 cubic meter).

Surveying measurements were taken to calculate the pond geometry. A level and tripod were used to measure elevation along the pond bottom and side slopes. Elevation measurements were collected along transects with a horizontal spacing between measurements of approximately 4 to 6 feet (1.2 to 1.8 m), depending on the site. The length and width of the pond bottom were measured with a steel tape measurer. The side slopes (change in elevation divided by change in horizontal distance) ranged from 0.3 to 0.7 for the three sites.

4.2 Data Analysis for the Full-Scale Tests

The rate of infiltration was estimated from full-scale test data by performing a water balance on the infiltration pond. The following expression gives the volume of water that infiltrates during time interval Δt:

$$V_{\inf} = Q_{in}(\Delta t) - A_{surf}(\Delta z) \qquad (4.1)$$

where V_{inf} is the volume of water that infiltrates during the time interval (L^3), Q_{in} is the flow rate into the pond (L^3/t), A_{surf} is the area of the pond surface (L^2), and Δz is the change in water depth during the time interval (L). The sign convention that is used in equation 4.1 is that a positive Δz denotes an increase in the depth of the water in the pond.

Except for ponds with rectangular cross-sections, the area of the water surface, A_{surf}, will be a function of the depth of the water in the pond, Δz. The surface area for rectangular ponds can be calculated by using the following expression:

$$A_{surf} = (L * W) + \frac{2\Delta z}{s}(L + W) + \frac{4\Delta z^2}{s^2} \qquad (4.2)$$

where L and W are the length and width of the pond bottom and s is the side slope of the pond. The slope is defined as the change in elevation divided by change in horizontal distance.

The infiltration rate is generally defined as the volume of water that infiltrates per unit time per unit area of the wetted pond bottom:

$$I = \frac{V_{\inf}}{A_{wet}\Delta t} \qquad (4.3)$$

where I = infiltration rate (L/t) and A_{wet} is wetted area of the pond bottom (L^2).

Equations 4.1 and 4.3 can be combined to give the following expression for infiltration rate:

$$I = \frac{V_{\inf}}{A_{wet}\Delta t} = \frac{Q_{in}}{A_{wet}} - \frac{A_{surf}\Delta z}{A_{wet}\Delta t} \qquad (4.4)$$

During the early portion of the test when the pond is being filled, the flow rate into the pond (Q_{in}) and the change in depth (Δz) are both positive values. During the later stage of the test the flow rate is 0.0 and the change in depth is a negative number. In both stages the infiltration rate is a positive value.

Except for ponds with vertical sides, the wetted area of the pond bottom will depend upon the depth of water in the pond. The wetted area (A_{wet}) for a rectangular pond is given by the following expression:

$$A_{wet} = L*W + \left(2L + 2W + \frac{4\Delta z}{s}\right)\sqrt{\Delta z^2 + \frac{\Delta z^2}{s^2}} \qquad (4.5)$$

4.3 Description of Sites Used for the Full-Scale Tests

Full-scale flood tests were conducted at four infiltration facilities in western Washington. One facility was located in Clark County, one facility was in King County, and two facilities were located in Kitsap County. The particular locations were chosen on the basis of the size of the ponds, the expected infiltration rate, and the willingness of the storm water managers in these counties to cooperate in the study. Small- to medium-sized ponds, in the range of 2,000 to 10,000 ft^3 (56 to 180 m^3) were chosen to reduce the amount of water that would be required for the flood tests. Ponds with anticipated infiltration rates in the range of 0.1 to 10 inches per hour ($7x10^{-5}$ to $7x10^{-3}$ cm/s) were chosen because these represent "typical" sites. Sites with infiltration rates significantly less than this are generally undesirable because of the size of the pond that would be required to infiltrate water from a typical design storm. Sites with infiltration rates significantly larger than this are undesirable because of water quality considerations (WDOE, 2001).

Site specific data, soil, design infiltration rate, and pond descriptions are found in Appendix D.

4.3.1 Clark County Pond

In November, 2000 a flood test was performed at a storm-water infiltration pond in Clark County. The pond, which is shown in Figure 4.2, is located in a residential area in the northern part of Vancouver. The pond is enclosed with a chain-link fence. No information was available regarding the age of the pond or area of the basin that drains into the pond.

The pond bottom is rectangular with dimensions 75 feet by 25 feet (23 meters by 7.6 meters). The side slopes were surveyed to be 0.3V:1H and the depth of the pond is approximately 6 feet (1.8 meters). A 3-foot (1-meter) high retaining wall constructed with concrete blocks is located on the north side of the infiltration pond. The retaining wall is permeable because of open spaces between the concrete blocks. The water flows into the infiltration pond from a pre-treatment area located on the grassy plateau above the retaining wall. Stormwater discharges to the pretreatment area from two pipes located at opposite ends of the grassy plateau.

The pond bottom and side slopes are covered with patches of moss and grass. Two trees are located in opposite diagonal corners of the pond. The side slopes of the pond are covered in patches of grass.

4.3.2 Balsam 7-11 Pond, Kitsap County

In September 2000 a flood test was performed at the Balsam 7-11 stormwater infiltration pond in Kitsap County. The infiltration pond (Figure 4.3) is located in east central Kitsap County, south of Sinclair Inlet. The site is located at the eastern end of a convenience store parking lot adjacent to a major thoroughfare. The estimated area of

the basin that drains into the pond is 7 acres (0.03 km^2) (Wiltsie, 1998). Stormwater that discharges into the pond comes from both residential and commercial developments. The water outlet pipe is located on the south end. Litter (such as wrappers, old shoes, and other articles of clothing) was found in the bottom of the pond. A chain-link fence encloses the pond.

The pond was designed in 1977. The pond bottom is rectangular, 7 feet (2.1 meter) wide by 53 feet (16.1 meter) long. The side slopes were surveyed to be 0.7V:1H and the depth of the pond is approximately 7 feet (2.1 meter). There is no pre-treatment for the stormwater that discharges into the pond. The pond bottom and side slopes are dense with wetland plants. Sediment build-up has been removed from Balsam 7-11 within the last three years (Anderson, J., 2001).

4.3.3 Krista Firs Pond, Kitsap County

In October 2000 a flood test was performed at Krista Firs storm water infiltration pond in Kitsap County. This pond, which is shown in Figure 4.4, is located in a residential area less than 3 miles (4.8 km) southwest of the Balsam 7-11 facility. The basin area draining into the pond is approximately 10.6 acres (0.04 km^2) (Wiltsie, 1998). A chain-link fence encloses the pond.

The pond was designed in 1978. The pond bottom is rectangular with dimensions of 26 feet (7.9 meters) by 39 feet (11.9 meter). The pond side slopes were estimated to be 0.4V:1H and the depth of the pond is approximately 6 feet (1.8 meter). The water inlet is located in the north west corner of the pond. There is no pre-treatment for the stormwater that discharges into the pond.

The pond bottom has dense patches of moss and grass. Shrubs and large gravel (ranging from 10 to 100 mm in size) are scattered throughout the bottom of the pond.

The side slopes have patches of dry grass and moss. This pattern indicates moist conditions in the pond bottom, but not for the side slopes.

4.3.4 Cimarron Pond, King County

A flood test was performed at the Cimarron storm water infiltration pond in King County in April 2001. This pond, which is shown in Figure 4.5, is located in a residential area on the Sammamish Plateau in eastern King County and was constructed in 1981. The basin area draining into the pond is approximately 14.6 acres (0.06 km^2). The pond bottom is roughly triangular in shape with side dimensions of approximately 42 feet (12.8 meter) by 85 feet (25.9 meter) by 110 ft (33.5 meter). The pond side slopes were estimated to be 0.6V:1H and depth of the pond is approximately 5 feet (1.5 meter). A breached swale was included in the design for pre-treatment of the stormwater. The top 6 inches (15 cm) of the pond were filled with well-graded, clean sand and ¾-in. to 2 in. (2-cm to 5 cm) washed gravel placed beneath the sand. The average infiltration rate used for the design was 13.3 in/hr ($9.4x10^{-3}$ cm/s). The photograph included in Figure 4.5, which shows the pond essentially full of water, was taken in January of 2002 after several month of high precipitation. The pre-treatment swale was fully submerged and an over-flow discharge pipe was partially submerged at this time. This overflow pipe discharges into a nearby wetlands, which suggest a relatively high water table.

Falling head test infiltrometer tests were conducted at the Cimarron pond in an earlier study (S. Foley, 2000). The measured infiltration rates from these tests was 2.7 inches/hour ($1.9x10^{-3}$ cm/s). At the time of this earlier study, the soils from the bottom of the pond were found to have a high percentage of fines (12 to 20 percent).

4.4 Estimates of Infiltration Rates Based on the Full-Scale Tests

4.4.1 Clark County Pond

The basic data that were used to estimate infiltration rates at the Clark County site are shown in Table 4.1 and in Figure 4.6. Table 4.1 lists the flow rates, the duration of

the test, and the pond geometry. Figure 4.6 shows the depth of water as a function of time, measured at 10-minute intervals. The flow rate into the pond during the filling portion of the test was approximately 2000 ft^3/hr (250 gpm or 57 m^3/hr), and the filling stage lasted for approximately 2.5 hours. The water level in the pond reached a depth of approximately 21 inches (53 cm) during the filling portion of the test.

The draining phase, which lasted just under 70 hours, can be divided into two parts. During the first part, which lasted until hour 30, the change in water level followed an exponentially shaped curve that became flatter with time. Between hour 30 and the end of the test, the water level followed a linearly shaped curve with a slope that was essentially constant.

The water level data shown in Figure 4.6 can be used to estimate the infiltration rate as a function of time with Equation 4.4. Figure 4.7 shows the infiltration rate averaged over each 30-minute period. The infiltration rate increased with time during the filling portion of the test and reached a maximum rate of approximately 2 in/hr ($1.4x10^{-3}$ cm/s). After the discharge to the pond was stopped, the infiltration rate quickly decreased to approximately 0.25 in/hr ($1.8x10^{-4}$ cm/s). This rate remained roughly constant for the duration of the test.

The total volume of water that was discharged to the infiltration pond during the full-scale test at the Clark County site was approximately 4710 ft^3 (133 m^3). All of this water eventually infiltrated into the ground. Figure 4.8 shows the fraction of the total inflow that had infiltrated from the pond as a function of time. The total inflow is estimated by summing the infiltration rates shown in Figure 4.7 over the duration of the test. This total inflow is given in the last column of Table 4.1. Note that the total inflow that was calculated on the basis of estimated infiltration rates (Column "I" in Table 4.1) is different from the total inflow that was calculated on the basis of discharge to the pond

(Column "D" in Table 4.1). These differences are due to uncertainties in pond surface area and wetted pond bottom in Equation 4.4.

The fraction of the total inflow that had infiltrated at each time was calculated by summing the infiltration rates for all earlier times and then dividing this sum by the total inflow. For the Clark County site, approximately 20 percent of the total inflow occurred during the filling stage of the test.

The estimated infiltration rate was nearly constant after approximately 30 hours, as shown in Figure 4.7. A constant infiltration rate suggests that the hydraulic gradient that causes flow is also approximately constant during this period. Given that the water level in the pond decreased from approximately 10 inches (25 cm) at 30 hours to less than 1 inch (2.5 cm) at 70 hours, it appears that the water level or water pressure in the pond was not a primary component of the forces causing infiltration.

The rapid increase in infiltration during the filling portion of the test may have been caused in part by lateral flow along the sides of the ponds. This is similar to "bank storage" that occurs in stream channels. As the water level in the pond increases, flow is induced horizontally into the banks of the pond. This infiltration is in addition to the infiltration that occurs along the pond bottom. Once the water level in the pond begins to decrease, the horizontal flow is reversed and water drains into the pond along the sides and out of the pond along the bottom. This inflow, which reduces the net infiltration rate, decreases with time.

Figure 4.9 compares infiltration rates as a function of water level for the rising and falling limbs of the hydrograph. The graph shows that infiltration rates during the rising limb were significantly larger than the infiltration rates during the falling limb. In general, this is expected because the head gradient is largest for initially dry soils. However, these differences in infiltration rates could also be explained by lateral flow.

When the pond is filling up, flow in both the horizontal and vertical direction allows for more water storage in the sub-surface and thus a higher infiltration rate. When the water level in the pond decreases, the flow from the sides of the pond reverses direction.

The data shown in Figure 4.9 can be used to estimate the relative magnitude of the horizontal and vertical flows. As an example, when the depth of water in the pond is18 inches, the infiltration rate during the rising limb is approximately 1.7 in/hr ($1.1x10^{-3}$ cm/s) while the infiltration rate during the falling limb is approximately 0.8 in/hr ($5.6x10^{-4}$ cm/s). During the filling phase, the horizontal and vertical flows are both away from the pond, as shown in Figure 4.10a. Equation (4.6) describes vertical and horizontal flow from the pond during the filling phase:

$$V + H \cong 1.7 \text{ in/hr.} \qquad (4.6)$$

where V is vertical flow (L/t) and H is horizontal flow (L/t).

During the draining phase, the horizontal flow is into the pond and the vertical flow is away from the pond, as shown in Figure 4.10b. Equation (4.7) describes vertical and horizontal flow from the pond during the draining phase:

$$V - H \cong 0.8 \text{ in/hr.} \qquad (4.7)$$

Equations 4.6 and 4.7 can be solved simultaneously if V and H are assumed to be the same in both equations. This resulted in a horizontal flow of 0.45 in/hr (1.1 cm/hr) and a vertical flow of 1.25 in/hr (3.2 cm/hr). At the water depth of 18 inches (46 cm), the horizontal flow accounted for roughly 36 percent of the total infiltrating water. When the water level stopped rising, the water infiltrating vertically had the addition of the total horizontal flow volume of water that was coming back into the pond. This may explain

why the net infiltration rate quickly dropped as soon as the inflow from the hydrant was shut off.

4.4.2 Balsam 7-11 Pond, Kitsap County

The basic data that were used to estimate infiltration rates at the Balsam site are shown in Table 4.1 and Figure 4.11. The flow rate into the pond during the filling stage was approximately 1000 ft^3/hr (125 gpm or 28 m^3/hr). The pond was filled for approximately 2 hours and the water reached a maximum depth of approximately 31 inches (79 cm). The total volume of water discharged into the pond was 2290 ft^3 (64.8 m^3). Similar to the pond in Clark County, the drainage phase can be divided into two parts. During the first part of the draining phase, the water level decreased exponentially. This occurred between hour 2 and hour 6. Between hour 6 and the end of the test, the water level declined linearly.

Figure 4.12 shows the infiltration rate averaged over 30-minute periods. The maximum infiltration rate was approximately 12 in/hr ($8.5x10^{-3}$ cm/s) and occurred at the end of the filling phase. The infiltration rate fell to approximately 2 in/hr ($1.4x10^{-3}$ cm/s) during the later part of the test.

The linear part of Figure 4.11 demonstrates that the infiltration rate was roughly constant after approximately 6 or 7 hours. This infers a constant gradient during the second stage of the drainage phase. The water level in the pond decreased by approximately 15 inches (38 cm) during the last 6 hours of the drainage stage when the infiltration rate had reached a relatively steady state. This supports the idea that the water level in the pond may have been a significant driving force for infiltration.

Figure 4.13 shows the fraction of the total inflow that had infiltrated from the pond as a function of time. Approximately 30 percent of the total inflow occurred during the filling stage of the test. Figure 4.14 compares calculated infiltration rates as a

function of water level for the rising and falling limbs of the hydrograph. These calculations show that infiltration rates increased rapidly after the water level in the pond reached a depth of approximately 30 inches (76 cm).

4.4.3 Krista Firs Pond, Kitsap County

The basic data that were used to estimate infiltration rates at the Krista Firs pond are shown in Table 4.1 and in Figure 4.15. The information in Table 4.1 describes the flow rates, the duration of the test, and the pond geometry. Figure 4.15 shows the depth of water as a function of time. These depths were measured at 10-minute intervals. The flow rate into the pond was approximately 1850 ft^3/hr (230 gpm or 52 m^3). The pond was filled for approximately 2 hours, and the water reached a maximum depth of approximately 26 inches (66 cm). The total volume of water discharged into the pond was approximately 4190 ft^3 (119 m^3).

The draining phase of the test, which lasted for approximately 70 hours, can be divided into two parts. During the first part, from hour 3 to hour 30, the water level decreased exponentially. The water level declined linearly for the next 40 hours. However, there were two jumps in the curve: one after approximately 30 hours and one after approximately 55 hours. These times correspond to October 29 and October 30 2000. There was very little precipitation on October 29th (0.05 inches or 0.1 cm) and no precipitation on October 30th (National Oceanic and Atmospheric Administration, 2000). However, 0.30 inches (0.76 cm) and 0.13 inches (0.33 cm) of precipitation fell on October 27th and 28th, respectively. The jumps could be explained by this precipitation if the response time between precipitation and water levels was on the order of 2 days, but such a long response time is improbable.

Figure 4.16 shows the infiltration rate averaged over a 30-minute period. The maximum infiltration rate reached was approximately 13 in/hr (9.2×10^{-3} cm/s) and

occurred at the end of the filling phase. The infiltration rate dropped to a relatively steady rate of approximately 0.2 in/hr ($1.4x10^{-4}$ cm/s) after approximately 30 hours.

The estimated infiltration rate was nearly constant after approximately 20 hours, as shown in Figure 4.16. As was discussed for the Clark County test, a constant infiltration rate suggests that the hydraulic gradient that causes flow is also approximately constant during this period. Given that the water level in the pond was decreasing from approximately 15 inches (38 cm) at 20 hours to approximately 5 inches (13 cm) at 70 hours, it appears that the water level or water pressure in the pond was not a primary component of the forces causing infiltration.

Figure 4.17 shows the fraction of the total inflow that had infiltrated from the pond as a function of time. Approximately 20 percent of the total inflow occurred during the filling stage of the test. Figure 4.18 compares calculated infiltration rates as a function of water level for the rising and falling limbs of the hydrograph. These calculations show that infiltration rates increased rapidly after the water level in the pond reached a depth of approximately 26 inches (66 cm). Figure 4.18 compares infiltration rates as a function of water level for the rising and falling limbs of the hydrograph. The graph shows that infiltration rates during the rising limb were significantly larger than the infiltration rates during the falling limb.

4.4.4 Cimarron Pond, King County

The basic data that were used to estimate infiltration rates at Cimarron pond are shown in Table 4.1 and in Figure 4.19. The information in Table 4.1 describes the flow rates, the duration of the test, and the pond geometry. Figure 4.19 shows the depth of water as a function of time. These depths were measured at 5-minute intervals. The flow rate into the pond was approximately 1220 ft^3/hr (150 gpm or 35 m^3). The pond was filled for approximately 1.7 hours and the water reached a maximum depth of approximately 13 inches (33 cm). The total volume of water discharged into the pond

was approximately 2070 ft^3 (59 m^3) The test at the Cimarron pond was completed by placing four pressure transducers at different locations on the pond bottom. These transducers were at slightly different elevations, as shown in Figure 4.19. The average of these four transducers was used to calculate the depth of water in the pond and the infiltration rate.

Figure 4.20 shows the infiltration rate averaged over a 30-minute period. The maximum infiltration rate was approximately 1.9 in/hr ($1.3x10^{-3}$ cm/s) and occurred at the end of the filling phase. The infiltration rate dropped to a relatively steady rate of approximately 0.1 in/hr ($7.1x10^{-5}$ cm/s) after approximately 2 hours. The relatively high-frequency fluctuations may have been the result of precipitation events that occurred during the drainage period. Given these higher-frequency fluctuations, the estimated average infiltration rate was nearly constant after approximately 3 hours, as shown in Figure 4.20. Again, a constant infiltration rate suggests that the hydraulic gradient that causes flow is also approximately constant during this period. Figure 4.21 compares infiltration rates as a function of water level for the rising and falling limbs of the hydrograph. The graph shows that infiltration rates during the rising limb were significantly larger than the infiltration rates during the falling limb.

4.5 Implications of the Data

Lateral or horizontal flow may have occurred during the filling phases at all four ponds. This suggests that the ponds may have had a higher infiltration rate during the initial inflow of stormwater discharge. Once a maximum water level in the pond had been reached and the water level began to decline, the infiltration rate would decrease if the horizontal flow reversed and flowed back into the pond. The infiltration rates for the ponds eventually reached a nearly constant value. The early-time and long-term infiltration rates for the four ponds included in this study are summarized in Table 4.2.

If lateral flow is consistently important, more efficient designs may require a larger ratio of side area to bottom area. This design approach would necessitate maintenance for the sides as well as the bottom of the pond. If the soil on the sides and bottom are preserved with respect to vegetation and silt build-up, the horizontal as well as the vertical flow could be an effective means of infiltrating stormwater runoff into the subsurface.

Infiltration rates based on soil texture for the three sites are included in Table 4.2. These estimates are from the WDOE *Stormwater Management Manual for Western Washington: Volume III -- Hydrologic Analysis and Flow Control Design/BMPs* (2001).

The soil texture infiltration rate of sand over-estimated the actual full-scale measured rate at Krista Firs and King County. The soil texture rate for Balsam 7-11 under-estimated the actual full-scale rate, and the soil texture rate for Clark County closely estimated the actual full-scale rate. This reinforces that grain size texture alone does not include site-specific characteristics that may affect infiltration rates. Possible explanations for the differences between the full-scale measured rates and the estimated rates based on soil texture information are included in Chapter 5.

Table 4.1 – Summary of data for full-scale infiltration tests

A. Site	B. Inflow Rate (ft^3/hr)	C. Inflow Duration (hours)	D. Total Inflow (ft^3)	E. Draining Duration (hours)	F. Max. Water Depth (ft)	G. Bottom Area (ft^2)	H. Ratio of side area to bottom area	I. Total Infiltration (ft^3)
Clark	2060	2.5	4710	67.8	1.8	1860	0.5	4820
Balsam	1000	2.2	2290	12.4	2.6	370	1.6	2260
Krista	1840	2.3	4190	78.9	2.2	1030	0.8	3960
Cimarron	1220	1.7	2070	102.9	0.8	2040	0.15	1370

Table 4.2 – Summary of calculated infiltration rates.

Site	**Observed infiltration rates**		**Soil Texture Description**	**d_{10} (mm)**	**Estimated long-term rate from WDOE, 2001 (in/hr)**	
	Final rate (long-term)	**Maximum rate (short-term)**			**Rate from soil texture**	**Rate from d_{10}**
Clark County	0.23 in/hr (0.0016 cm/s)	2.5 in/hr (0.0018 cm/s)	Loam/Silty Loam	0.001 to 0.005	0.13-0.25	< 0.8
Balsam 7-11	2.1 (0.0015)	13.2 (0.0093)	Silty Loam	0.002 to 0.03	0.13-0.25	< 0.8
Krista Firs	0.33 (0.00023)	2.8 (0.002)	Sand	0.1 to 0.4	2	2-9
Cimarron	0.1 ($7.1x10^{-5}$)	1.9 (0.0013)	Silty sand loam	0.04 to 0.3	0.13-0.25	0.8-6.5

Figure 4.1 - Pressure transducer installed at Krista Firs, Kitsap County.

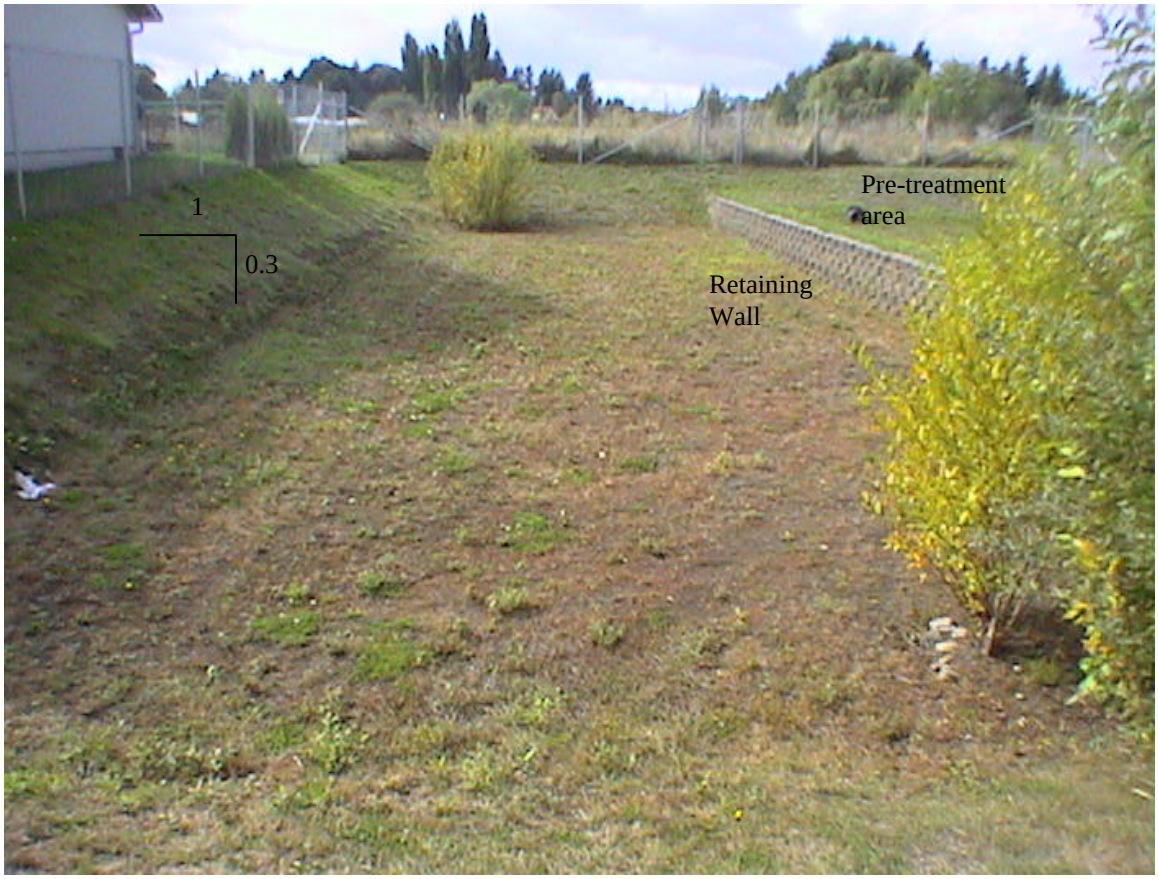

Figure 4.2 - Clark County pond, Clark County, 9616 NE 59th Ave., Vancouver, Washington, 98686.

Figure 4.3 - Balsam 7-11, Kitsap County, Lund Ave. SE and Jackson Ave., Port Orchard, Washington, 98366.

Figure 4.4 - Krista Firs, Kitsap County, K.C. Place and Cedar Rd E., Port Orchard, Washington, 98366.

Figure 4.5 – Cimarron, King County, N.E. 12th Place and 230th Avenue NE, Sammamish, Washington 98074.

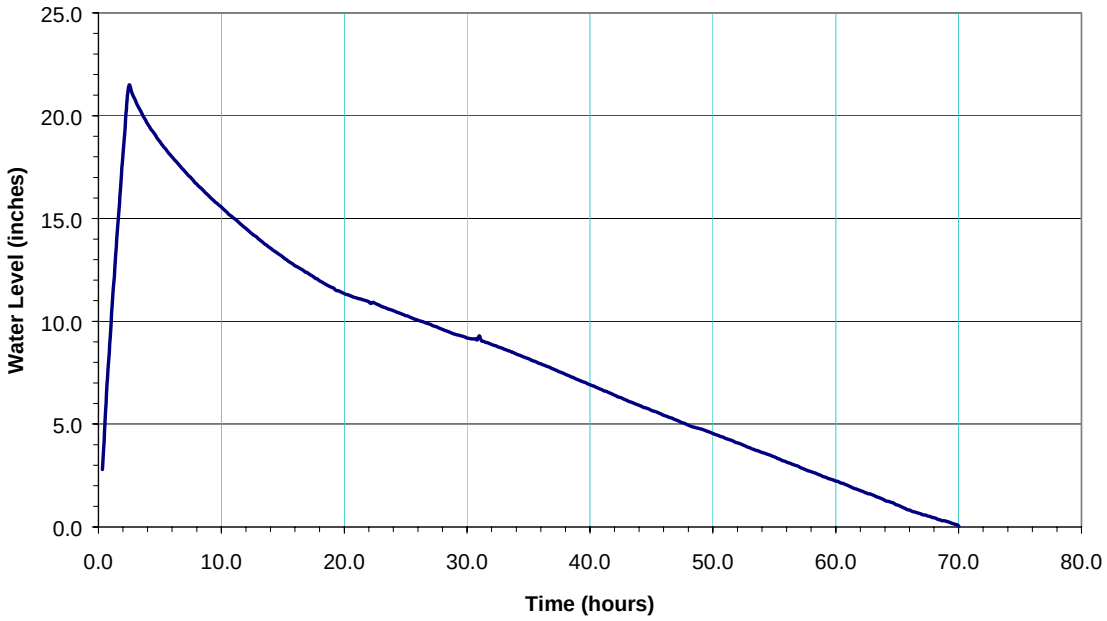

Figure 4.6 - Water levels during the full-scale test at the Clark County pond.

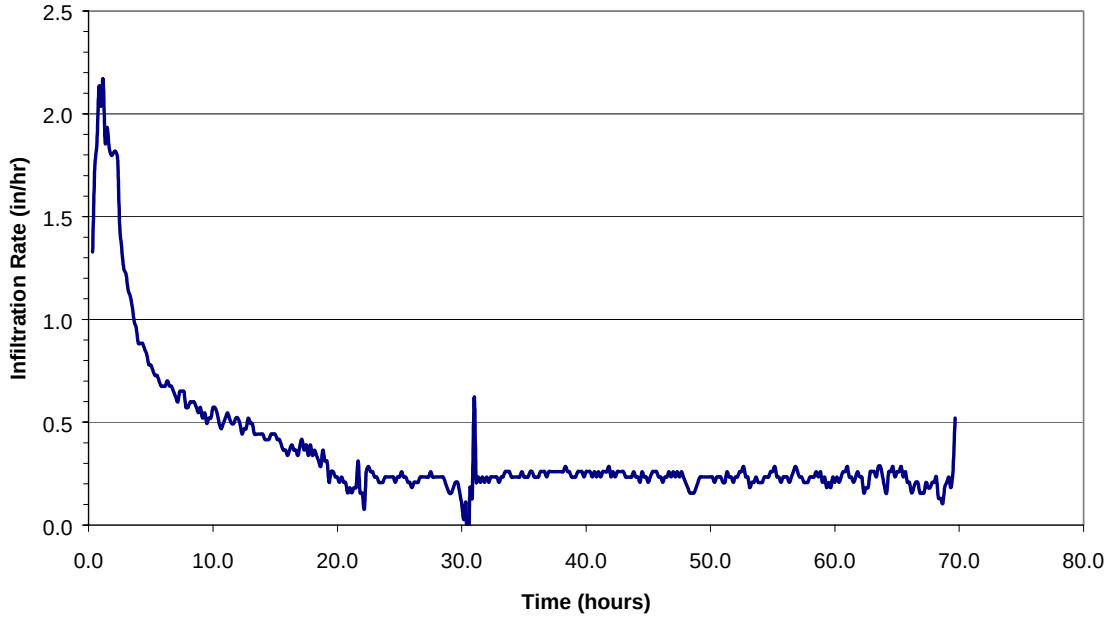

Figure 4.7 - Infiltration rate for Clark County averaged over 30-minute intervals.

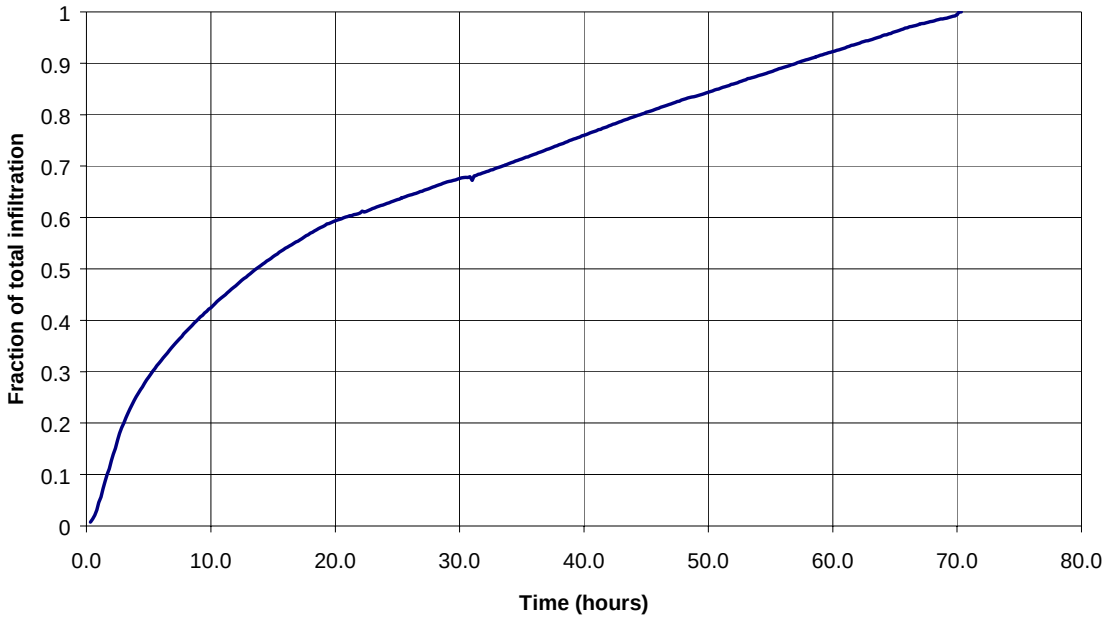

Figure 4.8 - Fraction of total inflow that had infiltrated as a function of time at the Clark County pond.

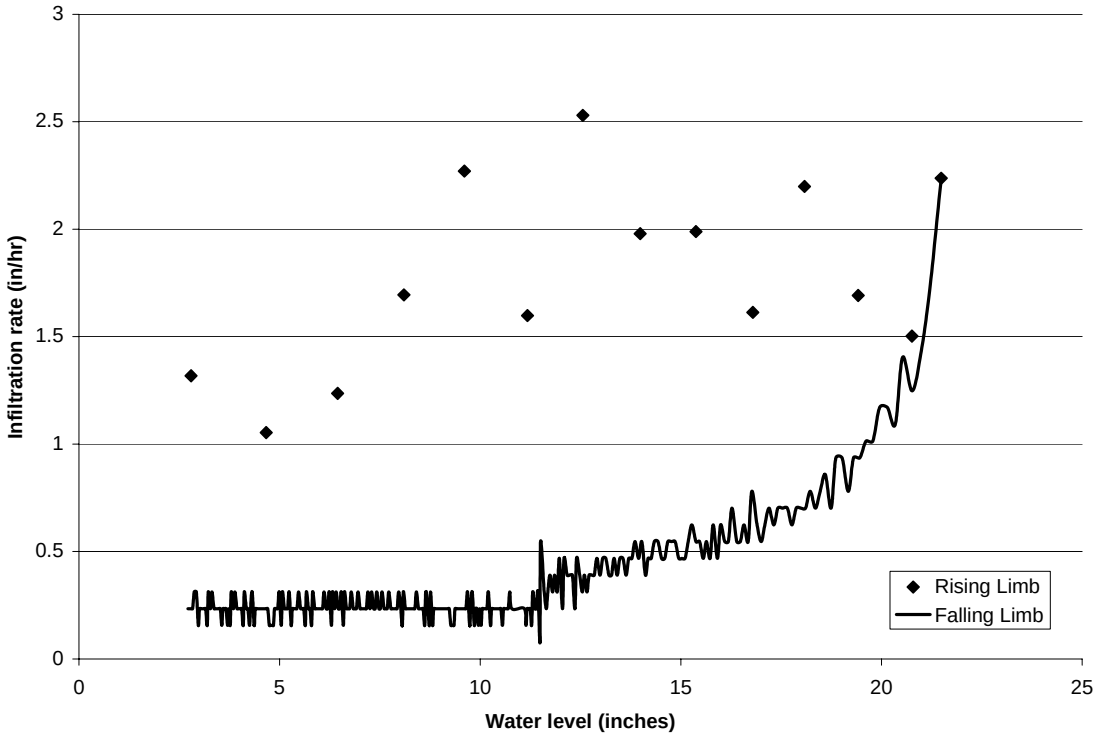

Figure 4.9- Infiltration rate versus water level for Clark County pond.

a) Filling - Equation (4.6) b) Draining - Equation (4.7)

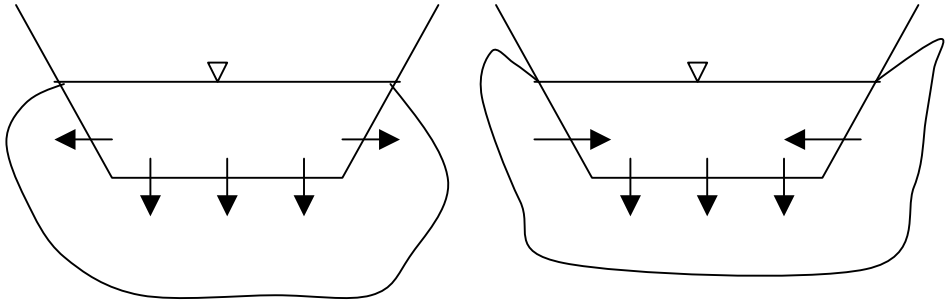

Figure 4.10 - Horizontal and vertical infiltration during the filling and draining stages.

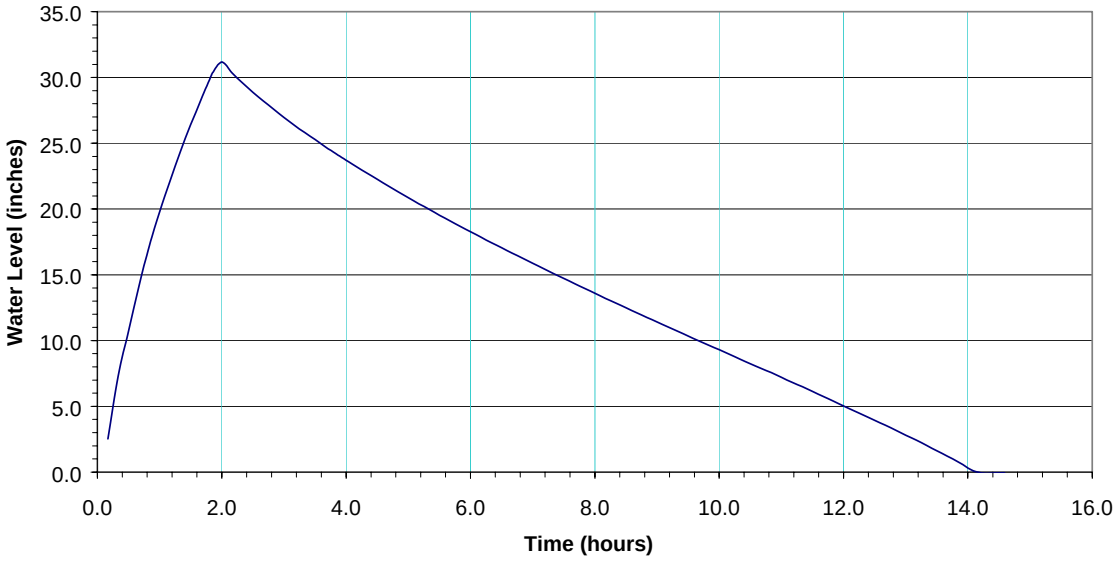

Figure 4.11 - Water levels during the full-scale test at the Balsam 7-11 pond.

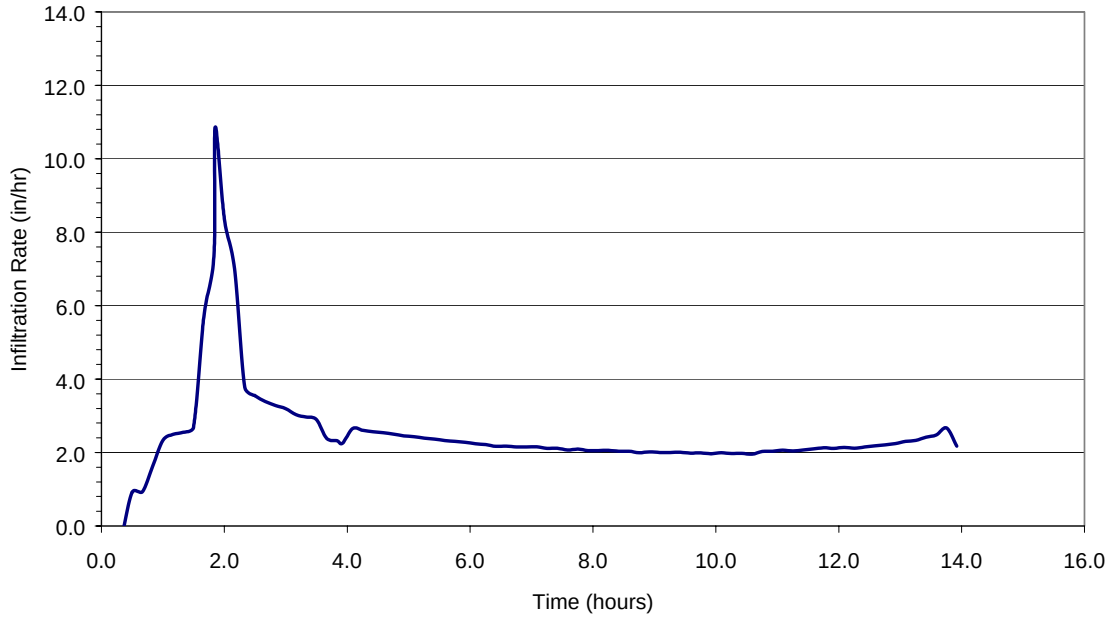

Figure 4.12 - Infiltration rate for Balsam 7-11 averaged over 30-minute intervals.

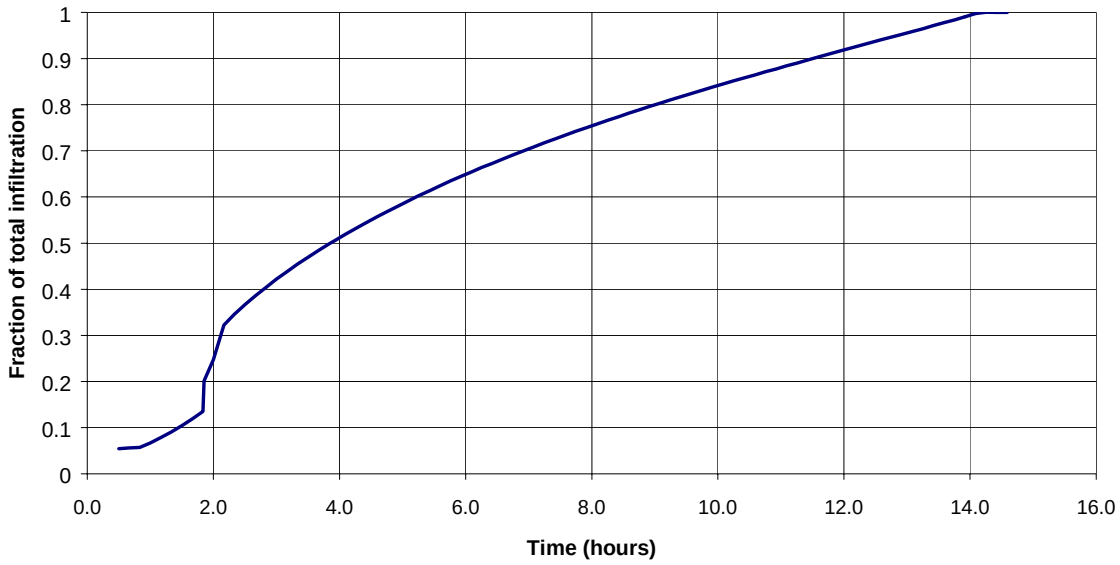

Figure 4.13 - Fraction of the total flow that had infiltrated as a function of time at the Balsam 7-11 pond.

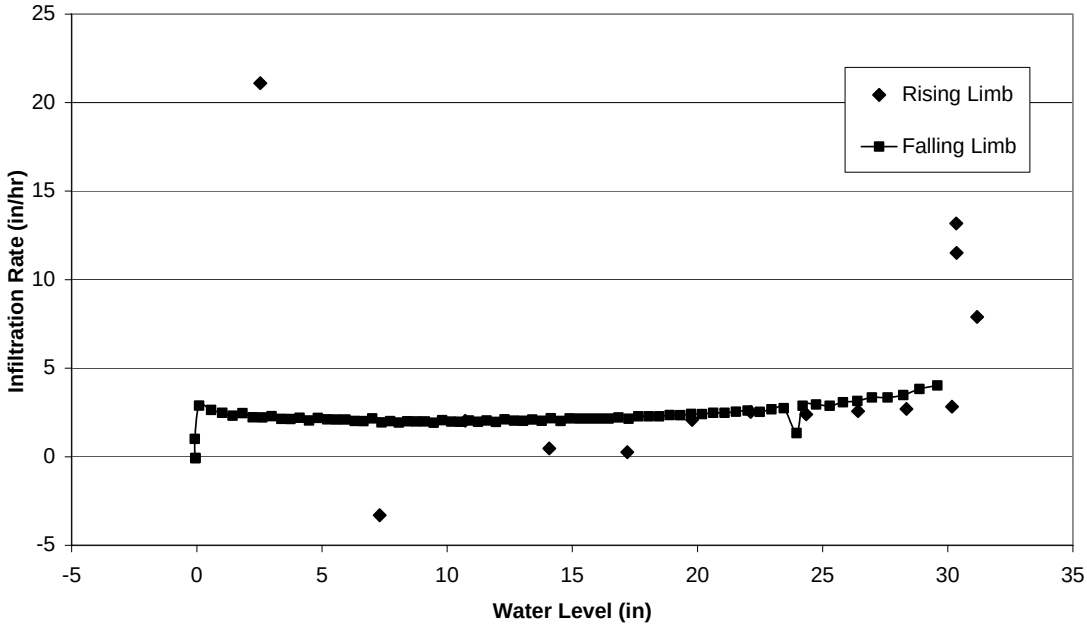

Figure 4.14 - Infiltration rate versus water level for Balsam 7-11 pond.

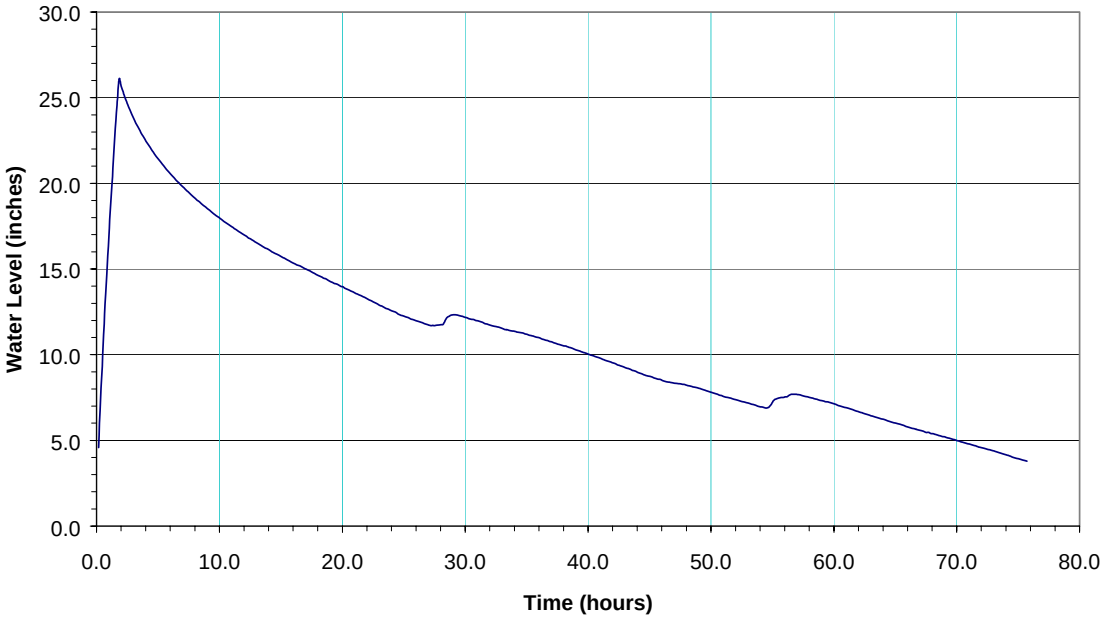

Figure 4.15 - Water levels during the full-scale test at the Krista Firs pond.

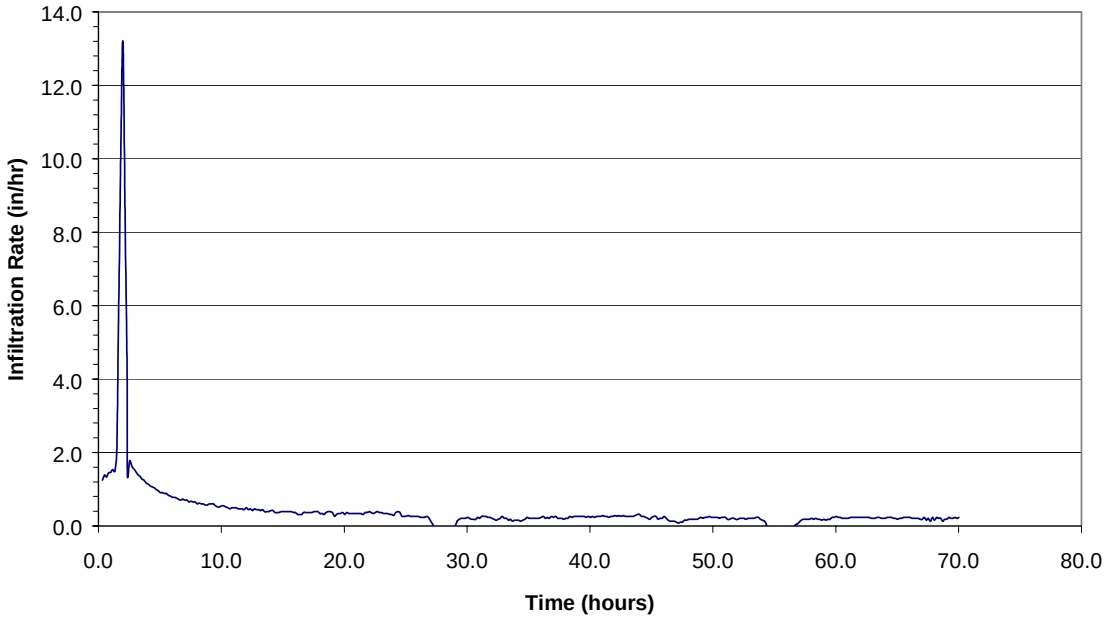

Figure 4.16 - Infiltration rate for Krista Firs averaged over 30-minute intervals.

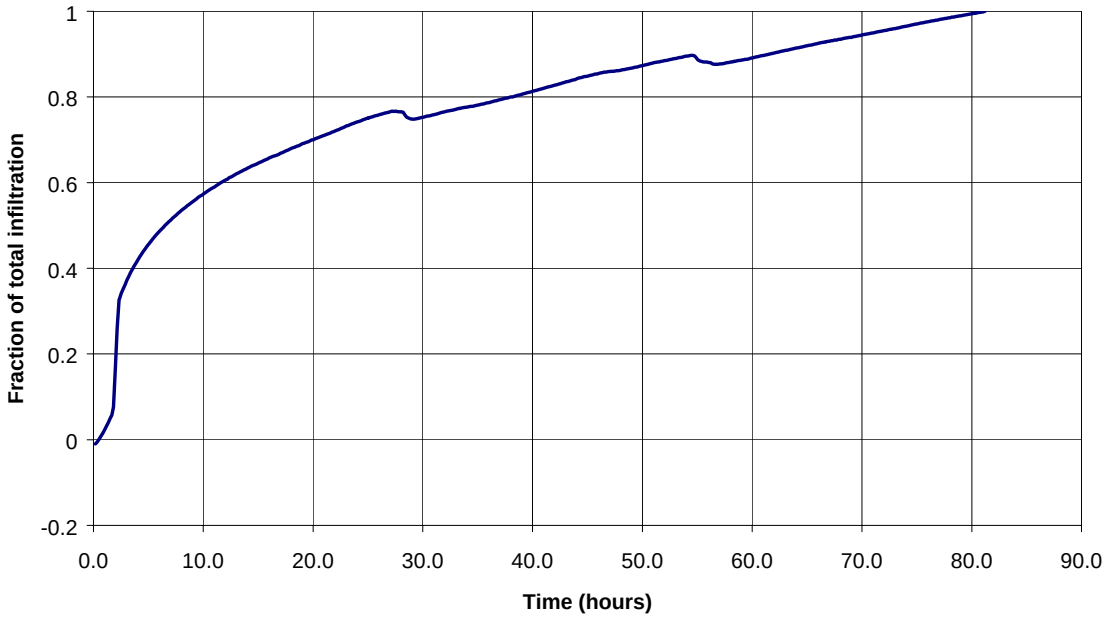

Figure 4.17- Fraction of total inflow that had infiltrated as a function of time at the Krista Firs pond.

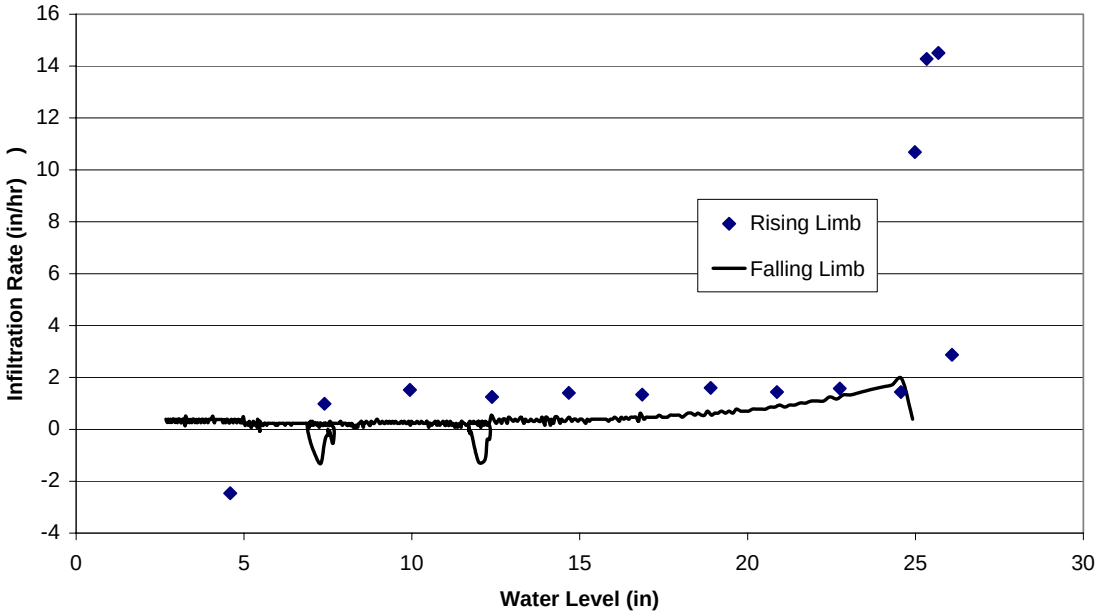

Figure 4.18 - Infiltration rate versus water level for Krista Firs pond.

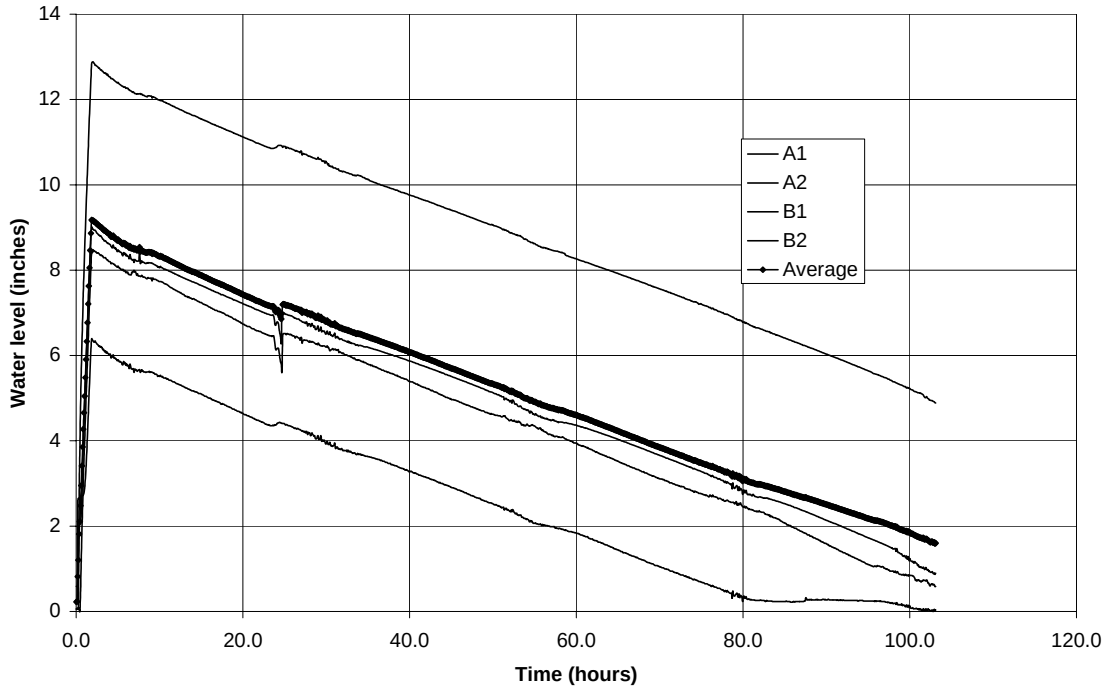

Figure 4.19 - Water levels during the full-scale test at the Cimarron pond.

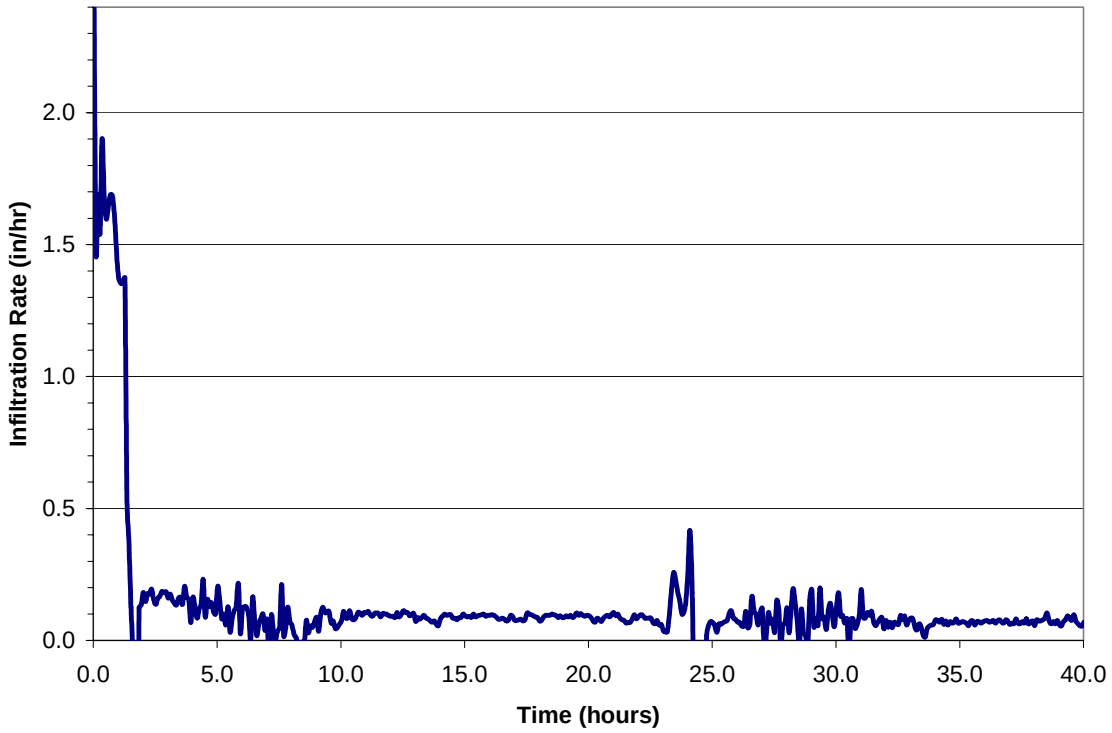

Figure 4.20 - Infiltration rate for Cimarron averaged over 30-minute intervals.

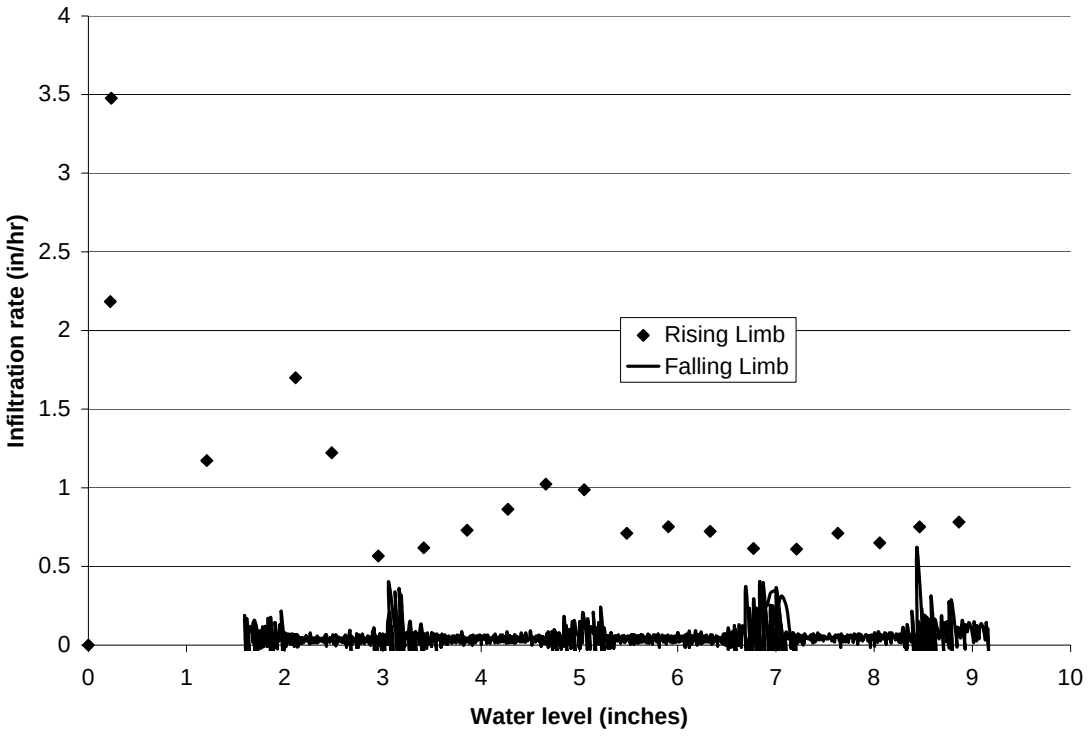

Figure 4.21 - Infiltration rate versus water level for Cimarron pond.

5 COMPARISON OF FIELD-SCALE INFILTRATION RATES WITH SMALL-SCALE, SATURATED HYDRAULIC CONDUCTIVITY VALUES

Saturated hydraulic conductivity estimated from measuring air conductivity, a regression equation derived from grain size parameters, and the Hazen formula were compared to full-scale infiltration rates calculated during this study and given in literature.

5.1 Analyses of Estimated Saturated Hydraulic Conductivity and Measured Full-Scale Infiltration Rates

Table 5.1 summarizes measured full-scale infiltration rates and estimated saturated hydraulic conductivity rates for 16 sites. Full-scale infiltration tests were calculated for four sites during this study (see Chapter 4). Full-scale monitored rates for the other 12 sites were taken from literature. The 16 sites are described more fully in Appendix D.

Column A in Table 5.1 includes a descriptor of how the full-scale tests were conducted. Two types of test were used. For the first type of test, denoted with "C" in Table 5.1, water levels in the ponds were measured continuously. The slope of this water level versus time curve is used to estimate the infiltration rate. For the second type of test, denoted with "S" in Table 5.1, a single "stage" measurement was collected for each infiltration event. This stage measurement represents the highest level of the water in the pond during a particular time interval between observations. In general, the specific date or time at which these levels reached their maximum values were not measured. With the stage measurement approach, infiltration rates can only be calculated by estimating when the water level reached its maximum value. The continuous measurements are obviously more reliable than the stage measurements.

The estimated saturated hydraulic conductivity values given in columns B, C, and D in Table 5.1 are derived from discrete soil samples collected from several depths at several different horizontal locations beneath each of the infiltration ponds. The number

of samples that were collected at each horizontal location was determined based upon field observations. The intent was to collect a sample from each discrete layer at each horizontal location. Table 5.2 gives an example of how the data from these multiple samples were combined to obtain a single "effective" or "equivalent" hydraulic conductivity estimate for each infiltration pond. Soil samples were collected at four different horizontal locations at the Springfield, Thurston County site. At three of these horizontal locations, samples were collected from three different layers. At the fourth location, samples were collected from only two different layers. Hydraulic conductivity values were estimated for each soil sample using the Hazen equation, the full regression equation, and laboratory measurements of air conductivity. The example included in Table 5.2 uses hydraulic conductivity estimates based on the Hazen equation. Hydraulic conductivity estimates from different layers at a single horizontal location were combined using the harmonic mean:

$$K_{equiv} = \frac{d}{\sum \frac{d_i}{K_i}} \qquad (5.1)$$

where d is the total depth of the soil column, d_i is the thickness of layer "i" in the soil column, and K_i is the saturated hydraulic conductivity of layer "i" in the soil column.

The harmonic mean given by equation 5.1 is the appropriate effective hydraulic conductivity for flow that is perpendicular to stratigraphic layers (Freeze and Cherry, 1979). For the Springfield site, these harmonic means range from 6 inches/hour for locations 1 and 4 to 12 inches/hour for location 3, as shown in the last column in Table 5.2. The harmonic means for each location are then averaged to obtain a single estimated hydraulic conductivity for each infiltration pond. This average is equal to 8.7 inches/hour for the Springfield site. The data used to estimate equivalent hydraulic conductivity values for other sites are given in Appendix E.

Table 5.3 compares the observed full-scale infiltration rates with estimates of saturated hydraulic conductivity developed using the log regression equation. The ratio included in Table 5.3 is the observed full-scale infiltration rate (column A in Table 5.2)

divided by the saturated hydraulic conductivity value from (column C in Table 5.2). In all cases, the observed infiltration rate is less than the estimated saturated hydraulic conductivity. In some cases, the observed infiltration rate is more than two orders of magnitude smaller than the estimated saturated hydraulic conductivity. Table 5.3 also includes a description of factors that may affect the full-scale infiltration rate and cause it to be lower than the estimated hydraulic conductivity value from grain size analyses or air conductivity values. These factors include biofouling, siltation, poor bottom vegetation, and low gradients due to high water tables. On average, for the sixteen sites included in Table 5.3, the average observed full-scale infiltration rate was approximately 50 times smaller than the average estimated saturated hydraulic conductivity value. In terms of hydraulic gradients, this relationship between observed infiltration rates and estimated hydraulic conductivity values suggests that the gradient term in the infiltration equation (Equation 1.1) may be significantly less than 1.0.

The data included in Table 5.3 are generally consistent with comparisons of full-scale infiltration rates and estimates from short-term, small scale infiltrometer tests, as illustrated in Figure 5.1. This figure compares measured, long-term infiltration rates with measured infiltrometer tests at sites included in Table 5.3. Recommended rates from the WDOE manual (WDOE, 2001) based on the d_{10} soil parameter are also included in Figure 5.1. These results show that full-scale rates are roughly 10 to 100 times smaller than the rates from infiltrometer tests, similar to what is described in Table 5.3. A proposed range of values based on maintenance and influent control is also included in Figure 5.1.

5.2 Limitations to Each Approach

The use of the air permeameter approach in a laboratory setting to estimate field-scale saturated hydraulic conductivity is limited by the disturbance of soil samples. The structure of the soil as it exists in the field is difficult, if not impossible, to reproduce for laboratory samples.

Non-uniform soil samples can result in voids in the air permeameter cylinder. These voids allow preferential pathways for the air to flow through and thus produce higher air conductivity estimates. In general, the shortcomings of this type of testing procedure arise from disturbed soil samples and non-uniform soil structure. Density, porosity, soil structure, and packing play a significant role in both water and air conductivity. When these parameters are mechanically altered, small-scale effects are lost.

There are limitations in determining infiltration based on soil texture as well. Although soil texture can provide good insight into the potential infiltration rate of a soil type, site-specific characteristics also influence the actual infiltration rate. Specific site characteristics that should be considered when infiltration potential is estimated include flow direction, heterogeneity of the soil formation, depth from the bottom of the pond to the water table, and impermeable surfaces in the subsoil. Soil texture alone does not incorporate these other factors. Another consideration is that infiltration rates of soils with the same textural classification can still differ because of structure and packing.

Table 5.1—Comparison of estimated saturated hydraulic conductivity and long-term full-scale infiltration rates.

Site	A. Long-term Full-scale (in/hr)	B. K_{equiv} Hazen (in/hr)	C. K_{equiv} Regression (in/hr)	D. K_{equiv} Lab K_s (in/hr)
Clark County Pond	0.23 (C1)	0.01	4	20
Beaverdam, King County	1.9 (C1)	350	390	180
Cimarron, King County	0.1 (C1)	51	46	c
Balsam 7-11, Kitsap County	2.1 (C1)	0.04	4	17
Krista Firs, Kitsap County	0.33 (C1)	36	55	204
Airdustrial, Thurston County[1]	1.7 (C2)	35	70	81
Bush, Thurston County[1]	>10 (S)	110	130	232
Echo Glen, Thurston County[1]	13.5 (S)	370	290	a
Lacey Lid, Thurston County[1]	0.3 (C2)	23	64	60
Margaret McKenny, Thurston County[1]	2 (C2)	43	63	145
Ridgeview, Thurston County[1]	>4 (S)	570	670	a
Springfield, Thurston County[1]	3 (C2)	9	32	14
State Farm, Thurston County[1]	7 (S)	45	73	83
Sweetbriar, Thurston County[1]	0.4 (C2)	37	78	28
Westwood Baptist, Thurston County[1]	1.0 (C2)	14	35	30
Wood Glen, Thurston County[1]	2.3 (C2)	56	84	104

[1] Data from Wiltsie, E., *Stormwater Facilities Performance Study, Infiltration Pond Testing and Data Evaluation*, Thurston County, Washington, August 10, 1998.

"a"—soil texture was too coarse to measure using the air permeameter method

"b"—the soil was too fine to determine a d_{10} value

"c"—Soil samples not available for lab tests

(C1) – Denotes estimates derived from continuous water level measurements during periods with known inflow.

(C2) – Denotes estimates derived from continuous water level measurements without direct measurements of inflow volumes.

(S) – Denotes estimates derived from single maximum stage measurement without direct measurements of inflow volumes.

Table 5.2 – Example calculations for equivalent hydraulic conductivity for the Springfield, Thurston County site using the Hazen approximation.

Layer	**Layer thickness (inches)**	**d_{10} (mm)**	**K_w (cm/s)**	**K_w (in/hr)**	**$K_{equivalent}$ (in/hr)**
1	13	0.05	2.2E-03	3	
1	8	0.08	5.6E-03	8	
1	10	0.18	2.8E-02	40	6
2	9	0.09	7.0E-03	10	
2	6	0.13	1.5E-02	21	
2	17	0.09	7.0E-03	10	11
3	14	0.07	4.3E-03	6	
3	8	0.54	2.5E-01	360	
3	7	0.23	4.6E-02	65	12
4	18	0.06	3.1E-03	4	
4	8	0.34	1.0E-01	143	6
Averages:				**61**	**8.7**

Table 5.3—Ratios of observed full-scale infiltration rates to saturated hydraulic conductivity estimated using the log regression equation (column C in Table 5.1)

Site	Ratio of observed full scale infiltration to estimated saturated hydraulic conductivity	Factors affecting Full-Scale Rate
Clark County Pond	0.058	Biofouling evident from dense patches of moss. Lateral flow noted.
Beaverdam, King County	0.005	Evidence of high water table. No continued maintenance.
Cimarron, King County	0.002	Obvious biofouling and possible groundwater mounding. No pre-treatment or continued maintenance
Balsam 7-11, Kitsap County	0.525	Sediment build-up had been recently removed prior to test. No pretreatment. Recent maintenance.
Krista Firs, Kitsap County	0.006	Biofouling - pond bottom has dense patches of moss. No pretreatment.
Airdustrial, Thurston County	0.024	Siltation and severe silt-fouling noted. Shallow groundwater noted. Poor vegetation noted.
Bush, Thurston County	>0.077	Periodic shallow groundwater noted. Poor bottom vegetation noted.
Echo Glen, Thurston County	0.047	Some localized plugging noted on pond bottom from fine-grained materials not included in lab samples. Good maintenance noted.
Lacey Lid, Thurston County	0.005	Obvious biofouling with moss. Groundwater mounding noted ("bottom very close to seasonal high groundwater water level") Poor bottom vegetation noted.
Margaret McKenny, Thurston Co.	0.032	Fouling due to moss and silt noted. Intermittent groundwater mounding. Poor bottom vegetation noted.
Ridgeview, Thurston County	>0.006	Ratio is likely much less than 150. No ponding was observed in any storms. Poor maintenance noted.
Springfield, Thurston County	0.094	Groundwater mound observed. Initial infiltration rate (15 in/hr) approximately 5 times larger than final rate (3 in/hr). No pretreatment.

Table 5.3—continued.

Site	Ratio of full scale observed infiltration to estimated saturated hydraulic conductivity	Factors affecting Full-Scale Rate
State Farm, Thurston County	0.096	Biofouling prior to full scale tests. Earlier tests suggest biofouling has reduced full-scale rate by a factor of 3. No pretreatment.
Sweetbriar, Thurston County	0.005	Groundwater mounding observed. No pretreatment. Silt fouling noted. Poor vegetation noted.
Westwood Baptist, Thurston Co.	0.029	Shallow groundwater and low-permeability till layer (< 6 ft) under portions of facility
Wood Glen, Thurston County	0.027	Periodic groundwater mounding noted. Moss-covered bottom and poor vegetation cover noted. No pretreatment.
Average	**0.07**	

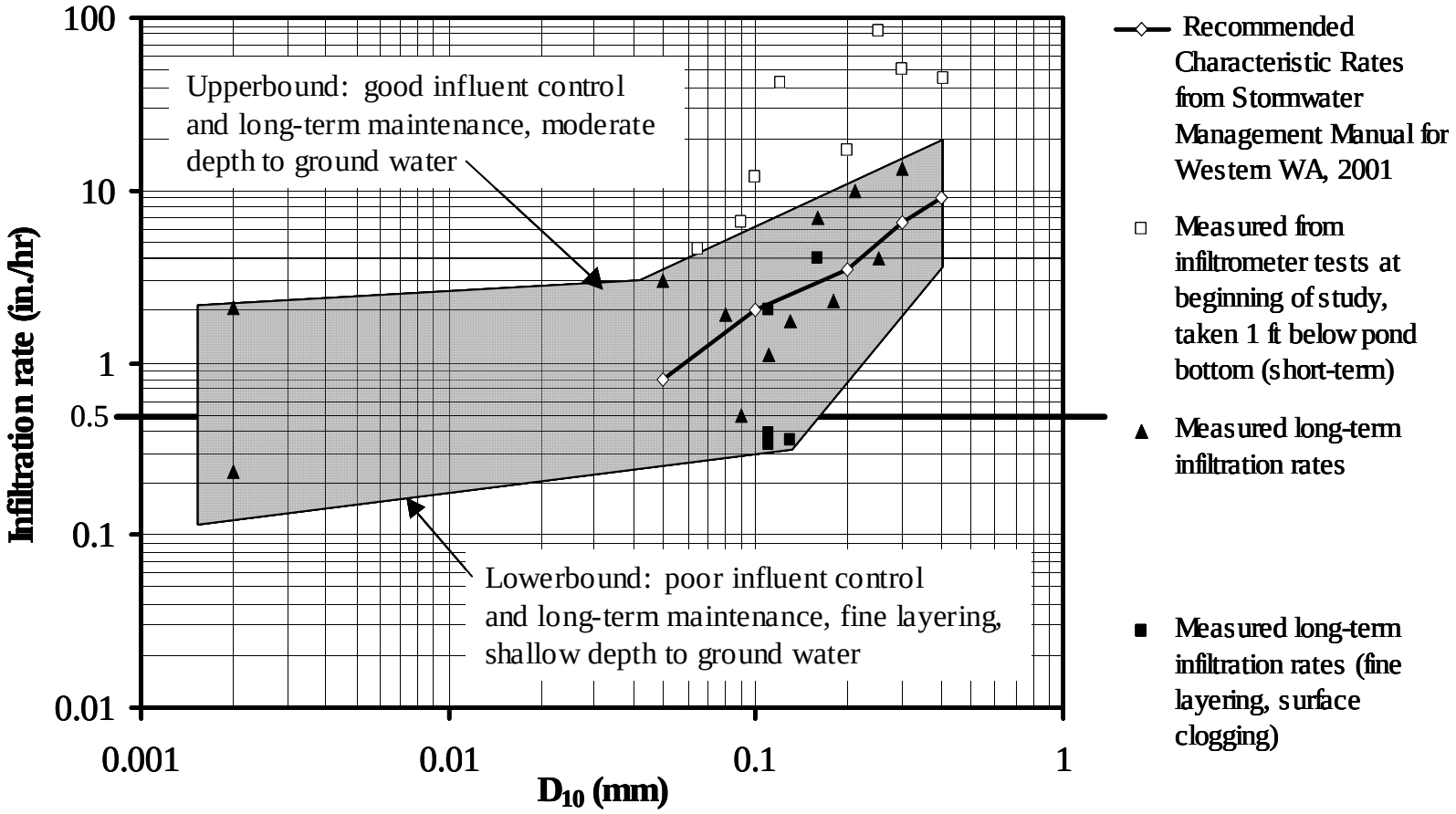

Figure 5.1 – Comparison of small scale, short-term infiltrometer tests with long-term, full-scale observations.

6 VALIDATION OF BASE MODEL ASSUMPTIONS

Results from a steady-state saturated flow model were compared to results from a transient unsaturated model to evaluate errors that are introduced when a simplified, steady-state, saturated model is used to simulate flow from infiltration ponds. Sections 6.1 and 6.2 describe the two model types used in the comparison, and sections 6.3 and 6.4 quantify and discuss the error introduced by steady-state, saturated flow assumptions.

6.1 Description of Saturated and Unsaturated Flow Models

6.1.1 Saturated Flow Model

The groundwater flow model MODFLOW was used for the steady-state saturated flow simulations (McDonald and Harbaugh, 1988). This finite difference model simulates saturated flow in three dimensions. Because the unsaturated transient model described below was a 2-dimensional model, the third dimension in MODFLOW was not used. Figure 6.1 is a cross-sectional view of the model domain and the applied boundary conditions for the simplified infiltration facility used in the comparison study. The geometry of the facility was similar to a trench in terms of width (3 feet or 1 meter). This geometry was necessary because of limitations on spatial resolution associated with the unsaturated model, as described below. However, this geometry also emphasized the differences between the saturated and unsaturated flow models, which was the goal of the simulations described in this section. The trench or pond was located in the upper left-hand corner to take advantage of symmetry. To simplify the comparison, the water level in the pond was set to 1.6 ft (0.5 meters) above the pond bottom by specifying a constant head boundary condition within the pond.

The boundary conditions are shown in Figure 6.1. The left boundary acted as a no-flow boundary because of symmetry. The bottom boundary was treated as impervious and is representative of a deep low-permeability layer. Because of the depth of the model (145 feet) and the relatively high permeability of more shallow layers, this bottom boundary does not significantly affect near-surface hydraulic gradients or infiltration from the simulated facilities. Outflow from the domain was allowed along

the right hand boundary below the water table. As of result of the boundary conditions, water that left the pond flowed down to the water table and out below the water table. The depth to the water table from the pond floor was 3 meters, typical for infiltration ponds in Western Washington.

Table 6.1 lists all of the model parameters used for the saturated model. Three values for saturated hydraulic conductivity were used in the evaluations to represent a range of values typically found beneath infiltration ponds. The model output gave water table location and the flow exiting the pond. The infiltration rate for the pond was solved for by dividing the flow by the wetted perimeter of the pond.

6.1.2 Unsaturated Flow Model

The 2-dimensional saturated-unsaturated finite-difference model VS2DH 3.0 was used for the transient unsaturated flow model simulations (Hsieh et al., 2000). The unsaturated hydraulic characteristics were represented by the van Genuchten equation (van Genuchten, 1980):

$$\theta = \frac{\theta_s - \theta_r}{[1 + (\alpha|\psi|)^{\beta}]^{1-\frac{1}{\beta}}} \qquad (6.1)$$

Where θ is the volumetric moisture content (dimensionless), θ_r is the residual moisture content (dimensionless), θ_s is the saturated moisture content (dimensionless), ψ is the suction head (L), α is the van Genuchten alpha parameter (L^{-1}), and β is the van Genuchten beta parameter (dimensionless).

Figure 6.2 is a cross-section view of the model domain and applied boundary conditions. Table 6.2 lists the parameters used in the Van Genuchten equation. Hydrostatic equilibrium was assumed for the initial condition. The initial condition was a flat water table with dry soil above the water table and around the pond (as shown in Figure 6.2). The transient simulations were run for 30 hours. As an example of the model output,

Figure 6.3 shows the advance of the wetting front in a medium sand at three different times.

The transient unsaturated flow model is more complicated to use than the steady-state saturated flow model. The unsaturated forms of the governing equations are highly nonlinear and are difficult to solve numerically (Anderson and Woessner, 1992). Also, the additional relationships that must be specified in unsaturated flow modeling, such as between hydraulic conductivity and pressure head, are very sensitive to small changes in moisture content. This sensitivity causes instabilities to develop during the numerical solution. Using small nodal spacing (on the order of inches or centimeters) and small times steps (on the order of seconds) can minimize these instabilities but requires long computational times. VS2D only allows 85,000 nodes, which prohibits modeling a large region when centimeter-scale grid spacing is required.

6.2 Comparison of Infiltration Rates

The evaluation of the steady-state, saturated flow assumption is separated into two distinct discussions. The first discussion considers errors in assuming that the infiltration exiting the pond has reached steady-state. The second discussion considers the assumption of saturated flow. In evaluating these assumptions, the two numerical models presented above were used to compare calculated infiltration rates exiting the infiltration pond in both models. For each unique situation, both models simulated flow using the same boundary conditions, hydraulic parameters, and model dimensions.

6.2.1 Steady-State vs. Transient

Two scenarios were developed to examine how quickly the flow from an infiltration pond will reach steady-state and how the infiltration rate depends on the proximity of the constant head boundary condition to the pond. The length from the center of the pond to the outer edge of the constant head boundary was set to 10 and 50 meters (33 and 165 feet) for the first and second scenarios, respectively. Figures 6.4 and 6.5 show the infiltration rate versus time for both models when the hydraulic conductivity of the soil was 34 in/hour (0.024 cm/s). The main difference between these two results

was the decrease in the steady-state saturated flow infiltration rate as the boundary was moved farther away from the pond. However, in the transient simulation, the wetting front did not migrate fast enough with low permeable soils for the boundary condition to affect the infiltration rate within the time assumed in the analysis.

In scenario 1, the transient model reached a steady infiltration rate after approximately 5 hours. This quick response occurred because the wetting front reached the boundary condition, which set the gradient. When the boundaries were extended to a distance of 165 feet (50 meters) in the second scenario, the infiltration rates decreased to a value close to a different steady-state infiltration rate. This trend would continue as the distance to the boundary was increased, until the boundary conditions were distant enough that they would not affect the wetting front migration in the transient simulation. Figures 6.6 through 6.9 show the infiltration rate versus time in both scenarios for two additional hydraulic conductivities. For these lower permeable units, the transient simulations were identical for both scenarios since the water did not flow fast enough to be influenced by the boundary conditions within the 30-hour time period. The steady-state saturated simulations, however, produced different infiltration rates because the location of the boundary will always affect the infiltration rate at steady-state.

A small kink in the curve develops at around 3 hours in both figures 6.6 and 6.7. At this time, the wetting front reached the water table and caused the infiltration rate to drop at a quicker rate. If the water table had been farther from the bottom of the infiltration pond, the infiltration rate would not have shown this sudden decrease. The same kink can also be seen in figures 6.8 and 6.9 after 9 hours of infiltration. It is also present in figures 6.4 and 6.5; however, because the wetting front moved through the subsurface so quickly, it occurs before only 1 hour of infiltration.

6.2.2 Saturated vs. Unsaturated

In addition to modeling under the assumption of steady-state flow, the assumption of saturated flow instead of unsaturated flow must be evaluated. In Figure 6.4, it is clear that the transient simulation had reached a steady infiltration rate after 5 hours because

there were no changes in the rate for over 25 hours. Therefore, the differences between the infiltration rates of the saturated and unsaturated models had to all be due to differences in modeling the two types of flow. To quantify the difference in infiltration rates that occur when a saturated flow model versus an unsaturated flow model is used, additional simulations were run. The previous simulations (figures 6.6 to 6.9) could not be used because a steady infiltration rate was not attained. Two additional simulations were performed to determine the difference present at the lower hydraulic conductivity values of 3.4 in/hr (0.0024 cm/s) and 1.1 in/hr (0.00081 cm/s). In these additional simulations, the distance to the constant-head boundary was reduced to 13 feet (4 meters) to allow the transient models to reach a steady infiltration rate. Figures 6.10 and 6.11 give the results of using the smaller model domain. In both cases, a steady infiltration rate was achieved within the time period modeled. The differences between the two values resulted from modeling a saturated or unsaturated flow model. The difference between the saturated and unsaturated flow models was lowest in highly permeable soils and increased as the hydraulic conductivity of the soil decreased. Table 6.3 shows that the error in the final steady-state infiltration rate varied from 19 to 36 percent over a range of hydraulic conductivities typically found beneath infiltration ponds in Western Washington.

6.3 Validity of the Steady-State Saturated Flow Assumption

The results of the model comparison suggest that, under certain hydraulic conditions, the errors introduced by assuming steady-state saturated flow may be acceptable for simulating flow from infiltration ponds. In permeable materials with shallow water tables, the system will reach steady-state within a relatively short amount of time, and differences between saturated flow and unsaturated flow will be low. Conversely, when ponds are constructed at sites in lower permeability materials, the errors in the steady-state saturated flow model results may be large. It is important to note, however, that the results from the steady-state saturated flow simulations always give conservative estimates of infiltration rates because infiltration rates calculated under these assumptions are always less than transient unsaturated flow infiltration rate estimates. Additionally, the relative relationships that are established in the evaluation

that follows will still hold true. The absolute values of infiltration will have large errors for systems with low permeable soils.

In very general terms, assumptions regarding saturated, steady-state systems will result in errors for infiltration rates that are larger than a factor of 1 or 2 but less than an order of magnitude. The errors will be largest for sites with relatively deep groundwater tables in high-permeability sites (where the infiltration does not cause significant groundwater mounding), and for infiltration events that occur early in the wet season when soils tend to be relatively dry. The steady-state, saturated assumption will provide reasonable approximations for systems with shallow water tables and for sites with long wet seasons.

Errors in the steady-state saturated assumptions should be considered relative to errors introduced by characterization and generalization of aquifer properties and by the enforcement of boundary conditions. There is significant uncertainty in any hydraulic conductivity estimate, which can vary over an order of magnitude from one point to another. Also, treating the boundary conditions for the models as constant head introduces error because uncertainty is associated with the water table level.

Table 6.1—Modeling parameters

Texture Class (Unified Soil Classification)	**Total Porosity***	**Residual Moisture Content (θ_r)***	**Saturated Hydraulic Conductivity**	
			(cm/s)	**(in/hr)**
Medium SAND	0.375	0.02	$2.4x10^{-2}$	34
Fine SAND	0.377	0.075	$2.4x10^{-3}$	3.4
Sandy SILT	0.496	0.15	$8.1x10^{-4}$	1.1

* Parameters only necessary in unsaturated model

Table 6.2 — Parameters used for Van Genuchten Equation

Texture Class (Unified Soil Classification)	**α (cm^{-1})**	**α (in^{-1})**	**β (dimensionless)**
Medium SAND	4.31	10.9	3.1
Fine SAND	1.04	2.64	6.9
Sandy SILT	0.847	2.15	4.8

Table 6.3 — Infiltration Rate Errors between Unsaturated and Saturated Model Results

Texture Class (Unified Soil Classification)	**Infiltration Rate Error between Saturated and Unsaturated Model (%)**
Medium SAND	19%
Fine SAND	32%
Sandy SILT	36%

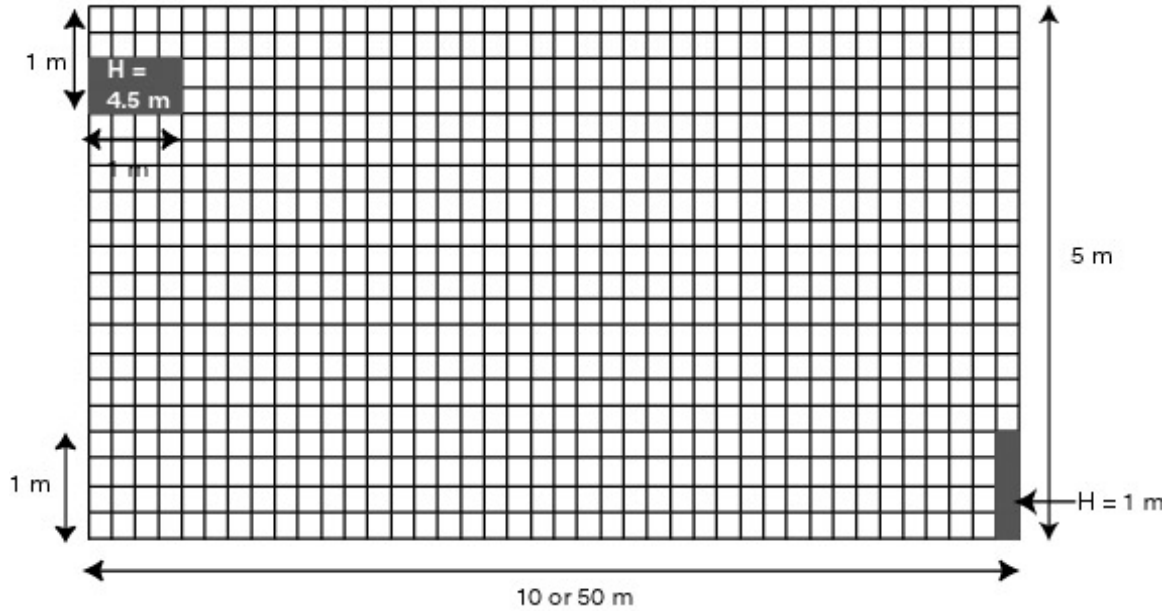

Figure 6.1—Cross-section view of steady-state saturated flow model used in comparison study

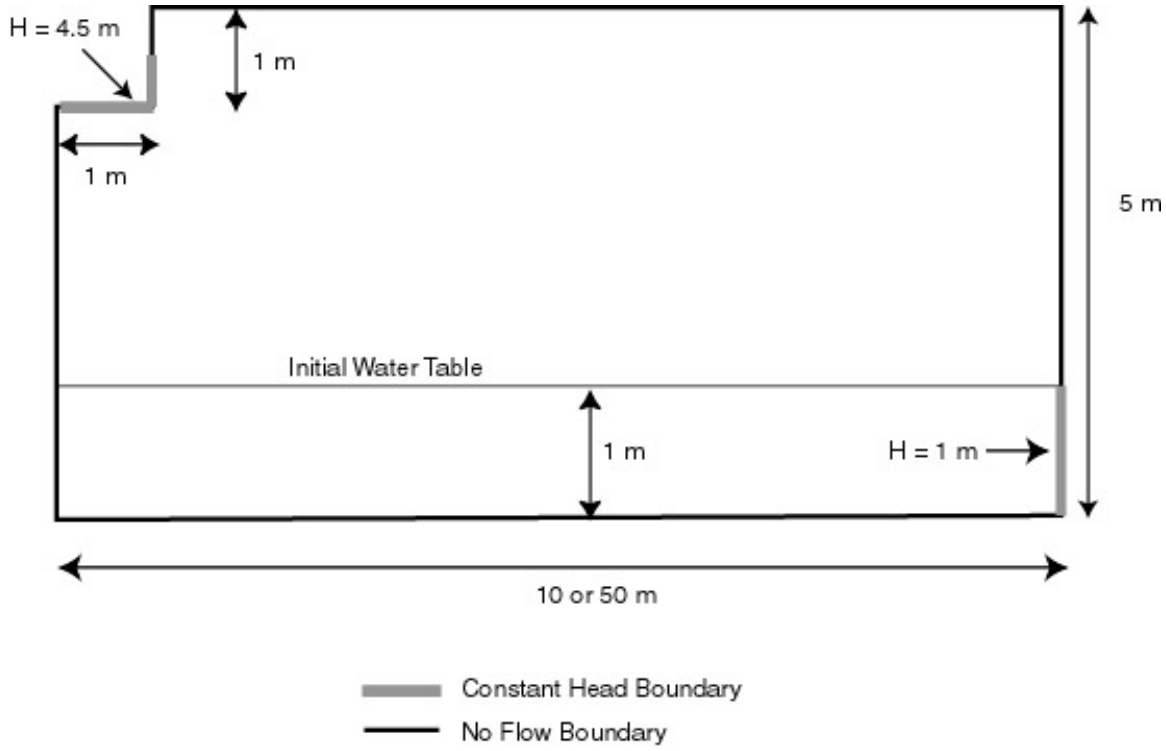

Figure 6.2—Cross-section view of transient unsaturated flow model used in comparison study

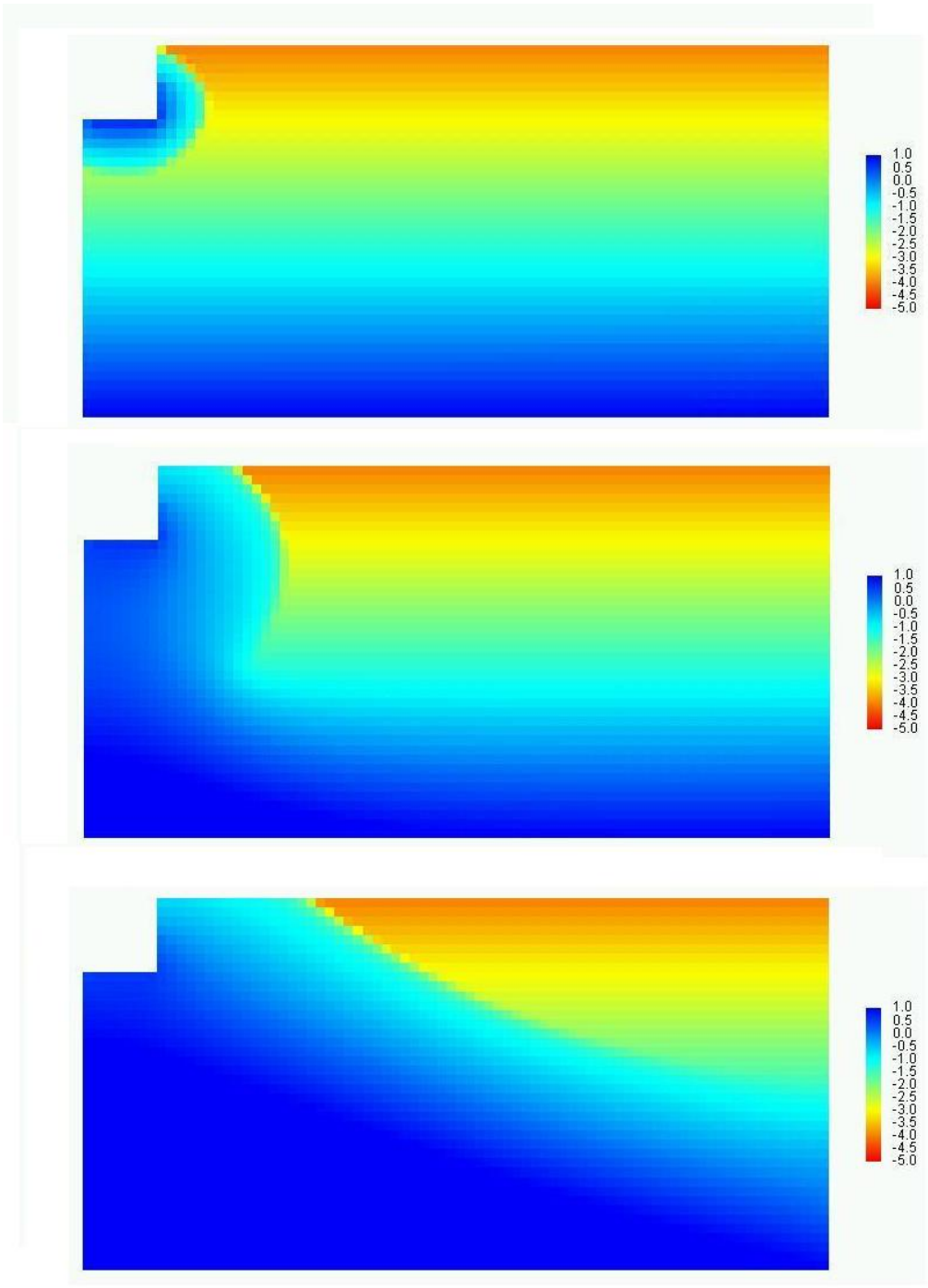

Figure 6.3—Pressure head contour map showing the advance of the wetting front at t = 0.024, 0.4, and 2.3 hours (legend units in meters)

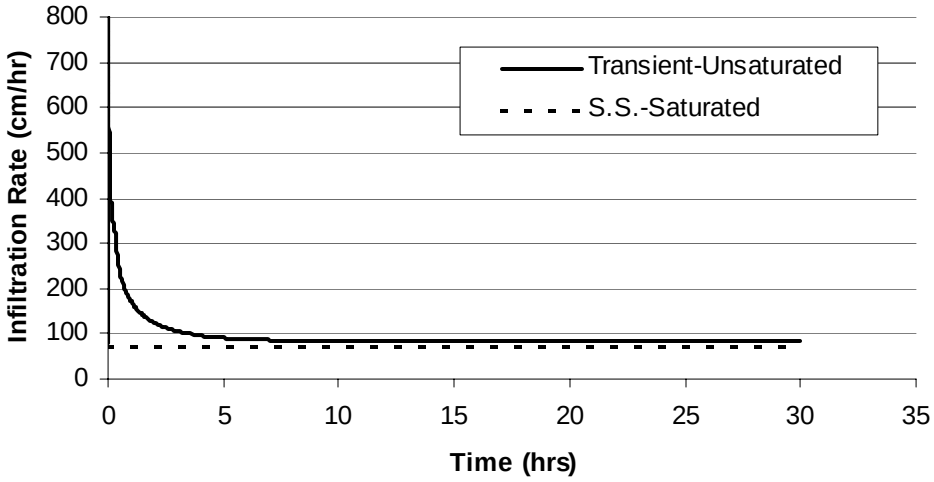

Figure 6.4—Infiltration rate versus time for K = 34 in/hr (0.024 cm/s) in Scenario 1

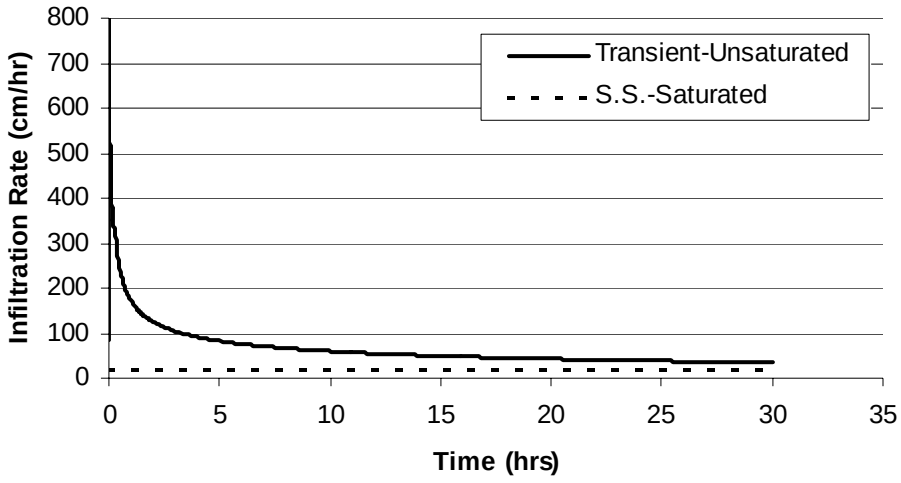

Figure 6.5—Infiltration rate versus time for K = 34 in/hr (0.024 cm/s) in Scenario 2

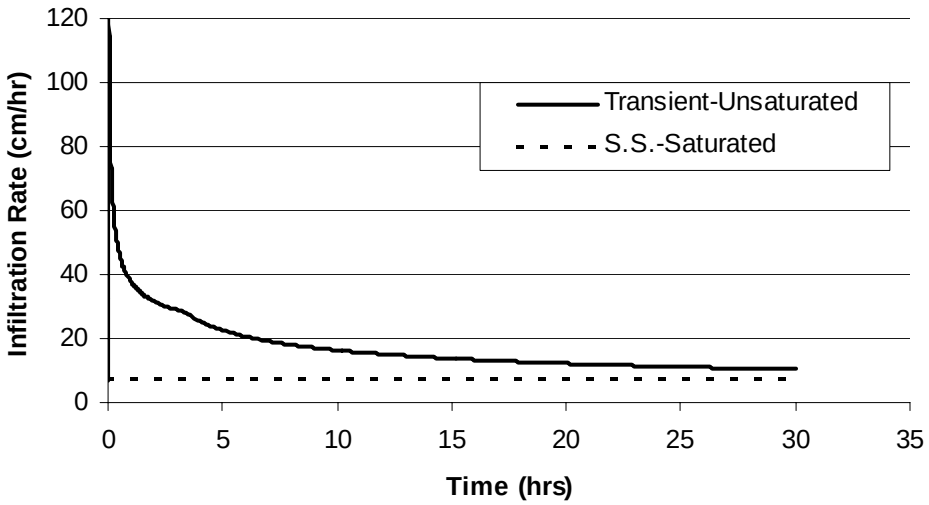

Figure 6.6—Infiltration rate versus time for K = 3.4 in/hr (0.0024 cm/s) in Scenario 1

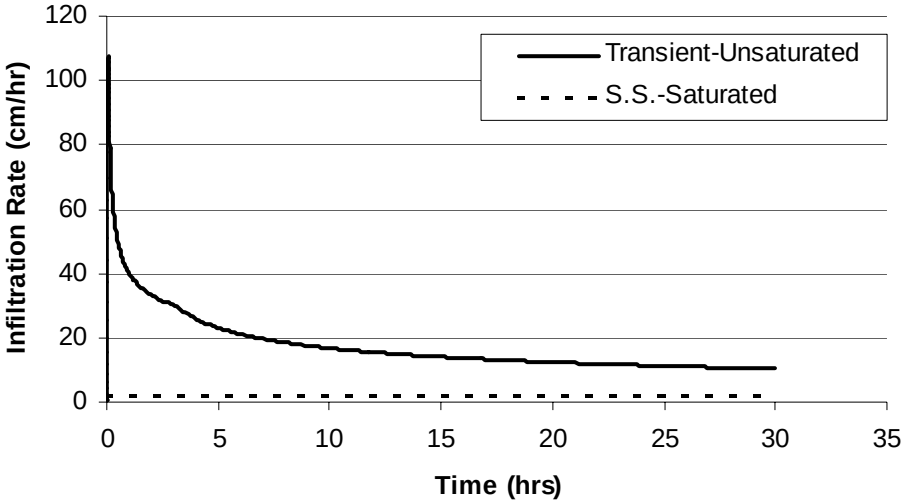

Figure 6.7—Infiltration rate versus time for K = 3.4 in/hr (0.0024 cm/s) in Scenario 2

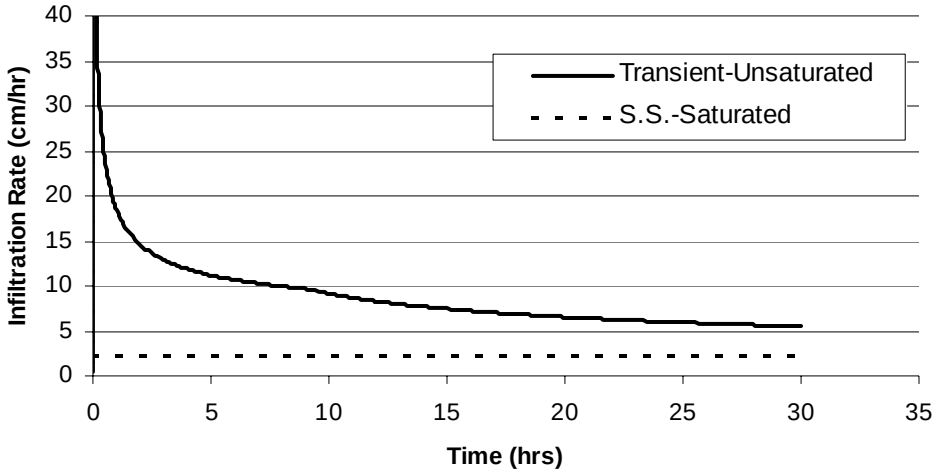

Figure 6.8—Infiltration rate versus time for K = 1.1 in/hr (0.00081 cm/s) in Scenario 1

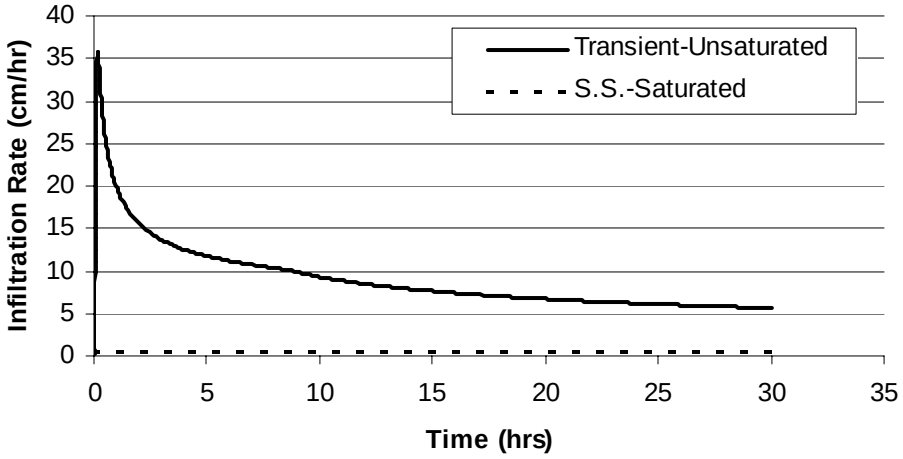

Figure 6.9—Infiltration rate versus time for K = 1.1 in/hr (0.00081 cm/s) in Scenario 2

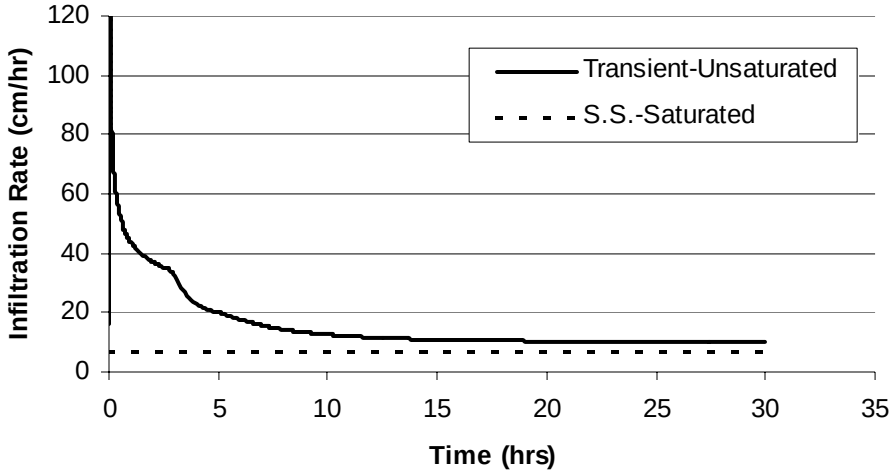

Figure 6.10—Infiltration rate versus time for K = 3.4 in/hr (0.0024 cm/s) in small model

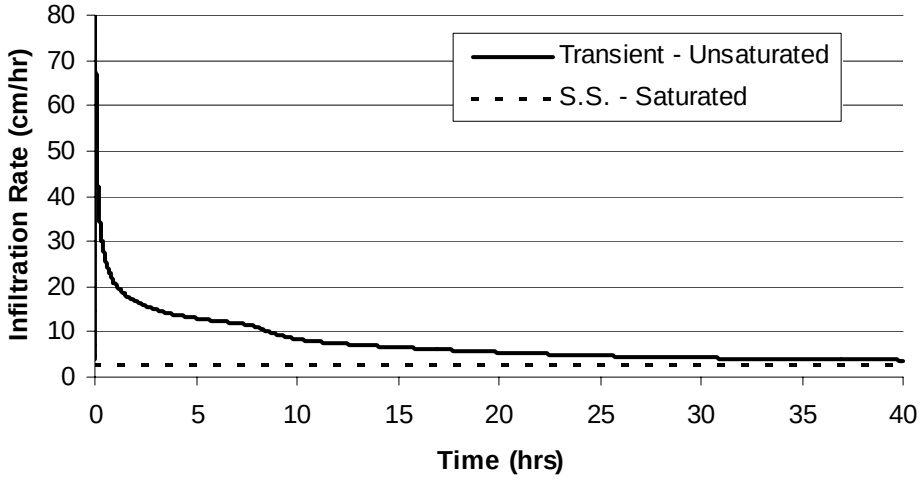

Figure 6.11—Infiltration rate versus time for K = 1.1 in/hr (0.00081 cm/s) in small model

7 EVALUATION OF INFILTRATION POND PERFORMANCE

In this section, 3-dimensional, steady-state, saturated flow model simulations are used to examine the influence of different parameters on the overall effectiveness of infiltration ponds. A base model of the Lacey-Lid infiltration pond in Thurston County, Washington, is presented; the effect of site-specific parameters on infiltration rates are examined; and the benefits of possible design modifications are considered. Finally, model simulations are used to examine hydraulic gradients beneath infiltration ponds.

7.1 Thurston County Base Model Description

A base model of a "typical" pond was developed in MODFLOW to evaluate different design alternatives. This model was loosely based on the geometry and observed geology beneath the Lacey-Lid infiltration pond in Thurston County, Wash. (see Figure 7.1) as described in the *Water Resources Investigations Report 92-4109* (Drost et al., 1999). The 3-dimensional grid representing the pond covered an area of 5100 ft by 5000 ft (1555 m by 1524 m). The pond was located in the center of the model domain, had an area of 120 by 240 ft (36.6 by 73.2 m), and was 5 ft (1.5 m deep). The elevation at the bottom of the model was set at 0 ft, and the top of the model was set at 145 ft (44.2 m).

The model is divided into five fields that represent regions with distinct hydrogeologic properties. Table 7.1 describes the hydraulic parameters used in the base model. Figure 7.2 is a cross-section view through the center of the pond showing the location of each field.

The hydraulic parameters in these fields were changed to test the sensitivity of the pond to different conditions. For example, when a gravel bed beneath the pond was simulated, the hydraulic conductivity of field 5 was increased to a value consistent with gravel.

7.1.1 Boundary-Conditions

A no-flow boundary was enforced along the perimeter of the layers above the regional water table. The layers beneath the water table had a constant head boundary equal to the elevation of the water table. The confining unit (layer 30) had a no-flow boundary along the perimeter. The perimeter around the bottom layer had a constant head boundary that was equal to 3 ft (0.91 m) less than the water table elevation. The water level in the pond was set to 5 ft (1.5 m) above the pond bottom by specifying a constant head of 140 ft (44.2 m). The hydraulic gradient between the upper unconfined unit and the lower confined unit remained for all of the simulations. A recharge rate of 12 in/yr (30.5 cm/yr) was applied to the surface of the entire model to reduce the effects of the boundary conditions to the flow field.

7.1.2 Grid

The model contained 86 rows, 86 columns, and 31 layers. The dimensions of the rows and columns ranged from 2 ft (0.6 meters) to 150 ft (45.7 m). The finest row and column spacing existed around the perimeter of the infiltration pond and was required to accurately simulate lateral flow. The grid spacing gradually increased away from the pond to a maximum value of 150 ft (45.7 m). The rows and columns along the model perimeter had a dimension of 30 ft (9.1 m). Figure 7.3 shows a plan view of the grid spacing with a blow-up around the edge of the infiltration pond. The layers were most thin beneath the pond and above the water table. The top 25 layers were each 1-ft (0.3-m) thick. The next three layers were 2-ft (0.6-m) thick. The lowest three layers had thicknesses of 40, 30, and 50 ft (12.2, 9.2, and 15.2 m), respectively.

7.2 Evaluations of Hydraulic Gradients Beneath Infiltration Ponds

7.2.1 Importance of Hydraulic Gradients in Infiltration Pond Performance

As discussed in Section 1, the design of an infiltration pond requires an accurate estimation of the hydraulic gradient. Some design approaches found in the literature (Ferguson, 1994; Stahre and Urbonas, 1990) recommend using a constant vertical hydraulic gradient of 1.0. This assumption makes the infiltration rate equal to the hydraulic conductivity of the subsurface material. Unfortunately, this simplified method,

which is common practice, does not account for the possibility of hydraulic gradients being less than 1.0. If a hydraulic gradient of 1.0 is used in the design process, the pond size may be undersized. Prolonged gradients of less than 1.0 will cause flooding from the infiltration pond since the pond will only have been designed to store all the water from the appropriate design storm. Conversely, a cost is also associated with underestimating the hydraulic gradient. This will result in land being used for an infiltration pond that could have been used for other purposes.

7.2.2 Gradient Changes in Transient Unsaturated Flow Model

The transient unsaturated flow model introduced in section 6.2 was used to monitor the time evolution of the hydraulic gradient beneath an infiltration pond for different soil types during a 30-hour recharge period. Darcy's law was used to solve for the hydraulic gradient at each time step. Since the flow leaving the pond at each time step is known, the hydraulic gradient can be solved for:

$$i = \frac{Q}{A \cdot K} \qquad (7.1)$$

where *i* is the hydraulic gradient (L/L), A is the area of the wetted perimeter (L^2), and *K* is the hydraulic conductivity of the material beneath the pond (L/T). The wetted area of the pond is defined as bottom area plus the depth of water in the pond times the perimeter length. This assumes that the walls of the pond are vertical and the bottom is horizontal.

Figure 7.5 is a graph of the hydraulic gradients beneath a pond over time for a sandy soil (K=34 in/hr or 2.4×10^{-2} cm/s) and shows how the hydraulic gradient decreases to below 1.0 after only 2 hours of infiltration. Figures 7.6 and 7.7 show the same time series for a fine sand and sandy loam with hydraulic conductivities of 3.4 and 1.1 in/hr (2.4×10^{-3} and 8.1×10^{-4} cm/s), respectively. The hydraulic gradient of the pond in Figure 7.6 decreases to below one after 17 hours, whereas the hydraulic gradient in Figure 7.7 remains greater than 1.0 within the 30-hour period.

These results demonstrate that, in highly permeable soils, assuming a hydraulic gradient of 1.0 is not conservative. Conversely, in low permeable soils, assuming a

hydraulic gradient of 1.0 may be conservative. In the sections that follow, steady-state models are used to estimate infiltration rates and gradients in the vicinity of infiltration ponds and trenches. The results shown in Figures 7.5 through 7.7 should be considered when evaluated these estimates. The steady-state calculations will generally be conservative because they result in the lowest gradients, as shown in Figures 7.5 through 7.7.

7.3 Factors in Pond Performance

7.3.1 Water Table Elevation and Lateral Flow

A series of simulations were performed to quantify the change in the infiltration rate that occurs from water table fluctuation and to determine the amount of lateral flow from infiltration ponds. Figure 7.4 is a cross-section view of the model through the pond, giving an example of the model output. The white area beneath the infiltration facility in Figure 7.4 denotes the saturated portion of the water table aquifer. This figure shows the water table mound that forms beneath the infiltration facility at steady-state conditions. This mound, which is formed in all simulations described in this chapter, controls the rate of infiltration. Table 7.2 gives the model infiltration rates and percentage of water leaving the sides and bottom of the pond for pairs of water table elevations and hydraulic conductivities. Model simulations were run with water table elevations of between 120 and 140 ft (36.6 and 39.6 m). These elevations correspond to groundwater depths between 0 and 20 feet, measured relative to the bottom of the pond. Hydraulic conductivity values ranged from 1.5 in hr to 150 in/hr (0.001 to 0.11 cm/s). This range corresponds to typical values for sites that are considered for infiltration facilities (Ferguson, 1994).

The substantial decrease in infiltration rate that occurs when the depth to groundwater decreases emphasizes the importance of understanding regional water table variations at a proposed infiltration site. If, for example, a PIT is performed in the summer when regional water table elevations are low, the measured infiltration rate could be twice the rate that would be observed in the winter when the water table levels rise.

Changes in water table elevation have little effect on the percentage of the flow that occurs through the sides of the infiltration pond. Under all the conditions modeled, there was a slight increase in the lateral flow as the water table approached the pond bottom, but nearly one-third of the flow from the infiltration pond left through the sides.

7.3.2 Confining Unit

Table 7.3 summarizes the changes in infiltration rate due to variations in the hydraulic conductivity of the confining unit (Field 2). The percentage of change in infiltration rate was calculated between the base model case and the values listed in Table 7.3. These changes were the greatest when the hydraulic conductivity was reduced from the base value of 5 in/hr to 0.05 in/hr (0.0035 to 3.5 x 10^{-5} cm/s).

7.3.3 Anisotropy

The effects that anisotropy have on the infiltration rate are shown in Table 7.4. Simulations were done under isotropic conditions and then compared to systems that had ratios of 3:1 and 10:1 between the horizontal and vertical hydraulic conductivity. These ratios of anisotropy are typical of natural systems. The hydraulic conductivity in the horizontal remained the same, and the vertical value was reduced to obtain the appropriate ratio. These results show that, as expected, decreasing the vertical hydraulic conductivity will reduce the infiltration rate out the bottom of the pond dramatically. The increase in the amount of water exiting the sides of the pond is not enough to maintain previous levels of infiltration, which causes a decrease in the overall infiltration out of the pond.

7.3.4 Water Level in the Pond

The sensitivity to the water level in the pond was investigated by changing the constant head boundary in Field 3 (the inside of the pond) to represent lower levels of water in the pond. The results of Table 7.5 suggest that the decrease in the total infiltration rate that accompanies lowering the water level in a pond is a result of a decrease in the amount of lateral flow. The amount of water that exited the bottom of the pond was similar for all pond depths.

7.3.5 Pond Geometry

Table 7.6 shows infiltration rate variations resulting from changes in the pond geometry. For all the ponds the area of the footprint, the depth of the pond, and the water level in the pond were the same. The aspect ratio included in Table 7.6 is defined as the ratio of the pond length to the pond width. Figure 7.8 is a plot of the relative infiltration rate versus aspect ratio. (Relative infiltration rate is defined as the ratio of the infiltration rate divided by the infiltration rate for a pond with the same size but with an aspect ratio of 1.0. This relative infiltration rate can also be considered a "correction factor" that is used to estimate infiltration rates for ponds with aspect ratios different from 1.0, as described below.) Figure 7.8 illustrates that the infiltration rate increases approximately linearly as a pond becomes more elongate. The increase in the infiltration rate can be attributed to the increase in the lateral flow that occurs as the pond perimeter increases.

The data presented in Table 7.6 and Figure 7.8 can be used to develop a correction factor to account for the effects of aspect ratio. The infiltration rate for a pond with an aspect ratio greater than 1.0 can be estimated by multiplying the correction factor times the infiltration rate for a pond with an aspect ratio equal to 1.0. This approach is discussed in more detail in Chapter 8. The following equation can be used to describe the results included in Table 7.6 and Figure 7.8:

$$CF_{aspect} = 0.02A_{ratio} + 0.98 \qquad (7.2)$$

where A_{ratio} is the aspect ratio for the pond (length/width) and CF_{aspect} is the correction factor for ponds with aspect ratios greater than 1.0. Equation 7.2 should not be used for ponds with aspect ratios greater than approximately 20.

Table 7.7 illustrates the effects of pond size on hydraulic gradients. Hydraulic gradients are calculated from infiltration rates using Equation (7.1). The results in Table 7.7 show that the gradient decreases as the pond size or area increases. Correction factors for pond area can be developed using an approach analogous to the correction

factors for aspect ratio described in the previous paragraph. The correction for pond size, CF_{size}, is given by the following expression:

$$CF_{size} = 0.73(A_{pond})^{-0.76} \quad (7.3)$$

where

CF_{size} = correction factor for size of the pond

A_{pond} = area of the pond bottom in acres

This expression for correction factor was developed for ponds with bottom areas between 0.6 and 6 acres in size. Figure 7.9 shows the relationship between Equation (7.3) and the calculated correction factor based on computer simulations. (The correction factor calculated using computer simulations is obtained by taking the ratio of the gradient calculated for a larger pond to the gradient calculated using a smaller pond with the same aspect ratio.) For small ponds (ponds with area equal to 2/3 acre), the correction factor is equal to 1.0. For large ponds (ponds with area equal to 6 acres), the correction factor is 0.2.

7.3.6 Effects of Thickness of Subsurface Layers

The stratigraphy or subsurface layering that was assumed for the base case simulations is described in Figure 7.2. This base case was developed assuming the bottom or base of the groundwater flow system is 145 feet beneath the ground surface. Additional simulations were developed to investigate the effects of a thicker sequence of subsurface layers. The vertical dimensions of the layers shown in Figure 7.2 were doubled to evaluate these effects. The base of the model was kept at elevation zero, but the top of the lower aquifer (Field 4 in Figure 7.2) was increased from elevation 50 feet to elevation 100 feet, the top of the confining unit (Field 3 in Figure 7.2) was increased from elevation 80 feet to elevation 160 feet, and the ground surface was increased from elevation 145 feet to elevation 290 feet. The depth of the pond was also doubled, from 5 feet to 10 feet.

The results of the simulations for the deeper groundwater flow system are included in Table 7.8. The first four rows in Table 7.8 give gradients for a small pond (0.66 acres) with the deep system. The last four rows consider a large pond (6.0 acres) with the deep system. These results will be used in Chapter 8 to evaluate the validity of regression equations that relate gradient to pond size, depth to groundwater, and depth of water in the pond.

7.3.7 Design Alternatives

7.3.7.1 Gravel Base

A series of simulations were run to quantify changes in infiltration rate due to replacement of the natural soil beneath a pond with a gravel material. Table 7.9 summarizes the changes in infiltration rates that resulted from the addition of 3 ft (0.9 m) of highly permeable material beneath the footprint of the infiltration pond. The range of hydraulic conductivity tested represented typical values for gravel material (Fetter, 1994). The increase in the total infiltration rate ranged from 0.8 percent to 1.8 percent for all the water table elevations considered. While the amount of flow out the bottom of the pond increased substantially, this was counteracted by a decrease in the amount of lateral flow, which resulted in an insignificant increase in total infiltration rate.

7.3.7.2 Gravel Column Modification

A gravel column with a high hydraulic conductivity was simulated from the pond bottom down to an elevation of 116 ft (35.4 m) (4 ft or 1.2 meters below the regional groundwater elevation). The column was 10 ft by 10 ft (3 by 3 m) in area and had a hydraulic conductivity of 50,000 in/hr (35.3 cm/s). The addition of the column increased the infiltration rate from 6.97 to 6.98 in/hr (17.69 to 17.72 cm/hr). This insignificant change indicates that adding a gravel column will not affect a pond's performance during steady-state saturated conditions. The small effect is due to the hydraulic gradient term. Adding a gravel chimney has little impact if no significant hydraulic gradient exists to drive groundwater flow.

The major caveat to these results is that they were determined under the assumption of steady-state saturated flow. Results reported in Section 6.3 demonstrated that the error in these assumptions varies according to the subsurface properties, but in general they are small in comparison to errors introduced in the characterization and generalization of subsurface aquifer parameters and enforcement of boundary conditions.

7.4 Evaluations of Infiltration from Trenches

Infiltration from unlined trenches was simulated using the same general model as was used for the infiltration pond simulations described in previous sections. The infiltration trench was simulated using the same flow field geometry, hydraulic conductivity distributions, and boundary conditions shown in Figures 7.2 through 7.4. The only difference between the pond simulations and the trench simulations was the length of the facility. For the infiltration trench, the facility was assumed to extend the full length of the flow field so that the flow system was effectively a two-dimensional, vertical cross section.

The "base-case" simulation for the infiltration trench assumed a trench with a depth of 2 feet (0.61 m.) and with side slopes of 1V:2H. The water level in the trench was assumed to be 2 feet deep (elevation = 145 feet or 44.2 m.) and the water table was assumed to be at elevation 120 feet (36.6 m), as shown in Figure 7.2. The base case hydraulic conductivity values were the same as the base case for the pond simulations, as summarized in Table 7.1.

Table 7.10 summarizes the results of simulated infiltration rates from trenches as a function of water elevation. For the base case scenario, with a water table 25 feet below the ground surface (23 feet or 7 m below the bottom of the trench), the infiltration rate is approximately 12.7 in/hr (32 cm/hr). The effective hydraulic gradient given in Table 7.10 is defined as the ratio of the infiltration rate to the saturated hydraulic conductivity for field 1, which is the upper layer in the flow field. These results show that the effective gradient is approximately equal to the depth to the water table in feet, divided by 100. Between 25% and 30% of the infiltration leaves the trench in a

horizontal direction. The fraction of horizontal flow increases as the depth to the water table decreases, as would be expected.

Table 7.11 summarizes the results of sensitivity studies for a variety of factors that affect the performance of infiltration trenches. The results in Table 7.11 are similar to the results shown earlier for infiltration ponds.

One important effect on pond performance is the clogging due to siltation or biofouling. Table 7.12 illustrates the simulated reduction in infiltration that occurs if a 2-inch (5-cm) thick layer beneath an infiltration trench becomes clogged so that the its hydraulic conductivity is reduced by a factor of 50 ("moderate" clogging) or 350 ("high" clogging). Column "B" in Table 7.12 gives the effective or equivalent vertical hydraulic conductivity values calculated using Equation 5.1 assuming 23 feet to the water table with a hydraulic conductivity of 50 in/hr. The two-inch layer of low-permeability material at the pond bottom reduces the effective hydraulic conductivity to 37 in/hr for a 50:1 reduction and to 14 in/hr for a 350:1 reduction. However, the infiltration rates and gradients do not change proportionally, as shown in columns D and E. This is because of the effects of lateral flow. Reductions in vertical flow from the bottom of the trench are offset by increases in lateral flow, particularly for trenches with deeper water levels, as shown in Column F. Because the reduction in permeability only occur along the trench bottom, flow that leaves the trench laterally will move vertically through the unimpacted soils adjacent to the trench.

The impacts of clogging on infiltration will become more important as the ratio of bottom area to side area increases (e.g. for ponds instead o trenches.) Table 7.12 suggests that the higher water levels that occur in more narrow trenches with steeper side slopes will be impacted less by clogging than flatter trenches with shallow water. This is because there will be less horizontal flow from the trenches with shallow water.

Table 7.1—Descriptions and hydraulic parameters for each field

Field	Description	Hydraulic Conductivity (in/hr)	Porosity
1	Region around and below the infiltration pond, but above the confining unit	50	0.21
2	Simulates a confining unit between the upper unconfined aquifer and the lower confined aquifer	5	0.21
3	The inside of the pond that simulates no aquifer matrix; The depth is 5 feet and it cuts across 5 layers.	n.a.	1
4	Simulates a confined aquifer	50	0.21
5	3 feet directly beneath the footprint of the infiltration pond	50	0.21

Table 7.2—Infiltration rates and gradient for different water table depths below pond bottom

Depth of Water Table (ft)	Hydraulic conductivity beneath facility (in/hr)	Infiltration Rate (in/hr)	Calculated Gradient	Percent of Total Infiltration	
				Bottom	Sides
20	1.5	0.3	0.200	69	31
	2.5	0.4	0.160		
	5	0.7	0.140		
	25	3.6	0.144		
	50*	7.0	0.140		
	150	19.4	0.129		
15	1.5	0.2	0.133	68	32
	2.5	0.3	0.120		
	5	0.6	0.120		
	25	3.0	0.120		
	50	5.8	0.116		
	150	16.2	0.108		
10	1.5	0.1	0.067	67	33
	2.5	0.2	0.080		
	5	0.4	0.080		
	25	2.3	0.092		
	50	4.5	0.090		
	150	12.8	0.085		
5	1.5	0.08	0.053	66	34
	2.5	0.1	0.040		
	5	0.3	0.060		
	25	1.6	0.064		
	50	3.2	0.064		
	150	9.1	0.061		
0	1.5	0.01	0.007	66	34
	2.5	0.04	0.016		
	25	0.9	0.036		
	50	1.8	0.036		
	150	5.2	0.035		

* Base Model Case

Table 7.3—Effect of confining unit on infiltration rates and gradients for different water table depths below pond bottom

Depth of Water Table (ft)	Hydraulic Conductivity in Field 2 (in/hr)	Infiltration Rate (in/hr)	Calculated Gradient	Percent Change in Infiltration Rate		
				Total	Bottom	Sides
20	0.05	4.8	0.10	-45	-53	-24
	1.5	6.4	0.13	-9	-11	-10
	5	7.0	0.14	--	--	--
	15	7.6	0.15	+8	+10	+4
15	0.05	4.0	0.08	-44	-51	-24
	5	5.3	0.11	-9	-11	-5
	15	6.3	0.13	+8	+10	+4
10	0.05	3.1	0.06	-44	-50	-24
	5	4.2	0.08	-9	-10	-5
	15	4.9	0.10	+8	+9	+4

Table 7.4—Changes in infiltration rates caused by anisotropy

Ratio of Horizontal to Vertical Hydraulic Conductivity	Change in Infiltration Rate (%)		
	Total	Bottom	Sides
1:1	--	--	--
3:1	-23	-26	+14
10:1	-74	-86	+34

Table 7.5—Changes in infiltration rates caused by varying water depths in pond

Depth of Water in Pond (ft)	Change in Infiltration Rate (%)		
	Total	Bottom	Sides
5	--	--	--
4	-8	-0.78	-22
3	-11	-0.84	-30
2	-17	-1.78	-43

Table 7.6—Infiltration rates for different pond aspect ratios

Aspect ratio	Pond Perimeter (ft)	Pond Dimensions (ft x ft)	Infiltration Rate (in/hr)	Correction factor for aspect ratio*	Flow out sides (%)
1	680	170 x 170	6.9	1.0	30.7
2	720	120 x 240	7.0	1.02	31.4
8	1080	480 x 60	8.0	1.16	35.5

*Correction factor given by Equation 7.2

Table 7.7—Infiltration rates for different pond areas

Hydraulic conductivity beneath facility (in/hr)	Pond Area (acres)	Pond Dimensions (ft x ft)	Calculated Gradient	Correction factor for pond area from model	Correction factor for pond area from regression*
5	0.66	120x240	0.16	1.00	1.00
5	1.49	180x360	0.09	0.54	0.54
5	2.64	240x480	0.06	0.35	0.35
5	5.95	360x720	0.03	0.18	0.19
50	0.66	120x240	0.14	1.00	1.00
50	1.49	180x360	0.08	0.54	0.54
50	2.64	240x480	0.05	0.35	0.35
50	5.95	360x720	0.03	0.19	0.19

*Regression equation given by Equation 7.3

Table 7.8—Effect of changes in subsurface geometry and pond size on gradients

K (in/hr)	Subsurface geometry	Pond size (ft x ft)	Water table depth + depth of pond	Calculated Gradient
5	Deep	120x240	30	0.172
50	Deep	120x240	30	0.137
5	Deep	120x240	60	0.344
50	Deep	120x240	60	0.273
5	Deep	360x720	30	0.033
50	Deep	360x720	30	0.026
5	Deep	360x720	60	0.065
50	Deep	360x720	60	0.052

Table 7.9—Infiltration rate changes due to addition of gravel base

Depth of Water Table (ft)	Hydraulic Conductivity of Field 5 (in/hr)	Change in Infiltration Rate (%)		
		Total	Bottom	Sides
20	125	+0.8	+5.7	-10.8
	500	+1.5	+12.7	-27.0
	1250	+1.8	+15.7	-34.7
25	125	+0.8	+5.8	-10.6
	500	+1.5	+13.0	-26.9
	1250	+1.8	+16.0	-34.7
10	125	+0.8	+5.9	-10.6
	500	+1.4	+13.2	-26.7
	1250	+1.7	+16.3	-34.3

Table 7.10—Infiltration rates from trenches for different water table elevations

Water table elevation (ft)	Water table depth (ft)	Infiltration rate (in/hr)	Calculated Gradient	Horizontal flow (%)
120*	**23**	**12.7**	**0.25**	**25%**
125	18	10.5	0.21	26%
130	12	8.2	0.16	27%
135	8	5.7	0.11	28%
140	3	3.2	0.06	29%

*Denotes base case simulation

Table 7.11—Sensitivity evaluations for infiltration rates from trenches

Hydraulic conductivity of Field 1 (in/hr)	Infiltration rate (in/hr)	Calculated Gradient	Horizontal flow (%)
25	6.4	0.26	25%
50*	**12.7**	0.25	**25%**
150	37.3	0.25	25%
Horizontal:Vertical Anisotropy			
1*	**12.7** in/hr	0.25	**25%**
3	11.7	0.23	39%
10	9.8	0.20	57%
Hydraulic conductivity of confining unit (in/hr)			
5*	**12.7** in/hr	0.25	**25%**
1.5	12.2	0.24	25%
0.3	10.9	0.22	26%
0.1	9.7	0.19	26%
Horizontal to vertical side slope			
1:1	12.5 in/hr	0.25	47%
2:1*	**12.7**	0.25	**25%**
3:1	12.8	0.26	15%
4:1	12.9	0.26	10%

*Denotes base case simulation

Table 7.12—Reduction in infiltration rates in trenches due to bottom clogging (after Duchene et. al, 1994)

A	B	C	D	E	F	
Reduction in hydraulic conductivity for 2-inch layer beneath trench	**Effective vertical hydraulic conductivity beneath trench (in/hr)**	**Depth of water in the trench (ft)**	**Infiltration rate based on model results (in/hr)**	**Calculated gradient based on hydraulic conductivity in Field #1 of 50 in/hr**	**Reduction in infiltration rate (percentage)**	
					Total	**Horiz.**
no reduction[1]	**50**	**2.0**	**12.7**	**0.25**	none	none
50:1	37	3.2	12.2	0.24	-4	+16
50:1	37	1.6	11.8	0.24	-7	+15
50:1	37	0.8	10.2	0.20	-20	+10
no reduction[1]	**50**	**2.0**	**12.7**	**0.25**	none	none
350:1	14	3.2	11.9	0.24	-6	+17
350:1	14	1.6	11.3	0.23	-11	+15
350:1	14	0.8	9.7	0.19	-24	+12

[1]Base-case simulation

Figure 7.1—Lacey-Lid infiltration pond in Thurston County, Wash.

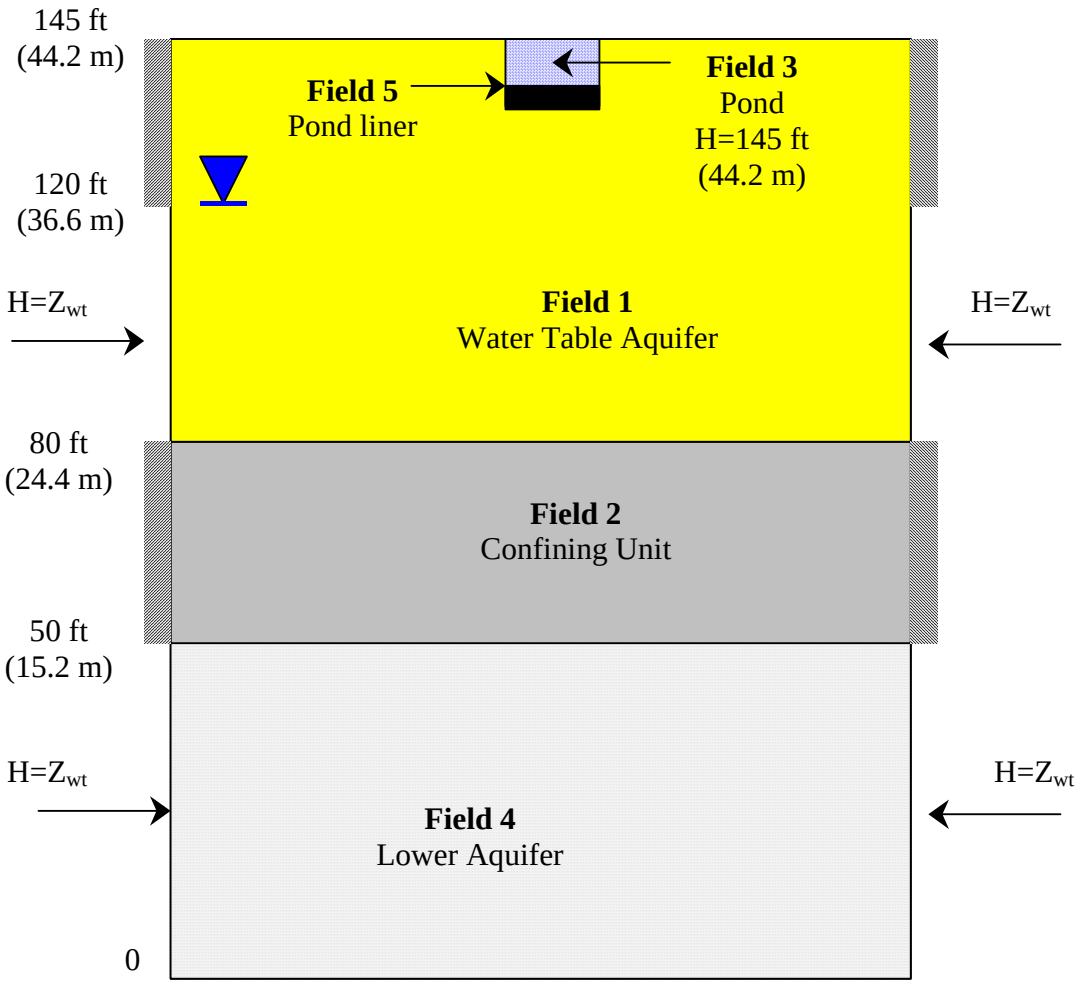

Figure 7.2—Cross-section view of modeled domain showing locations of five fields

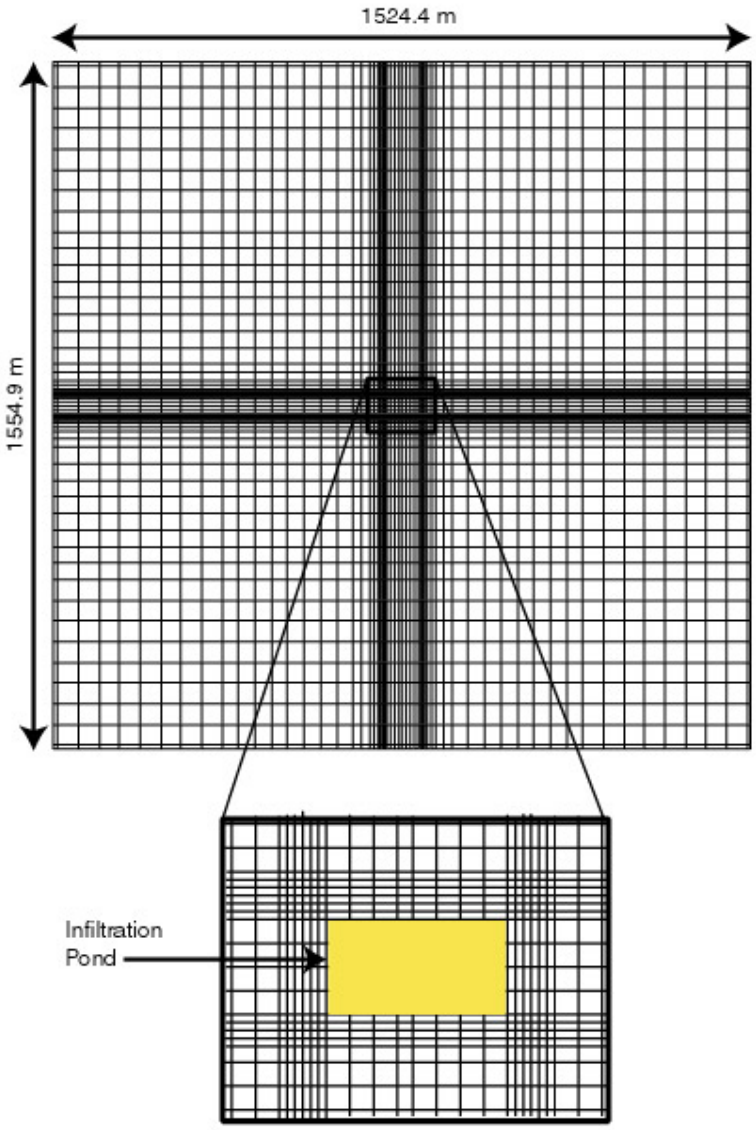

Figure 7.3—Plan view of row and column spacing

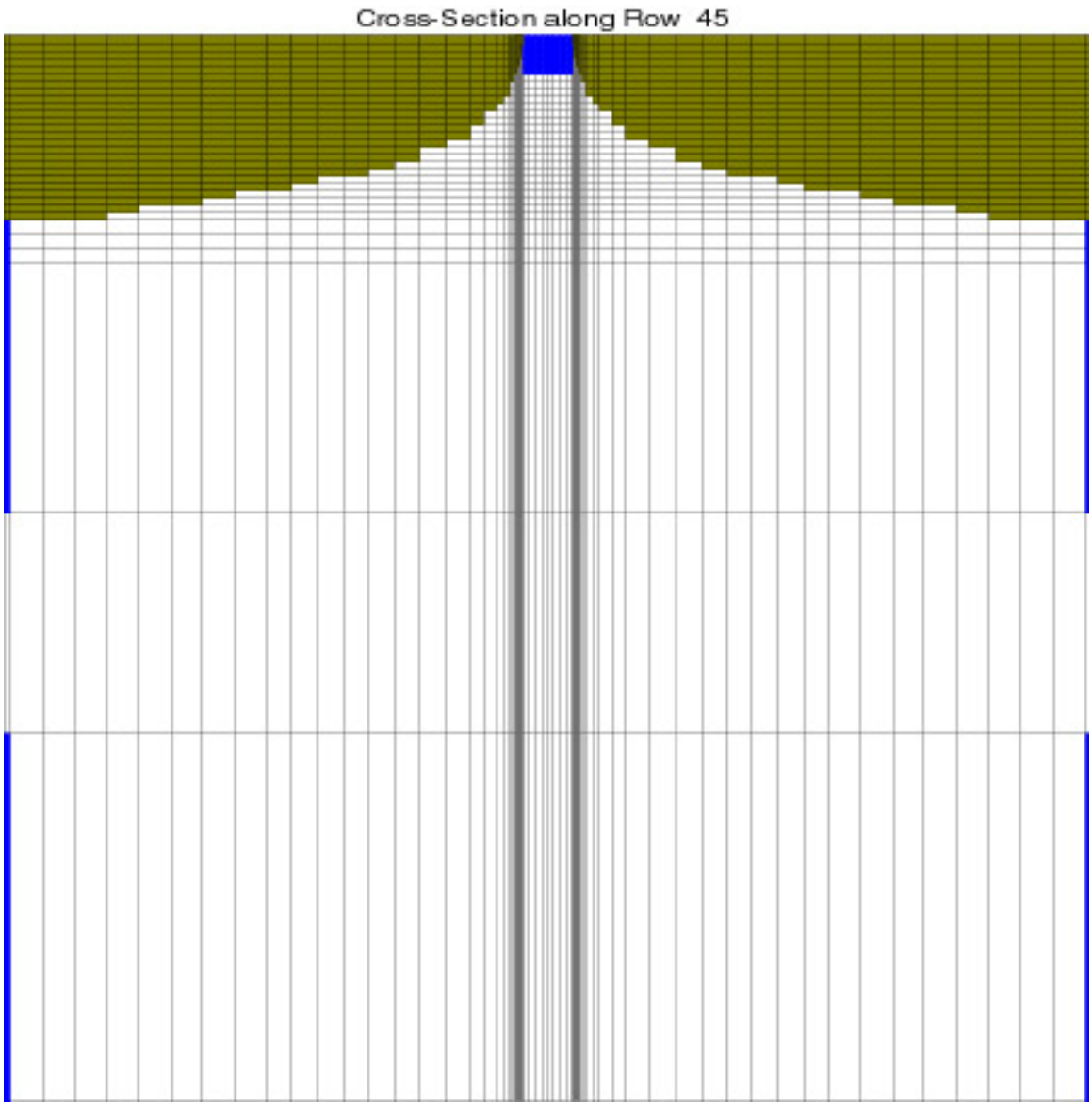

Figure 7.4—Cross-section view of flow from Lacey-Lid infiltration pond

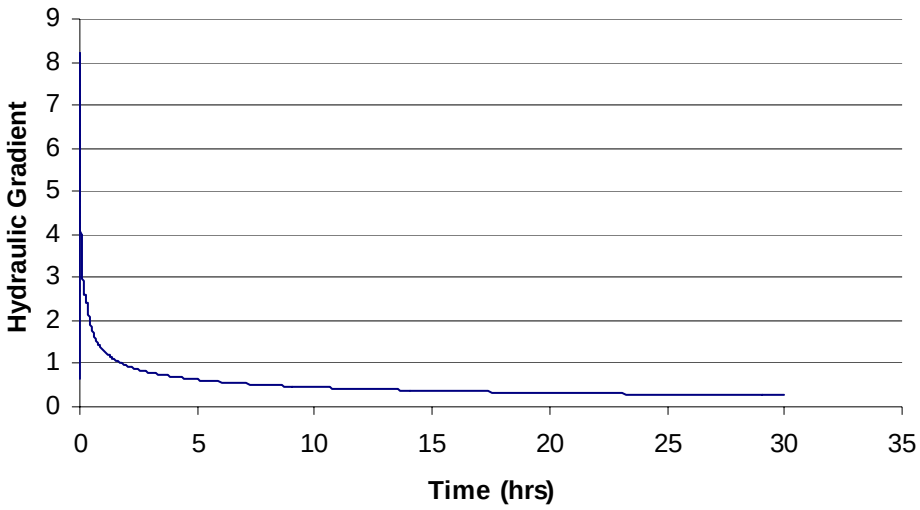

Figure 7.5—Hydraulic gradient versus time for K = 34 in/hr ($2.4x10^{-2}$ cm/s)

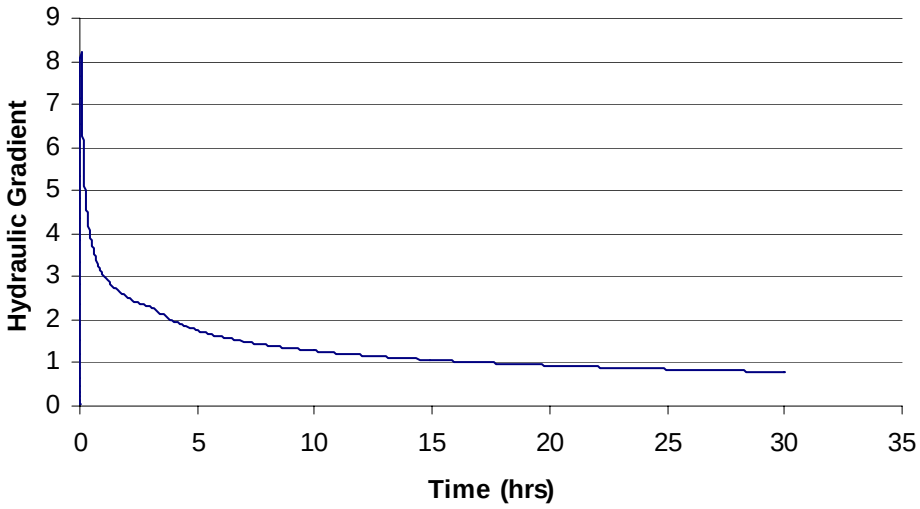

Figure 7.6—Hydraulic gradient versus time for K = 3.4 in/hr ($2.4x10^{-3}$ cm/s)

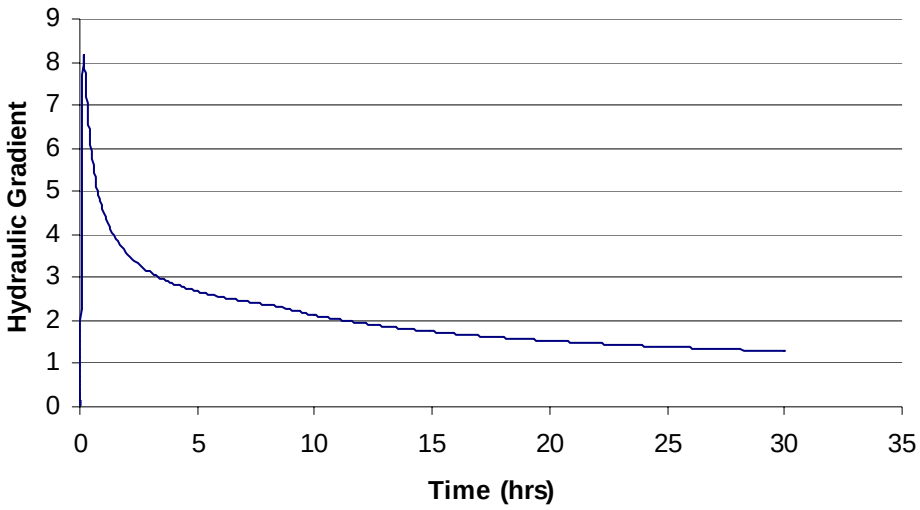

Figure 7.7—Hydraulic gradient versus time for K =1.1 in/hr ($8.1x10^{-4}$ cm/s)

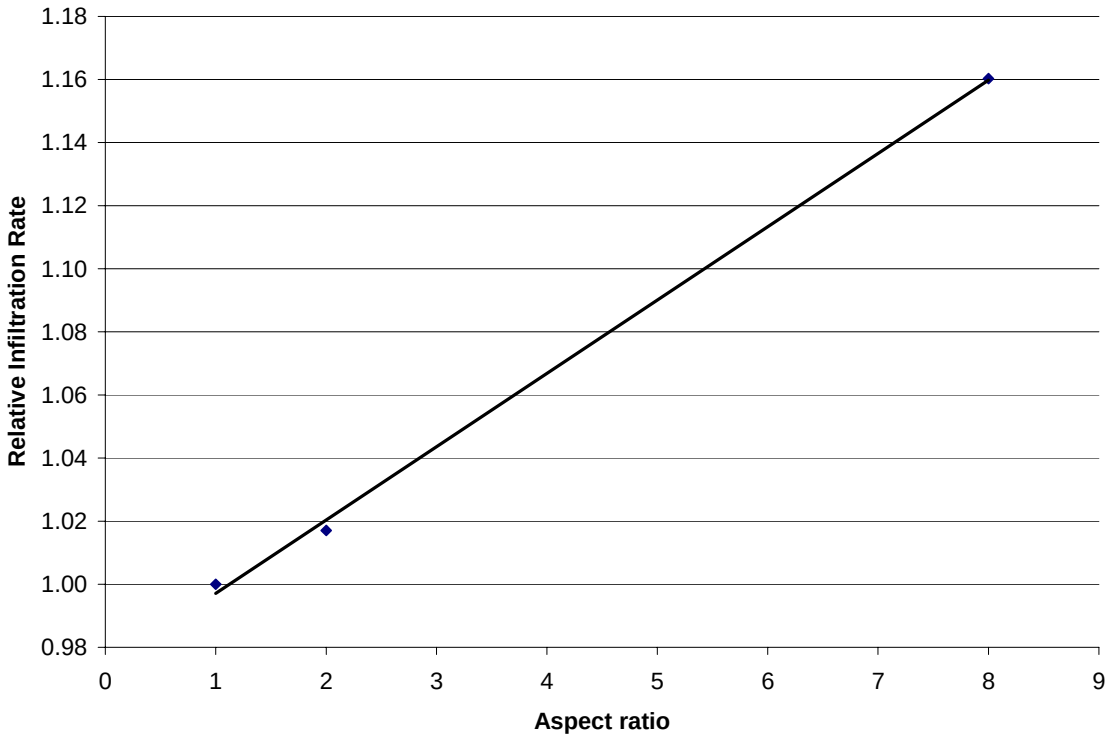

Figure 7.8—Relative Infiltration rate versus pond aspect ratio

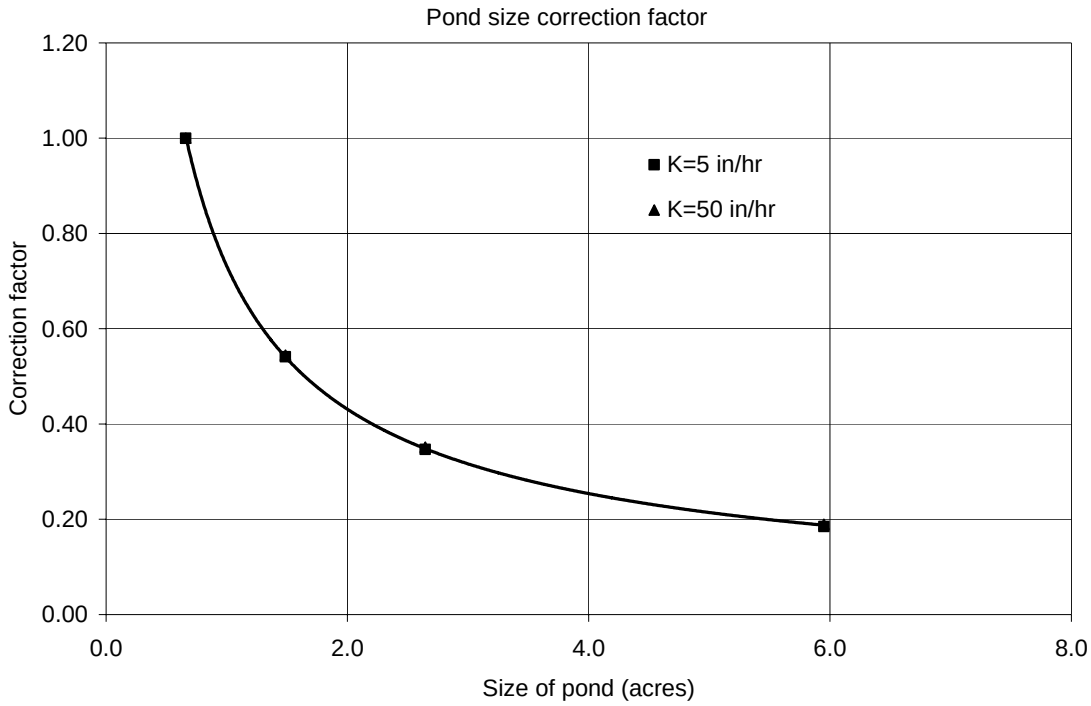

Figure 7.9– Correction factors for pond size given by Equation (7.3)

8 CONCLUSIONS AND DESIGN RECOMMENDATIONS

The following conclusions and design recommendations were developed from the results of the studies described in this report.

8.1. Effects of Hydraulic Gradient

- Short-term infiltration tests will tend to over-estimate long-term infiltration rates, as shown by the Green-Ampt approximation. The initial infiltration rate is significantly larger than the saturated hydraulic conductivity because the hydraulic gradient term is larger than 1.0. As more water infiltrates, the gradient approaches a value of 1.0, and the infiltration rate approaches the saturated hydraulic conductivity.
- If recharge or infiltration is sufficient to cause the wetting front to reach a regional or perched water table, the hydraulic gradient may drop to a value significantly less than 1.0, and the infiltration rate may be much less than the saturated hydraulic conductivity. This is a very important concept and one that is overlooked in design approaches in which infiltration rates are estimated solely on the basis of soil types or saturated hydraulic conductivity estimates.
- A transient, unsaturated flow model was used to monitor the time evolution of the hydraulic gradient beneath an infiltration pond for different soil types during a 30-hour recharge period. The results demonstrated that, in highly permeable soils, assuming a hydraulic gradient of 1.0 is not conservative. Conversely, in low permeability soils, assuming a hydraulic gradient of 1.0 may be conservative.

8.2 Estimating Saturated Hydraulic Conductivity from Soil Gradation Data

- Equation C-13, shown in Table 8.1, produces estimates of hydraulic conductivity that have a sum of mean square errors that is approximately 35 percent smaller than the mean square errors produced by the Hazen equation for the set of synthetic and natural soils used in this study. This polynomial equation uses data that are readily available from grain size analyses and should be considered an

alternative for the Hazen equation, especially for more coarse-grained soils with a hydraulic conductivity larger than approximately 0.05 cm/s.

8.3 Full-Scale Infiltration Tests

- Full-scale infiltration tests conducted at four sites in western Washington showed that the infiltration rate increases with time during the filling portion of the test. After the discharge to the pond is stopped, the infiltration rate quickly decreases to a rate that may be several times smaller than the initial rate. The rapid increase in infiltration during the filling portion of the test may be caused in part by lateral flow along the sides of the ponds. This is similar to "bank storage" that occurs in stream channels. As the water level in the pond increases, flow is induced horizontally into the banks of the pond. This infiltration is in addition to the infiltration that occurs along the pond bottom. Once the water level in the pond begins to decrease, the horizontal flow is reversed and water drains into the pond along the sides and out of the pond along the bottom. This inflow, which reduces the net infiltration rate, decreases with time.
- Infiltration rates based on soil texture for four sites are included in Table 8.2. These estimates are from the WDOE *Stormwater Management Manual for the Puget Sound Basin* (2001). The infiltration rates based on soil textures over-estimated the actual full-scale measured rate at Krista Firs (Kitsap County) and at Cimarron (King County). The soil texture rate for Balsam 7-11 (Kitsap County) under-estimated the actual full-scale rate, and the soil texture rate for Clark County closely estimated the actual full-scale rate.
- Saturated hydraulic conductivity values estimated from measuring air conductivity and from regression equations derived from grain size parameters were compared to full-scale infiltration rates calculated during this study and given in literature. The estimated saturated hydraulic conductivity values were up to two orders-of-magnitude larger that the full-scale infiltration rates for some sites and were two orders-of-magnitude smaller in other cases. This reinforces that grain size texture alone does not include site-specific characteristics that may affect infiltration rate

8.4 Comparison of Modeling Approaches

- Results from a steady-state saturated flow model were compared to results from a transient unsaturated model to evaluate errors that are introduced when the simplified model is used to simulate flow from infiltration ponds. These results show that the steady-state assumption may significantly under-estimate infiltration rates and that the amount of this under-estimation is dependent upon site-specific hydrologic information.
- Computer simulations were used to quantify the difference in estimated infiltration rates that occur when a saturated flow model is used versus an unsaturated flow model. The difference between the saturated and unsaturated flow models is lowest in highly permeable soils and increases as the hydraulic conductivity of the soil decreases. The modeling results suggest that using steady-state models will tend to under-estimate the infiltration rate from 20 to 40 percent over the range of hydraulic conductivities typically found beneath infiltration ponds in Western Washington.

8.5 Design Alternatives from Computer Simulations

- The results of computer simulations suggest the infiltration rate increases linearly as a pond becomes more elongate. The increase in the infiltration rate can be attributed to the increase in the lateral flow that occurs as the pond perimeter increases.
- A gravel column with a high hydraulic conductivity was simulated from the pond bottom down to the regional groundwater table. The addition of the column increased the infiltration rate by less than 1 percent. This insignificant change indicates that adding a gravel column will not affect the pond's performance during steady-state saturated conditions. The small effect is due to the hydraulic gradient term. Adding a gravel chimney has little impact if no significant hydraulic gradient exists to drive groundwater.
- If lateral flow is consistently important, more efficient designs may require a larger ratio of side area to bottom area. This design approach would necessitate

maintenance for the sides as well as the bottom of the pond. If the soil on the sides and bottom are preserved with respect to vegetation and silt build-up, the horizontal as well as the vertical flow could be an effective means of infiltrating storm-water runoff into the subsurface.

8.6 A Suggested Design Approach

This section summarized a suggested design approach based on the results of this study and on information from the literature. The steps described below and summarized on Figure 8.1 are aimed at achieving two main objectives. The first objective is to describe procedures used to develop designs for infiltration facilities. These designs will include recommendations for the size and shape of infiltration ponds or infiltration trenches. The second objective is to help identify situations in which more refined and sophisticated analyses should be brought to bear in the design process. These more sophisticated analyses may include additional field or laboratory tests and more realistic analytical tools including analytical groundwater flow models and computer simulations.

8.6.1 Estimate the volume of stormwater that must be infiltrated by the proposed or planned facility

The volume of stormwater that must be infiltrated and the rate at which this must occur are generally specified by local, regional, or state requirements. In many cases, the volume and required rates of discharge are controlled by both water quality and water quantity concerns. Although the methods for estimating the stormwater volume is beyond the scope of this manual, it is useful to recognize the general ways in which this stormwater volume or discharge can be described.

There are three primary ways in which the stormwater discharges are generally described: 1) a single-value or fixed volume of runoff water, 2) a single-event or single-storm runoff hydrograph (i.e. runoff volume versus time), and 3) a continuous hydrograph that considers multiple events or storms over some longer period of time. The first and most simple way of describing stormwater discharge is as a total volume of water that much be infiltrated in a prescribed period of time. This is the approach that is generally used for water quality considerations related to how quickly the pond empties.

Table 8.3 describes time requirements used by different state and federal agencies. For example, the WDOE design requirement that the pond empty within 24 hours focuses on the runoff that is generated by a storm that is defined as the 24-hour storm with a 6-month return frequency (a.k.a., 6-month, 24-hour storm). (Note: For areas in western Washington, the 6-month, 24-hour storm can be estimated as 72% of the 2-year, 24-hour rainfall amount.). The volume of run-off from this storm that is discharged to the infiltration facility is often determined using a "curve-number" method that relates a land area's total runoff volume to the precipitation it receives and to its natural storage capacity. This approach is described in Volume III, Chapter 2, Section 2.3.2 of the WDOE manual (2001). The important thing to note about this approach is that it results in a single number that represents the total volume of water that will be discharged to the stormwater facility, denoted as V_{design} in the sections below.

The second method for describing stormwater discharges is the single-event or single-storm runoff hydrograph. The hydrograph describes the volume of runoff versus time for some specified precipitation event. An example single-event hydrograph for a 6-month, 24 hour storm in Western Washington is included Figure 8.2. The single-event hydrograph method is used primarily for calculations aimed at insuring that the pond empties within 24 hours. For example, the WDOE stormwater manual (2001) describes the Santa Barbara Unit Hydrograph (SBUH) method for estimating the hydrograph from the 6-month, 24-hour storm. This description is included in Volume III, Chapter 2, Section 2.3.2 of the WDOE manual (2001). Because the unit hydrograph approach results in a time-series of inflows to the infiltration facility, spreadsheet solutions are generally required to account for the balances between time-dependent inflow, outflow, infiltration rates, and pond storage changes. These time-varying conditions generally preclude more simple designed approaches that are based on tables or graphs. (For example, Akan (2002) gives solutions for time-dependent infiltration rates that result from time-varying inflow rates and subsurface saturation conditions).

The third and most involved method for describing stormwater discharges uses a continuous hydrograph that considers the runoff from multiple events or storms over

some longer period of time. This approach generally requires a computer-based rainfall-runoff model, such as the WSDOT's MGSFLOOD model, U.S. EPA's HSPF model or the Danish Hydraulic Institute's MIKE SHE model. The continuous runoff hydrographs that result from these models can be used to design infiltration facilities if they are linked with some approach for estimating infiltration rates. In the most general case, these infiltration rates will change with time during the storm event. These transient infiltration rates can be estimated using computer-based groundwater flow models such as USGS's MODFLOW. The continuous runoff hydrographs can also be linked with more simple approaches for estimating infiltration rates, including the steady-state rates described below. It should be noted, however, that these steady-state rates may over- or under-estimate actual time-dependent rates, depending upon site-specific conditions. The continuous-hydrograph approach is generally required to meet water quantity requirements if the infiltration pond is designed with an overflow system that discharges to a stream or surface water body. This method is described in Section 2.2 and Appendix III-B of Volume III of the WDOE manual (2001).

8.6.2 Choose a trial geometry and estimate depth in the pond

The methodology described below for estimating infiltration rates is based on regression equations to estimate gradients. These equations depend upon the size of the pond, A_{pond}, and upon the depth of water in the pond, D_{pond}. Larger ponds result in smaller gradients and deeper ponds result in higher gradients. This dependency introduces some difficulty or complications into the design process because the gradient is needed to select the size of the pond and the size of the pond is needed to estimate the gradient. An iterative approach is recommended, wherein a trial pond size and depth are assumed, perhaps based on experience at similar sites. The design approach described below can then be used to check the trial design. After the design has been fully developed, the trial pond size should be compared to the design pond calculated below and revised as necessary.

The initial trial geometry, including length, width, and depth of the facility, will generally be based on the characteristics of the property or site that is proposed for the

infiltration facility. Computer simulations and observations suggest that elongated facilities with a larger fraction of side area to bottom area may result in higher infiltration rates. Facilities that result in deeper water depths within the facilities also result in higher infiltration rates. If possible, trial geometries should reflect these results. The volume of the infiltration facility for trial geometry should be based on the design volume, V_{design}, described in Section 8.6.1. The margin or factor safety that is used in this calculation should reflect the site-specific consequences that would occur if the actual stormwater volume exceeds the design volume.

8.6.3 Perform subsurface site characterization and data collection

The WDOE (2001) stormwater manual includes recommendations for subsurface site characterization and data collection activities that are relevant for the design procedures described in this manual. These recommendations are summarized in Table 8.4. The WDOE recommendations related to depths of soil borings or test pits should be viewed as minimum requirements. The results of computer simulations described in Chapter 7 suggest that relatively deep features in the subsurface may affect the performance of infiltration ponds and trenches. The identification of small-scale layering and stratigraphy can be particularly important in terms of the potential for groundwater mounding. Continuous and careful sampling is recommended to depths at least as large as the WDOE requirements.

8.6.4 Estimate saturated hydraulic conductivity from soil information, laboratory tests, or field measurements

A variety of methods can be used to estimate saturated hydraulic conductivity. These methods, which are summarized below, include estimates based on grain size information, laboratory permeameter tests, air conductivity measurements, infiltrometer tests, and pilot infiltration tests. Some of the advantages and disadvantages of these various methods are summarized in Table 8.5.

8.6.4.1 Estimate values based on grain size information

Given the requirements for soil sampling and grain size analyses summarized in Table 2, saturated hydraulic conductivity estimates should be developed based on grain size distributions for all layers encountered during the site characterization phase. These estimates from soil gradation data are more reliable than estimates based solely on USDA soil type.

A variety of methods are available for estimating saturated hydraulic conductivity values from grain size information. One of the most simple and most commonly used approaches is the Hazen equation:

$$K_s = Cd_{10}^2 \qquad (8.1)$$

where K_s is the saturated hydraulic conductivity in cm/sec, C is a conversion coefficient, and d_{10} is the grain size for which 10% of the sample is more fine (10% of the soil particles have grain diameters smaller than d_{10}). For K_s in units of cm/s and for d_{10} in units of mm, the coefficient, C, is approximately 1.

A second approach for estimating saturated hydraulic conductivities for soils typical of western Washington was proposed in Chapter 3:

$$\log_{10}(K_s) = -1.57 + 1.90d_{10} + 0.015d_{60} - 0.013d_{90} - 2.08f_{fines} \qquad (8.2)$$

where d_{60} and d_{90} are the grain sizes in mm for which 60% and 90% of the sample is more fine and f_{fines} is the fraction of the soil (by weight) that passes the number-200 sieve. This approach is based on a comparison of hydraulic conductivity estimates from air permeability tests with grain size characteristics. Other regression relationships between saturated hydraulic conductivity and grain size distributions are available from the literature (e.g. Freeze and Cherry, 1979; Fetter, 1994; Rawls et al., 1982; Rawls and Brakensiek, 1985).

Grain size samples can also be used to estimate hydraulic conductivity through air conductivity tests using the following relationship, as described in Chapter 2:

$$K_s = C_f K_{air} \qquad (8.3)$$

The correction factor C_f, is dependent upon the viscosity and density of air and water. If the air conductivity is measured at laboratory temperatures, and if the hydraulic conductivity is also for laboratory temperatures, then the correction factor is equal to 15. This is based on an assumed laboratory temperature of 20° C. If the air conductivity is measured at laboratory temperatures, and if the hydraulic conductivity is for field temperatures, then the correction factor is approximately 11.5. This is based on an assumed field temperature of 10° C. A simple apparatus for estimating air conductivity from grain size samples is described in Massmann and Johnson (2001).

It should be noted that the estimates given by equations (8.1) through (8.3) should be viewed as "order-of-magnitude" estimates. If measurements of hydraulic conductivity are available from laboratory or field tests (as described in sections 8.6.4.2 and 8.6.4.3), these data should be weighed more heavily in selecting values of hydraulic conductivity for design purposes.

8.6.4.2 Estimate values based on laboratory tests

The grain size methods described in the previous section will give order-of-magnitude estimates for hydraulic conductivity for soils that are relatively coarse-grained (sands and some silty sands). For more fine-grained soils, these methods are prone to significant error. Laboratory saturated hydraulic conductivity tests are recommended for fine-grained soils or whenever feasible. These tests should be conducted on samples that are compacted to a density similar to what is anticipated for actual subsurface conditions. Fixed-head and falling-head tests using both rigid-wall and flexible-wall permeameters are commonly used in the geotechnical laboratories. If this type of data is available, it should be considered in the design process.

8.6.4.3 Estimate values based on field tests

If data from field tests of saturated hydraulic conductivity are available, these should be considered in the design. These field tests typically include single-ring and

double-ring infiltrometer tests or pilot infiltration tests (PIT) similar to what is described in Appendix V-B in Volume V of the WDOE stormwater manual (2001).

Recent developments have also shown that field-tests of air conductivity can also be used to estimate saturated hydraulic conductivity values, in much the same way as laboratory tests. Descriptions of these types of field tests are included in Iverson et al (2001a and 2001b), Fish and Koppi (1994), Liang et al. (1996), and Seyfried and Murdock (1997).

8.6.4.4 Incorporate hydraulic conductivity estimates for layered soils.

In many cases, estimated saturated hydraulic conductivity values are derived from discrete soil samples collected from several depths at several different horizontal locations beneath each of the infiltration ponds. The goal should be to collect at least one sample from each discrete layer at each horizontal location. Table 8.6 gives an example of how the data from these multiple samples can be combined to obtain a single "effective" or "equivalent" hydraulic conductivity estimate for an infiltration facility. Soil samples were collected at four different horizontal locations at the example site. At three of these horizontal locations, samples were collected from three different layers. At the fourth location, samples were collected from only two different layers. Hydraulic conductivity values were estimated for each soil sample using the Hazen equation. Hydraulic conductivity estimates from different layers at a single horizontal location can be combined using the harmonic mean:

$$K_{equiv} = \frac{d}{\sum \frac{d_i}{K_i}} \qquad (8.4)$$

where d is the total depth of the soil column, d_i is the thickness of layer "i" in the soil column, and K_i is the saturated hydraulic conductivity of layer "i" in the soil column.

The depth of the soil column, d, would typically include all layers between the pond bottom and the water table. However, for sites with very deep water tables (> 100 feet) where groundwater mounding to the base of the pond is not likely to occur, it is

recommended that the total depth of the soil column in Equation 8.4 be limited to approximately 20 times the depth of pond. This is to insure that the most important and relevant layers are included in the hydraulic conductivity calculations. Deep layers that are not likely to affect the infiltration rate near the pond bottom should not be included in Equation 8.4.

The harmonic mean given by equation (8.4) is the appropriate effective hydraulic conductivity for flow that is perpendicular to stratigraphic layers (Freeze and Cherry, 1979). For the example site, these harmonic means range from 6 in/hr for locations 1 and 4 to 12 in/hr for location 3, as shown in the last column in Table 8.6. The harmonic means for each horizontal location are then averaged to obtain a single estimated hydraulic conductivity for each infiltration pond. This average is equal to 8.7 in/hr for the example site.

The approach described by Equation (8.4) and shown in Table 8.6 is applicable for combining hydraulic conductivity estimates that are derived from a variety of methods, including grain size analyses, laboratory tests, and field tests. When combining these values, it is important to recognize the layer or which for which the test is relevant.

8.6.5 Estimate the hydraulic gradient

The infiltration rate from a pond or trench is given by the product of the saturated hydraulic conductivity and the hydraulic gradient. The hydraulic gradient describes the driving forces that cause flow from the infiltration facility. The two primary forces are gravity and capillary suction. The relative importance of these forces and the subsequent gradient depends upon a variety of factors, including duration of the infiltration event, local and regional geology, and depth to groundwater.

In general, there are two cases or end-points for estimating gradients. One end-point is sites with relatively shallow groundwater and the second is sites with relatively deep groundwater. For those sites with thick unsaturated zones, infiltration can be

approximated by the Green-Ampt equation (e.g. Chin, 2000). This approach assumes ponded water at the ground surface and a wetting front that extends to some depth, L. The wetting front is assumed to move downward as a sharp interface. The soil is assumed saturated above the wetting front (the water content is assumed equal to the porosity). The water content below the wetting front is assumed equal to some lower initial value. The gradient is approximated by the following expression:

$$gradient \approx \frac{D_{pond} + L + h_{wf}}{L} \qquad (8.5)$$

where D_{pond} is the depth of water in the pond or infiltration facility, L is the depth of the wetting front below the bottom of the pond, and h_{wf} is the average capillary head at the wetting front, with units of length. For infiltration ponds and trenches, the average capillary head, h_{wf}, will be small relative to the depth of water in the facility and the depth of the wetting front so this term can be dropped from equation (8.5).

The term "L" in equation (8.5) represents the depth of the wetting front. Because this changes with time as water infiltrates at the ground surface, the gradient also changes with time. The gradient will start out at some value significantly greater than 1 and will approach 1 as the wetting front moves downward. For most infiltration events, the gradient will reach a value of 1 relatively quickly as compared to the duration of the event, as described in Chapter 7. A gradient of 1 would be appropriate for these cases. For very short infiltration events or for soils that are relatively fine-grained (e.g. sandy loam), a gradient of 1.5 may be justified.

For the shallow groundwater sites, the possibility of groundwater mounding must be considered in designing infiltration facilities. This mounding will reduce the hydraulic gradient to a value that is often significantly less than 1.0, and the infiltration rate may be much less than the saturated hydraulic conductivity. This is a very important concept and one that is overlooked in design approaches in which infiltration rates are estimated solely on the basis of soil types or saturated hydraulic conductivity estimates. It should be noted that mounding may also result if perched water-table conditions occur due to

low-permeability layers beneath site and above the water table. (In very general terms, a layer would be characterized as "low-permeability" in this context if the estimated hydraulic conductivity of the layer is less than 10% of the hydraulic conductivity assigned to the overlying materials and if the hydraulic conductivity of this layer is less than the infiltration rate from the pond. As a first approximation, a layer could be characterized as low permeability in this context if it is less than 0.5 inches per hour and if it is less than 10% of the overlying materials.)

For deep groundwater sites, where the effects of mounding will generally be small, the gradient will not typically be reduced by infiltration from the facility. For these deep sites, the gradient will be approximately equal to 1.0, as described by the Green-Ampt equation. The approach described below uses regression equations to estimate the hydraulic gradient. These equations were developed based on computer simulations described in Chapter 7 for sites where water table mounds will develop. These regression equations can also be applied to sites with deep groundwater by limiting the gradient to a maximum value of 1.0.

The results of computer simulations described in Chapter 7 were based on the geometry and observed geology beneath the Lacey-Lid infiltration pond in Thurston County, Wash. as described in the *Water Resources Investigations Report 92-4109* (Drost et al., 1999). Based on the results of these computer simulations, the effective gradient under steady-state conditions beneath a medium-sized infiltration facility can be approximated with the following expression:

$$\text{gradient} = \text{i} \approx \frac{D_{wt} + D_{pond}}{138.62(K^{0.1})} CF_{size} \qquad (8.6)$$

where K is saturated hydraulic conductivity in feet/day, D_{wt} is the depth in feet from the base of the infiltration facility to the water table or to the first low-permeability layer, and D_{pond} is the depth of water in the pond, in feet. The regression equation given above was developed using computer simulations for ponds with infiltration rates that ranged from 0.2 to 20 inches per hour (saturated K values from 1.5 to 150 in/hour). The data that

were used to develop the regression equation given by Equation 8.6 are included in Table 7.2.

Equation (8.6) was developed by first choosing a functional form for the gradient relationship. It was assumed, based on the data in Table 7.2, that the gradient would be approximately linearly proportional to the depth of the water table and the depth of water in the pond. These two variables were added together to describe this linear proportionality. A variety of relationships between gradient and hydraulic conductivity were considered, including polynomial, exponential, power-law, and linear relationships. A power-law relationship between gradient and hydraulic conductivity was found to fit the data best. A trial and error approach was used to select the exponent term in the power relationship (i.e., the "0.1" value in Equation 8.6). Finally, the coefficient in the denominator (138.62) was determined by minimizing the difference between the gradient predicted with the model and the gradient predicted with the regression equation.

The correction for pond size, CF_{size}, was given in Chapter 7 as Equation 7.3 and is shown in Figure 7.9. This equation correction factor is repeated below:

$$CF_{size} = 0.73(A_{pond})^{-0.76} \qquad (8.7)$$

where

CF_{size} = correction factor for size of the pond

A_{pond} = area of the pond bottom in acres

This expression for correction factor was developed for ponds with bottom areas between 0.6 and 6 acres in size. For small ponds (ponds with area equal to 2/3 acre), the correction factor is equal to 1.0. For large ponds (ponds with area equal to 6 acres), the correction factor is 0.2.

Chapter 7 also includes the results of computer simulations for infiltration trenches in which the length dimension is much larger than the width. Based on the

results of these computer simulations, the effective gradient under steady-state conditions beneath an infiltration trench can be approximated with the following expression:

$$\text{gradient} = \text{i} \approx \frac{D_{wt} + D_{trench}}{78(K^{0.05})} \qquad (8.8)$$

where K is saturated hydraulic conductivity in feet/day, D_{wt} is the depth in feet from the base of the infiltration trench to the water table or to the first low-permeability layer, and D_{trench} is the depth of water in the trench, in feet. The regression equation given by Equation 8.8 was developed using computer simulations for trenches with infiltration rates that ranged from 0.2 to 20 inches per hour (saturated K values from 1.5 to 150 in/hour). The data that were used to develop the regression equation given by Equation 8.8 are included in Table 7.10 and the first three rows of Table 7.11. There is no correction factor required for trench size.

Equation (8.8) was developed using the same approach as was used to develop the regression for ponds (Equation 8.6). The gradient was assumed to be approximately linearly proportional to the depth of the water table and the depth of water in the pond. These two variables were added together to describe this linear proportionality. A power-law relationship between gradient and hydraulic conductivity was found to fit the data best. A trial and error approach was used to select the exponent term in the power relationship (i.e., the "0.05" value in Equation 8.8). Finally, the coefficient in the denominator (78.0) was determined by minimizing the difference between the gradient predicted with the model and the gradient predicted with the regression equation.

The relationships given in Equation 8.6 and 8.8 are based on estimates of infiltration rates derived from the computer simulations presented in Chapter 7. These relationships were derived by estimating infiltration rates as a function of depth to groundwater using the computer model. The results of these computer simulations allowed a relationship to be developed between the infiltration rate and the depth to groundwater. As the depth to groundwater was decreased in the computer model, the infiltration rate also decreased. This observed relationship can be incorporated into

Darcy's law through the gradient term. As the depth to groundwater decreases, the gradient also decreases. Equations 8.6 and 8.8 provide estimates for relating the depth to groundwater and the gradient.

Figure 8.3 compares the gradients for ponds estimated using Equation (8.6) with the gradients calculated using the model. The data shown with circles is the data used to develop Equation (8.6), given in Table 7.2. Additional computer simulations were then conducted using larger ponds and ponds with deeper water tables to evaluate the robustness of the regression equation. The results of these additional simulations are included in Table 7.7 and 7.8. The open squares show the results of this verification. The data and computer models used in the regressions are more fully described in Chapter 7. Figure 8.3 shows that the regression equation provides very good estimates of the modeled systems with gradients less than approximately 0.2. The equation also provides reasonable estimates for gradients for systems with deeper water tables. Furthermore, the regression equation is conservative for the deep water table ponds in that the estimated gradients are smaller than the model predictions. Figure 8.4 compares gradients for trenches calculated using Equation 8.8 with the gradients calculated using the model. These gradients from the model are included in Tables 7.10 and 7.11. The results in Figure 8.4 show that the regression equation provides good estimates of the modeled systems with gradients less than approximately 0.3.

It is important to note that the relationships described in Equations (8.6) through (8.8) are approximations that were derived from a set of computer simulations for a particular facility in a particular hydrogeologic system. It is believed that these equations are representative of facilities at sites where the depth to groundwater is from several feet to approximately 100 feet. For systems deeper than 100 feet, where the Green-Ampt equation will provide a better representation of the infiltration processes, a gradient of 1.0 is recommended in lieu of the gradients given by Equations (8.6) and (8.8).

It should also be noted that Equations (8.6) and (8.8) do not incorporate the effects of perched water tables that result beneath the infiltration facility. Under some

hydrogeologic conditions, water-table mounding may occur above low-permeability layers that lie above the "normal" or regional water table. This mounding can result in an unsaturated zone between the saturated, perched water and the normal or regional water table. Under these conditions, the appropriate depth that should be used in Equations (8.6) and (8.8) is not the depth to the regional water table, but rather the depth to the low-permeability layer that may cause perched conditions. In very general terms, a layer could be characterized as "low-permeability" in this context if the estimated hydraulic conductivity of the layer is less than 10% of the hydraulic conductivity assigned to the overlying materials and if the hydraulic conductivity of this layer is less than the infiltration rate from the pond. As a first approximation, a layer could be characterized as low permeability in this context if it is less than 0.5 inches per hour and if it is less than 10% of the overlying materials.

Equation (8.6) shows that the gradient depends upon the size of the pond, A_{pond}, upon the depth of water in the pond, D_{pond}. Larger ponds result in smaller gradients and deeper ponds result in higher gradients. This introduces some difficulty in that the gradient is needed to select the size of the pond and the size of the pond is needed to estimate the gradient. An iterative approach is recommended, wherein a trial pond size and depth is assumed, perhaps based on experience in similar sites. The trial pond size is used in Equation (8.7) to get a pond correction factor and the depth of water is used in Equation (8.6) to estimate the gradient. The trial pond size should be compared to the actual pond size calculated below to determine if a revised correction factor is required.

8.6.6 Estimate the infiltration rate by multiplying gradient and hydraulic conductivity.

Based on Darcy's law, the infiltration rate can be estimated by multiplying the saturated hydraulic conductivity from Section 8.6.4 with the hydraulic gradient determined in section 8.6.5:

$$f = K\left(\frac{dh}{dz}\right) = Ki \qquad (8.9)$$

where f is the specific discharge or infiltration rate of water through a unit cross-section of the infiltration facility (L/t), K is the hydraulic conductivity (L/t), dh/dz is the hydraulic gradient (L/L), and "*i*" is a "short-hand" notation for the gradient (given by Equation (8.6) or (8.8) for ponds and trenches at sites with shallow water tables, or a value of approximately 1 for ponds and trenches at sites with deep water tables).

8.6.7 Apply correction factors for biofouling, siltation, and pond geometry

The infiltration rate given in Equation (8.9) was developed assuming that the hydraulic conductivity of the soil beneath the infiltration facility will remain equal to the value measured in the field or laboratory tests or estimated using soil information. Depending upon the level of pre-treatment and the maintenance program that is put in place at the facility, the long-term infiltration rates may be reduced significantly by factors such as siltation and biofouling. Siltation is more likely to occur if there is not sufficient pre-treatment of the storm water or in locations where the drainage basin is prone to erosion because of recent land disturbances or steep slopes. Biofouling is more likely to occur if the pond is located beneath trees and other vegetation or in shaded locations.

If effective pre-treatment and reliable long-term maintenance cannot be guaranteed, the infiltration rates used in Equation 8.9 should be reduced. Table 8.7 gives infiltration rate reduction factors to account for biofouling and siltation effects for infiltration ponds and trenches. These factors, which are somewhat subjective, were developed based on a comparison of the field observations described in Chapter 5 and the computer simulations described in 7. The field site descriptions contained in Appendix D include descriptions of pond conditions, including vegetation, indications of siltation or biofouling, evidence of maintenance practices, and presence of pretreatment facilities. The computer simulations used to develop Equations (8.6) and (8.8), as described in Chapter 7, did not include effects of siltation or biofouling. The correction factors included in Table 8.7 were developed by comparing the infiltration rates estimated with the computer model with infiltration rates observed in the field. The infiltration rates

calculated using Equation (8.9) should be multiplied by these correction factors to account for the effects of siltation and biofouling.

Although siltation and biofouling may be less prevalent in infiltration trenches as compared to infiltration ponds, field data have not been collected that would allow correction factors to be estimated for these trenches. The conservative approach would be to use the same correction factors for trenches as for ponds. However, the computer simulation results described in Table 7.12 suggest that reductions in hydraulic conductivity due to bottom clogging from siltation and biofouling may have relatively small effects on overall infiltration rates and gradients for trenches. This is because of the larger amounts of lateral flow that occurs in trenches relative to ponds. Reductions in vertical flow from the bottom of the trench are offset by increases in lateral flow, particularly for trenches with deeper water levels. Based on these results, it may be more appropriate to use correction factors that are included Column D in Table 8.7.

Computer simulations described in Chapter 7 also suggest that ponds with large aspect ratios (defined as pond length divided by pond width) have higher infiltration rates than ponds with lower aspect ratios. The data shown in Figure 7.8 were used to develop an equation for correction factor that can be used to account for these results. This equation, which is included as Equation 7.2 in Chapter 7, is repeated below:

$$CF_{aspect} = 0.02A_{ratio} + 0.98 \qquad (8.10)$$

where A_{ratio} is the aspect ratio for the pond (length/width). In no case should the correction factor for aspect ratio be greater than 1.4.

The correction factors for siltation and biofouling and for aspect ratio are multiplied by the infiltration rate given by Equation (8.9):

$$f_{corr} = (CF_{silt/bio})(CF_{aspect})\, f = (CF_{silt/bio})(CF_{aspect})Ki \qquad (8.11)$$

where $CF_{silt/bio}$, is the correction factor for siltation and biofouling, CF_{aspect} is the correction factor for aspect ratio, and f is the "uncorrected" infiltration rate given by Equation 8.9. (Note: The aspect ratio correction is not applied to trench configurations.)

Once an infiltration rate has been estimated using Equation (8.11), it should be compared with rates from the literature, from design manuals, and from observations at other similar facilities in similar hydrogeologic environments for verification purposes. For example, the rates can be compared to those rates given in the WDOE stormwater manual (see Tables 8.8 through 8.10 below). Table 8.8 gives rates that are based on USDA soil type, Table 8.9 gives rates that are based on soil gradation analyses, and Table 8.10 gives correction factors that are used to reduce infiltration rate estimates from field-scale tests, including PIT tests.

In many instances, the infiltration rates estimated using Equation (8.11) will be significantly larger than the rates given in Tables 8.8 through 8.10. The rates given in Tables 8.8 through 8.10 from the WDOE manual were developed based on observations at field sites in western Washington. Many of these sites have reduced infiltration rates due to maintenance and design issues, as described in Chapter 4 and Wiltsie (1998). The rates in Tables 8.8 through 8.10 were also developed for sites with relatively shallow water tables and will likely be overly conservative for sites with deep water tables and thick unsaturated zones. Figure 5.1 illustrates the range of values for infiltration rates that can be expected based on maintenance and design practices.

The infiltration rates given by Equation (8.11) may, in fact, be larger or smaller than the rates given in Tables 8.8 through 8.10 or in Figure 5.1 for reasons that are reality-based. The important question is whether an explanation can be developed for the differences. For example, if the value given by Equation (8.11) is for a site with coarse gravel and a deep water table, it may be significantly larger than the rates in the figures, tables, or other databases. Similarly, if the site is located in low-permeability materials with a shallow water table and no pretreatment, the value from Equation (8.11) may be smaller than previously-observed values.

Other safety factors could also be applied to the infiltration rate at this step in exceptional circumstances to account for other uncertainties. It should be noted that there are "built-in" safety factors related to the hydrologic analyses used to estimate the volume of infiltrated water, V_{design}. These safety factors are related to the design storm that is used to generate runoff for the infiltration facility.

The infiltration rate given by Equation (8.11) can be combined with the gradient equation given by Equation (8.6) to obtain a relationship between hydraulic conductivity, gradient, and infiltration for infiltration ponds:

$$Q_{ponds} = KiA_{total} \approx K\left[\frac{D_{wt} + D_{pond}}{138.62(K^{0.1})} CF_{size}\right](CF_{silt/bio})(CF_{aspect})A_{total} \quad (8.12)$$

A similar equation can be developed for trenches by combining Equations (8.8) and (8.11):

$$Q_{trench} = KiA_{trench} \approx K\left[\frac{D_{wt} + D_{trench}}{78(K^{0.05})}\right](CF_{silt/bio})A_{trench} \quad (8.13)$$

8.6.8 Design approaches for single-event hydrographs

In most cases, flow from the infiltration facilities will occur through both the sides and the bottom of the facility. It may be useful in some instances to quantify the magnitude of these two components in order to assess the effects of bottom plugging and other maintenance issues. Based on observations and computer simulations described in Chapters 5 and 7, horizontal flow from facilities may be significant and is sensitive to the average depth of water during the infiltration event.

The total flow out the sides and bottom of the facility can be estimated to a first approximation with the following expressions:

$$Q = Q_{sides} + Q_{bottom} = f_{corr}(A_{sides} + A_{bottom}) = f_{corr}(A_{total}) \quad (8.14)$$

where f is the infiltration rate of water through a unit cross-section of the infiltration facility (L/t) estimated using Equation (8.11), Q is the volumetric flow rate (L^3/t), A_{sides} and is the cross-sectional area of the submerged pond sides in a vertical plane, A_{bottom} is the cross-sectional area of the pond bottom in a horizontal plane, and A_{total} is the total area of both sides and bottom. In the general case, the value for both A_{sides} and A_{bottom} will depend upon the depth of water in the facility. Reasonable first approximations can be derived using values based on one-half the maximum depth of water for the design storm. As a minimum, the total flow rate, Q, times the required draining time, T_{req} (e.g. from Table 8.3) should be greater than the design volume, V_{design}.:

$$(Q)T_{req} \geq V_{design} \quad (8.15)$$

8.6.9 Design approaches for continuous hydrographs

The required infiltration rates given by equation (8.15) were developed based on the assumption that the complete design flow volume arrives "instantaneously" at the infiltration facility. The WDOE storm-water manual (2001) specifies that the infiltration facility must be designed to drain completely within 24 hours **after the flow to it has stopped**. For the 24-hour design event, flow will not stop arriving to the infiltration facility until at least 24 hours after the storm begins. The WDOE manual effectively allows at least 48 hours from the beginning of the storm event before the water must be infiltrated.

For typical inflow hydrographs, similar to what is shown in Figure 8.2, most of the stormwater arrives relatively early in the storm event, which allows more than 24 hours for it to become infiltrated. The methodologies described by Equation (8.15) do not include this "extra" time. More importantly, the single-event hydrograph does not directly account for the effects of a long sequence of multiple precipitation events.

Continuous flow models such as WSDOT's MGSFLOOD model or U.S. EPA's HSPF can be used to incorporate the transient effects described by continuous hydrographs. One approach for accomplishing this is to include the infiltration facility in the runoff or flow models using a stage-discharge relationship. This stage-discharge relationship describes the flow rate as a function of the depth of water in the pond or trench. The infiltration equations given by Equations (8.12) and (8.13) can be used for these purposes. These equations effectively provide stage-discharge relationships for ponds and trenches. Both the gradient term and the area term in Equations (8.12) and (8.13) depend upon the depth or stage of water in the pond or trench. These stage discharge relationships can be directly implemented within the continuous flow models to evaluate the change in depth in the facility with time.

The typical design approach for using continuous hydrographs for facilities without overflow features would be to select a pond geometry that would provide a minimum freeboard for the continuous design hydrograph. The magnitude of this minimum freeboard would be dependent upon the consequences of overflow from the facility.

For facilities that include overflow features or design components, the design approach would be to select the pond geometry to meet the performance objective for water quantity considerations given by Minimum Technical Requirement #7 (MTR #7) in the WDOE Stormwater Management Model (Volume I, Chapter 2, page 2-31). This requirement specifies that stormwater discharges to streams must mimic certain aspects of pre-developed conditions, as described in Section 1.

8.6.10 Consider computer simulations to refine design

More sophisticated computer-based simulations should be considered for many sites. It is likely that these simulations will result in facilities that are less over-designed than the facilities that would result from infiltration rates given in the WDOE stormwater manual (2001). These simulations should be especially considered for the following situations:

1) Sites with significant heterogeneity and stratigraphy, particularly sites where subsurface lateral flow through higher-permeability strata may be extensive.
2) Sites where transient effects of inflow rates are likely to be important, as discussed in Section 8.6.9.
3) Sites with water table depths or depths to low-permeability layers that are greater than 100 feet. These types of sites were not included in the computer simulations described in Chapter 7 and the regression equation given by Equations (8.6) and (8.8) may significantly under-estimate the actual gradient.

Steady-state, saturated simulations similar to what can be developed using the USGS MODFLOW computer code will generally give conservative results that are more realistic than the procedures described in this manual. For particularly important sites, transient, unsaturated models may be warranted, similar to what is described in Chapter 7.

8.6.11 Post design-evaluations

Full-scale tests should be conducted at all sites on a periodic basis. If a source of water is available (e.g. nearby fire hydrants or water trucks), these tests should be conducted using controlled and measured inflow rates that result in significant ponding in the facility. If water sources are not available, inflow rates should be monitored if at all possible.

By monitoring inflow rates, relationships can be developed that give infiltration rates as a function of stage or water level in the facility. These types of relationships are particularly valuable if computer-simulations are used to evaluate the design performance, or if continuous hydrographs are used in the design approach. Appendix A describes methods for conducting and analyzing data from the full-scale tests with known inflow rates.

In cases where the full-scale tests indicate infiltration rates that are significantly less than the design rates, the facility may need to be modified. If the lower rates are expected to be caused by soil plugging or bio-fouling, then remediation of the existing

pond may be possible. For some sites, particularly those where the lower rates are due to unexpectedly high groundwater levels, there may be little that can be done, other than increasing the areal extent of the facility or designing an overflow system. The approaches described in this manual can be used to re-evaluate these design options. In many instances, more refined and sophisticated analyses will be warranted.

8.7 Example calculations using the suggested design approach

This section describes examples calculations used to estimate infiltration rates for ponds. The focus of the calculations is on estimating infiltration rates using the approaches and equations described in Sections 8.6.4 through 8.6.7. The examples are based on field data collected at four existing facilities described in the Thurston County study (Wiltsie, 1998). Infiltration rates are estimated for the following sites: Airdustrial, Lacy Lid, Sweetbriar, and Woodward Glen. These four sites were selected because of the availability of data describing groundwater levels. Descriptions of the four sites are included in Appendix D and in Table 8.11.

8.7.1 Estimate saturated hydraulic conductivity from soil information

Saturated hydraulic conductivity values will be estimated in the examples using soil texture information, as described in Section 8.6.4.1. Table 8.12includes soil texture information that was collected at the four sites. The grain-size curves that used to develop this data are included in Appendix C.

The first column in Table 8.12 describes the number of horizontal locations at which soil samples were collected at each facility. The second column describes the number of layers that were encountered at each horizontal location and the third column gives the thickness of each of these layers. Columns E through H in Table 8.12 gives soil texture information. This information includes D_{10}, D_{60}, and D_{90} grain size diameters and the fraction of fine-grained material, f_{fines}, for each horizontal location and for each layer.

The soil texture information can be used to estimate the saturated hydraulic conductivity value using the log-regression equation (Equation 8.2):

$$\log_{10}(K_s) = -1.57 + 1.90d_{10} + 0.015d_{60} - 0.013d_{90} - 2.08\mathrm{f}_{\mathrm{fines}} \quad (8.2)$$

Column I in Table 8.12 gives saturated hydraulic conductivity values in cm/s for each location and layer calculated using Equation 8.2. These values represent "point" measurements for the hydraulic conductivity of each layer at each location. The values for each layer can be combined using Equation 8.4 to give an equivalent hydraulic conductivity for each location:

$$K_{equiv} = \frac{d}{\sum \frac{d_i}{K_i}} \quad (8.4)$$

These equivalent hydraulic conductivity values are given in Column J in Table 8.12.

Finally, the equivalent hydraulic conductivity values for each location can be averaged to obtain a single estimate of saturated hydraulic conductivity value for each facility. This averaging is described in Column K in Table 8.12. The average hydraulic conductivity values in units of ft/day are included in Column L.

8.7.2 Estimate the hydraulic gradient

The hydraulic gradient at each site can be estimated using Equation 8.6:

$$\text{gradient} = \mathrm{i} \approx \frac{D_{wt} + D_{pond}}{138.62(K^{0.1})} CF_{size} \quad (8.6)$$

where K is saturated hydraulic conductivity in feet/day, D_{wt} is the depth in feet from the base of the infiltration facility to the water table or to the first low-permeability layer, and D_{pond} is the depth of water in the pond, in feet.

The correction for pond size, CF_{size}, is given by Equation 8.7:

$$CF_{size} = 0.73(A_{pond})^{-0.76} \quad (8.7)$$

where

CF_{size} = correction factor for size of the pond

A_{pond} = area of the pond bottom in acres

Equation 8.7 was developed for ponds with bottom areas between 0.6 and 6 acres in size. For small ponds (ponds with area equal to 2/3 acre), the correction factor is equal to 1.0. All of the example facilities were smaller than 2/3 acre so that correction factor for pond size is 1.0 in all cases.

Table 8.13 summarizes gradient calculations. The depths to the water table at the four sites, D_{wt}, and the depth of water in the pond D_{pond}, were estimated based on data that were collected using pressure transducers at each site. These data are described in Wiltsie et al. (1998). The hydraulic conductivity values in column E were estimated using the log regression equation, as described in the previous section. Column F gives estimated gradient for each location.

8.7.3 Estimate the uncorrected infiltration rate

The infiltration rates are estimated by multiplying the saturated hydraulic conductivity with the hydraulic gradient, as described by Equation 8.9:

$$f = K\left(\frac{dh}{dz}\right) = Ki \quad (8.9)$$

Table 8.14 summarizes the calculated infiltration rates for the example sites.

8.7.4 Apply correction factors for pond geometry and for biofouling and siltation

The infiltration rates calculated in Table 8.14 do not include corrections for pond geometry or for biofouling and siltation caused by poor maintenance and/or insufficient pretreatment. The correction factor for pond geometry is given by Equation 8.10:

$$CF_{aspect} = 0.02A_{ratio} + 0.98 \quad (8.10)$$

Table 8.15 includes aspect ratios for the four example ponds. The calculated correction factor for pond geometry is also included in Table 8.15.

Correction factors for biofouling and siltation are included in Table 8.7. These correction factors describe both biofouling and poor maintenance. The report by Wiltsie (1998) includes descriptions of pond conditions, including biofouling and maintenance practices. The correction factors in Table 8.16 were estimated based on these descriptions. Two estimates of infiltration rate are included for the Airdustrial site. The first estimate assumes poor maintenance with a correction factor for siltation and biofouling equal to 0.3. The second estimate assumes a maintained facility with a correction factor equal to 1.0. These two estimates were developed to allow comparisons with observed infiltration rates from tests that were conducted both before and after maintenance activities at the actual field site.

The infiltration rates calculated in Table 8.15 are corrected using the correction factors for aspect ratio and for maintenance and biofouling in Table 8.16. These corrected infiltration rates are calculated using Equation (8.11):

$$f_{corr} = (CF_{silt/bio})(CF_{aspect})\, f = (CF_{silt/bio})(CF_{aspect})Ki \quad (8.11)$$

8.7.5 Comparison of observed and calculated infiltration rates

Table 8.17 provides a comparison of the measured infiltration rates with the estimates that were developed using the suggested design approach. The rates are reasonably similar, in part because the correction factors used for siltation and biofouling were originally developed based on observations at these ponds. Table 8.17 also includes estimates used the WDOE approach based on the D_{10} grain size diameters. The values calculated using the equations suggested in the current study incorporate more site-specific characteristics, including pond size, depth to groundwater, and depth of water in the pond. These additional characteristics allow more variability in the estimated

infiltration rates, as shown in Table 8.17. The WDOE recommended rates based on USDA soil textural classification and D_{10} measurements (reproduced in Tables 8.8 and 8.9) do not explicitly consider hydraulic gradient. The WDOE rates are based on observations from sites in Western Washington with shallow groundwater tables and with absent or inconsistent pretreatment and maintenance practices. As expected, these rates are reasonably similar to the rates estimated using the approach developed in the current study for these particular sites in Western Washington. The two approaches would give significantly different results for facilities with deeper water tables and with better pretreatment and maintenance activities.

Table 8.1—Sum of mean square error of synthetic and natural soils for selected equations.

	Regression Equation	Sum of mean square error
C.1	$K_s = 0.87\, d_{10}^2$	5.43
C.13	$\text{Log}(K_s) = -1.57+1.90\, d_{10} +0.015\, d_{60} - 0.013\, d_{90} -2.08 fines$	4.72

Note: d_{10}, d_{60}, and d_{90} are the grain sizes in mm at which 10, 60, and 90 percent of the material by weight is smaller, fines is the fraction of material passing 0.075 mm (#200) sieve, and K_{sat} is the saturated hydraulic conductivity in units of cm/sec.

Table 8.2—Summary of calculated infiltration rates.

Site	Long-term infiltration rate (in/hr)	Short-term infiltration rate (in/hr)	Soil Texture Description	Estimated long-term rate from soil texture (WDOE, 2001) (in/hr)
Clark County	0.23	2.5	Loam/Silty Loam	0.13/0.25
Cimarron	0.1	1.9	Silty sand loam	0.25
Balsam 7-11	2.1	13.2	Silty Loam	0.25
Krista Firs	0.33	2.8	Sand	2

Table 8.3 – Example water quality performance objectives for infiltration facilities

Agency	Recommended or allowable storage time, T_{req}	Reference
Federal Highway Administration	**72 hours**	*Urban Design Drainage Manual*, Hydrologic Engineering Circular No. 22, Washington D.C., 1996.
Maryland Department of the Environment	**48 hours**	*Maryland Stormwater Design Manual*, Center for Watershed Protection , Annapolis, MD 1998.
California Department of Transportation	**24 hours**	*Stormwater quality handbook*, Project Training and Design Guide, Sacramento, CA, 2000.
Washington Department of Ecology	**24 hours**	*Stormwater Management Manual for Western Washington*, Publication 99-13, Olympia, WA, 2001.

Table 8.4 – WDOE requirements for subsurface characterization at infiltration facilities (from WDOE, 2001)

WDOE (2001) Requirements	Comments and Recommendations
Subsurface explorations (test holes or test pits) to a depth below the base of the infiltration facility of at least 5 times the maximum design depth of ponded water proposed for the infiltration facility. (p. 3-62)	This should be viewed as a minimum requirement. Infiltration rates from stormwater facilities can be affected by relatively deep features in the groundwater flow system, particularly for sites with subsurface layering. Deeper features may be especially important in western Washington where there are long periods of precipitation that may cause groundwater mounding and where facilities may receive runoff from multiple storms. In many cases, it may be prudent to continue subsurface explorations to depths of 50 feet or greater.
Continuous sampling (representative samples from each soil type and/or unit within the infiltration receptor) to a depth below the base of the infiltration facility of 2.5 times the maximum design ponded water depth, but not less than 6 feet. (p. 3-62)	This should be viewed as a minimum requirement. It may not be conservative, especially for ponds that receive runoff from multiple storms and for sites with subsurface layering. Relatively small-scale layering can affect infiltration performance, even if these features occur relatively deep beneath the facility. Continuous samples and more detailed sampling to greater depth is probably warranted in many cases.
For basins, at least one test pit or test hole per 5,000 ft ^{2} of basin infiltrating surface (in no case less than two per basin) (p. 3-62)	This is a reasonable amount of investigation.
For trenches, at least one test pit or test hole per 50 feet of trench length (in no case less than two per trench). (p. 3-62)	This is a high density of test pits, especially as compared to the sampling frequency for ponds
Prepare detailed logs for each test pit or test hole and a map showing the location of the test pits or test holes. Logs must include at a minimum, depth of pit or hole, soil descriptions, depth to water, presence of stratification. (p. 3-63)	This is a reasonable and appropriate recommendation.

WDOE (2001) Requirements	Comments and Recommendations
As a minimum, one soil grain-size analysis per soil stratum in each test hole shall be performed within 2.5 times the maximum design water depth, but not less than 6 feet.	Grain size analyses should be performed on samples from all strata encountered in the soil borings. Deeper borings are recommended.
Soil characterization for each soil unit (soils of the same texture, color, density, compaction, consolidation and permeability) encountered should include: grain-size distribution, textural class (USDA), percent clay content (include type of clay, if known, color/mottling, and variations and nature of stratification	These are prudent and reasonable recommendations.
Installation of ground water monitoring wells (at least three per infiltration facility, unless the highest ground water level is known to be at least 50 feet below the proposed infiltration facility)	This is a prudent and reasonable recommendation. Note that if wells are installed to 50 feet, continuous or near-continuous soil samples are recommended for the full depth.
Monitor the seasonal ground water levels at the site during at least one wet season.	This is a prudent and reasonable recommendation
Estimate of the volumetric water holding capacity of the infiltration receptor soil.	This is a prudent and reasonable recommendation
Existing ground water flow direction and gradient ,lateral extent of infiltration receptor, horizontal hydraulic conductivity of the saturated zone	These are prudent and reasonable recommendations.
Impact of the infiltration rate and volume at the project site on ground water mounding, flow direction, and water table; and the discharge point or area of the infiltrating water. A ground water mounding analysis should be conducted at all sites where the depth to seasonal ground water table or low permeability stratum is less than 15 feet and the runoff to the infiltration facility is from more than one acre.	Groundwater mounding analyses are prudent. However, the one-acre requirement for a mounding analysis is arbitrary. This should be based on the anticipated depth of stormwater discharge. Low-permeability strata below 15 feet may also affect mounding and should be considered in mounding analyses.

Table 8.5 – Comparison of methods for estimating saturated hydraulic conductivity values for unconsolidated soils above the water table.

Method	**Advantages**	**Disadvantages**
Regressions using grain size information	Inexpensive; rapid sample collection; can often collect many samples to evaluate heterogeneity and layering	Errors may be significant (a factor or 10 or more), especially for soils with large percentages of fine materials or swelling clays
Laboratory permeameter tests	Measures effects of swelling, well-accepted methods and protocols	Typically disturbed samples; requires specialized equipment and expertise
Field infiltrometer tests	Measures unsaturated flow processes; gives in-situ results that reduce the effects of sample disturbance	Time consuming, only possible with near-surface soils that can be exposed in excavations; should be used to estimate saturated hydraulic conductivity and not infiltration rate
Pilot infiltration tests	Gives large-scale estimate that incorporates effects of heterogeneity	Large volumes of water are typically required; only possible with near-surface soils that can be exposed in excavations
Packer permeability tests in boreholes	Allows in-situ measurements at depth, allows specific strata to be tested	Expensive and time-consuming, requires specialized equipment and expertise, large volumes of water may be required
Estimates from air conductivity	No water is required; tests can be done in the field or in the laboratory; relatively rapid test;	Requires specialized equipment and expertise; errors may be significant if swelling occurs; methods and protocols not yet well-accepted

Table 8.6 – Example calculations for equivalent hydraulic conductivity using the Hazen approximation

Layer	Layer thickness (inches)	D_{10} (mm)	K_w (cm/s)	K_w (in/hr)	$K_{equivalent}$ (in/hr)
1	13	0.05	2.2E-03	3	
1	8	0.08	5.6E-03	8	
1	10	0.18	2.8E-02	40	6
2	9	0.09	7.0E-03	10	
2	6	0.13	1.5E-02	21	
2	17	0.09	7.0E-03	10	11
3	14	0.07	4.3E-03	6	
3	8	0.54	2.5E-01	360	
3	7	0.23	4.6E-02	65	12
4	18	0.06	3.1E-03	4	
4	8	0.34	1.0E-01	143	6
Averages:				**61**	**8.7**

Table 8.7 —Infiltration rate reduction factors to account for effects of biofouling and siltation

A	B	C	D
Potential for biofouling	**Degree of long-term maintenance and performance monitoring**	**Infiltration rate reduction factor**	
		Ponds	**Trenches**
Low	Average to high	0.9	0.9
Low	Low	0.6	0.8
High	Average to high	0.5	0.75
High	Low	0.2	0.6

Table 8.8—Recommended infiltration rates based on USDA soil textural classification (from Table 3.7 in Vol. III and Table 7.1 in Vol. V, WDOE, 2001)

	Short-Term Infiltration Rate, in/hr (cm/hr)	**Correction Factor**	**Estimated Long-Term Infiltration Rate, in/hr (cm/hr)**
Clean sandy gravels and gravelly sands (i.e., 90% of the total soil sample is retained in the #10 sieve)	20 (50)	2 (5)	10 (25)
Sand	8 (20)	4 (10)	2 (5)
Loamy Sand	2 (5)	4 (10)	0.5 (1.3)
Sandy Loam	1 (2.5)	4 (10)	0.25 (0.64)
Loam	0.5 (1.3)	4 (10)	0.13 (0.33)

Table 8.9—Recommended infiltration rates based on ASTM gradation testing (from Table 3.8 in Vol. III and Table 7.2 in Vol. V, WDOE, 2001)

D10 Size from ASTM D422 Soil Gradation Test mm	**Estimated Long-Term Infiltration Rate, in/hr (cm/hr)**
>0.4	9 (23)
0.3	6.5 (16.5)
0.2	3.5 (8.9)
0.1	2.0 (5)
0.05	0.8 (2)

Table 8.10—Correction factors to be used with in-situ infiltration measurements to estimate long-term design infiltration rates (from Table 3.9 in Vol. III and Table 7.3 in Vol. V, WDOE, 2001)

Issue	**Partial Correction Factor**
Site variability and number of locations tested	CFv = 1.5 to 6
Degree of long-term maintenance to prevent Siltation and bio-buildup	CFm = 2 to 6
Degree of influent control to prevent siltation and bio-buildup	CFi = 2 to 6
Total correction factor	CF = CFv + CFm + CFi

Table 8.11 – Description of ponds used in example calculations

Site Name	Site Address	Pond Age (years)	Pond Bottom Surface Area (ft^2)	Pond Volume (ft^3)	Pond Geometry
Airdustrial	Bonniewood Dr SW and 70th Ave Tumwater, WA	7	6,400	34,000	Rectangular
Lacey Lid	Yelm Hwy and Corporate Ctr Lacey, WA	10	17,100	248,276	Rectangular
Margaret McKenny	Morse-Merryman Rd SE and Quentin St.; Lacey, WA	10	6,720	72,352	Rectangular
Sweetbriar	Boulevard Rd and 45th Av. SE Lacey, WA	8	15,000	92,123	Triangular
Woodard Glen	Lister Rd NE and Cherry Blossom Olympia, WA	21	2,000	8,700	Small trapezoidal

Table 8.12 - Estimates of saturated hydraulic conductivity developed using the log-regression relationship

A	B	C	D	E	F	G	H	I	J	K
Site	**Location**	**Layer**	**Thickness**	**d_{10}**	**d_{60}**	**d_{90}**	**fines**	**K_s (cm/s)**	**K_{equiv} (cm/s)**	**K_{equiv} (ft/day)**
Airdustrial	1	1	67"	0.2	0.3	0.4	0.02	5.8E-02	5.8E-02	
	2	1	48"	0.13	0.31	0.7	0.03	4.0E-02	4.0E-02	
								Average K_{equiv}	**4.9E-02**	**140**
Lacey Lid	1	1	69”	0.11	0.26	0.4	0.03	3.7E-02	3.7E-02	
	2	1	50”	0.16	0.32	0.7	0	5.3E-02	5.3E-02	
								Average K_{equiv}	**4.5E-02**	**128**
Margaret McKenny	1	1	22"	0.34	12	31	0.02	6.34E-02		
	1	2	20"	0.23	1	10	0	5.55E-02		
	1	3	12"	0.11	0.8	11	0.06	2.37E-02	4.4E-02	
								Average K_{equiv}	**4.4E-02**	**126**
Sweetbriar	1	1	36”	0.16	0.28	0.4	0	5.34E-02		
	1	2	9”	0.11	0.28	0.41	0.03	3.72E-02		
	1	3	24”	0.18	0.3	0.5	0	5.82E-02	5.2E-02	
	2	1	36”	0.18	0.29	0.4	0.02	5.30E-02		
	2	2	30”	0.21	0.52	0.94	0	6.60E-02	5.8E-02	
								Average K_{equiv}	**5.5E-02**	**156**
Woodard Glen	1	1	15"	0.55	9	11.7	0	2.84E-01		
	1	2	28"	0.2	0.55	1.5	0.01	5.92E-02	8.2E-02	
	2	1	36"	0.18	0.28	0.4	0.01	5.56E-02		
	2	2	6"	0.2	40	100	0	1.24E-02	3.7E-02	
								Average K_{equiv}	**5.9E-02**	**168**

Table 8.13– Estimates of hydraulic gradient for the example sites

A	B	C	D	E	F
Facility	**A_{pond} (acres)**	**D_{wt} (feet)**	**D_{pond} (feet)**	**K (ft/day)**	**Calculated gradient**
Airdustrial	0.15	3.0	1.0	140	0.018
Lacey Lid	0.52	2.5	0.4	128	0.013
Margaret McKenny	0.15	3.5	1.3	126	0.021
Sweetbriar	0.34	3.2	1.7	156	0.021
Wood Glen	0.05	3.2	0.6	168	0.016

Table 8.14 – Estimates of uncorrected infiltration rates for the example sites

A	B	C	D	E
Facility	**K (ft/day)**	**K (in/hr)**	**Calculated gradient**	**Calculated infiltration rate (in/hr)**
Airdustrial	140	70	0.018	1.23
Lacey Lid	128	64	0.013	0.83
Margaret McKenny	126	63	0.021	1.33
Sweetbriar	156	78	0.021	1.64
Wood Glen	168	84	0.016	1.38

Table 8.15 – Correction factors for aspect ratios

Facility	Aspect Ratio	CF_{aspect}
Airdustrial	1.0	1.0
Lacey Lid	18.0	1.3
Margaret McKenny	5.7	1.1
Sweetbriar	1.5	1.0
Woodward Glen	1.4	1.0

Table 8.16 – Correction factors for siltation and biofouling

Facility	Descriptions Regarding Siltation and Biofouling	CF_{aspect}	$CF_{silt/bio}$	Infiltration (in/hr)	
				Uncorrected	Corrected
Airdustrial	Not maintained	1.0	0.3	1.23	0.37
Airdustrial	Maintained	1.0	1	1.23	1.23
Lacey Lid	Silt fouling	1.3	0.5	0.83	0.56
Margaret McKenny	Partially maintained	1.1	0.9	1.33	1.31
Sweetbriar	Not maintained	1.0	0.3	1.64	0.50
Woodward Glen	Maintained	1.0	1	1.38	1.39

Table 8.17. Comparison of measured infiltration rates with the estimated rates

A	B	C	D	E
Facility	**Estimated infiltration (in/hr)**	**Observed infiltration rate (in/hr)**	**Rate estimated from WDOE[a] (in/hr)**	**D_{10} (mm)**
Airdustrial (pre-maintenance)	0.37	0.3	2	0.09
Airdustrial (post-maintenance)	1.23	1.7	2	0.09
Lacey Lid	0.56	0.3	2	0.12
Margaret McKenny	1.31	2.0	3.5	0.25
Sweetbriar	0.50	0.4	0.8	0.065
Woodward Glen	1.39	2.3	0.2	0.1

[a]Rate based on D_{10} using Table 3.8 in Vol. III and Table 7.2 in Vol. V, WDOE, 2001

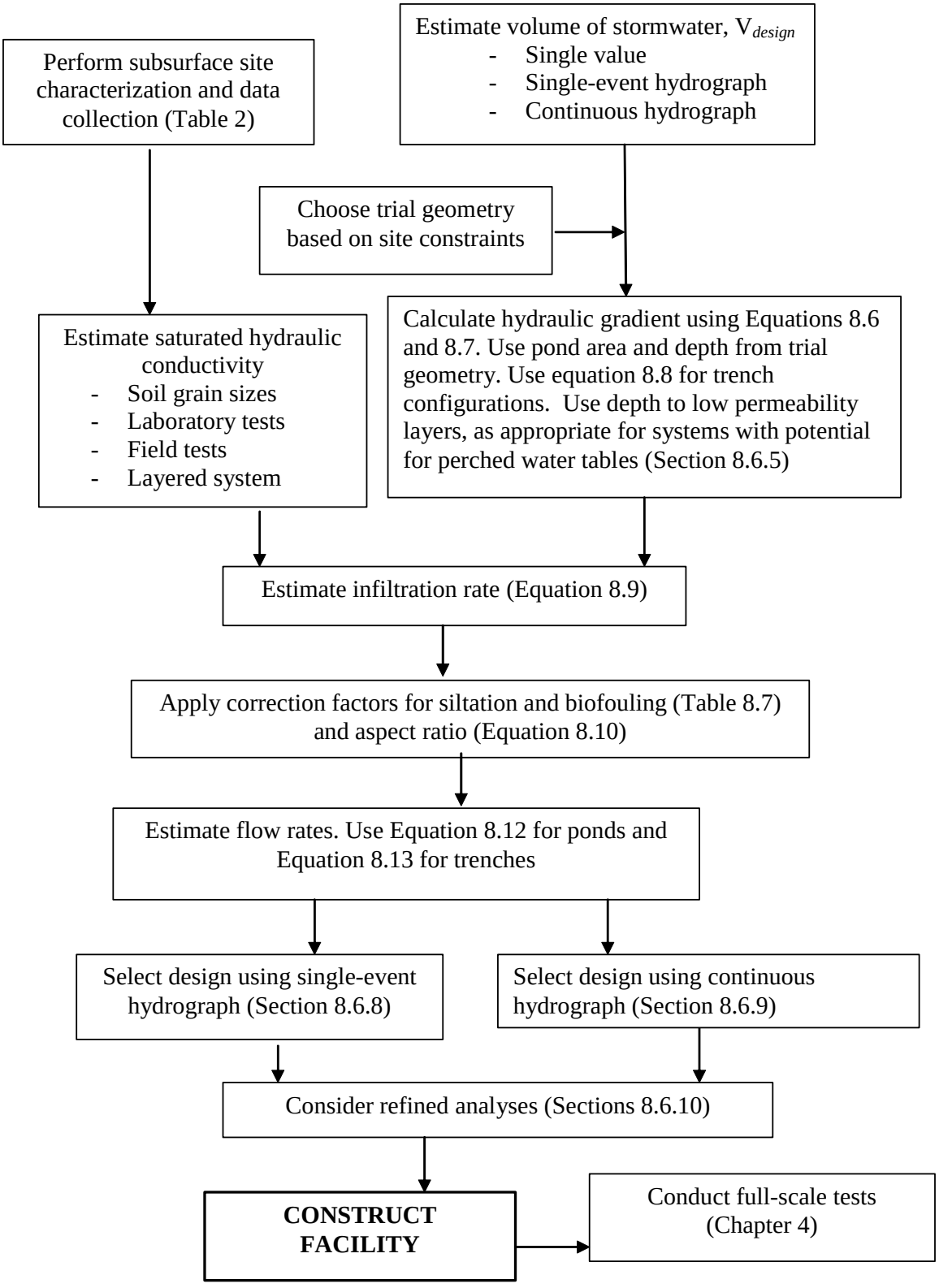

Figure 8.1 – Flow chart summarizing design approach for ponds

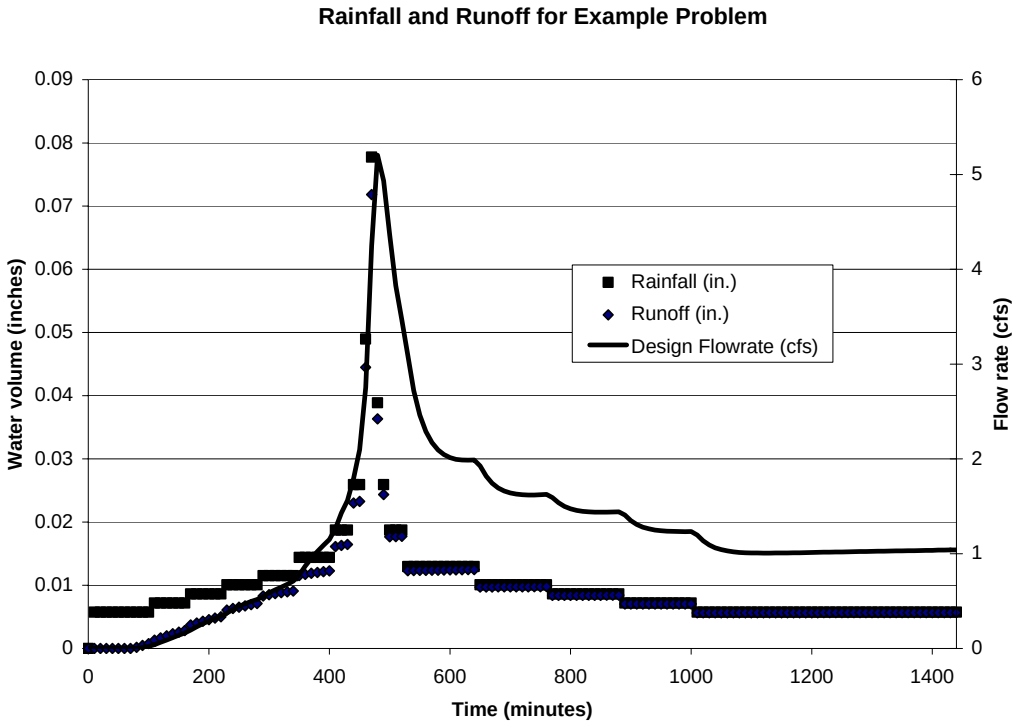

Figure 8.2– Example single-event hydrograph used for infiltration pond design

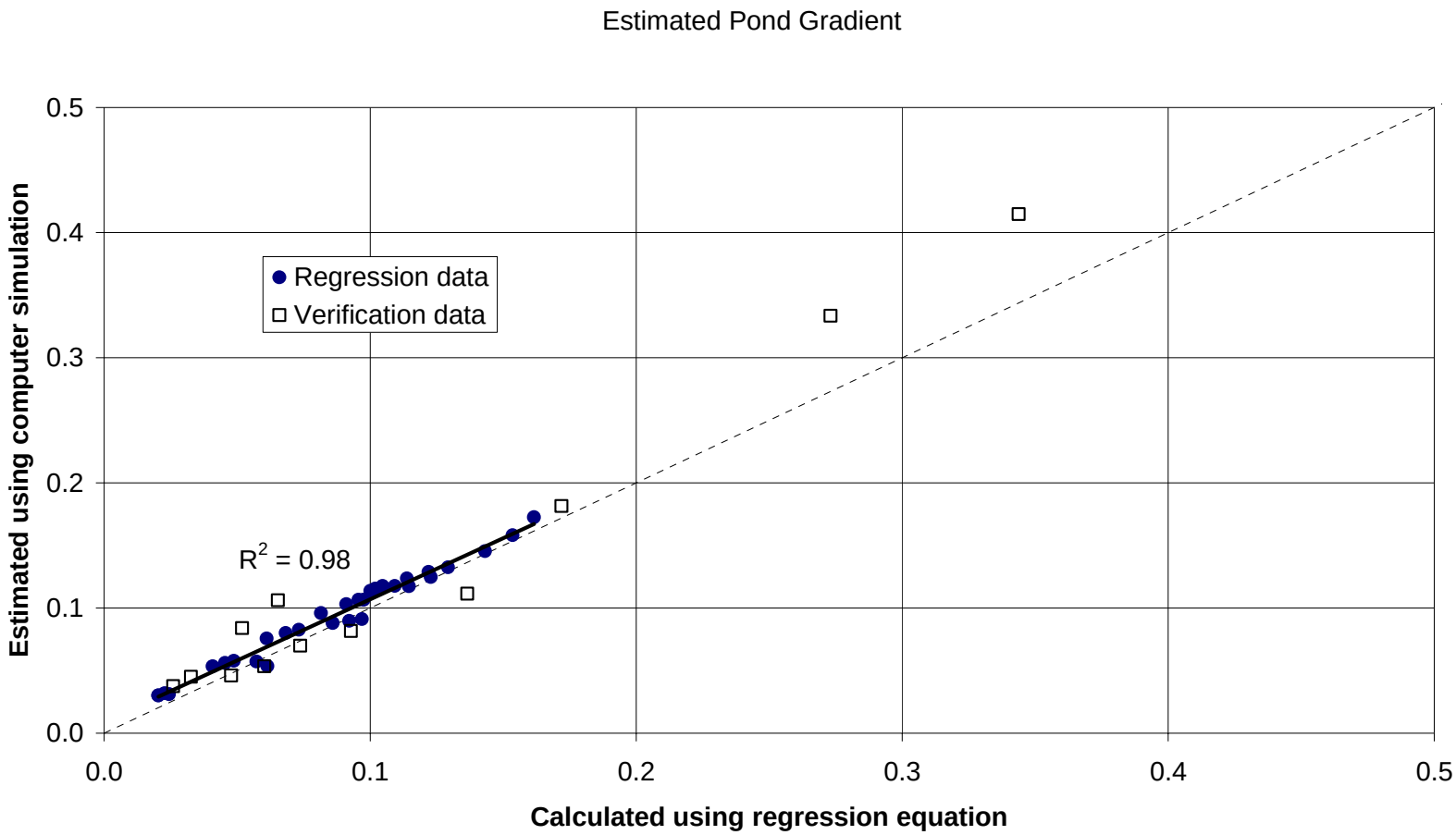

Figure 8.3 – Comparison of gradients for ponds calculated using Equation (8.6) with gradients simulated using computer models

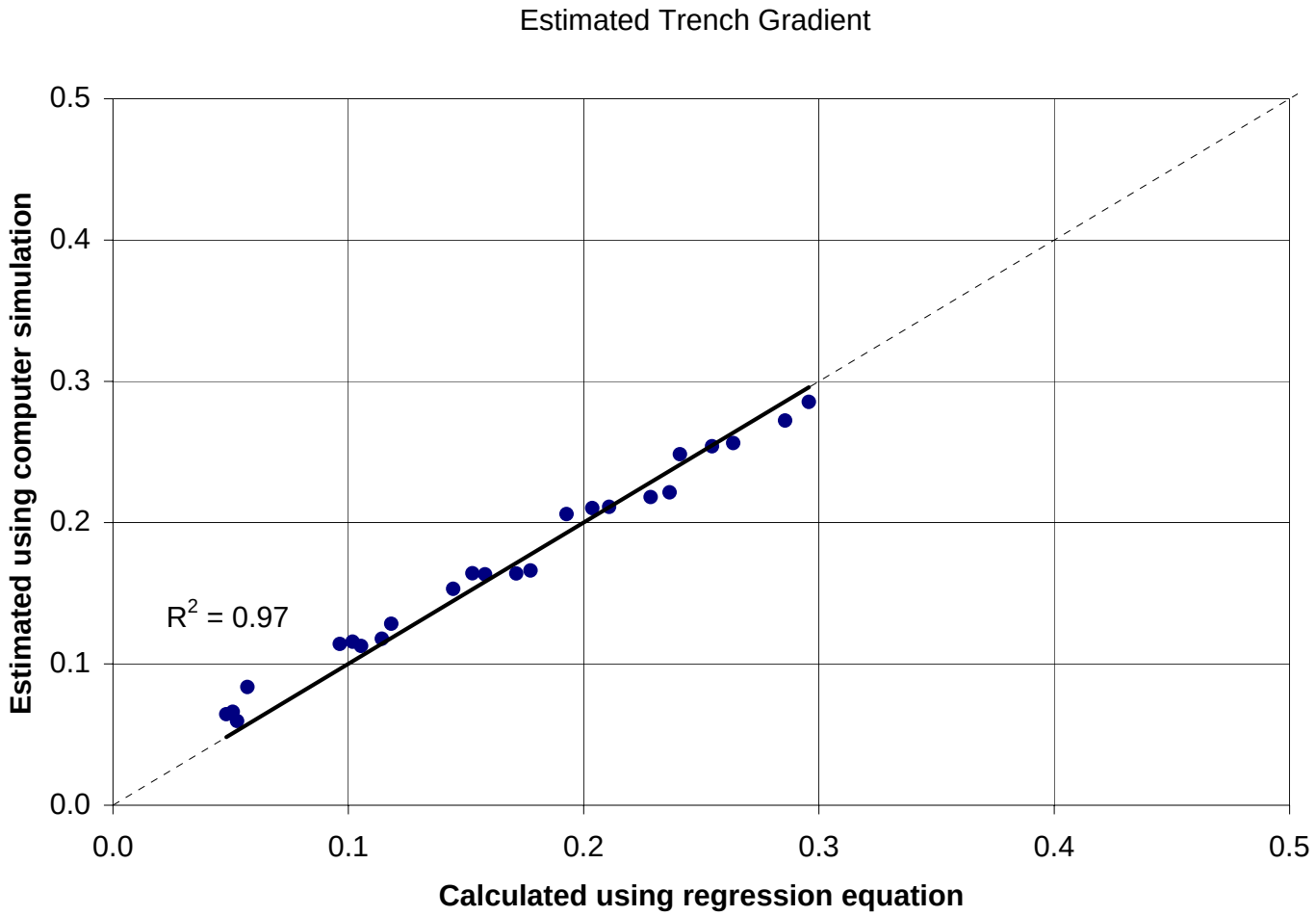

Figure 8.4– Comparison of gradients for trenches calculated using Equation (8.8) with gradients simulated using computer models

ACKNOWLEDGMENTS

The authors wish to acknowledge the generous help and support provided during the study by Tony Allen and Keith Anderson at the Washington State Department of Transportation. Steve Foley at King County, Jerry Anderson at Kitsap County, Ed McMillan at Clark County, and Scott Lindblum at Thurston County were especially helpful. Each provided access to stormwater facilities in their jurisdictions, freely offered data and information related to these facilities, and shared their considerable experiences and insights.

REFERENCES

Anderson, J., *personal interview*, Surface and Storm Water Management Department, Kitsap County, January, 2001.

Anderson M.P. and W.W. Woessner, *Applied groundwater modeling : simulation of flow and advective transport*, Academic Press, San Diego, 1992.

Akan, A.O., Sizing stormwater infiltration structures, *Journal of Hydraulic Engineering*, ASCE, 128 (5): 534-537, May, 2002.

Blackwell, P.S., A.J. Ringrose-Voase, N.S. Jayawardane, K.A. Olsson, D.C. McKenzie, and W.K. Mason, The use of air-filled porosity and intrinsic permeability to air to characterize structure of macropore space and saturated hydraulic conductivity of clay soil, *Journal of Soil Science*, 41, pp. 215-228, 1990.

Bouwer, H., *Groundwater Hydrology*, McGraw-Hill Book Company, 1978.

Bouwer, H. and R.C. Rice, Effect of water depth in groundwater recharge basins on infiltration, *ASCE Journal of Irrigation and Drainage Engineering*, 115(4), pp. 556-567, 1989.

Butchart, C.D., *Using Air Conductivity and Soil Texture as Indicators of Infiltration Rates for Stormwater Infiltration Ponds*, M.S. Thesis, Department of Civil and Environmental Engineering, University of Washington, 2001.

California Department of Transportation, *Stormwater quality handbook, Project Training and Design Guide*, Sacramento, CA, 2000.

Carsel, R.F. and R.S., Parrish, Developing joint probability distributions of soil water retention characteristics, *Water Resources Research*, 24(5), pp. 755-769, 1988.

Chin, D.A., *Water Resources Engineering*, Prentice Hall, 2000.

Chow, V.T., D.R. Maidment and L.W. Mays, *Applied Hydrology*, McGraw-Hill Book Company, 1988.

Corey, A.T., Methods of Soil Analysis, Part 1, *American Society of Agronomy - Soil Science Society of America*, 1986.

Danielson, R.E. and P.L. Sutherland, Porosity, Methods of Soil Analysis, Part 1, *American Society of Agronomy - Soil Science Society of America*, 1986.

Davis, S.N. and R.J.M. DeWiest, *Hydrogeology*, John Wiley & Sons, Inc., 1966.

Davis, J.M., J.L. Wilson and F.M. Phillips, A portable air-minipermeameter for rapid in-situ field measurements, *Ground Water,* Vol 32, No. 2, pp. 258-266, 1994.

Drost, B.W. et al., Hydrology and quality of ground water in northern Thurston County, Washington, *Water Resources Investigations Report 92-4109*, U.S. Geological Survey; Denver, CO, 1999.

Duchene, M., E.A. McBean, and N.R. Thomson, Modeling of Infiltration from Trenches for Storm-water Contro, ASCE Journal of Water Resources Planning and Management, Vol. 120(3), pp. 276-293, 1992.

Federal Highway Administration, *Urban Design Drainage Manual, Hydrologic Engineering Circular No. 22*, Washington D.C., 1996.

Ferguson, B.K., *Stormwater Infiltration*, CRC Press, Inc., 1994.

Fetter, C.W., *Applied Hydrogeology*, Prentice-Hall, Inc., 1994.

Foley, S. *personal interview*, Department of Natural Resources, Water and Land Resources Division, King County, August, 2000.

Freeze A. and J. Cherry, *Groundwate*r, Prentice-Hall, Inc., 1979.

Hsieh, P.A., W. Wingle, and R.W. Healy, A graphical software package for simulating fluid flow and solute or energy transport in variably saturated porous media: *U.S. Geological Survey Water-Resources Investigations* Report 99-4130, 2000

Iversen B., P. Moldrup , P. Schjonning, and P.Loll. Air and water permeability in differently textured soils at two measurement scales, *Soil Science*, 166(10), pp. 643-659, October, 2001.

Janna, W.S., *Introduction to Fluid Mechanics*, PWS-Kent Publishing Company, 1993.

King County, *King County Surface Water Design Manual*, Seattle, Washington, 1998.

Loll P., P. Moldrup, P. Schjonning, and H. Riley, Predicting saturated hydraulic conductivity from air permeability: Application in stochastic water infiltration modeling, *Water Resource Resources*, 35(8), pp. 2387-2400, 1999.

Maryland Department of Natural Resources, Water Resources Administration, Stormwater Management Division, *Standards and Specifications for Infiltration Practices*, Maryland Department of Natural Resources, Annapolis, Maryland, 1984.

Maryland Department of the Environment and Center for Watershed Protection, *2000 Maryland Stormwater Design Manual, Volumes I and II*, Maryland Department of the Environment, Baltimore, Maryland, 2000.

Massmann, J.W., Applying groundwater flow models in vapor extraction system design, *ASCE Journal of Environmental Engineering*, Vol. 115, pp. 129-149, 1989.

Massmann, J.W. and L. Johnson, A set of exercises illustrating flow in porous media, *Ground Water*, Volume 34(4), July-August, pp. 499-503, 2001.

Mays, L.W., *Water Resources Handbook*, McGraw-Hill, 1996.

McDonald M.G. and A.W. Harbaugh, A modular three-dimensional finite-difference ground-water flow model, *Techniques of Water-Resources Investigations of the United States Geological Survey. Book 6, Modeling techniques ; chapter A1*, U.S. Geological Survey, 1988.

Meyer, P.D., M.L. Rockhold, and G.W. Gee, *Uncertainty Analyses of Infiltration and Subsurface Flow and Transport for SDMP Sites*, Pacific Northwest National Laboratory, 1997.

National Oceanic and Atmospheric Administration, 2000
http://www.seawfo.noaa.gov/climate/olympia/2000/OCT2000/103100.cli

Rawls, W.J., and D.L. Brakensiek, *Prediction of Soil Water Properties for Hydrologic Modeling*, Watershed Management in the Eighties, ASCE, 1985.

Rawls, W.J., D.L. Brakensiek and K.E. Saxton, *Estimation of Soil Water Properties*, Transations of the ASAE, 1982.

Salvucci, G.D. and D. Entekhabi, Explicit expressions for Green-Ampt (delta function diffusivity) infiltration rate and cumulative storage, *Water Resources Research*, Vol. 30, No. 9, pp. 2661-2663, 1994.

Schuh, W.M., Seasonal Variation of Clogging of an Artificial Recharge Basin in a Northern Climate, *Journal of Hydrology* 120 (1-4): pp 193-215, 1990

Seyfried, M.S. and M.D. Murdock, Use of air permeability to estimate infiltrability of frozen soil, *Journal of Hydrology*, 202(1-4), pp. 95-107, December, 1997.

Springer, D.S., H.A. Loaiciga, S.J. Cullen, and L.G. Everett, Air permeability of porous materials under controlled laboratory conditions, *Ground Water*, Vol. 36, No. 4, pp. 558-565, 1998.

Stahre P. and B. Urbonas, *Stormwater detention for drainage, water quality, and CSO management*, Prentice Hall Englewood Cliffs, N.J, 1990.

Stolar, S., M.S. Evaluation of Factors Affecting Infiltration Pond Performance, MS Thesis, Department of Civil and Environmental Engineering, University of Washington, 2001.

Stonestrom, D.A. and J. Rubin, *Air permeability and trapped-air content in two soils*, Water Resource. Resources., Vol. 25, No. 9, pp. 1959-1969, 1989.

Van Genuchten, M.T., A closed-form equation for predicting the hydraulic conductivity of unsaturated soils, *Soil Science Society of America Journal*, Vol. 44 (5), pp. 892-898, 1980.

Ward, A.D. and W.J. Elliot, *Environmental Hydrology*, Lewis Publishers, 1995.

Washington Department of Ecology, *Stormwater Management Manual for Western Washington: Volume III -- Hydrologic Analysis and Flow Control Design/BMPs*, Publication 99-13, August, 2001.

Water Environment Federation, *WEF Manual of Practice #23, Urban Runoff Quality Management*, Water Environment Federation & ASCE, 1998.

Weeks, E.P., *Field determination of vertical permeability to air in the unsaturated* zone, USGS professional paper 1051, Washington, D.C, 1978.

Wiltsie, E., *Stormwater Facilities Performance Study, Infiltration Pond Testing and Data Evaluation, Thurston County, Washington*, August 10, 1998.

Appendix A –Data used in Regressions for Synthetic Soil Samples

	Soil Texture Mixture									
Sample	**% 16**	**% 50**	**% 125**	**% Flour**	**Observed K_{air} (cm/s)**	**Fines**	**D_{10} (mm)**	**D_{60} (mm)**	**D_{90} (mm)**	**K_{sat} from K_{air} (cm/s)**
1a	100	0	0	0	6.50E-02	0.000	0.88	1.2	1.6	9.75E-01
1b	95	0	0	5	3.50E-02	0.050	0.82	1.2	1.6	5.25E-01
1c	90	0	0	10	2.20E-02	0.100	0.42	1.2	1.6	3.30E-01
1d	85	0	0	15	1.10E-02	0.149	0.025	1.1	1.6	1.65E-01
1e	80	0	0	20	4.30E-03	0.199	0.014	1.1	1.6	6.45E-02
2a	0	100	0	0	2.70E-03	0.000	0.19	0.32	0.38	4.05E-02
2b	0	95	0	5	1.10E-03	0.050	0.17	0.31	0.38	1.65E-02
2c	0	90	0	10	3.50E-04	0.100	0.1	0.3	0.38	5.25E-03
2d	0	85	0	15	9.90E-05	0.149	0.025	0.29	0.38	1.49E-03
2e	0	80	0	20	4.20E-05	0.199	0.014	0.28	0.38	6.30E-04
3a	0	0	100	0	3.80E-04	0.537	0.034	0.08	0.1	5.70E-03
3b	0	0	95	5	2.50E-04	0.560	0.03	0.08	0.1	3.75E-03
3c	0	0	90	10	1.60E-04	0.583	0.022	0.078	0.1	2.40E-03
3d	0	0	85	15	1.20E-04	0.606	0.014	0.073	0.097	1.80E-03
3e	0	0	80	20	7.50E-05	0.629	0.009	0.07	0.096	1.13E-03
4a	40	20	40	0	3.70E-03	0.215	0.046	0.42	1.3	5.55E-02
4b	38	19	38	5	2.10E-03	0.254	0.038	0.38	1.3	3.15E-02
4c	36	18	36	10	1.00E-04	0.293	0.031	0.35	1.3	1.50E-03
4d	34	17	34	15	4.50E-05	0.332	0.02	0.31	1.2	6.75E-04
4e	32	16	32	20	2.70E-05	0.371	0.012	0.29	1.2	4.05E-04
5a	20	60	20	0	2.20E-03	0.107	0.07	0.32	1	3.30E-02
5b	19	57	19	5	2.40E-04	0.152	0.05	0.31	1	3.60E-03
5c	18	54	18	10	1.30E-04	0.196	0.035	0.3	1	1.95E-03

	Soil Texture Mixture									
Sample	**% 16**	**% 50**	**% 125**	**% Flour**	**Observed K_{air} (cm/s)**	**Fines**	**D_{10} (mm)**	**D_{60} (mm)**	**D_{90} (mm)**	**K_{sat} from K_{air} (cm/s)**
5d	17	51	17	15	4.90E-05	0.241	0.024	0.28	1	7.35E-04
5e	16	48	16	20	3.30E-05	0.285	0.014	0.28	1	4.95E-04
6a	20	40	40	0	1.40E-03	0.215	0.046	0.28	1.1	2.10E-02
6b	19	38	38	5	2.30E-04	0.254	0.04	0.27	1.1	3.45E-03
6c	18	36	36	10	1.00E-04	0.293	0.032	0.26	1.1	1.50E-03
6d	17	34	34	15	6.30E-05	0.332	0.02	0.25	1.1	9.45E-04
6e	16	32	32	20	4.30E-05	0.371	0.012	0.24	1	6.45E-04
7a	20	20	60	0	4.80E-04	0.322	0.04	0.17	1	7.20E-03
7b	19	19	57	5	2.80E-04	0.356	0.035	0.1	1	4.20E-03
7c	18	18	54	10	1.64E-04	0.390	0.03	0.1	1	2.46E-03
7d	17	17	51	15	1.00E-04	0.423	0.017	0.096	1	1.50E-03
7e	16	16	48	20	4.80E-05	0.457	0.01	0.095	1	7.20E-04
8a	60	20	20	0	1.30E-02	0.107	0.07	1	1.5	1.95E-01
8b	57	19	19	5	9.40E-03	0.152	0.05	1	1.5	1.41E-01
8c	54	18	18	10	6.40E-03	0.196	0.036	0.95	1.4	9.60E-02
8d	51	17	17	15	1.50E-04	0.241	0.024	0.9	1.3	2.25E-03
8e	48	16	16	20	1.20E-04	0.285	0.014	0.9	1.3	1.80E-03
9a	40	40	20	0	1.50E-02	0.107	0.07	0.43	1.2	2.25E-01
9b	38	38	19	5	1.50E-03	0.152	0.05	4	1.2	2.25E-02
9c	36	36	18	10	7.50E-05	0.196	0.035	0.35	1.2	1.13E-03
9d	34	34	17	15	3.50E-03	0.241	0.023	0.34	1.1	5.25E-02
9e	32	32	16	20	4.30E-05	0.285	0.014	0.33	1.1	6.45E-04
10a	33	33	33	0	9.90E-04	0.177	0.05	0.36	1.2	1.49E-02
10b	32	32	32	4	2.00E-04	0.212	0.042	0.35	1.2	3.00E-03
10c	30	30	30	10	5.70E-05	0.261	0.032	0.32	1.1	8.55E-04
10d	28	28	28	16	5.30E-05	0.310	0.019	0.3	1.1	7.95E-04

	Soil Texture Mixture									
Sample	**% 16**	**% 50**	**% 125**	**% Flour**	**Observed K_{air} (cm/s)**	**Fines**	**D_{10} (mm)**	**D_{60} (mm)**	**D_{90} (mm)**	**K_{sat} from K_{air} (cm/s)**
10e	27	27	27	19	3.10E-05	0.334	0.014	0.3	1.1	4.65E-04
11a	0	25	75	0	4.00E-04	0.403	0.035	0.093	0.3	6.00E-03
11b	0	75	25	0	9.50E-04	0.134	0.06	0.28	0.37	1.43E-02
11c	25	0	75	0	2.40E-04	0.403	0.035	0.093	1.1	3.60E-03
11d	75	0	25	0	5.00E-03	0.134	0.06	1	1.5	7.50E-02
11e	25	75	0	0	2.10E-03	0.000	0.2	0.35	1.1	3.15E-02
11f	75	25	0	0	1.50E-03	0.000	0.26	1	1.5	2.25E-02
12a	50	50	0	0	4.60E-03	0.000	0.23	0.94	1.2	6.90E-02
12b	0	50	50	0	3.70E-04	0.269	0.04	0.23	0.35	5.55E-03
12c	50	0	50	0	7.00E-04	0.269	0.04	0.94	1.2	1.05E-02
13a	80	20	0	0	1.50E-02	0.000	0.3	1	1.5	2.25E-01
13b	85	10	5	0	3.00E-02	0.027	0.3	1	1.5	4.50E-01
13c	85	10	0	5	2.10E-02	0.050	0.3	1	1.5	3.15E-01
13d	90	10	0	0	4.50E-02	0.000	0.43	0.95	1.5	6.75E-01
13e	95	5	0	0	5.20E-02	0.000	0.83	0.95	1.5	7.80E-01
14a	95	0	5	0	3.90E-02	0.027	0.83	1	1.4	5.85E-01
14b	95	0	0	5	3.50E-02	0.050	0.83	1	1.4	5.25E-01
14c	75	15	10	0	2.00E-02	0.054	0.11	1	1.4	3.00E-01
14d	80	10	10	0	2.00E-02	0.054	0.11	1	1.4	3.00E-01
14e	80	10	0	10	1.20E-02	0.100	0.075	1	1.4	1.80E-01
15a	85	5	5	5	2.00E-02	0.077	0.11	1	1.6	3.00E-01
15b	85	15	0	0	4.00E-02	0.000	0.31	1	1.6	6.00E-01

Appendix B - Measured air conductivity and the corresponding saturated hydraulic conductivity for soil samples collected at field sites

Site	Test Pit# layer (#) depth"	K_{air} (cm/s)	K_{air} (cm/hr)	K_{equiv} (cm/hr)	$K_{average}$ (cm/hr)	K_w (cm/hr)
Clark County	TH1 (1) 14"	1.00E-03	3.60E+00			
	TH2 (1) 10"	9.20E-04	3.31E+00			
	TH3 (1) 9"	5.50E+04	1.98E+08			
	TH4 (1) 6"	1.30E-03	4.68E+00	5	5	55
Beaverdam, King County	TH1 (1) 4"	7.00E-02	2.52E+02			
	TH1 (2) 6"	5.90E-03	2.12E+01			
	TH1 (3) 3"	6.00E-02	2.16E+02	42		
	TH2 (1) 4"	2.50E-03	9.00E+00			
	TH2 (2) 4"	7.30E-02	2.63E+02			
	TH2 (3) 4"	6.50E-02	2.34E+02	25		
	TH3 (1) 4"	2.50E-03	9.00E+00			
	TH3 (2) 12"	6.60E-02	2.38E+02	32		
	TH4 (1) 4"	2.50E-03	9.00E+00			
	TH4 (2) 8"	5.90E-02	2.12E+02	25	31	357
Balsam 7-11, Kitsap Co.	TH1 (1) 10"	2.90E-03	1.04E+01			
	TH1 (2) 18"	5.00E-05	1.80E-01	0		
	TH2 (1) 7"	5.40E-04	1.94E+00			
	TH2 (2) 14"	3.90E-03	1.40E+01			
	TH2 (3) 24"	2.70E-03	9.72E+00	6	3	38
Krista Firs, Kitsap Co.	TH1 (1) 13"	6.20E-03	2.23E+01	22		
	TH1 (2) 14"	Too fast to measure.				
	TH2 (1) 27"	3.80E-03	1.37E+01			
	TH2 (2) 30"	2.00E-03	7.20E+00	9		
	TH3 (1) 10"	1.40E-02	5.04E+01	50	27	314
Airdustrial, Th. Co.	TH1 (1) 67"	5.10E-03	1.84E+01	18		
	TH2 (1) 48"	2.50E-03	9.00E+00	9	14	157
Bush, Th. Co.	TH1 (1) 20"	7.50E-03	2.70E+01			
	TH1 (2) 20"	7.50E-03	2.70E+01			
	TH1 (3) 35"	1.90E-02	6.84E+01	38		
	TH2 (1) 33"	1.50E-02	5.40E+01			
	TH2 (2) 30"	9.00E-03	3.24E+01	43	40	463
Echo Glen, Th. Co.	TH1 (2) 7"	1.10E-02	3.96E+01			
	TH1 (3) 14"	Too fast to measure.				
	TH1 (4) 12"	Too fast to measure.				
	TH1 (5) 7"	4.00E-02	1.44E+02	62	62	714
Lacey Lid, Th. Co.	TH1 (1) 69"	2.00E-03	7.20E+00	7		
	TH2 (1) 50"	3.60E-03	1.30E+01	13	10	116
Margaret McKenny, Th. Co.	TH1 (1) 22"	5.90E-03	2.12E+01			
	TH1 (2) 20"	9.20E-03	3.31E+01			
	TH1 (3) 12"	6.00E-03	2.16E+01	25	25	283
Ridgeview, Th. Co.	TH1 (1) 32"	Too fast to measure.				

Site	Test Pit# layer (#) depth"	K_{air} (cm/s)	K_{air} (cm/hr)	K_{equiv} (cm/hr)	$K_{average}$ (cm/hr)	K_w (cm/hr)
	TH1 (2) 5"	3.40E-02	1.22E+02			
	TH1 (3) 11"	Too fast to measure.				
	TH1 (4) 15"	5.70E-03	2.05E+01			
	TH2 (1) 35"	Too fast to measure.				
	TH2 (2) 12"	Too fast to measure.				
	TH2 (3) 15"	Too fast to measure.				
	TH3 (1) 60"	Too fast to measure.		26	26	298
Springfield, Th. Co.	TH1 (1) 13"	3.40E-04	1.22E+00			
	TH1 (2) 8"	1.10E-03	3.96E+00			
	TH1 (3) 10"	3.20E-03	1.15E+01	2		
	TH2 (1) 9"	3.50E-04	1.26E+00			
	TH2 (2) 6"	2.00E-03	7.20E+00			
	TH2 (3) 17"	2.20E-03	7.92E+00	3		
	TH3 (1) 14"	2.50E-04	9.00E-01			
	TH3 (2) 8"	1.00E-02	3.60E+01			
	TH3 (3) 7"	7.80E-03	2.81E+01	2		
	TH4 (1) 18"	4.00E-04	1.44E+00			
	TH4 (2) 8"	7.40E-03	2.66E+01	2	2	27
State Farm, Th. Co.	TH1 (1) 38"	5.40E-03	1.94E+01			
	TH1 (2) 27"	2.80E-03	1.01E+01	14	14	161
Sweetbriar, Th. Co.	TH1 (1) 36"	1.40E-03	5.04E+00			
	TH1 (2) 9"	3.80E-04	1.37E+00			
	TH1 (3) 24"	3.00E-02	1.08E+02	5		
	TH2 (1) 36"	1.10E-03	3.96E+00			
	TH2 (2) 30"	1.40E-03	5.04E+00	4	5	54
Westwood Baptist, Th. Co.	TH1 (1) 11"	5.10E-04	1.84E+00			
	TH1 (2) 10"	4.40E-04	1.58E+00			
	TH1 (3) 6"	4.00E-03	1.44E+01	2		
	TH2 (1) 15"	1.30E-04	4.68E-01			
	TH2 (2) 6"	1.20E-03	4.32E+00			
	TH2 (3) 5"	1.20E-02	4.32E+01	1		
	TH3 (1) 6"	1.70E-04	6.12E-01			
	TH3 (2) 6"	8.50E-03	3.06E+01			
	TH3 (3) 16"	1.50E-03	5.40E+00	2		
	TH4 (1) 10"	2.20E-03	7.92E+00			
	TH4 (2) 10"	2.80E-04	1.01E+00			
	TH4 (3) 11"	6.50E-04	2.34E+00	2		
	TH5 (1) 4"	2.20E-04	7.92E-01			
	TH5 (2) 14"	3.40E-03	1.22E+01	3		
	TH6 (1) 6"	5.70E-04	2.05E+00	2	2	23
Woodard Glen, Th. Co.	TH1 (1) 15"	1.40E-02	5.04E+01			
	TH1 (2) 28"	5.80E-03	2.09E+01	26		
	TH2 (1) 36"	2.70E-03	9.72E+00			
	TH2 (2) 6"	1.80E-03	6.48E+00	9	18	203

Appendix C – Grain Size Curves for Synthetic and Natural Soils

C.1 Grain Size Curves for Synthetic Soil Samples

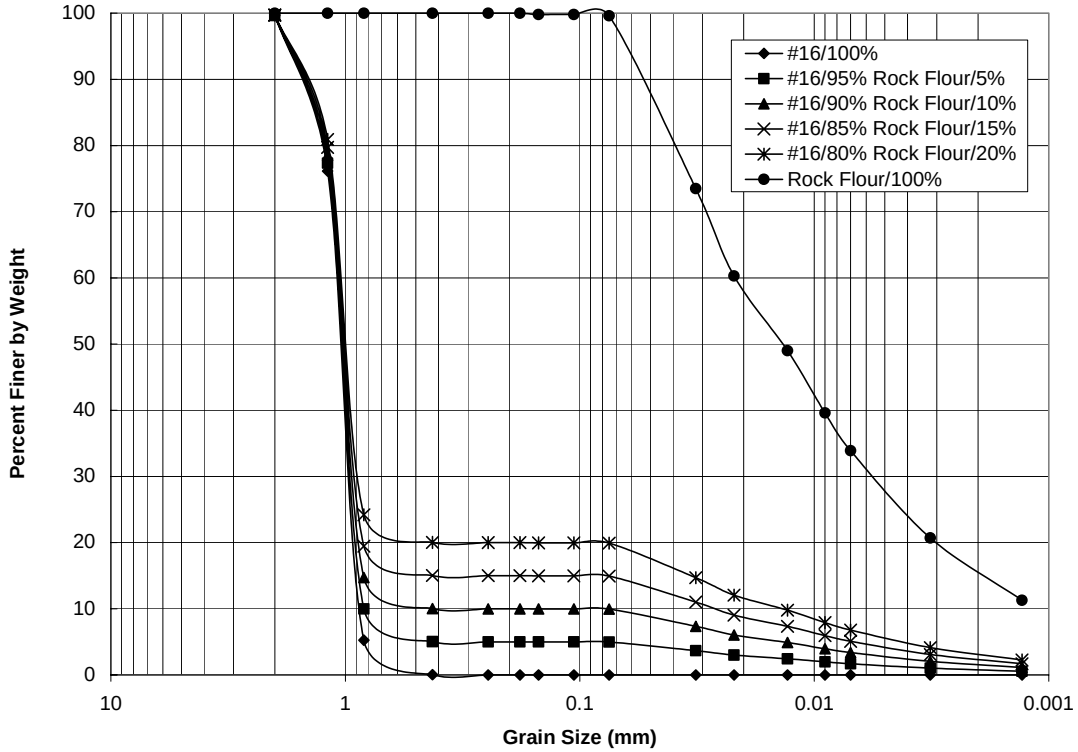

Figure C.1 – Grain size distribution for #16 synthetic soil and rock flour

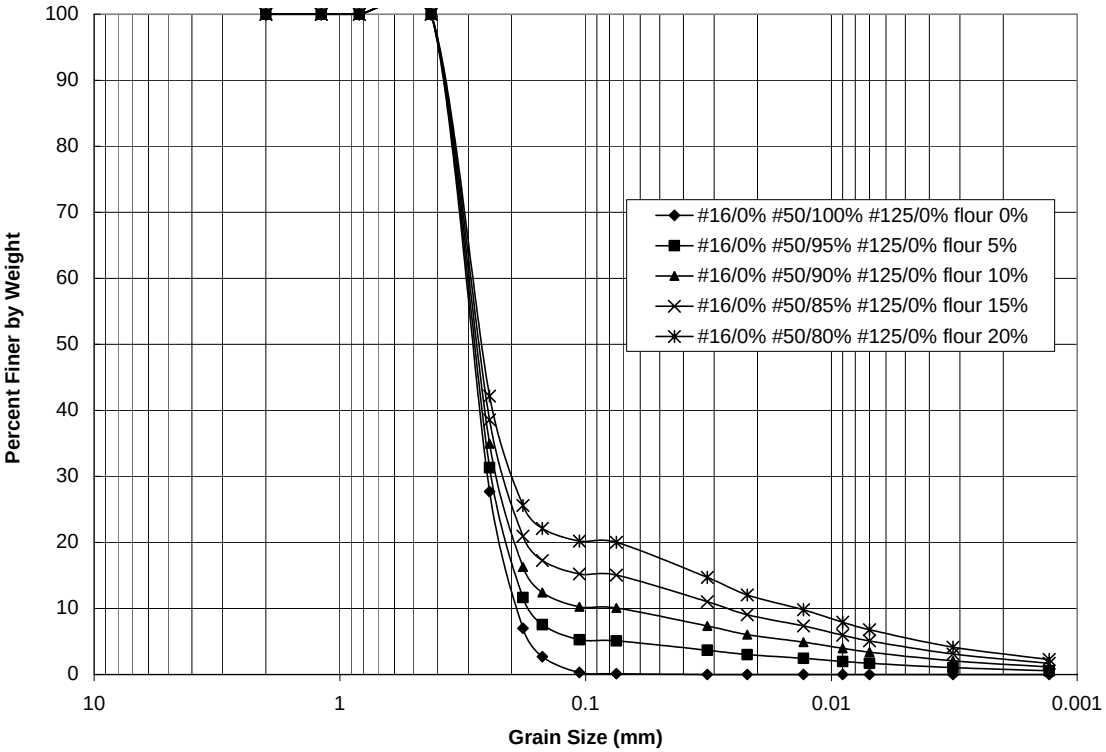

Figure C.2 – Grain size distribution for #50 synthetic soil

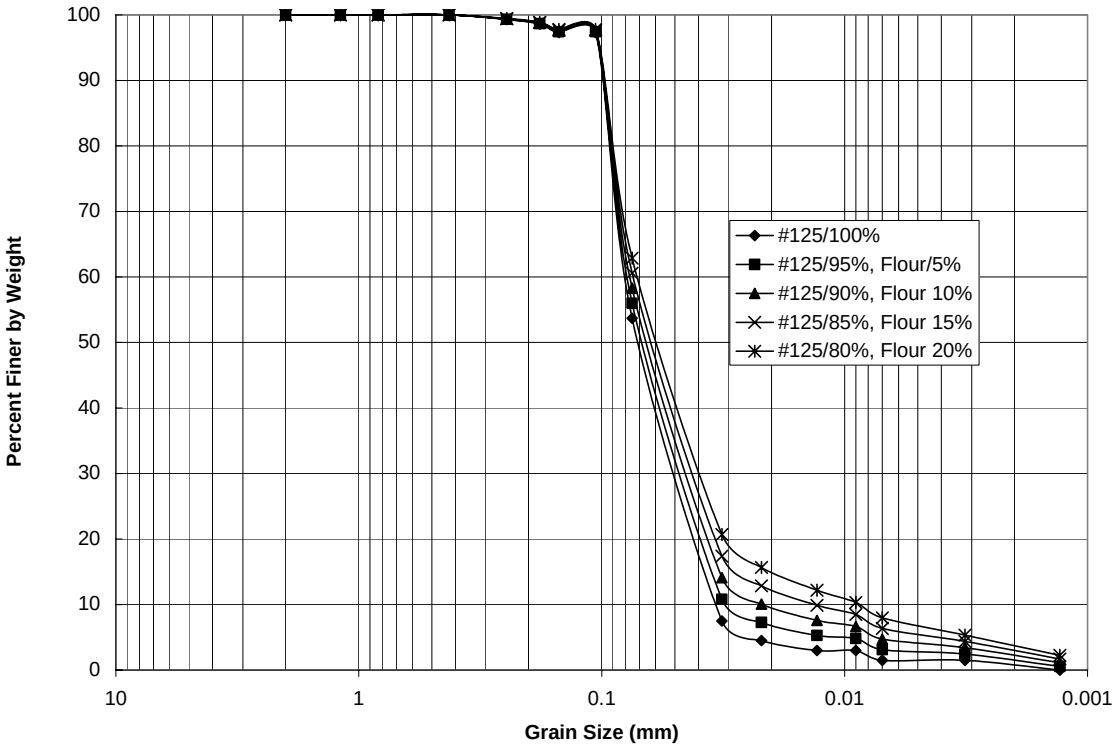

Figure C.3 – Grain size distribution for #125 synthetic soil

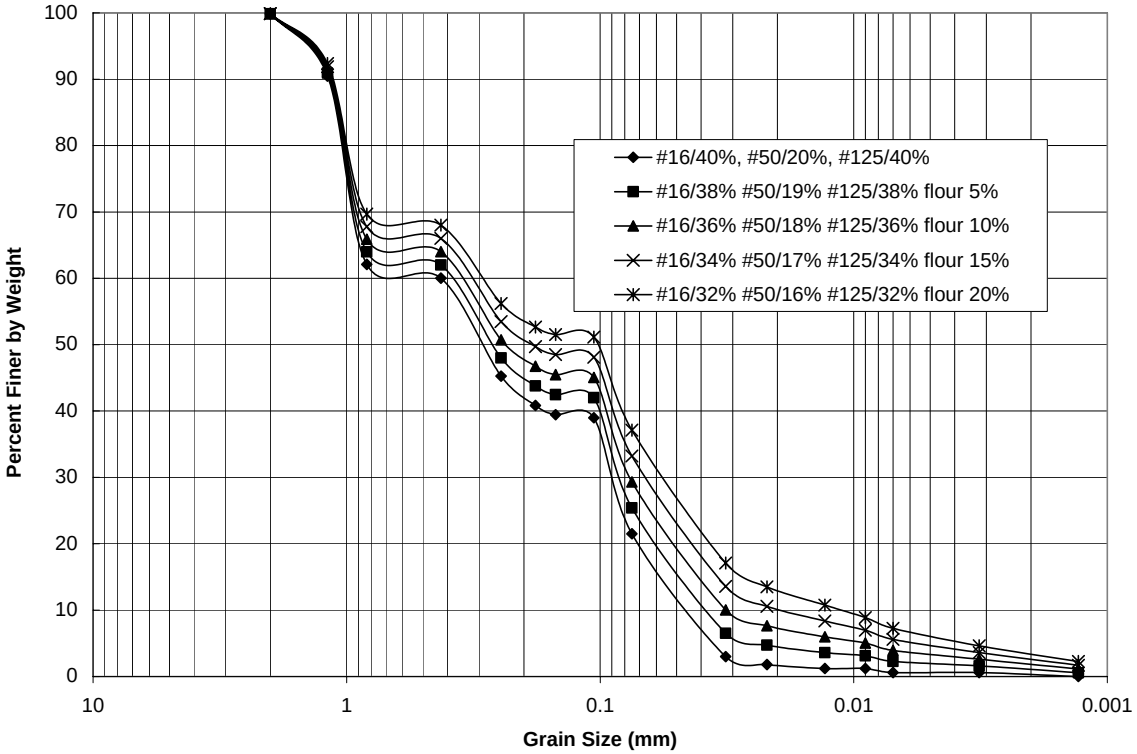

Figure C.4 – Grain size distribution for #16/40% #50/20% #125/40% synthetic soil

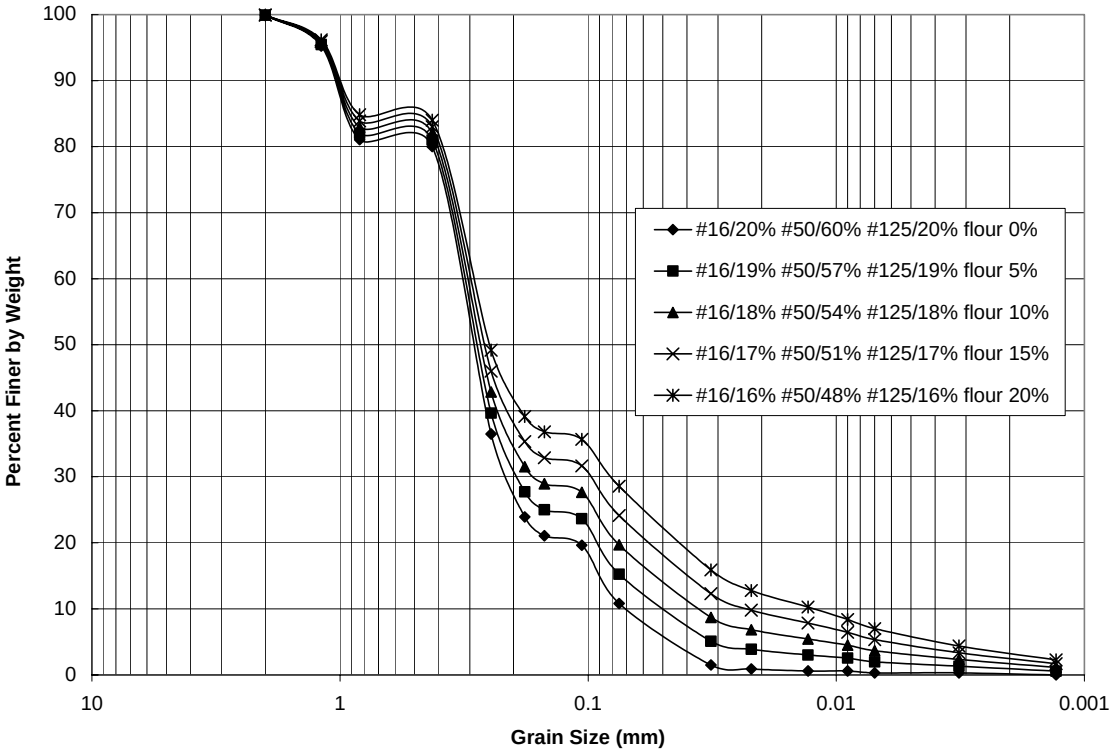

Figure C.5 – Grain size distribution for #16/20% #50/60% #125/20% synthetic soil

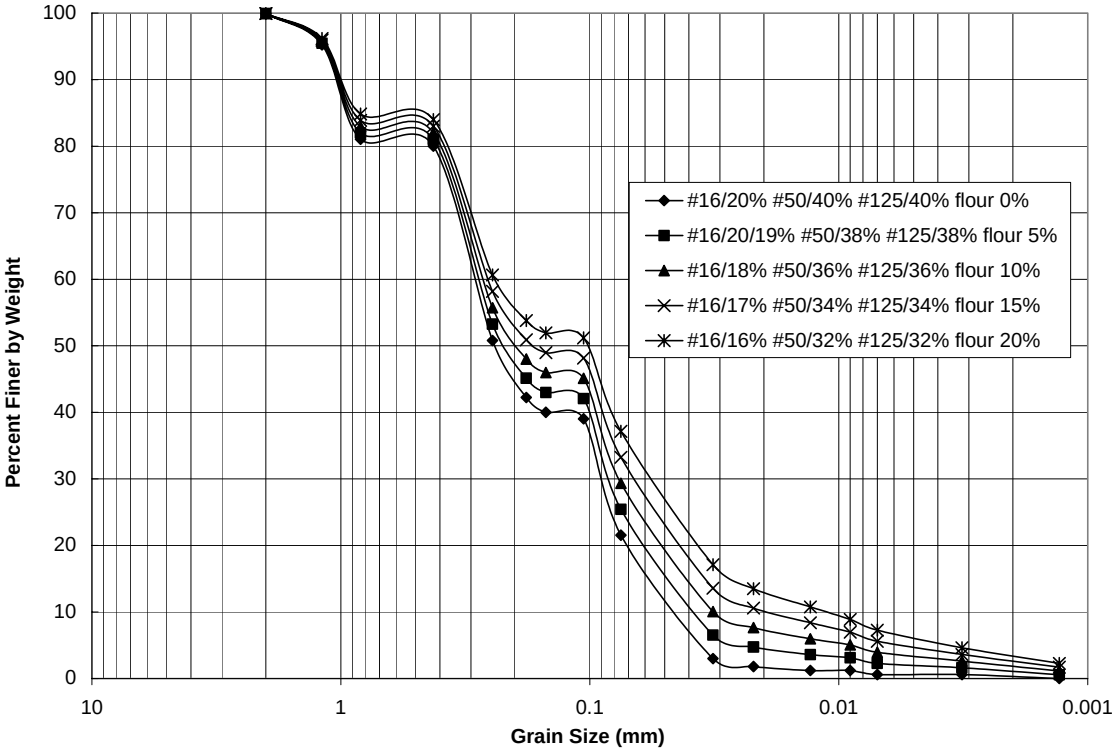

Figure C.6 – Grain size distribution for #16/20% #50/40% #125/40% synthetic soil

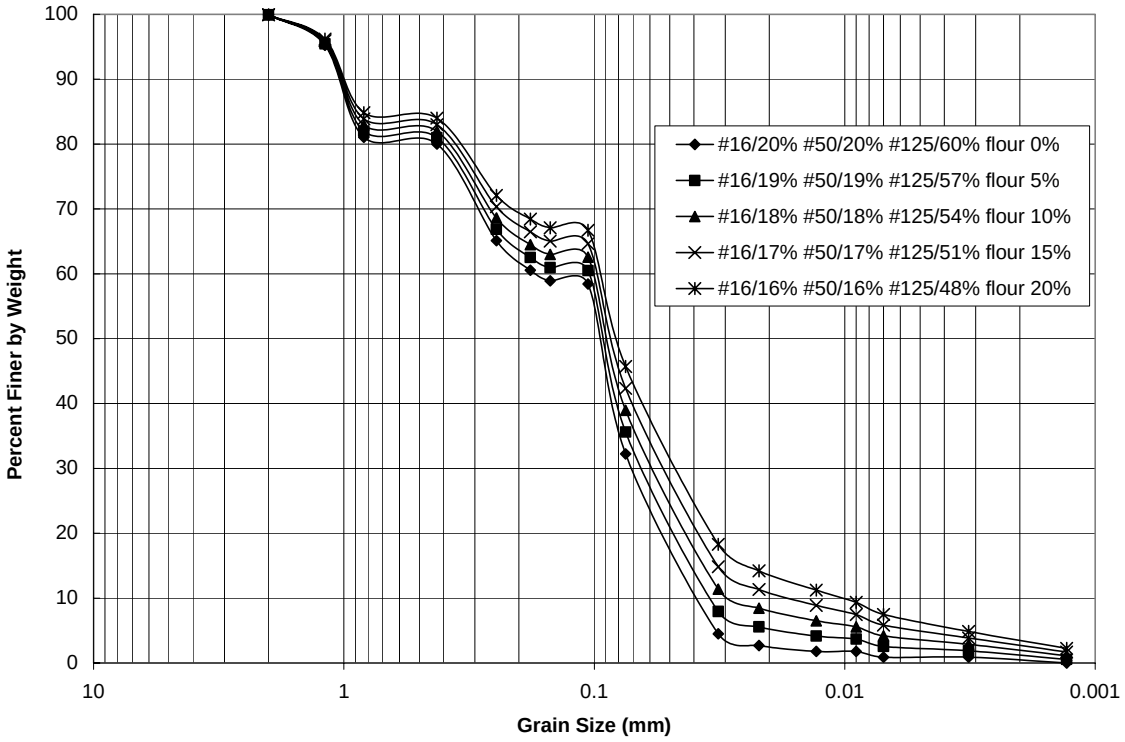

Figure C.7 – Grain size distribution for #16/20% #50/20% #125/60% synthetic soil

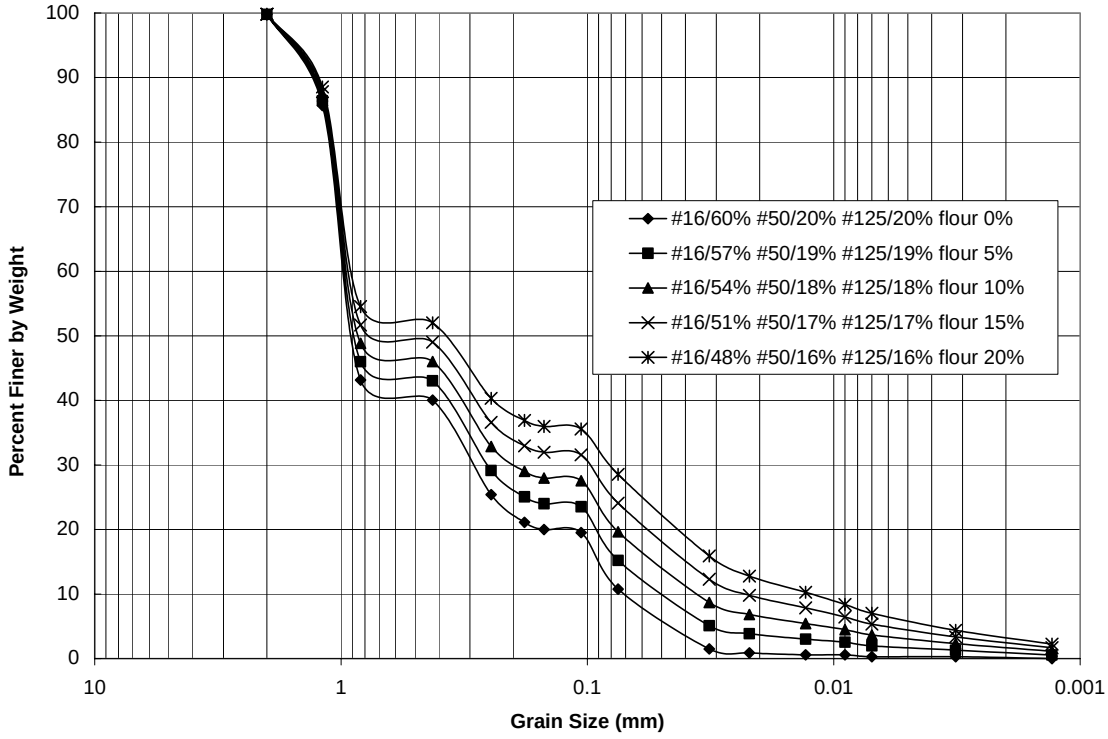

Figure C.8 – Grain size distribution for #16/60% #50/20% #125/20% synthetic soil

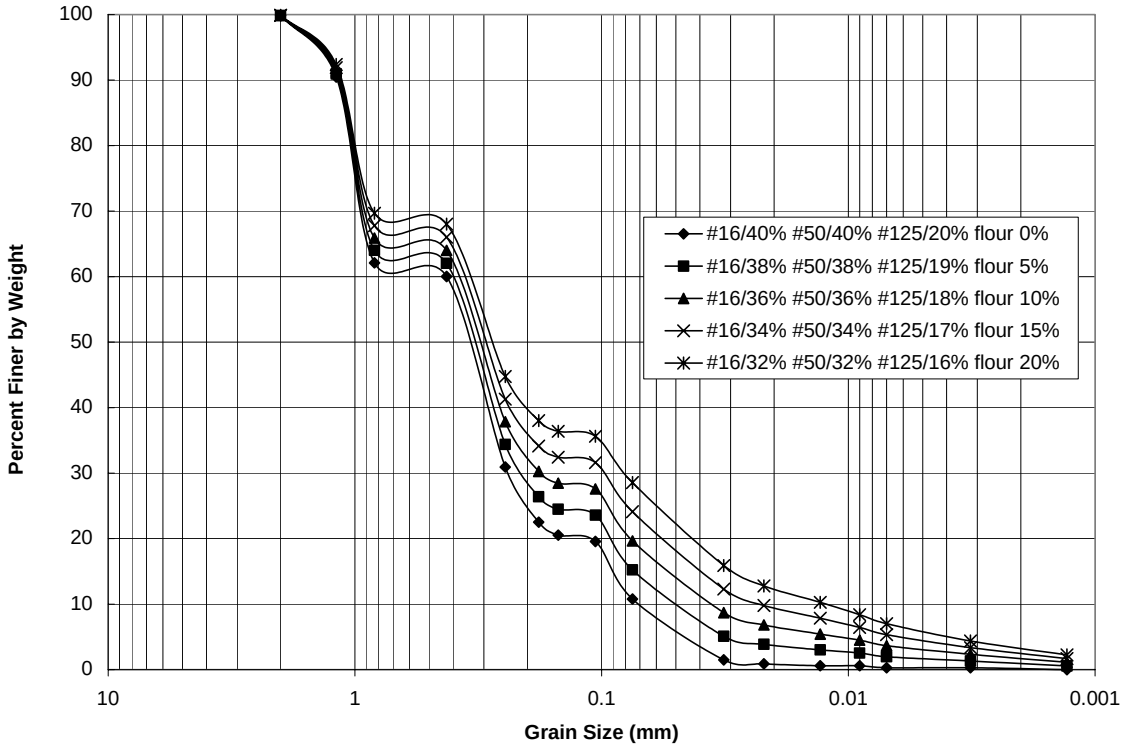

Figure C.9 – Grain size distribution for #16/40% #50/40% #125/20% synthetic soil

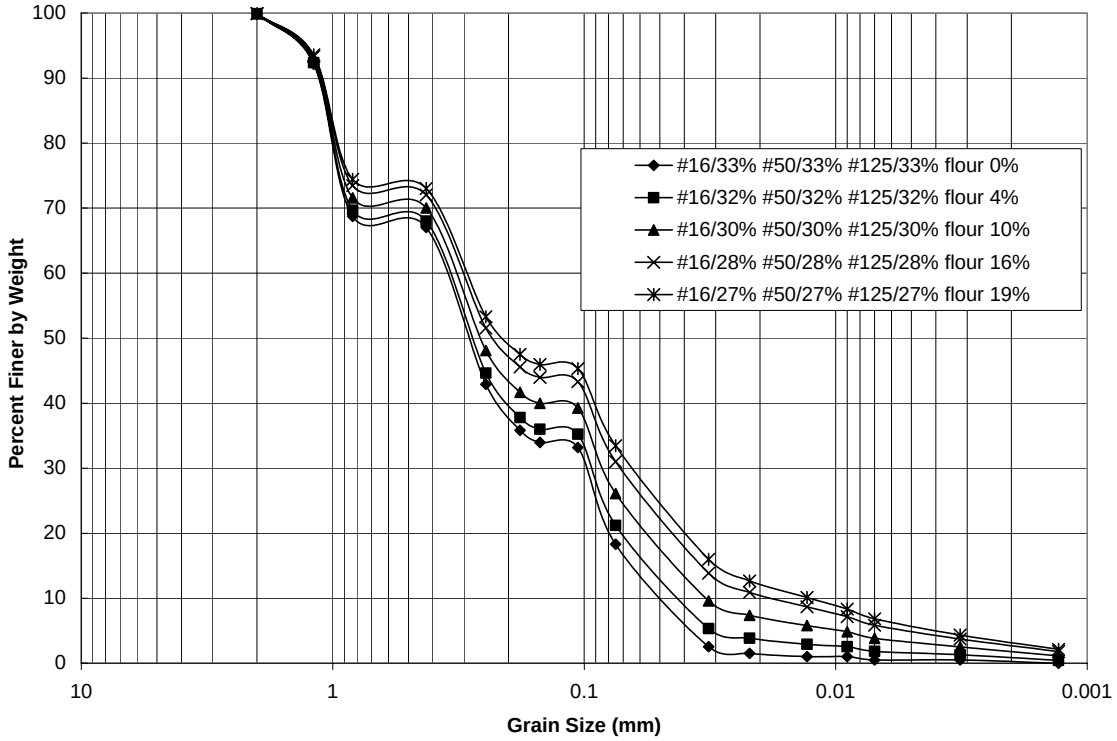

Figure C.10 – Grain size distribution for #16/33% #50/33% #125/33% synthetic soil

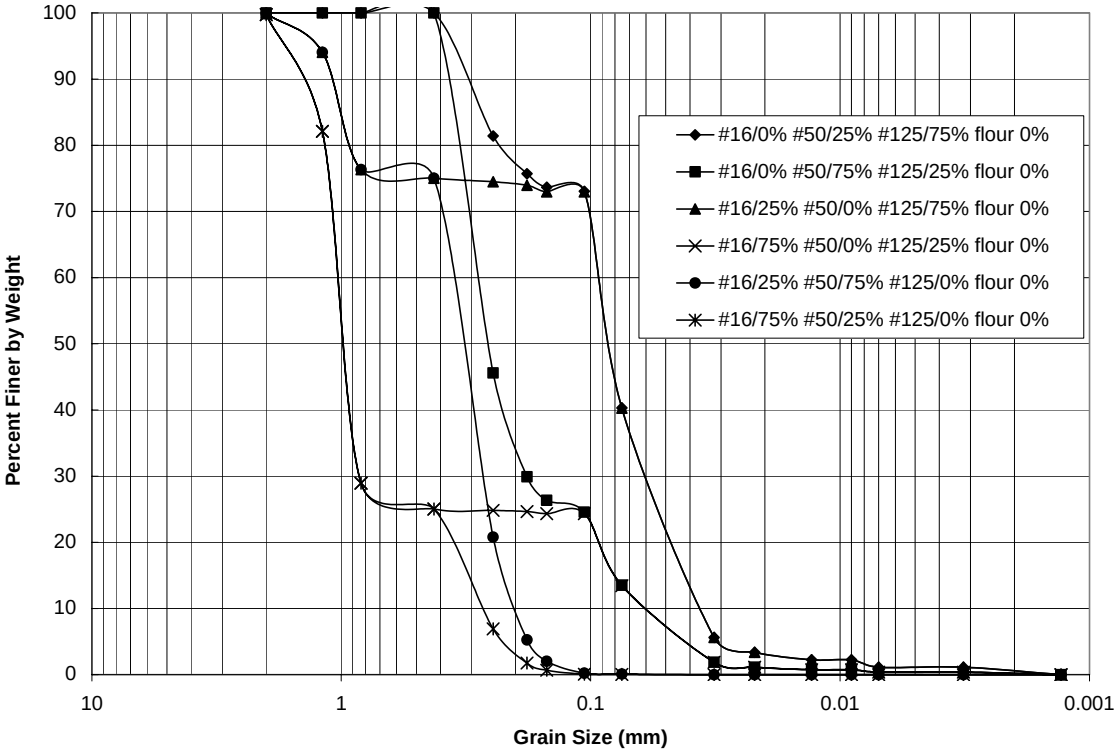

Figure C.11 – Grain size distribution for 25%-75% synthetic soil

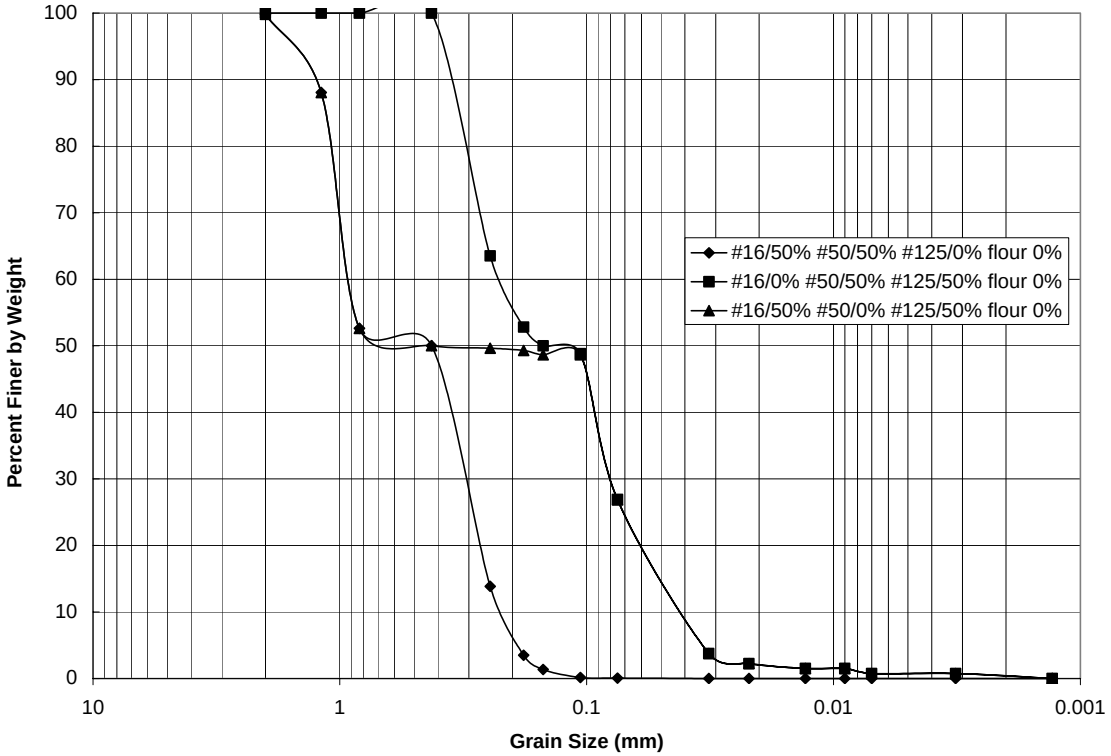

Figure C.12 – Grain size distribution for 50%-50% synthetic soil

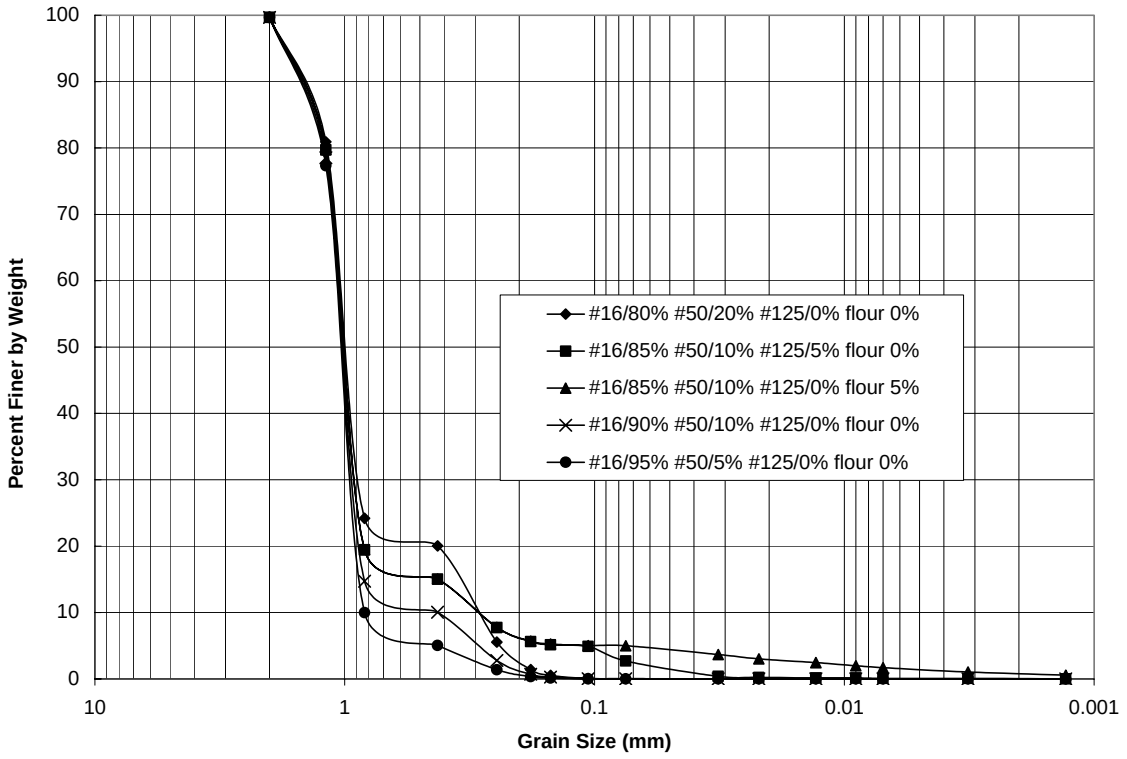

Figure C.13 – Grain size distribution for Mixed Synthetic Samples synthetic soil

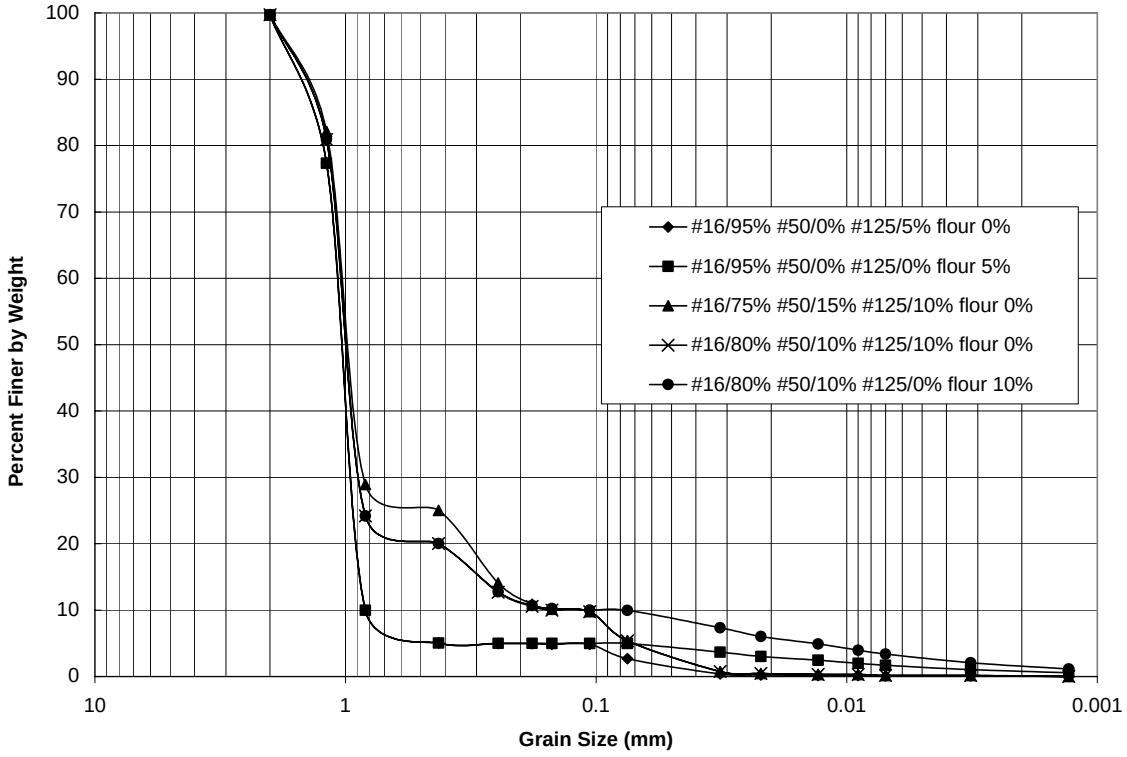

Figure C.14 – Grain size distribution for Mixed Synthetic Samples synthetic soil

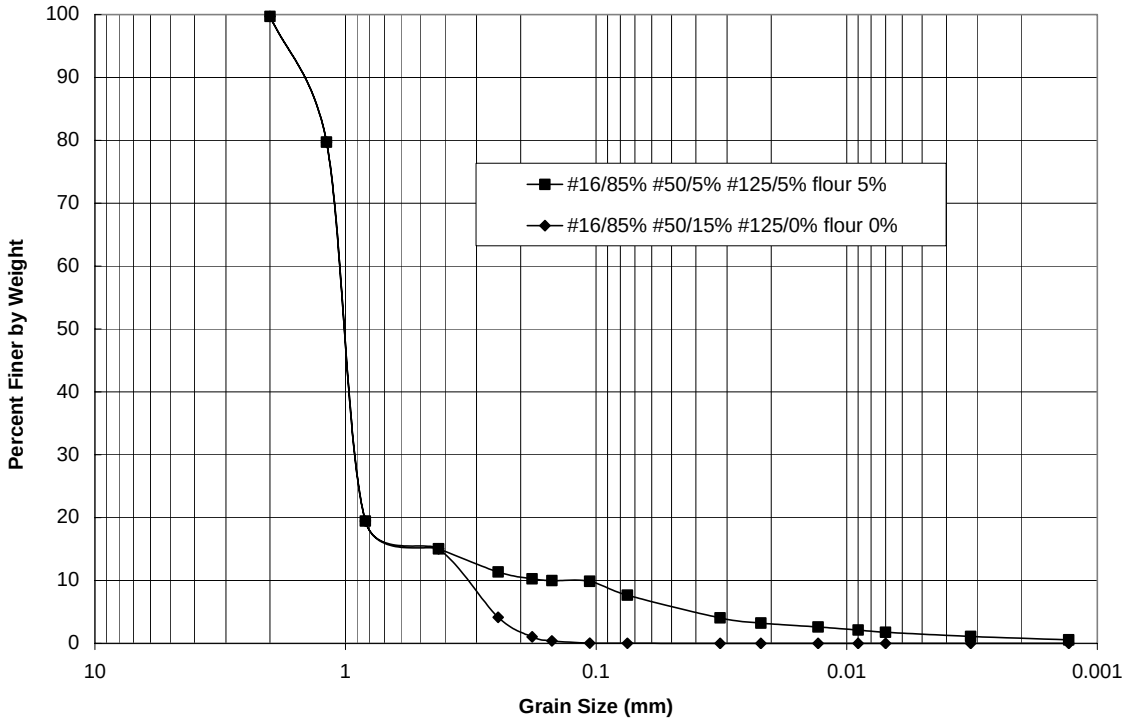

Figure C.15 – Grain size distribution for Mixed Synthetic Samples synthetic soil

C.2 Grain Size Curves for Natural Samples

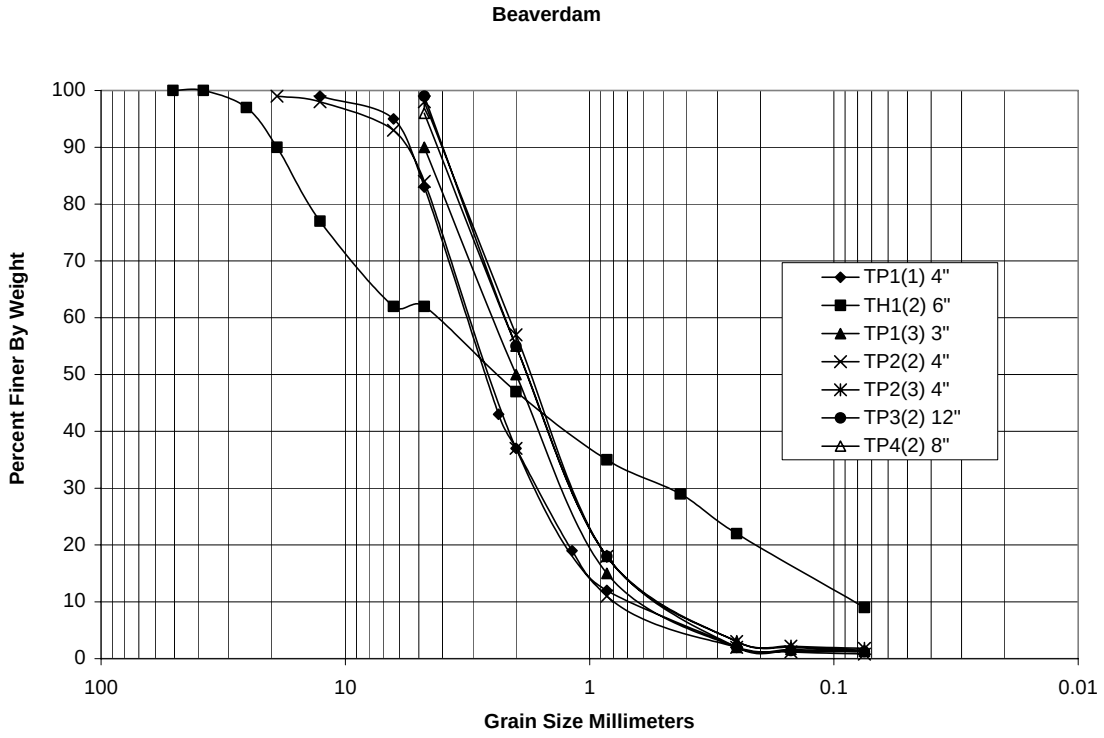

Figure C.16 – Grain size distribution for Beaverdam, King County pond

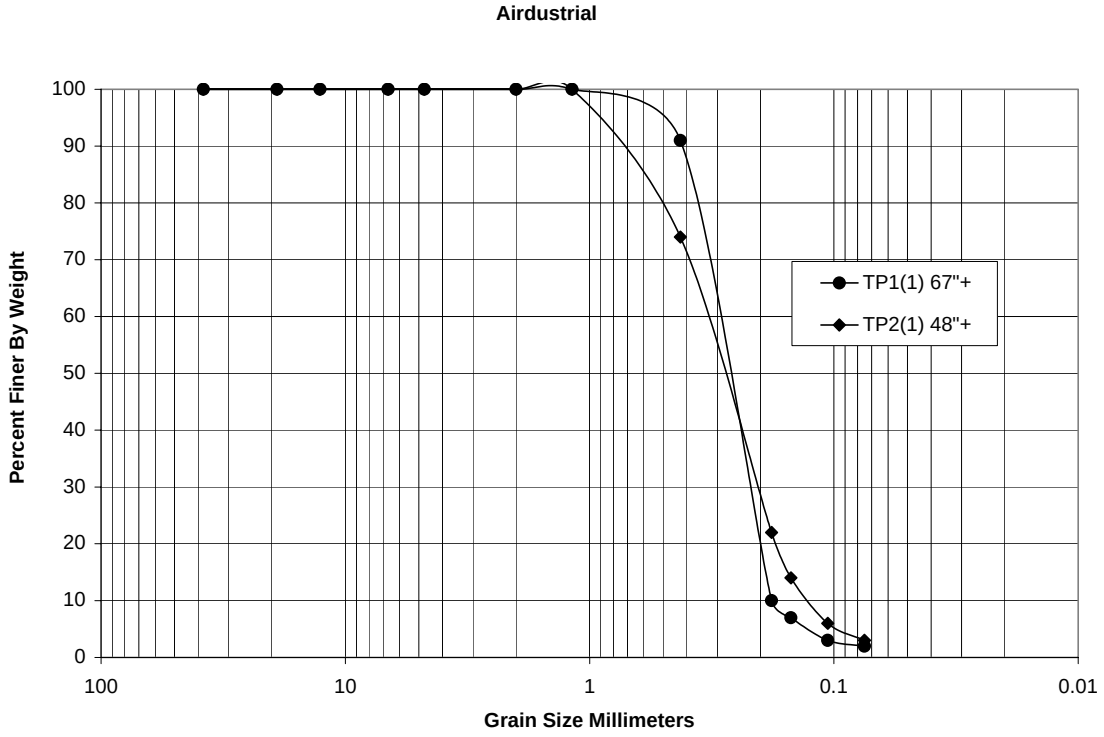

Figure C.17 – Grain size distribution for Airdustrial, Thurston County infiltration pond

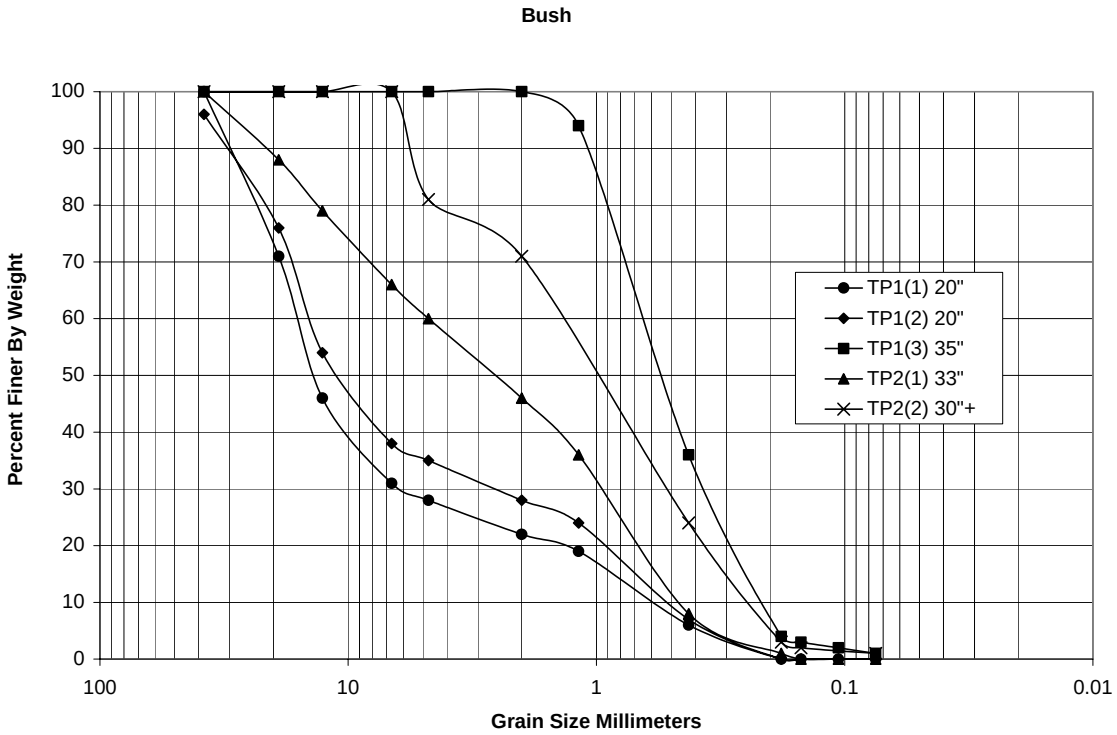

Figure C.18 – Grain size distribution for Bush, Thurston County infiltration pond

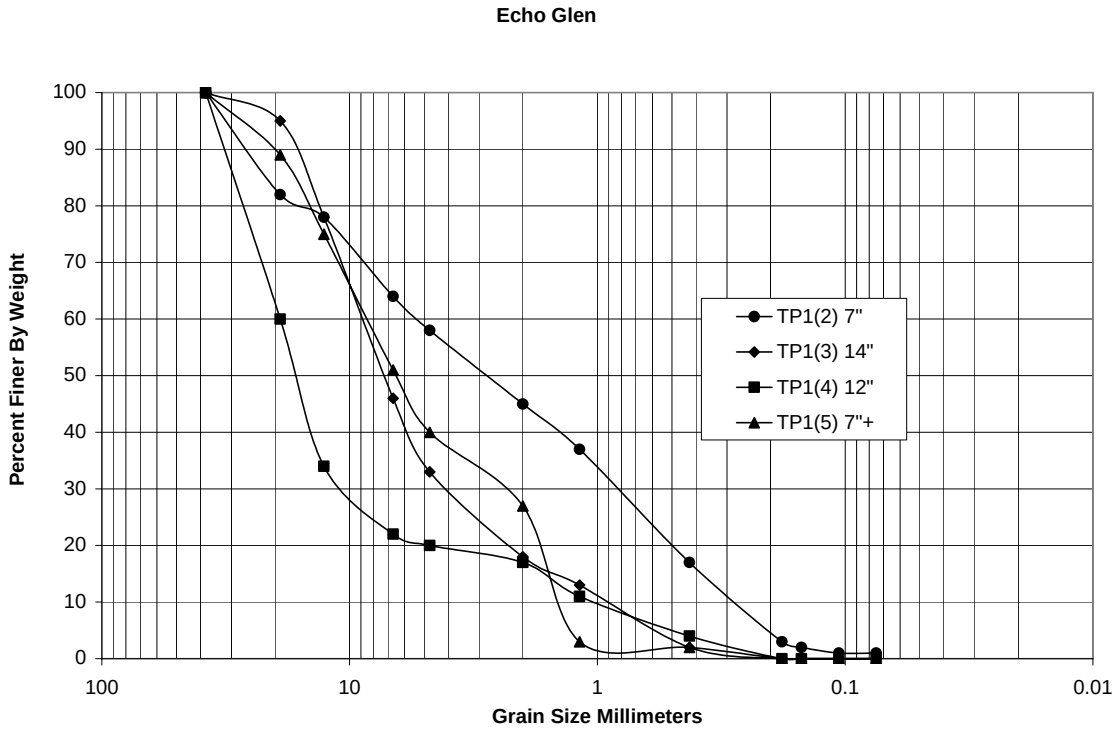

Figure C.19 – Grain size distribution for Echo Glen, Thurston County infiltration pond

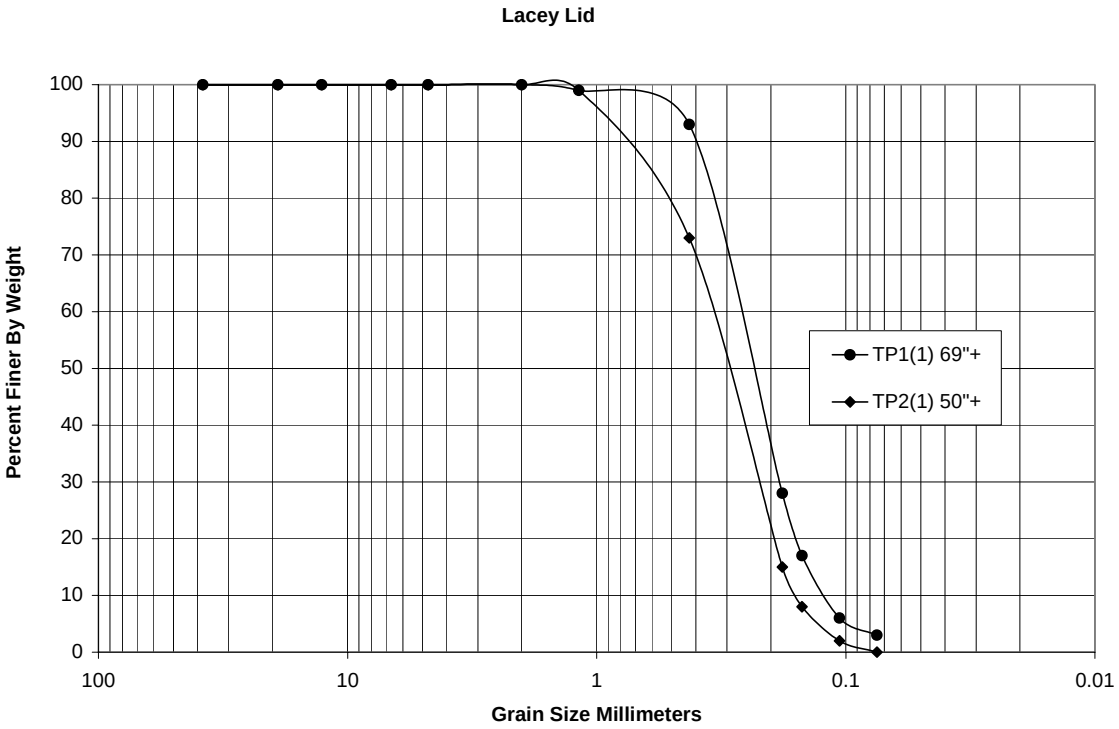

Figure C.20 – Grain size distribution for Lacy Lid, Thurston County infiltration pond

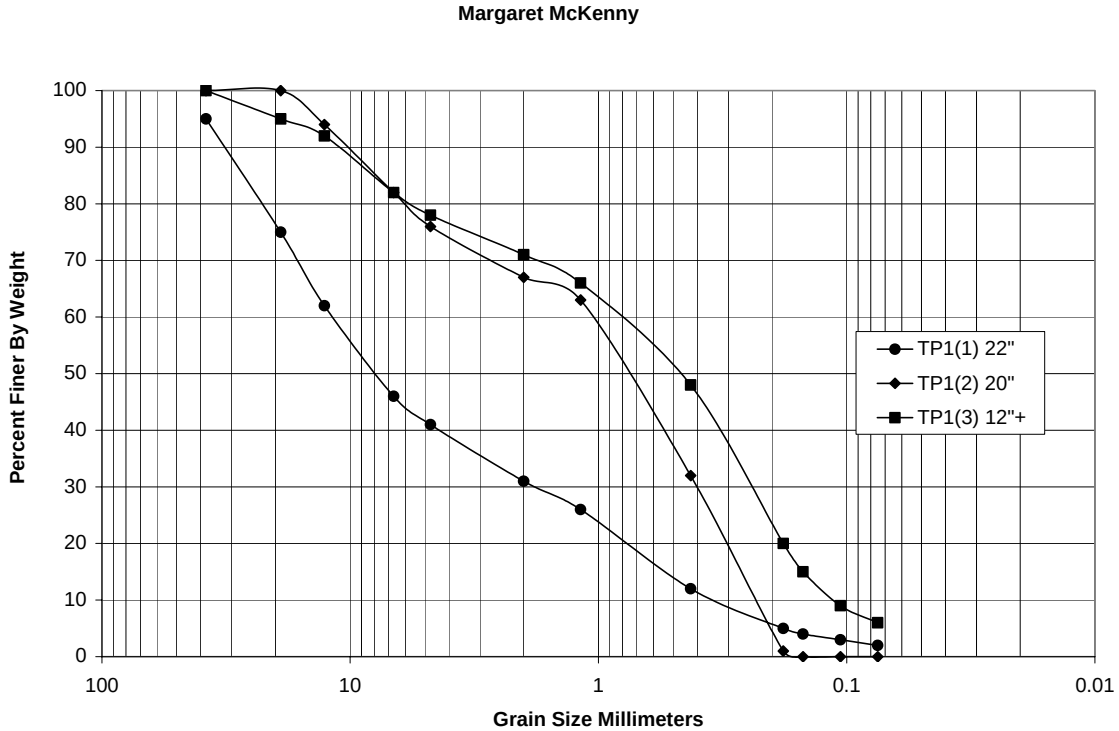

Figure C.21 – Grain size distribution for Margaret McKenny, Thurston County infiltration pond

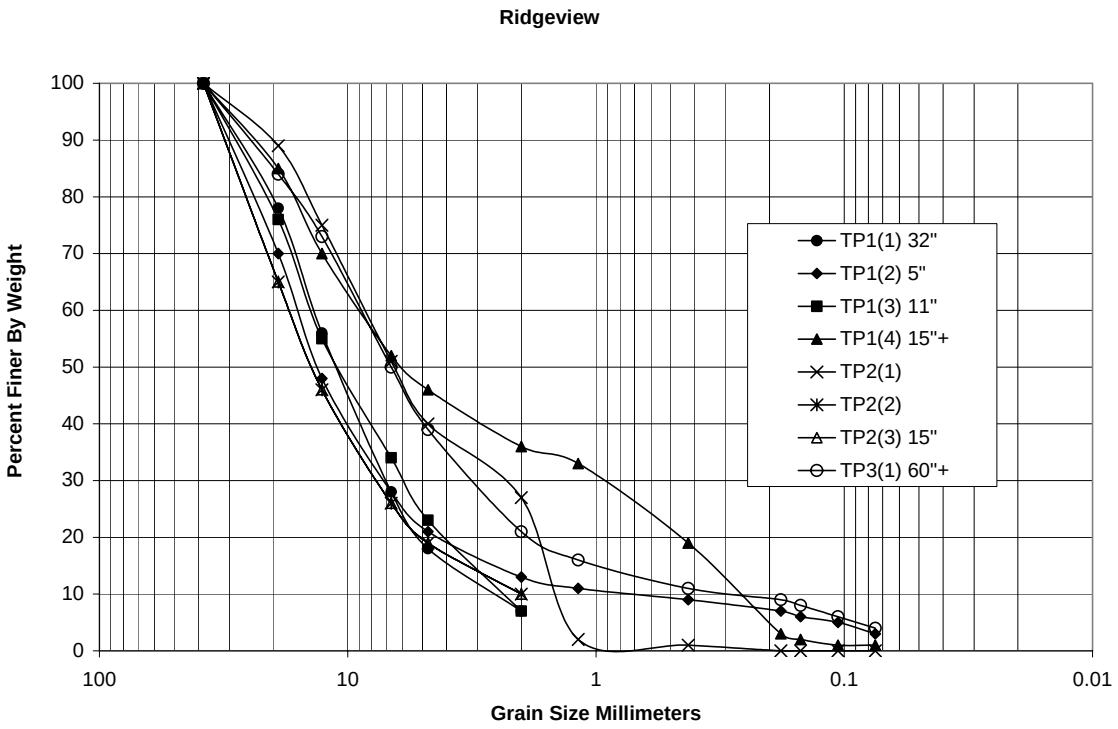

Figure C.22 – Grain size distribution for Ridgeview, Thurston County infiltration pond

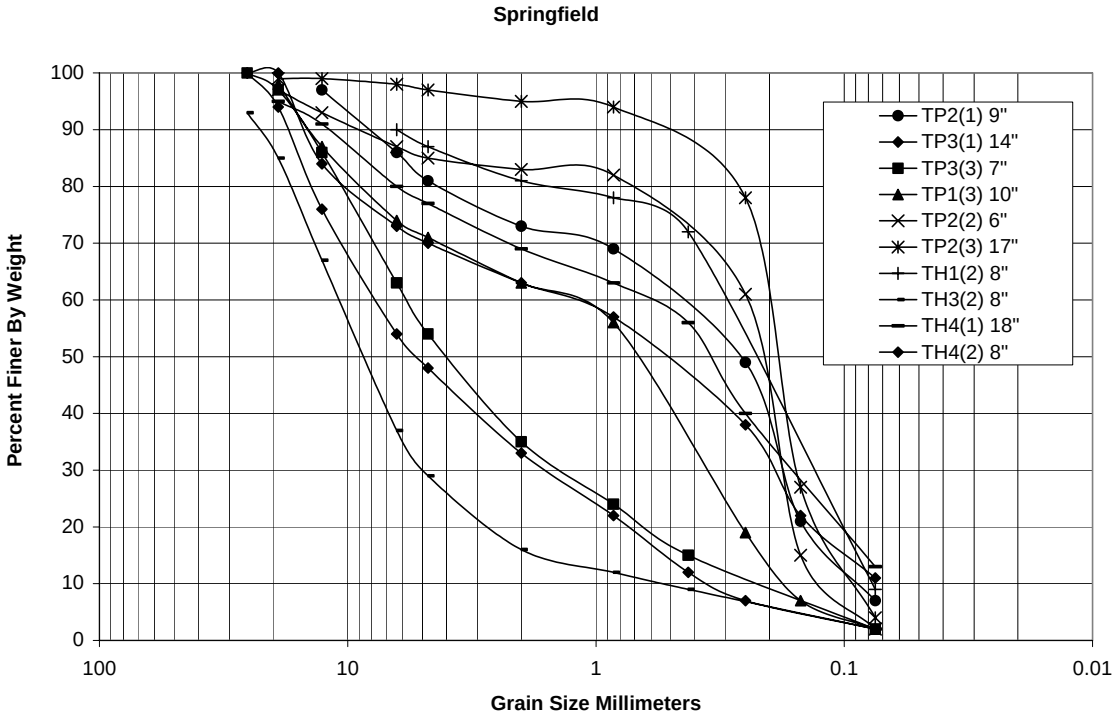

Figure C.23 – Grain size distribution for Springfield, Thurston County infiltration pond

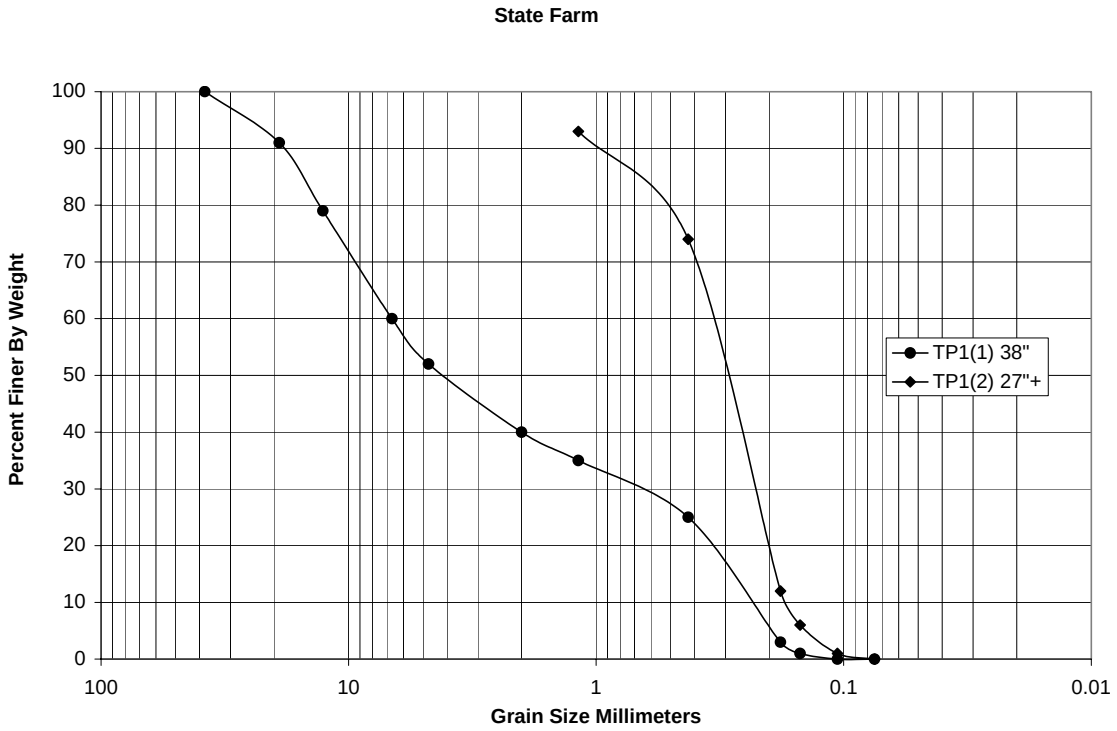

Figure C.24 – Grain size distribution for State Farm, Thurston County infiltration pond

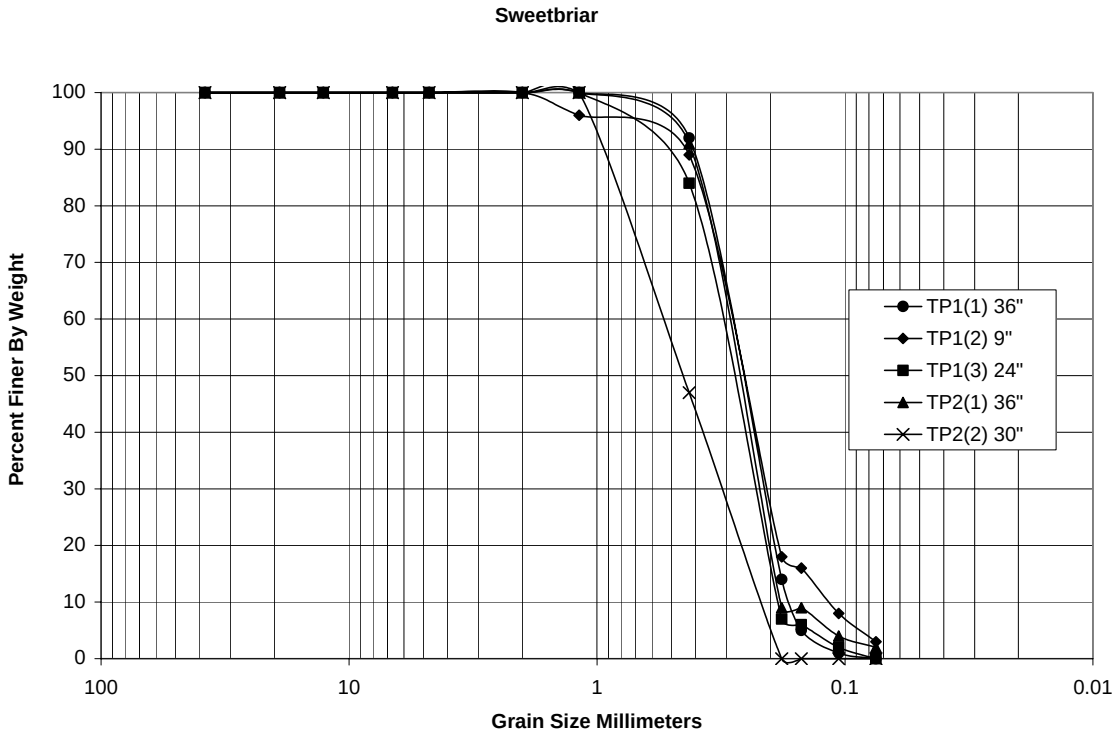

Figure C.25 – Grain size distribution for Sweetbriar, Thurston County infiltration pond

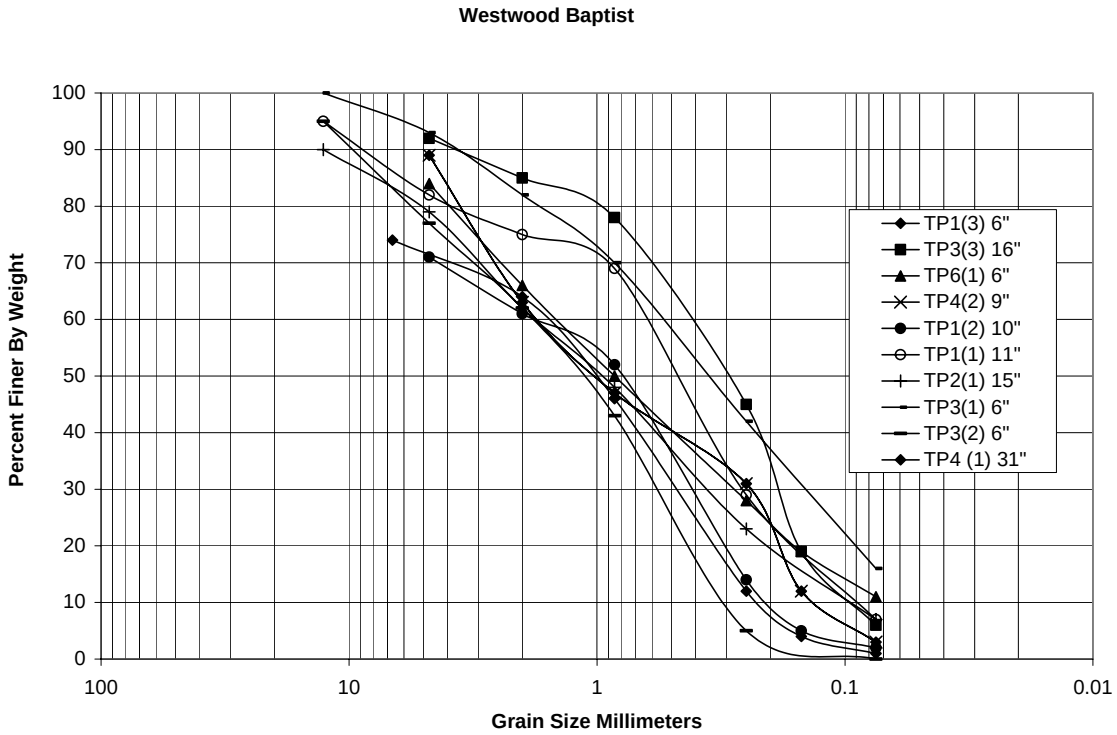

Figure C.26 – Grain size distribution for Westwood Baptist, Thurston County infiltration pond

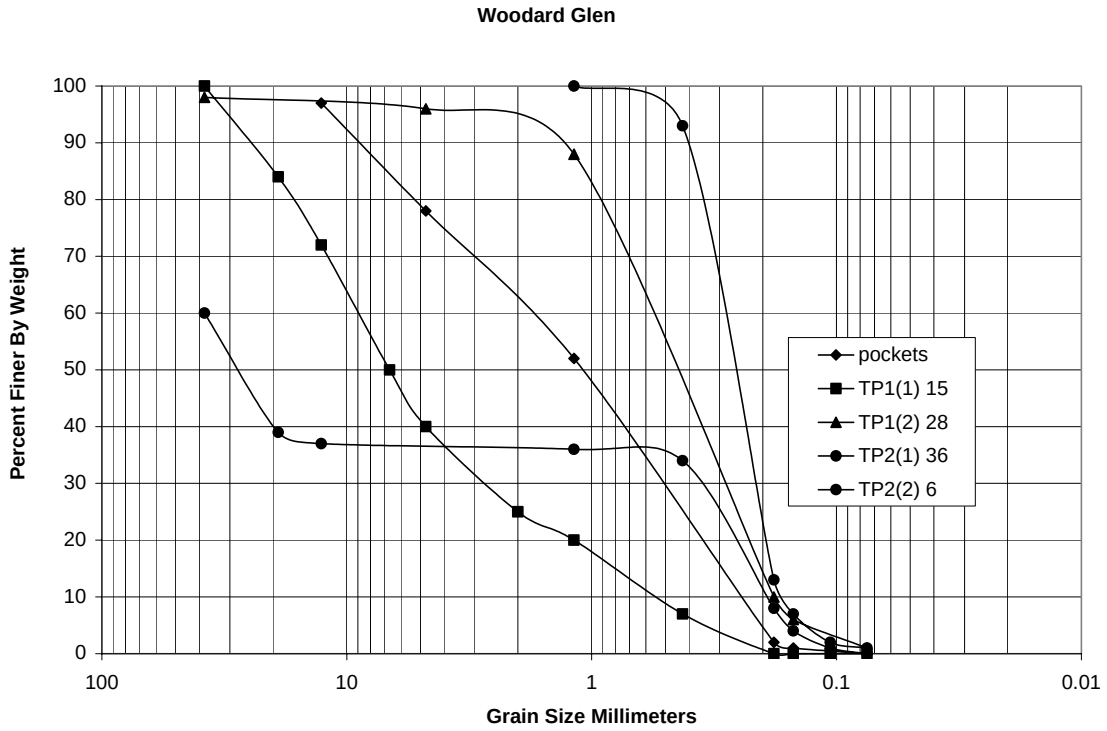

Figure C.27 – Grain size distribution for Woodward Glen, Thurston County infiltration pond

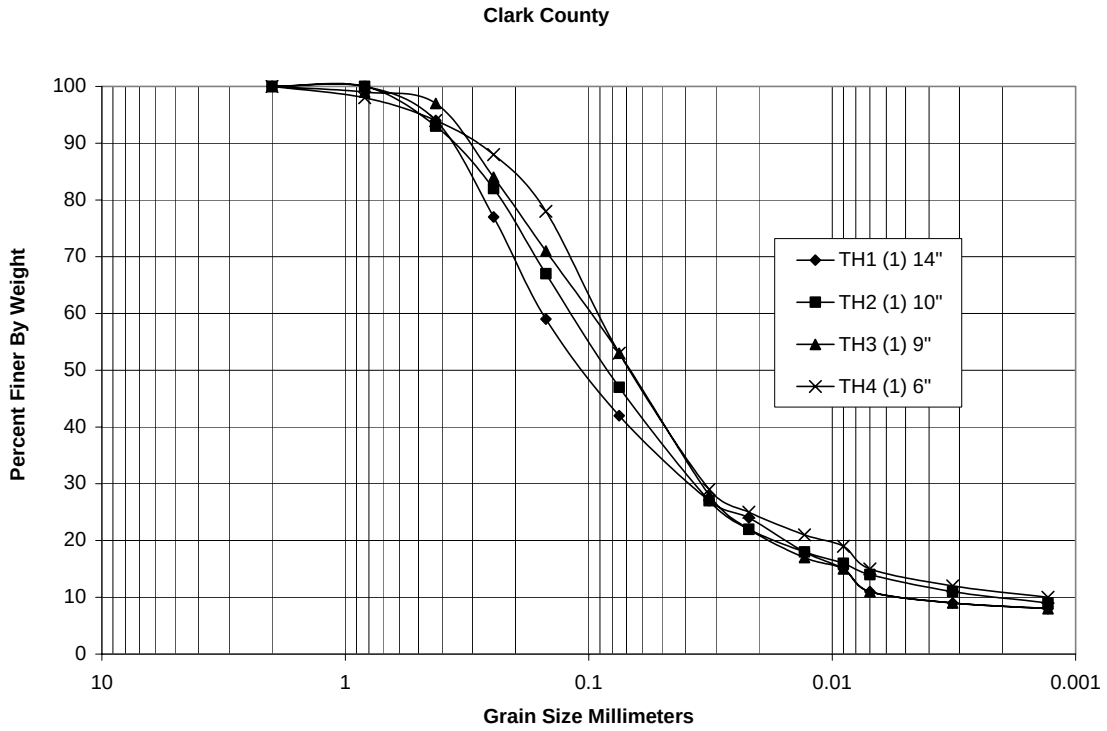

Figure C.28 – Grain size distribution for Clark County infiltration pond

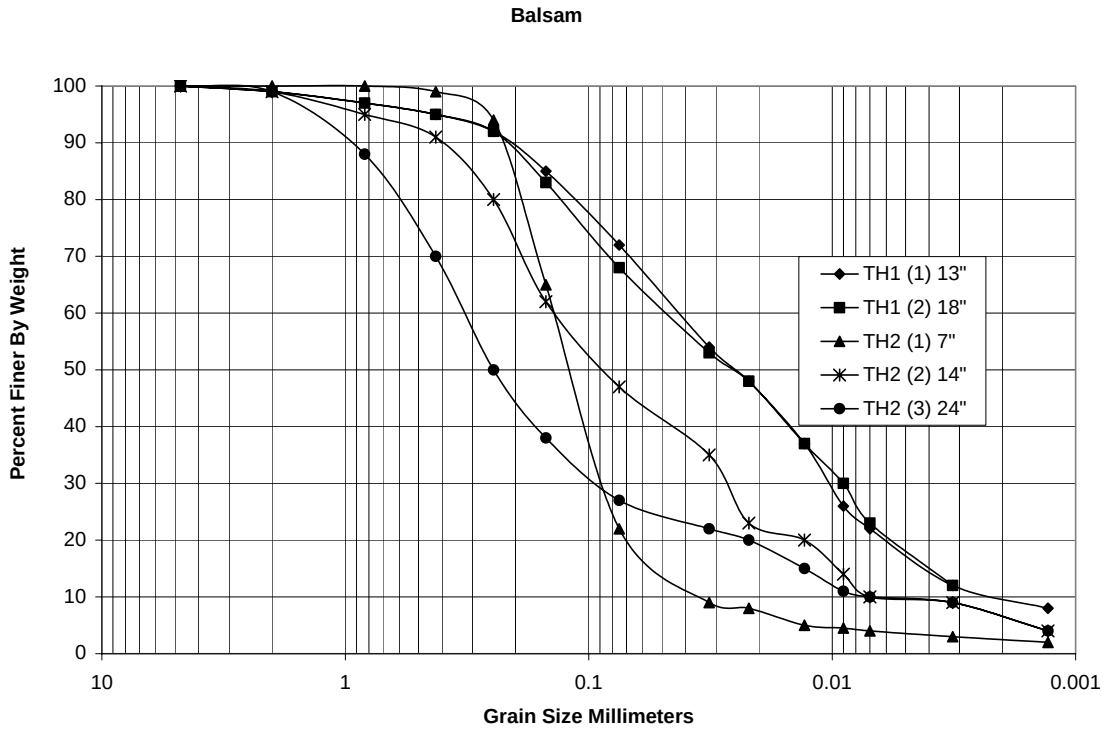

Figure C.29 – Grain size distribution for Balsam, Kitsap County infiltration pond

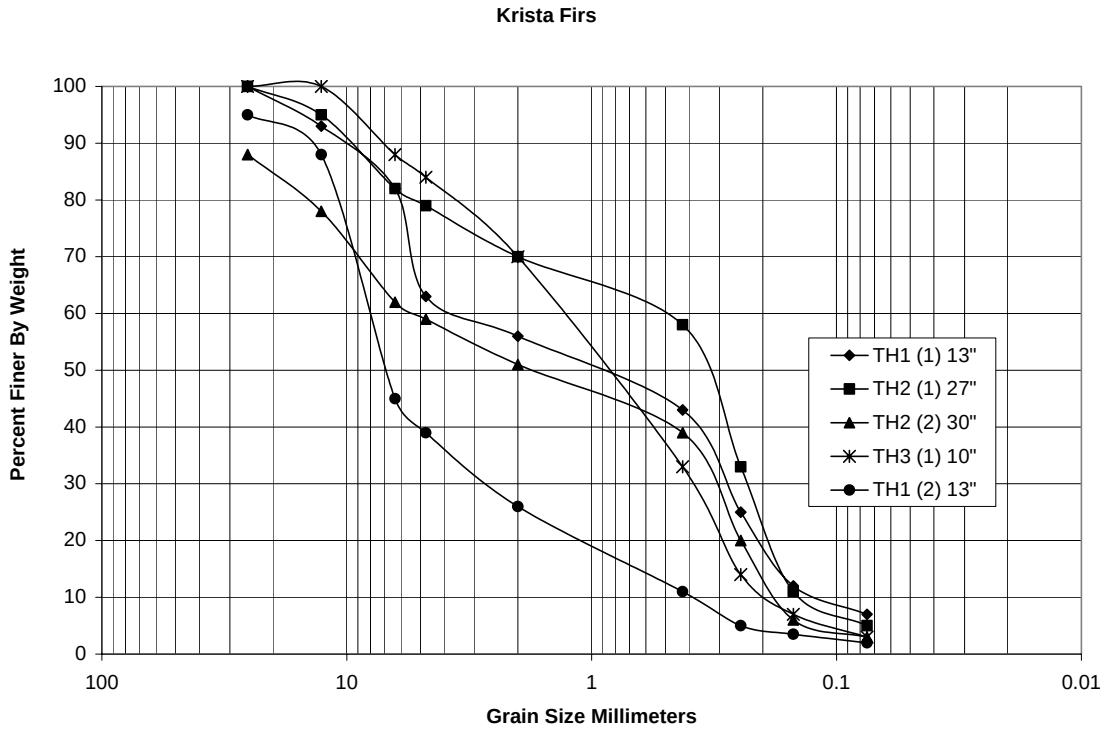

Figure C.30 – Grain size distribution for Krista Firs, Kitsap County infiltration pond

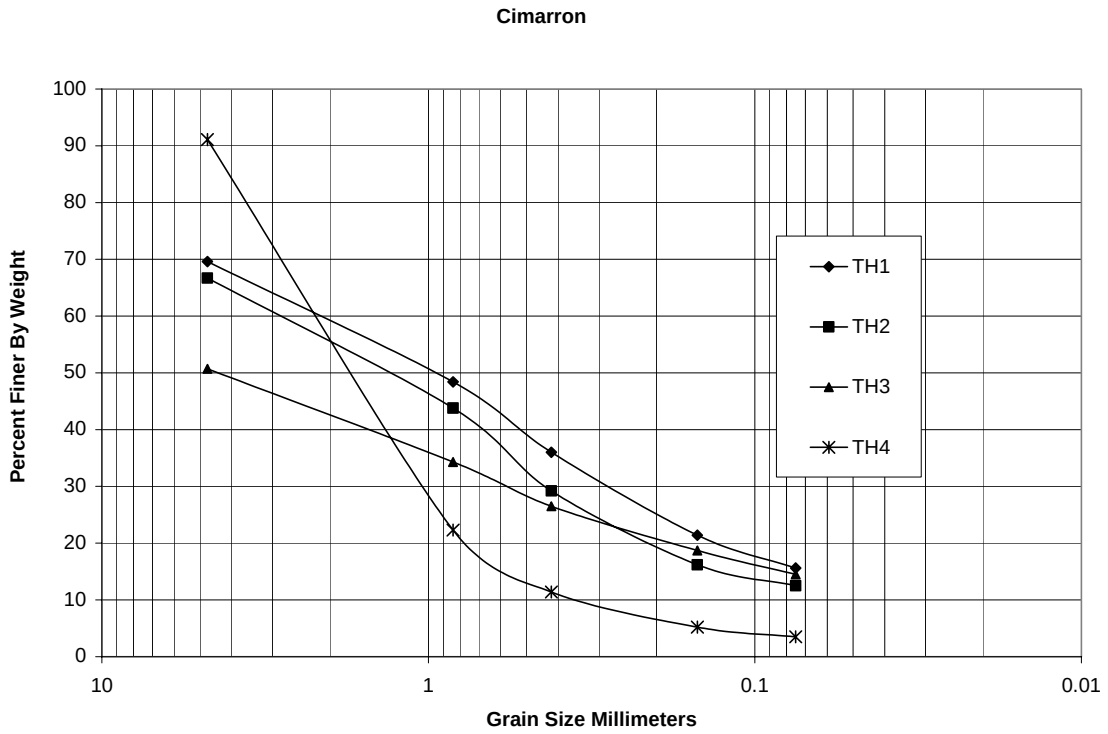

Figure C.31– Grain size distribution for Cimarron, King County infiltration pond

Appendix D - Description of Ponds used in the Full Scale Tests

Site Name	Site Address	Pond Age (years)	Pond Bottom Surface Area (ft^2)	Top Surface Area (ft^2)	Pond Volume (ft^3)	Pond Geometry
Clark Co.	Clark Co. 9616 NE 59th Av Vancouver, WA 98686	UNK	1,856	3,148	UNK	Rectangular
Beaverdam	King Co. SE Main St and 244th Av SE	UNK	~5,500	UNK	UNK	Trapezoidal
Balsum 7-11	Kitsap Co. Lund Av SE and Jackson Av Port Orchard, WA 98366	24	1,062	1,742	7200	Rectangular
Kirsta Firs,	Kitsap Co. K.C. Place and Cedar Rd E Port Orchard, WA 98366	23	1,030	2,078	3888	Rectangular
Airdustrial[1]	Thurston Co. Bonniewood Dr SW and 70th Ave Tumwater, WA	7	6,400	10,200	34,000	Rectangular
Bush Middle School[1]	Thurston Co. Kimmie St and 83rd Av Tumwater, WA	10	5,085	11,300	36,866	Triangular
Echo Glen[1]	Thurston Co.	10	7075	30,575	148,296 (wet pond + infiltration pond).	L-shaped.
Lacey Lid[1]	Thurston Co.[1] Yelm Hwy and Corporate Ctr Lacey, WA	10	17,100	53,840	248,276	Rectangular

Site Name	Site Address	Pond Age (years)	Pond Bottom Surface Area (ft^2)	Top Surface Area (ft^2)	Pond Volume (ft^3)	Pond Geometry
Margaret McKenny[1]	Thurston Co. Morse-Merryman Rd SE and Quentin St Lacey, WA	10	6,720	19,590	72,352	Rectangular
Ridgeview[1]	Thurston Co. Steilacoom Rd and Sandra Lee Ct Lacey, WA	7	23,265	31,446	93,465	Rectangular
Springfield	Thurston Co. Lilly Rd NE and Maple View Dr Olympia, WA	N/A	1,104	UNK	UNK	Rectangular
State Farm[1]	Thurston Co. Evergreen Park Dr and Heritage Ct Olympia, WA	11	560	2,400	2,960	Small kidney shaped.
Sweetbriar [1]	Thurston Co. Boulevard Rd and 45th Av. SE Lacey, WA	8	15,000	25,800	92,123	Triangular
Westwood Baptist,	Thurston Co. Kaiser Rd and Everygreen Pkwy Olympia, WA	7	171,000	UNK	5,800,000	Baseball field
Woodard Glen[1]	Thurston Co Lister Rd NE and Cherry Blossom Olympia, WA	21	2,000	3,800	8,700	Small trapezoidal

[1] Sites given in the Thurston County Performance Study.

[2] Infiltration Rates calculated using hind-cast analysis.

Site Name	Observed Soil Type	Design Infiltration Rate and Testing Method	Full-scale Infiltration Rate (cm/hr)	Bottom Cover and Condition	Comments
Clark Co.	Loam/Silty loam	UNK		Mostly bare with patches of mixed grasses.	Biofilter
Beaverdam	Sand		5	Gravelly bottom. No vegetation.	Biofilter
Balsum 7-11	Silty Loam	UNK	6	Dense with tall grass. Color and wide leaf vegetation indicate moist/wet conditions.	No pre-treatment. Thick wetland vegetation covers the pond bottom.
Kirsta Firs	Sand	20+"/hr	1	Poor vegetation of mixed grasses, frequent bare area with granular exposed areas.	No pre-treatment.
Airdustrial	Loamy sand	2,84 in/hr.	2	Isolated tufts of grass, bare patches, little top soil, fine sediment coating. Pond bottom silt covered due to failing biofilter swale.	Biofilter swale. Reached groundwater at 5.5 ft in August.
Bush Middle School[1]	Loamy sand	15 in/hr. (infiltrometer)	[2] >25	Mixed grasses, poor vegetation, much bare area, highly granular exposed area.	Bio-filtration swale. Seasonally high groundwater at 2 to 3 ft from pond bottom.
Echo Glen[1]	Sand	6 in/hr.	[2] >34	Sod grass. Full cover/dense.	Wet pond pre-treatment
Lacey Lid[1]	Loamy medium sand	UNK	1	Mixed grasses and moss.	Wet pond pre-treatment. Groundwater reached at 6 ft in August.
Margaret McKenny[1]	Gravely sandy loam	20 in/hr.	4	Scotch broom, hawkweed, mixed grasses and mosses. Pond bottom had silt covering.	Biofilter.

Site Name	Observed Soil Type	Design Infiltration Rate and Testing Method	Full-scale Infiltration Rate (cm/hr)	Bottom Cover and Condition	Comments
Ridgeview[1]	Gravely sandy loam	6 in/hr.	[2]>10	Scotch broom and gravel.	Wet pond pre-treatment.
Springfield	Sandy loam, loamy sand	3 in/hr.	38-8, rate dropped as volumne of infiltrated water increased.	Patches of grass and moss.	No pre-treatment. Neighborhood known to have shallow groundwater table in winter.K48
State Farm[1]	Loamy medium sand	20 in/hr. 2 infiltrometer tests.	11	Mixed grasses. Thick vegetation.	No treatment. Water level at 11 to 12 ft.
Sweetbriar[1]	Fine sandy loam	4.8 in/hr.	1	Scotch broom, mixed grasses and moss. Grass with bare patches, little top soil and mossy areas.	No pre-treatment. Groundwater mounding beneath pond bottom.
Westwood Baptist	Loamy sand	6 in/hr.	1	Hard pan layers.	Biofilter. 8 ft to groundwater, 27 ft to till.
Woodard Glen[1]	Loamy sand	UNK	4	Mixed grasses and moss. Bare patches with little topsoil, mossy patches. Moss and fine sediment clogging pond bottom.	No-pretreatment.

[1] Sites given in the Thurston County Performance Study.

[2] Infiltration Rates calculated using hind-cast analysis.

Appendix E – Estimated saturated hydraulic conductivity values for field sites

Site	Layer	Thickness	d_{10} (mm)	d_{60} (mm)	d_{90} (mm)	fines	K_w (cm/s)	K_{equiv} (cm/s)	K_{equiv} (in/hr)
Clark County	TH1(1)	14"	0.003	0.12	0.38	0.42	3.57E-03	3.6E-03	
	TH2(1)	10"	0.0023	0.1	0.32	0.47	2.81E-03	2.8E-03	
	TH3(1)	9"	0.005	0.09	0.3	0.53	2.13E-03	2.1E-03	
	TH4(1)	6"	0.0013	0.09	0.3	0.53	2.10E-03	2.1E-03	
Average K_{equiv}								**2.7E-03**	**3.8**
Beaverdam, King County	TH1(1)	4"	0.7	3	5.2	0.00	5.40E-01		
	TH1(2)	6"	0.08	1	6	0.16	1.51E-02		
	TH1(3)	3"	0.62	2.5	4.7	0.01	3.57E-01	3.1E-02	
	TH2(1)	4"	0.7	3	5.2	0.00	5.40E-01		
	TH2(2)	4"	0.8	3	5.2	0.01	8.06E-01		
	TH2(3)	4"	0.55	2.2	4	0.02	2.59E-01	4.3E-01	
	TH3(1)	3"	0.7	3	5.2	0.00	5.40E-01		
	TH3(2)	12"	0.55	2.2	4	0.01	2.67E-01	3.0E-01	
	TH4(1)	6"	0.7	3	5.2	0.00	5.40E-01		
	TH4(2)	8"	0.55	2.2	4	0.02	2.63E-01	3.4E-01	
Average K_{equiv}								**2.7E-01**	**390**
Cimarron, King County	TH1	n.a.	0.04	2	40	0.156	4.73E-03	4.7E-03	
	TH2	n.a.	0.04	3	40	0.125	5.69E-03	5.7E-03	
	TH3	n.a.	0.04	10	100	0.145	1.06E-03	1.1E-03	
	TH4	n.a.	0.4	2	5	0.035	1.19E-01	1.2E-01	
Average K_{equiv}								**3.3E-02**	**46**

Site	Layer	Thickness	d_{10} (mm)	d_{60} (mm)	d_{90} (mm)	fines	K_w (cm/s)	K_{equiv} (cm/s)	K_{equiv} (in/hr)
Balsam 7-11, Kitsap County	TH1(1)	10"	0.002	0.04	0.2	0.72	8.47E-04		
	TH1(2)	18"	0.002	0.05	0.21	0.68	1.03E-03	9.5E-04	
	TH2(1)	7"	0.03	0.13	0.21	0.22	1.05E-02		
	TH2(2)	24"	0.007	0.13	0.4	0.47	2.86E-03		
	TH2(3)	24"	0.008	0.31	1	0.27	7.40E-03	4.4E-03	
Average K_{equiv}								**2.7E-03**	**3.8**
Krista Firs, Kitsap County	TH1(1)	13"	0.11	3.8	10	0.07	2.59E-02		
	TH1(2)	13"	0.4	8	14	0.02	1.20E-01	4.3E-02	
	TH2(1)	27"	0.14	0.5	12	0.05	2.72E-02		
	TH2(2)	30"	0.18	5	25	0.03	2.81E-02	2.8E-02	
	TH3(1)	10"	0.2	1.3	7	0.03	4.67E-02	4.7E-02	
Average K_{equiv}								**3.9E-02**	**55**
Airdustrial, Thurston County	TH1(1)	67"	0.2	0.3	0.4	0.02	5.79E-02	5.8E-02	
	TH2(1)	48"	0.13	0.31	0.7	0.03	4.02E-02	4.0E-02	
Average K_{equiv}								**4.9E-02**	**70**
Bush, Thurston County	TH1(1)	20"	0.6	16	30	0	2.59E-01		
	TH1(2)	20"	0.5	15	30	0	1.61E-01		
	TH1(3)	35"	0.21	0.64	1.1	0.01	6.28E-02	9.9E-02	
	TH2(1)	33"	0.44	5	20	0.01	1.13E-01		
	TH2(2)	30"	0.24	1.3	5.8	0.01	6.35E-02	8.2E-02	
Average K_{equiv}								**9.1E-02**	**130**
Echo Glen, Thurston County	TH1(2)	7"	0.3	5.2	25	0.01	5.27E-02		
	TH1(3)	14"	0.9	9	15	0	1.19E+00		

Site	Layer	Thickness	d_{10} (mm)	d_{60} (mm)	d_{90} (mm)	fines	K_w (cm/s)	K_{equiv} (cm/s)	K_{equiv} (in/hr)
	TH1(4)	12"	0.6	20	31	0	2.89E-01		
	TH1(5)	7"	1.3	9	90	0	6.91E-01	2.0E-01	
Average K_{equiv}								**2.0E-01**	**290**
Lacey Lid, Thurston County	TH1(1)	69"	0.11	0.26	0.4	0.03	3.71E-02	3.7E-02	
	TH2(1)	50"	0.16	0.32	0.7	0	5.30E-02	5.3E-02	
Average K_{equiv}								**4.5E-02**	**64**
Margaret McKenny, Thurston County	TH1(1)	22"	0.34	12	31	0.02	6.34E-02		
	TH1(2)	20"	0.23	1	10	0	5.55E-02		
	TH1(3)	12"	0.11	0.8	11	0.06	2.37E-02	4.4E-02	
Average K_{equiv}								**4.4E-02**	**63**
Ridgeview, Thurston County	TH1(1)	32"	2.4	13	28	0	6.56E+02		
	TH1(2)	5"	0.6	15	30	0.03	2.16E-01		
	TH1(3)	11"	2.2	13	26	0	2.90E+02		
	TH1(4)	15"	0.25	9	25	0.01	4.85E-02	1.9E-01	
	TH2(1)	35"	1.4	8	20	0	8.80E+00		
	TH2(2)	14"	0.6	18	30	0	2.78E-01		
	TH2(3)	15"	2	19	30	0	1.32E+02	1.2E+00	
	TH3(1)	60"	0.3	9	25	0.04	5.22E-02	5.2E-02	
Average K_{equiv}								**4.7E-01**	**670**
Springfield, Thurston County	TH1(1)	13"	0.05	1	12	0.13	1.27E-02		
	TH1(2)	8"	0.077	0.3	6.1	0.09	2.03E-02		
	TH1(3)	10"	0.18	1.1	13	0.02	3.71E-02	1.8E-02	

Site	Layer	Thickness	d_{10} (mm)	d_{60} (mm)	d_{90} (mm)	fines	K_w (cm/s)	K_{equiv} (cm/s)	K_{equiv} (in/hr)
	TH2(1)	9"	0.09	0.42	8	0.07	2.24E-02		
	TH2(2)	6"	0.13	0.24	9	0.02	3.27E-02		
	TH2(3)	17"	0.09	0.2	0.5	0.04	3.23E-02	2.9E-02	
	TH3(1)	14"	0.068	1.3	14	0.11	1.44E-02		
	TH3(2)	8"	0.54	11	22	0.02	1.94E-01		
	TH3(3)	7"	0.23	5.8	14	0.02	5.29E-02	2.5E-02	
	TH4(1)	18"	0.06	0.6	11	0.13	1.35E-02		
	TH4(2)	8"	0.34	7.8	17	0.02	8.39E-02	1.8E-02	
Average K_{equiv}								**2.3E-02**	**32**
State Farm, Thurston County	TH1(1)	38"	0.23	6	19	0	5.03E-02		
	TH1(2)	27"	0.16	0.32	1	0	5.25E-02		
Average K_{equiv}								**5.1E-02**	**73**
Sweetbriar, Thurston County	TH1(1)	36"	0.16	0.28	0.4	0	5.34E-02		
	TH1(2)	9"	0.11	0.28	0.41	0.03	3.72E-02		
	TH1(3)	24"	0.18	0.3	0.5	0	5.82E-02	5.2E-02	
	TH2(1)	36"	0.18	0.29	0.4	0.02	5.30E-02		
	TH2(2)	30"	0.21	0.52	0.94	0	6.60E-02	5.8E-02	
Average K_{equiv}								**5.5E-02**	**78**
Westwood Baptist, Thurston County	TH1(1)	11"	0.09	0.6	9	0.07	2.19E-02		
	TH1(2)	10"	0.21	1.8	25	0.02	3.00E-02		
	TH1(3)	6"	0.23	1.6	40	0.01	2.16E-02	2.4E-02	
	TH2(1)	15"	0.09	2	15	0.07	1.91E-02		
	TH2(2)	6"	n/a						
	TH2(3)	5"	n/a						

Site	Layer	Thickness	d_{10} (mm)	d_{60} (mm)	d_{90} (mm)	fines	K_w (cm/s)	K_{equiv} (cm/s)	K_{equiv} (in/hr)
	TH3(1)	6"	0.06	0.5	4	0.16	1.45E-02		
	TH3(2)	6"	0.31	2	10	0	8.16E-02		
	TH3(3)	16"	0.09	0.4	4	0.06	2.65E-02	2.5E-02	
	TH4(1)		n/a						
	TH4(2)	9"	0.15	1.8	5	0.03	4.06E-02		
	TH4(3)	31"	n/a						
	TH5(1)	4"	n/a						
	TH5(2)	14"	n/a						
	TH6(1)	6"	0.07	1.5	7	0.11	1.81E-02		
Average K_{equiv}								**2.4E-02**	**35**
Woodard Glen, Thurston County	TH1(1)	15"	0.55	9	11.7	0	2.84E-01		
	TH1(2)	28"	0.2	0.55	1.5	0.01	5.92E-02	8.2E-02	
	TH2(1)	36"	0.18	0.28	0.4	0.01	5.56E-02		
	TH2(2)	6"	0.2	40	100	0	1.24E-02	3.7E-02	
Average K_{equiv}								**5.9E-02**	**84**